Probing the Structure and Dynamics of Intrinsically Disordered c-Myc PEST Fragment Using Spectroscopic Techniques

A Thesis Submitted in Partial Fulfillment of the

Requirements for the Degree of

Doctor of Philosophy

By

Mohd. Ziauddin Ansari

Department of Biosciences and Bioengineering
Indian Institute of Technology Guwahati
Guwahati, Assam- 781039, India

August 2018

INDIAN INSTITUTE OF TECHNOLOGY
GUWAHATI, Assam, India

Department of Biosciences and Bioengineering

STATEMENT

I do hereby declare that the matter embodied in this thesis is the result of investigations carried out by me in the Department of Biosciences and Bioengineering, Indian Institute of Technology Guwahati, India, under the guidance of Prof. Rajaram Swaminathan.

In keeping with the general practice of reporting scientific observations, due acknowledgements have been made wherever the work described is based on the findings of other investigators.

IIT Guwahati — Mohd. Ziauddin Ansari

August, 2018

INDIAN INSTITUTE OF TECHNOLOGY
GUWAHATI, Assam, India

Department of Biosciences and Bioengineering

CERTIFICATE

It is certified that the work described in this thesis, entitled "***Probing the Structure and Dynamics of Intrinsically Disordered c-Myc PEST Fragment Using Spectroscopic Techniques***" done by **Mohd. Ziauddin Ansari** for the award of degree of Doctor of Philosophy is an authentic record of the results obtained from the research work carried out under my supervision in the Department of Biosciences and Bioengineering, Indian Institute of Technology Guwahati, India, and this work has not been submitted elsewhere for a degree.

IIT Guwahati
August, 2018

Prof. Rajaram Swaminathan
Department of BSBE
IIT Guwahati

Dedicated to my Family

ACKNOWLEDGEMENTS

After many ups and downs and sacrifice of six years of my life, I am extremely happy to be in this position. And without the help of the people mentioned hereafter, I don't think I would have made it this far. I would like to express my sincere gratitude to all of them.

First and foremost, I want to express my deepest respect and sincere gratitude to my supervisor Prof. R. Swaminathan for giving me the opportunity to undertake a Ph.D. in his group. His continuous support, patience, enthusiasm, immense scientific ideas and motivation helped me in all the time of research and to explore the domain of work assembled in this thesis. He has been a great mentor, from whom I have learned a lot of things. He encouraged me not only to grow as a researcher but also as a person. I am indebted to him, for his faith in me and providing the right direction whenever I needed it the most.

Besides my advisor, I would also like to extend my sincere thanks to the Doctoral Committee members, Prof. K. Pakshirajan, Prof. B. K. Patel and Dr. S. P. Kanaujia for their encouragement, timely evaluation of my Ph.D. work and insightful suggestions, which help me a lot in the betterment of my thesis.

I thank our collaborator Dr. Rashna Bhandari (Laboratory of Cell Signalling, Centre for DNA Fingerprinting and Diagnostics, Hyderabad) and Dr. Padmavathi Lolla for providing us the clones of human c-Myc PEST fragment.

Thanks to the BSBE department staff members, for their co-operative nature. My sincere thanks to Central Instruments Facility, for service and support to Mass spectrometry facilities.

Thanks to IIT Guwahati and its administration for all the facilities that were made available to me and the Ministry of Human Resource Development (MHRD), India for the financial support.

Next, I wish to express my sincere thanks to my lab seniors Saumya Prasad and Shrutidhara Biswas for their enormous help and suggestion during my Ph.D. For making the lab a great place to work, I express my deep sense of gratitude to all my extraordinary

juniors Amrendra, Dileep, Anurag, Ekramul, Alka, Heeramoni, Vinay, Nayan, Aditya, Garima, Subhajit and Abheek. I am especially thankful to Amrendra, Dileep and Ekramul for their help during the thesis writing.

I would also like to express my sincere thanks to all my friends Wajid Ali, Vijya Laxmi, Asif Raza, Seraj Ahmad, Faheem, Sachin, Nafees, Renu and Gopal for their constant support and timely help. I thank them for making my stay at IIT Guwahati a memorable one.

My Ph.D. endeavor could not have been completed without the endless love, unending support, tolerance and blessings from my family. My deepest gratitude to my parents whose enormous sacrifices, unconditional love in every stage of my life motivated me overcomes all the challenges. Especially my father 'Mr. Liaqat Ali Ansari' whose firm believes in me and encouragement has given me all the strength to break through all the difficulties in life. I am also grateful to my brothers and younger sister, Nakhat for their unending love and emotional support in all the times. I owe every bit of my achievement to my family.

There were many other people who helped me both personally and professionally. Although it is not possible to pen down each of their names, I would like to thank each one of them for helping me in some of the other way during different stages of my Ph.D.

Finally, my deepest thanks to my wife, Amreen for her extreme support throughout this entire process and has made countless sacrifices to help me get to this point. Her support, motivation and help during this phase of my life cannot be expressed in words. Her understanding and unconditional love encouraged me to carry forward my work. She has truly been an immense support as a life partner.

Last but not the least; I am thankful to Almighty Allah for his continuous blessing during my research career to achieve these remarkable steps.

Mohd. Ziauddin Ansari *August, 2018*

LIST OF ABBREVIATIONS

ANS	8-Anilinonaphthalene-1-sulfonic acid
BSA	Bovine serum albumin
CD	Circular Dichroism
Dansyl	2-dimethyl aminonaphthalene 6-sulfonyl
DTNP	2,2'-dithiobis(5-nitropyridine)
DTT	1,4-Dithiothreitol
FRET	Förster Resonance Energy Transfer
Gdn.HCl	Guanidine Hydrochloride
IAEDANS	(1,5-IAEDANS, 5-((((2-Iodoacetyl)amino)ethyl) amino) Naphthalene-1-Sulfonic Acid)
IPTG	Isopropyl β-D-1-thiogalactopyranoside
MALDI	Matrix-assisted laser desorption ionization
NATA	N-acetyl tryptophan amide
SDS-PAGE	sodium dodecyl sulfate polyacrylamide gel electrophoresis
TCEP	Tris(2-carboxyethyl)phosphine
TFE	2,2,2-Trifluoroethanol
UV-Vis	Ultraviolet-Visible

THESIS ABSTRACT

Proteins are the most abundant and diverse intracellular biomolecules which have been thoroughly studied in past due to their numerous crucial functions in maintenance of biological processes. The newly discovered class namely Intrinsically Disordered Proteins (IDPs) which do not have any well-defined stable secondary or tertiary structure under the physiological conditions challenged and revised the traditional protein structure-function paradigm. Regardless of being flexible and lacking stable structure, IDPs have several structural and functional advantages over the ordered proteins and participates in many key biological functions such as signaling and cell cycle control. An extensive analysis of the structure, function and dynamics of IDPs is necessary for deciphering the elaborate physiological control of their functions and how such controls might fail in human diseases. In this context, we have chosen an IDP, human c-Myc PEST region whose structural determination and characterization of disordered properties has not been done before. The highly unstable c-Myc oncoprotein is a transcription factor which is involved in many essential cell processes. Its centrally located, highly acidic PEST region is responsible for quick degradation of c-Myc oncoprotein. The exact mechanism of PEST recognition and targeting of PEST containing proteins for degradation via proteasome is poorly understood and structural analysis of PEST region can provide better insights to understand their functional mechanism.

This thesis work is an attempt to understand and explore the structural and disorder properties of human c-Myc PEST fragment and its tryptophan inserted mutant (M1). The c-Myc PEST fragment was predicted to be highly disordered by using different disorder prediction tools. We observed anomalous SDS PAGE mobility and heat resistance in the c-Myc PEST fragment. The steady state fluorescence emission, fluorescence anisotropy and anisotropy decay analysis reveal solvent-exposed and unrestricted rotation of tryptophan in PEST M1 which in-turn indicates its disordered structure in the vicinity of tryptophan at C-terminus. Minor increase in ANS fluorescence intensity indicated presence of insignificant hydrophobic patches in PEST fragment. About five-fold high molecular weight and large hydrodynamic radius of PEST fragment as determined by size exclusion chromatography and dynamic light scattering revealed its random coil structure. This

random coil structure of PEST fragment was also confirmed by circular dichroism (CD). Further, about 3.5 fold increase in α-helical content of PEST fragment with 50% TFE suggest possibility of its interaction with other proteins.

Next we investigated the consequences of change in environment (like pH and counter ion) on the structure and dynamics of PEST fragment. We observed about two fold (1.7 to 3.3 ns) increase in the fluorescence lifetime of PEST M1 tryptophan with increasing pH (from 3 to 9). Higher steady state fluorescence anisotropy and residual anisotropy (r_∞) values at pH 3 and 5 revealed significant restricted rotational motion of PEST M1 tryptophan due to its well folded structure at C-terminus. About two fold increase [1.4 to 3.13 M^{-1} s^{-1} ($x10^9$)] in the value of bimolecular fluorescence quenching rate constant (k_q) was observed which suggests that tryptophan is buried in protein core at lower pH, compared to neutral and alkaline pH. The steady state and time-resolved fluorescence studies of dansyl (labeled at single cysteine) tagged PEST fragment revealed less folded form of PEST fragment at N-terminus in comparison with C-terminus at acidic pH. To analyze overall structural changes in PEST fragment at different pH; Förster Resonance Energy Transfer (FRET), ANS binding assay and CD analysis were carried out. FRET studies revealed that distance between cysteine^9-trytophan^{70} increased (from 24 to 32 Å) with increasing pH (from 3 to 9). About five fold increase in ANS fluorescence revealed the presence of significant hydrophobic patches in PEST fragment at acidic pH. CD analysis clearly indicated a major structural transition in PEST fragment upon changing the pH from acidic to basic. Tryptophan fluorescence measurements revealed no structural alteration in PEST fragment at pH 7.4 in presence of excess of counter ions (25 mM—500 mM NaCl).

We also observed involvement of single cysteine residue in dimerization of PEST fragments through disulphide bond formation. This dimer formation of PEST fragments was confirmed using different techniques like reducing and non-reducing SDS-PAGE, DTNP assay and mass spectrometry. Further, the structural and disordered properties of PEST dimer were extracted using different biophysical and spectroscopic techniques. About five fold increase in the molecular weight of PEST dimer was determined by size exclusion chromatography, revealing its random coil structure. Secondary structure analysis by CD revealed that dimerization induces some ordered structure in PEST fragment.

Fluorescence anisotropy decay investigations indicate more disorderedness in PEST dimer than its monomer at C-terminus as tryptophan is more free and dynamic in the dimer compared to its monomer.

Finally, the lack of structure promoting intrinsic spectral probes like tryptophan/tyrosine and richness of charged amino acids in wild type PEST fragment limits its structural analysis to a few techniques like circular dichroism and NMR. This led us to explore the new label free, simple and inexpensive method to investigate the conformational changes in IDPs. Here, we exploit the richness of charged amino acid population in IDPs to sense their structural transitions using Protein Charge Transfer Spectra (ProCharTS). The ProCharTS originate due to photoinduced electron transfers from: polypeptide backbone to NH_3^+ in lysine; COO^- in glutamate to polypeptide backbone; and COO^- in glutamate to NH_3^+ in lysine. Conformational changes induced in the PEST fragments by altering pH and temperature of aqueous medium was monitored by ProCharTS and confirmed by CD spectra. We observed that in presence of tryptophan, ProCharTS absorbance was substantially reduced, specifically at wavelengths where absorption by tryptophan was near its maximum. Significant changes in ProCharTS spectrum was observed with changing pH in the range 3—11, which correlated with changes in secondary structure of PEST fragments. ProCharTS intensity was sensitive to temperature induced changes in the secondary structure of PEST fragments between 25—85°C. Presence of 250 mM NaCl or KCl in the medium also altered the ProCharTS spectrum.

Taken together, this thesis work reveals structural and disorder properties of human c-Myc PEST fragment and highlights the utility of ProCharTS as a new label-free intrinsic probe to monitor structural transitions in IDPs.

Table of Contents

	Page No.
Acknowledgement	*i*
List of Abbreviations	*iii*
Abstract	*iv*

Chapter 1: Introduction and Review of Literature

1.1 Intrinsically Disordered Proteins (IDPs)	1
1.1.1 Functional anthology of IDPs	5
1.1.2 Special characteristics of IDPs	8
1.1.2.1 Amino acid composition	8
1.1.2.2 Charge and hydrophobicity	9
1.1.2.3 Many to one and one to many binding modes	10
1.1.2.4 Anomalous SDS-PAGE mobility	11
1.1.2.5 Enhanced proteolytic sensitivity	11
1.1.3 Influence of environment change on IDPs	12
1.1.3.1 Effect of pH	13
1.1.3.2 Effect of temperature	13
1.1.3.3 Effect of counter ions	14
1.1.3.4 Effect of binding partners	14
1.1.3.5 Effect of osmolytes	15
1.1.4 Techniques for recognizing and characterizing of IDPs	15
1.1.5 Advantage of protein being disordered	17
1.2 Human c-Myc PEST region	18
1.3 Objectives for the thesis work	23
1.4 Types of electronic spectra	25
1.4.1 Transitions involving π, σ, and n electrons	25
1.4.2 Transitions involving d and f electrons	26
1.4.3 Transitions involving charge-transfer electrons	26
1.5 Chromophores in Proteins	27

1.5.1 Peptide bond 27
1.5.2 Aromatic amino acids 28
1.5.3 Prosthetic groups and Co-Enzymes 29
1.6 Protein Charge Transfer Spectra (ProCharTS) 30

Chapter 2: Experimental Techniques, Materials and Methods

2.1 Experimental techniques 33
2.1.1 Absorbance 33
2.1.2 Fluorescence 35
2.1.2.1 Factors that affect fluorescence intensity 36
2.1.2.1.1 Internal Conversion 36
2.1.2.1.2 Quenching 36
2.1.2.1.3 Intersystem crossing 37
2.1.2.2 Steady state fluorescence 38
2.1.2.3 Steady-state fluorescence anisotropy 39
2.1.2.4 Time-resolved fluorescence decay 40
2.1.2.5 Time-resolved fluorescence anisotropy decay 43
2.1.2.6 Time-resolved intensity decay analysis 46
2.1.2.7 Time-resolved Anisotropy decay analysis 48
2.1.2.8 Fluorescence quenching 49
2.1.2.8.1 Static quenching 50
2.1.2.8.2 Dynamic or collisional quenching 50
2.1.2.9 Förster Resonance Energy Transfer (FRET) 52
2.1.3 Circular Dichroism 53
2.1.4 Dynamic Light Scattering 55
2.2 Materials 57
2.3 Methods 58
2.3.1 Amino acid composition and disorder prediction plots 58
2.3.2 Charge hydropathy plot and hydrophobic cluster analysis 58
2.3.3 Cloning, Expression and Purification of PEST Wt and PEST M1 59

2.3.3.1 Cloning of PEST Wt and PEST M1 59
2.3.3.2 Preparation of competent cells 59
2.3.3.3 Transformation 60
2.3.3.4 Expression and purification of PEST Wt and PEST M1 60
2.3.4 Sodium dodecyl sulfate polyacrylamide gel electrophoresis 61
2.3.5 Protein estimation 62
2.3.6 Mass Spectrometry analysis 62
2.3.7 Size exclusion chromatography 63
2.3.8 Dynamic Light Scattering measurements 64
2.3.9 UV-Visible absorption spectra 65
2.3.10 Labeling of PEST fragment with dansyl probe 65
2.3.11 Steady state fluorescence and anisotropy measurements 66
2.3.12 ANS binding assay 67
2.3.13 Time-resolved fluorescence and anisotropy measurements 68
2.3.14 Quenching of tryptophan with acrylamide 69
2.3.15 Intramolecular FRET measurements 70
2.3.16 Circular Dichroism analysis 71
2.3.17 Estimation of free thiol 72

Chapter 3: Purification and characterization of human c-Myc PEST fragment and its mutant

3.1 Introduction 73
3.2 Results and Discussion 75
3.2.1 Amino acid composition profile and disorder prediction plots 75
3.2.2 Charge hydropathy plot and hydrophobic cluster analysis 77
3.2.3 Purification of human c-Myc PEST fragment 79
3.2.4 Mass spectrometry analysis of PEST Wt and M1 80
3.2.5 Anomalous SDS-PAGE mobility and heat resistance 81
3.2.6 Determination of molecular weight and Stokes radius of PEST fragment by size exclusion chromatography 82
3.2.7 Dynamic light scattering measurements of PEST fragment 86

3.2.8 Absorption spectra of PEST Wt and M1 87
3.2.9 Steady state fluorescence and anisotropy analysis of PEST M1 88
3.2.10 Fluorescence lifetime and time-resolved anisotropy of PEST M1 90
3.2.11 ANS binding assay of PEST Wt and M1 92
3.2.12 Secondary structure analysis of PEST Wt and M1 by CD 93
3.2.13 Effect of TFE on structure of PEST Wt and M1 94
3.3 Conclusions 98

Chapter 4: Effect of pH and salt on structure and dynamics of human c-Myc PEST fragment and its mutant

4.1 Introduction 99
4.2 Results and Discussion 101
4.2.1 Steady state fluorescence intensity and fluorescence anisotropy studies of PEST M1 tryptophan 101
4.2.2 Tryptophan fluorescence lifetime analysis of PEST M1 105
4.2.3 Time-resolved anisotropy decay analysis of PEST M1 tryptophan 110
4.2.4 Quenching of PEST M1 tryptophan by acrylamide 113
4.2.5 Steady state fluorescence and anisotropy studies of dansyl 118
4.2.6 Fluorescence lifetime analysis of dansyl labeled PEST Wt and M1 120
4.2.7 Time-resolved anisotropy decay analysis of dansyl labeled PEST Wt and M1 123
4.2.8 Förster Resonance Energy Transfer (FRET) analysis 126
4.2.9 ANS binding assay of at different pH 131
4.2.10 Circular Dichroism (CD) analysis 133
4.2.11 Effect of salt (NaCl) on PEST fragment 135
4.3 Conclusions 138

Chapter 5: Unravelling the dimeric properties of human c-Myc PEST fragment and its mutant

5.1 Introduction 141
5.2 Results and Discussion 142
5.2.1 Estimation of free thiol group 142

5.2.2 Non-reducing and reducing SDS-PAGE 144
5.2.3 Mass analysis of PEST dimer 145
5.2.4 Size exclusion chromatography of PEST Dimer 147
5.2.5 Dynamic light scattering studies of PEST Dimer 150
5.2.6 Steady state fluorescence and anisotropy studies of PEST M1 dimer 152
5.2.7 Fluorescence lifetime analysis of PEST M1 dimer 154
5.2.8 Time-resolved anisotropy decay analysis of PEST M1 dimer 155
5.2.9 Circular Dichroism analysis of PEST Wt and M1 dimer 157
5.3 Conclusions 160

Chapter 6: Probing the structural transitions in human c-Myc PEST fragment and its mutant by Protein Charge Transfer (ProCharTS) Absorption Spectra

6.1 Introduction 161
6.2 Results and Discussion 162
6.2.1 Protein Charge Transfer (ProCharTS) Absorption Spectra of PEST 162
6.2.2 Comparison of absorption spectra with simulated Rayleigh Scatter 165
6.2.3 Effect of pH on the ProCharTS of PEST fragments 167
6.2.4 Effect of temperature on the ProCharTS of PEST fragments 169
6.2.5 Effect of salt on the ProCharTS of PEST fragments 174
5.3 Conclusions 176

Chapter 7: Thesis summary and future perspectives

7.1 Summary 177
7.2 Future perspectives 178

Appendix 179

List of Publications and Conferences 185

References 187

Chapter 1

Introduction and Review of literature

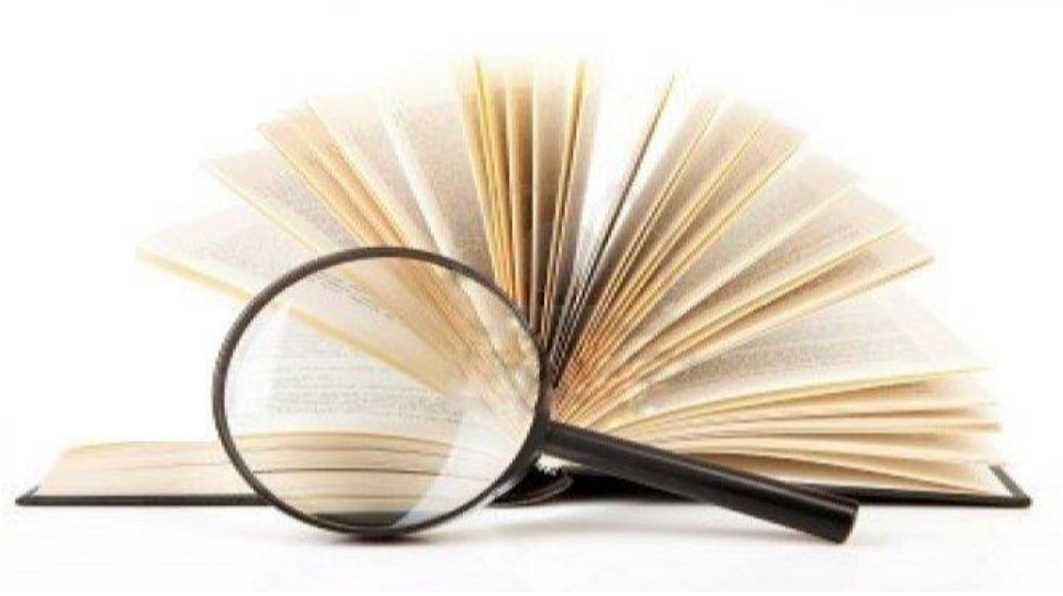

Biomolecules like carbohydrates, lipids, nucleic acids and proteins are crucially important for a cell to perform its normal functions. All these biomolecules are essential for survival and growth of living organism. Among all the biomolecules, proteins are the most abundant (about 55% of dry weight of the cell) and diverse biomolecules present in the living organism (Cooper and Ganem, 1997; Milo and Phillips, 2015). They carry out many crucial functions to maintain biological processes including storing and transporting of molecules like oxygen, catalyzing biochemical reaction, providing immune protection, transmitting nerve impulses, controlling differentiation and growth etc. (Berg et al., 2002; Daniel et al., 2003; di Prisco et al., 1991; Lesk, 2001). For better insight about the vast processes performed by proteins, their structural and functional determination is very important.

Since 1958 when three dimensional structure of myoglobin was discovered using X-ray analysis (Kendrew et al., 1958), understanding of protein structure and its function grew significantly. At the time, when only a few crystal structures of proteins were solved, some segments of protein were not resolved in electron density maps of X-ray crystallography and were still considered necessary for proper biological functions (Bloomer et al., 1978; Bode et al., 1978; Huber and Bennett Jr, 1983). The number of proteins and protein domains that have unordered or little ordered structure under the physiological conditions *in vitro* with significant roles in protein function is growing rapidly year after year. The prevalence and fundamental roles of these non-structured proteins or protein segments in biology were recognized in late 1990s as Intrinsically Disordered Proteins (IDPs) or Intrinsically Disordered Regions (IDRs).

1.1 Intrinsically Disordered Proteins (IDPs):

IDPs, known by different names such as natively unfolded proteins or intrinsically unstructured proteins or natively disordered proteins, have no well-defined stable secondary and/ or tertiary structures under the physiological conditions. Contrary to the ordered proteins, IDPs exist as a dynamic ensembles where the atom position as well as the dihedral angels of the peptide backbone changes significantly over time with no specific equilibrium values and naturally involve non-cooperative conformational changes. Thus, the protein's dynamical property defines its very existence of disorderedness. Regardless of being

flexible and lack of stable secondary or well-defined three dimensional structures, IDPs perform critical biological functions such as involvement in cell cycle control and signal transduction (Burgi et al., 2016; Dunker et al., 2008; Dyson and Wright, 2005; Fox and Kannan, 2017; Habchi et al., 2014; Uversky and Dunker, 2010; Weinreb et al., 1996; Wildegger et al., 1999).

IDPs/IDRs remains unstructured in unbound form, however in bound forms with their binding partners like different metal ions, membranes, osmolytes, DNA, RNA, proteins and macromolecular crowding agents they display ability to gain structure. Many instances are reported when even in the bound form; some portion of IDPs remains disordered (Burgi et al., 2016; Dyson and Wright, 2002; Dyson and Wright, 2005; Fox and Kannan, 2017; Spolar and Record, 1994; Sugase et al., 2007; Tompa, 2002). In comparison with structured globular proteins and domains, IDPs/IDRs are different in their amino acid composition, hydrophobicity, net charge, aromaticity, sequence complexity, flexibility and degree of amino acid substitutions over evolutionary time (Dunker et al., 2001; Habchi et al., 2014; Radivojac et al., 2007; Romero et al., 2001; Williams et al., 2001).

The traditional protein structure-function paradigm which supports the very fact that a defined ordered structure is a prerequisite for a protein to perform defined function is brought to question and is being challenged with the advent of newly discovered unstructured but biologically active proteins known as IDPs/IDRs. By resemblance with partially folded conformations of ordered proteins (such as pre-molten globule, molten globule and unfolded), IDPs are classified into three structurally different sub-classes known as native molten globules (also known as collapsed IDPs), native pre-molten globules and native coil (both are called as natively unfolded proteins or extended IDPs) (Ptitsyn, 1995a; Ptitsyn, 1995b; Tcherkasskaya and Uversky, 2001; Wright and Dyson, 1999). Figure 1.1A shows the illustration of different sub-classes of IDPs. Now the old structure-function paradigm about the proteins should be reformulated and should include the existence of IDPs.

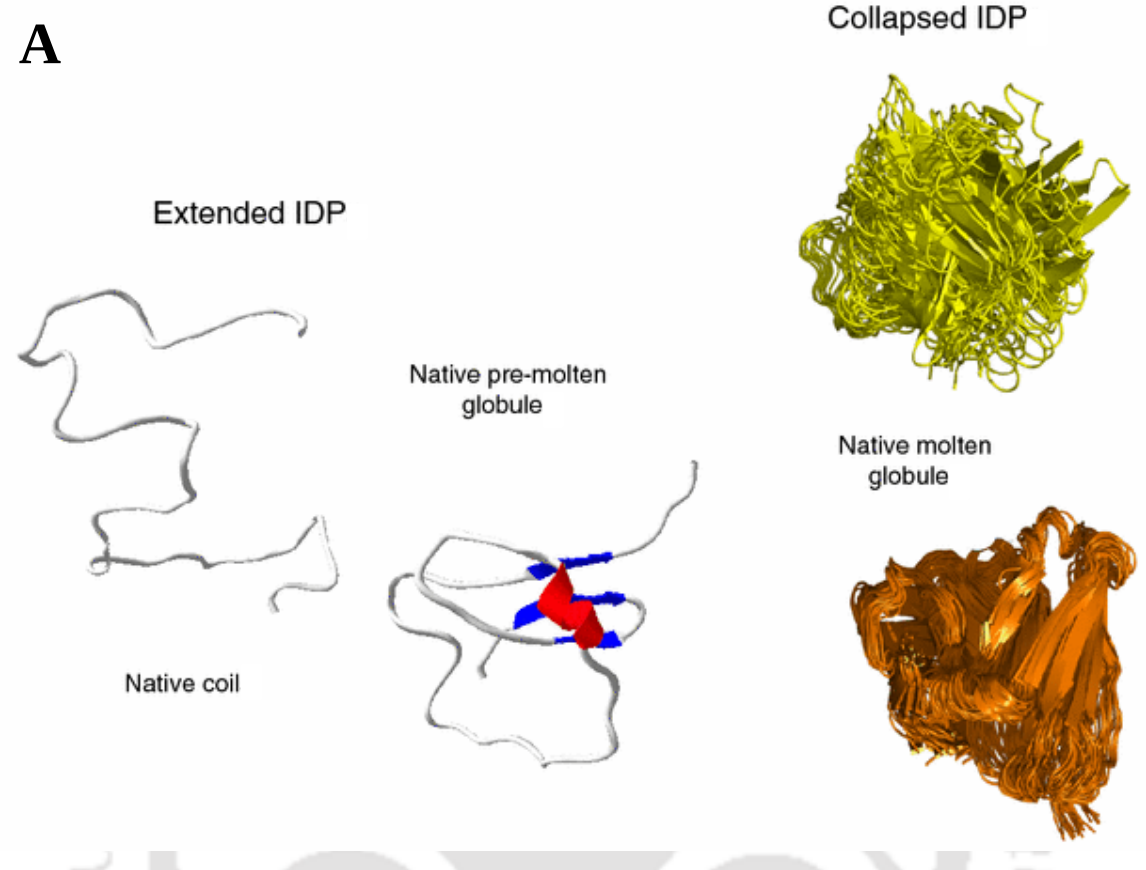

Figure 1.1A: Illustrative examples of model ID proteins. Two different extended forms (native coil and native pre-molten globule) are shown together with two examples of the collapsed IDPs (native molten globule-likes). Adapted from (Uversky, 2009).

An alternative theory called as "Protein Trinity" (shown in Figure 1.1B) was proposed by Dunker and Obradovic to explain the existence of IDPs (Dunker and Obradovic, 2001). According to Protein Trinity theory, any one of the three thermodynamics states, the solid like ordered state, the liquid like collapsed molten globule state, or the gas like extended (random coil) state can be the native or functional regions of proteins. Function of protein can arise from any one or from transition between three thermodynamics states. Later on, Protein Trinity theory was extended to Protein Quartet Model (display in Figure 1.1C) for including the fourth state (pre-molten globule). It explains that the function can arise from any of the four conformations or by transition between all four conformations (Uversky, 2002).

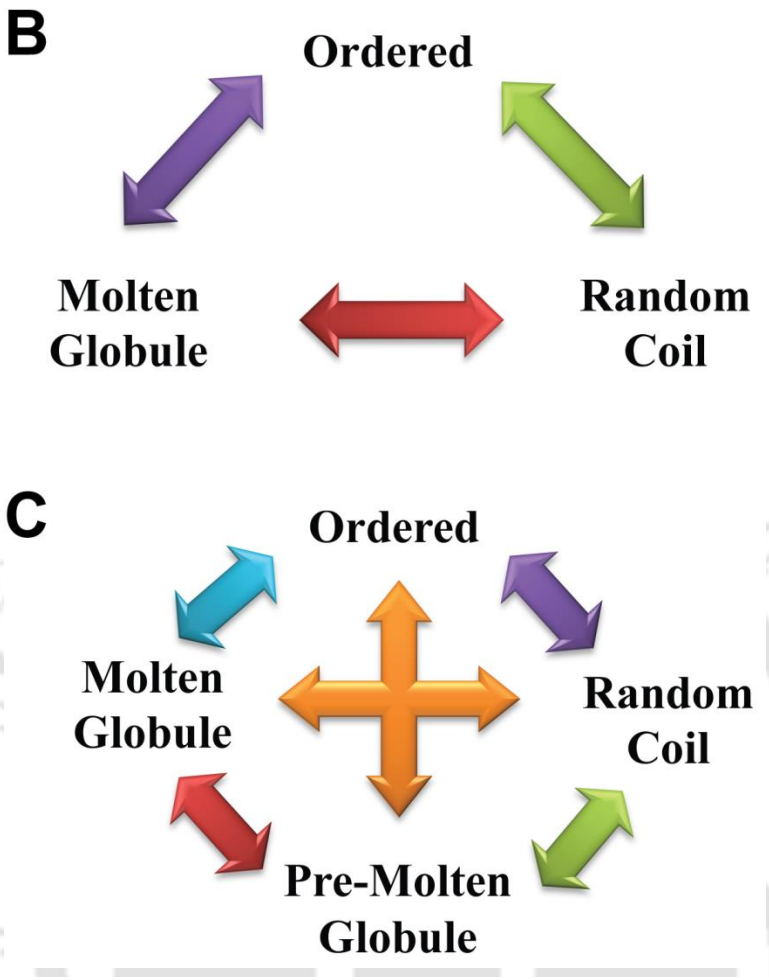

Figure 1.1: Extension of The Protein Trinity **[B]** to the Protein Quartet model of protein functioning **[C]**. Modified from (Uversky, 2002).

Bioinformatics studies point out that IDPs are highly abundant across different proteomes and their prevalence increases with the increase in complexity of the organisms (Dunker et al., 2000). An average of about 2.0 % of Archaeal, 4.2% of Eubacterial and 33% of eukaryotic proteins are predicted to be disordered (Fink, 2005; Oldfield et al., 2005) and more than 50% of eukaryotic proteins have long disordered region (Dunker et al., 2000). IDPs are frequently involved in critical processes like cell signaling and regulation (Dyson and Wright, 2005; Wright and Dyson, 2015) and widely associated with various human diseases including diabetes, cancer, neurodegenerative diseases and amyloidosis (Babu, 2016; Uversky et al., 2008). A high percentage of signaling, cancer, diabetes and neurodegenerative diseases associated proteins are predicted to possess long disordered

regions (Iakoucheva et al., 2002). Figure 1.1D shows the distribution of disordered proteins involved in binding, catalysis and transcription among *Escherichia coli*, yeast and human.

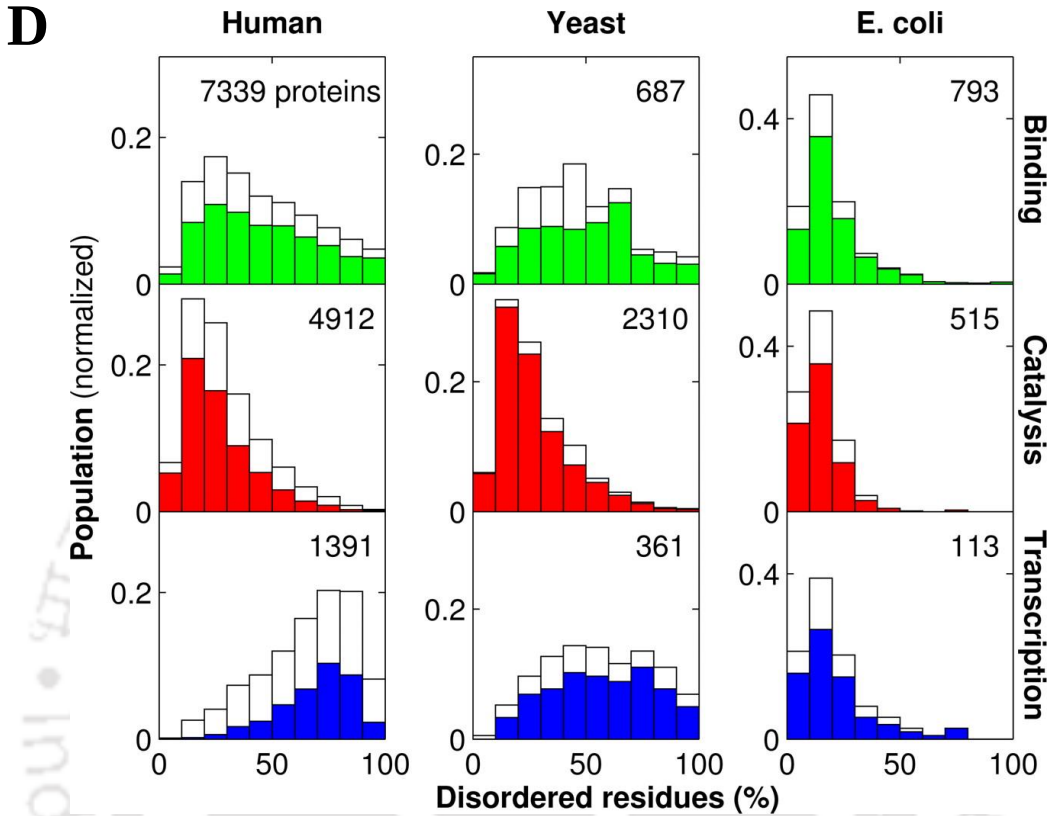

Figure 1.1D: Disorder distribution. Normalized histograms of the percentage of disordered residues in the sequence of human, yeast and *E. coli* proteins within the gene ontology categories of ‘‘protein binding’’, ‘‘catalytic activity’’, and ‘‘transcription regulator activity’’. The distributions after removing the overlap between the three categories are shown by the lower bars (shaded). Adapted from (Liu et al., 2009).

1.1.1 Functional anthology of IDPs

Functionally, IDPs are classified into six broad categories on the basis of their mode of action (Tompa, 2002; Tompa, 2003; Tompa and Csermely, 2004; Vucetic et al., 2007). These categories are called as RNA and protein chaperones, effectors, entropic chains, assemblers, display sites and scavengers (shown in Figure 1.1.1). About 28 different critical functions were assigned for IDPs such as molecular recognition through interaction with other proteins or nucleic acids (Dunker et al., 2002a; Dunker et al., 2002b; Habchi et al., 2014). In the six functional categories of IDPs, *entropic chains* display function directly from their ensemble structural states by producing force against structural changes or affect

the localization/orientation of attached domain (Dunker et al., 2002a). However, other five categories function through molecular recognition by permanent binding (*assemblers, effectors and scavengers*) or transient binding (*display sites and chaperons*) with target molecules.

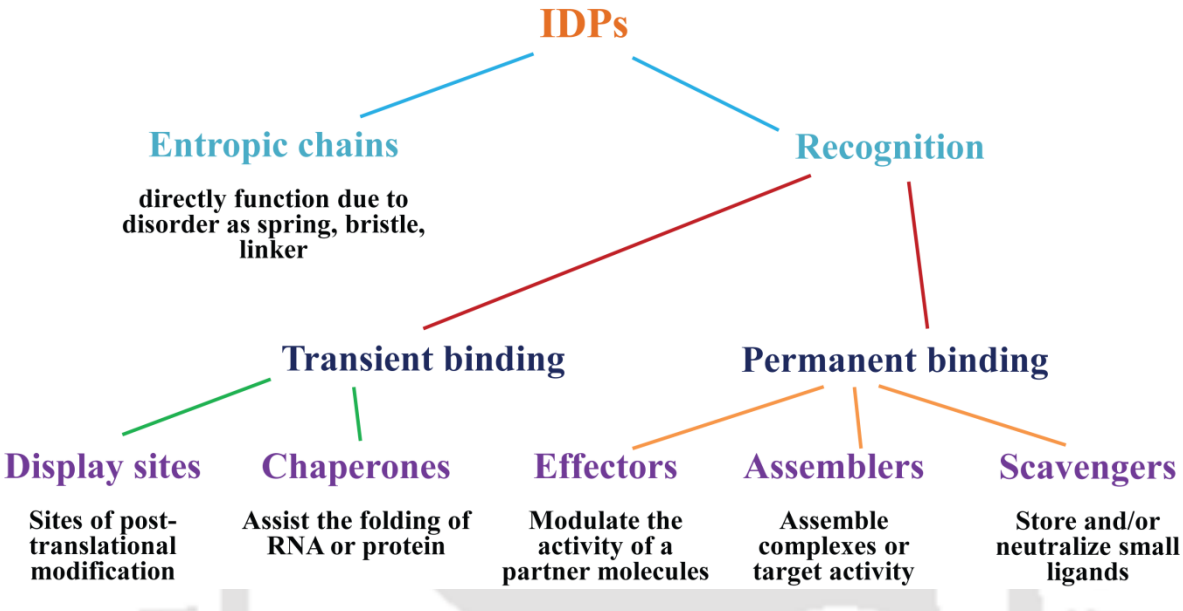

Figure 1.1.1: Functional classification scheme of IDPs. The function of IDPs stems either directly from their capacity to fluctuate freely about a large configurational space (entropic chain functions) or ability to transiently or permanently bind partner molecule(s). Modified from (Tompa, 2005).

Display sites perform its function in post-translational modification by providing flexible site to the active site of modifying enzyme with transient and specific binding (Cox et al., 2002; Iakoucheva et al., 2004). Another subclass, *Chaperones* proteins display their functions by directly evolving their disorder regions to recognize, solubilize or loosen the structure of incorrectly folded molecules. Entropy transfer model of disorder has been proposed as the mechanism of chaperone function. Statistical studies reveal that RNA *chaperons* are more disordered (40%) compared to proteins chaperones (15%) (Tompa and Csermely, 2004).

Effectors shows their functions by binding and modifying (inhibit or activate) the partner enzymes. The $p21^{cip1}$ and its homologous $p27^{Kip2}$ effector proteins inhibit the cyclin-dependent kinase (Cdks) and assemble the cyclin-Cdk complex which activates the Cdk (Olashaw et al., 2004; Tompa, 2002).

Next category, the *assemblers* help in the assembly of multiple proteins such as cytoskeleton, ribosome, chromatin and transcription initiation complex (Dyson and Wright, 2005). And last category, the *scavengers*, neutralize and/or store the small ligands by permanently binding with them (Tompa, 2002).

In general, IDPs are quite disordered and form transient states in their structures, they are usually involved in many key biological processes such as recognition, signaling, transcriptional and translational regulation and different control pathways via high-specificity/low-affinity binding with multiple partners (Babu, 2016; Ekman et al., 2006; Haynes et al., 2006; Patil and Nakamura, 2006; Wright and Dyson, 2015). Their transient structures provide them the flexibility to be bound to some ligands/proteins/nucleic acids and at the same time perform independent functions. The functional diversity because of disordered regions complements those of ordered protein regions (Uversky and Dunker, 2010; Vucetic et al., 2007). Many cell-signaling, neurodegenerative, cardiovascular and cancer-associated proteins have long disordered regions (Cheng et al., 2006; Hollstein et al., 1991; Iakoucheva et al., 2002; Oliner et al., 1993; Xue et al., 2010), suggesting that intrinsic disorderedness is an important criteria for signaling and regulation. Apart from signaling, post-translational modification is another important process concerning intrinsic disordered proteins. In eukaryotic cells, the enzymatic activity of many proteins, their association with other biomolecules or determination of their location in the cell is primarily determined by post-translational modifications. Among various post-translational modifications, protein phosphorylation is one of the most common and frequently observed phenomenon, and it is universally regarded that reversible protein phosphorylation is a signaling mechanism involved in almost all cellular processes (Khoury et al., 2011; Wright and Dyson, 2015). It has been found that IDPs/IDRs due to their flexible nature are often involved in molecular recognition and such protein post-translational modifications (Burgi et al., 2016; Dunker et al., 2002a; Iakoucheva et al., 2004; Nespoulous et al., 2012; Xie et al., 2007).

1.1.2 Special characteristics of IDPs

1.1.2.1 Amino acid composition

The origin of the significant differences in ordered and disordered proteins mainly lie in their primary structure because of their amino acids composition. Amino acid compositions of IDPs are much different in contrast with ordered proteins. IDPs are extremely depleted in hydrophobic (Ile, Leu and Val) and aromatic (Trp, Tyr and Phe) amino acid residues, which are responsible for folding and stabilizing the hydrophobic cores of folded globular proteins, thus providing more solvent accessibility and less hydrophobic regions. Moreover, they have low content of Cys and Asn residues. But, IDPs/ IDRs are significantly enriched in polar (Arg, Gly, Ser, Pro, Glu and Lys) and disorder promoting amino acid residues (Gly and Pro) (Habchi et al., 2014; Radivojac et al., 2007; Romero et al., 2001; Vacic et al., 2007; Williams et al., 2001). Figure 1.1.2.1 displays a comparison of amino acid frequencies found in IDPs with the ordered proteins.

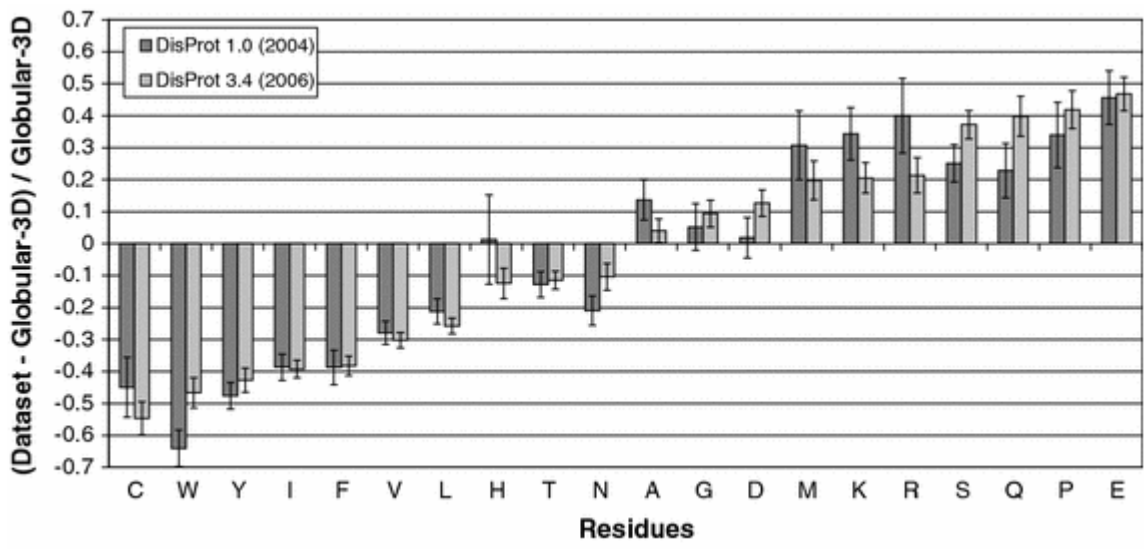

Figure 1.1.2.1: Amino-acid composition, relative to the set of globular proteins Globular-3D, of intrinsically disordered regions 10 residues or longer from the DisProt database. Dark gray indicates DisProt 1.0 (152 proteins), whereas light gray indicates DisProt 3.4 (460 proteins). Amino acid compositions were calculated per disordered region and then averaged. The arrangement of the amino acids is by peak height for the DisProt 3.4 release. Adapted from (Uversky, 2009).

1.1.2.2 Charge and hydrophobicity

One of the most prominent features of highly disordered proteins (native coil or native pre-molten globules) is their relatively high net charge (causes strong electrostatic repulsion) and low mean hydrophobicity (causes weak hydrophobic interaction) (Uversky et al., 2000a). This high net charge and low hydrophobicity is responsible for arising extended conformation in IDPs (Mao et al., 2010). Since, the amino acid sequences that are rich in polar, uncharged amino acids and lack hydrophobic residue are frequently shown to form diverse ensembles of collapse structures in aqueous medium (Crick et al., 2006; Dougan et al., 2009; Moglich et al., 2006; Mukhopadhyay et al., 2007; Vitalis et al., 2007; Walters and Murphy, 2009; Wang et al., 2006). Figure 1.1.2.2 depicts the charge hydropathy plot for ordered verses disordered proteins.

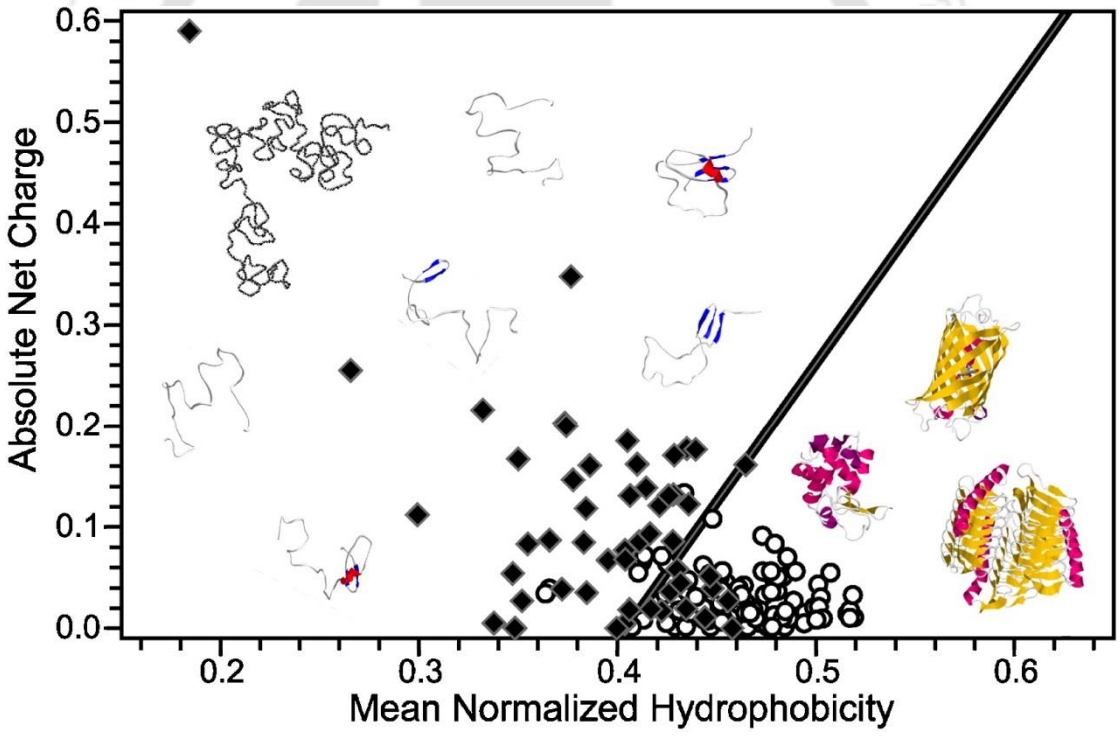

Figure 1.1.2.2: Peculiarities of amino acid composition of IDPs. Comparison of the mean net charge and the mean hydrophobicity for a set of 275 folded (open circles) and 91 natively unfolded proteins (black diamonds) are shown. The solid line represents the border between extended IDPs and compact globular proteins. Adapted from (Uversky, 2011).

1.1.2.3 Many to one and one to many binding modes

Many IDPs are termed to be promiscuous, being involved in frequent interactions with various partners. In protein–protein interaction networks, disordered proteins usually show at least two different mechanisms. 1) one to many mechanism, in which one IDP binds to many binding partners and 2) many to one mechanism, where several IDPs bind to one (often ordered) binding partner (Babu, 2016; Dunker et al., 2005; Fox and Kannan, 2017; Mittag et al., 2010a; Mittag et al., 2010b; Nash et al., 2001; Sigalov, 2010). Figure 1.1.2.3 depicts the illustration of p53 protein on how intrinsically disordered proteins are utilized by a hub of proteins and how disorder region confers miraculous structural plasticity to interact other proteins, allowing it to adopt several conformations after binding with diverse partners.

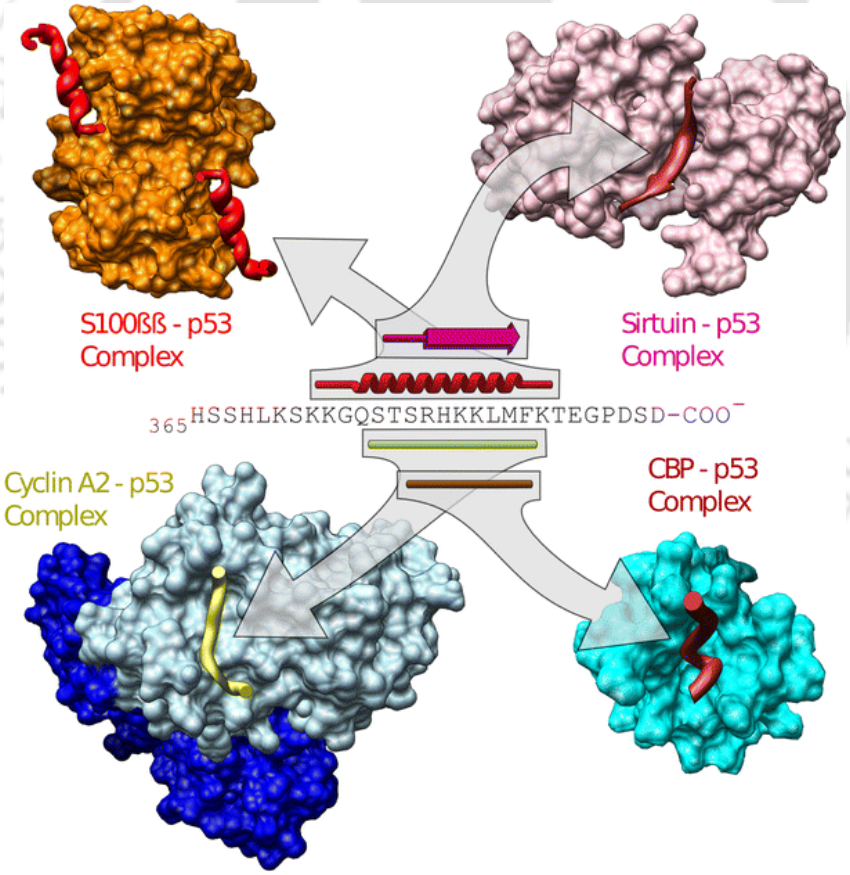

Figure 1.1.2.3: Sequence and structure comparison for the four overlapping complexes in the C-terminus of p53. The Primary, secondary and quaternary structure of p53 complexes. Adapted from (Uversky, 2009).

1.1.2.4 Anomalous SDS-PAGE mobility

IDPs show an anomalous behavior on Sodium Dodecyl Sulfate Polyacrylamide Gel Electrophoresis (SDS-PAGE) and they migrate very slowly through the SDS-PAGE. IDPs display larger apparent molecular weight compared to their actual molecular weight calculated from sequence or determined by mass spectrometry. The reason for the slower migration is their unusually high content of charged amino acids due to which they bind less with SDS and migrate more slowly through the gel in contrast to globular proteins (Cordero et al., 1992; Heyen et al., 2002; Kovacs et al., 2008). It was noticed that molecular weight of IDPs determined by SDS-PAGE is generally over estimated by 1.2-1.8 fold (Tompa, 2002).

1.1.2.5 Enhanced proteolytic sensitivity

Proteolytic enzymes require two main criteria to cleave any proteins 1) substrate (protein) should have a correct recognition sequence for a particular protease and 2) substrate should adapt structurally to the active site of protease (Fontana et al., 1997a; Fontana et al., 1986; Fontana et al., 1997b; Hubbard et al., 1994). Proteolytic recognition sequences in IDPs are more easily accessible and can adapt to the active site of protease due to their highly flexible structures (Fontana et al., 1997a; Fontana et al., 1997b; Hubbard et al., 1998). In contrast with ordered proteins, IDPs shows 5-7 fold more sensitivity to the proteolytic cleavage (Dunker et al., 2002a; Tompa, 2002; Uversky, 2002). Due to presence of high flexibility, very less enzyme:substrate ratio (1:100—1:1000) is required for rapid proteolysis of IDPs in comparison with the ordered proteins which needs high (1:10—1:50) enzyme:substrate ratio (Galea et al., 2006; Kovacs et al., 2008).

1.1.3 Influence of environment change on IDPs

Another peculiar characteristic of IDPs is; they are extremely sensitive to the change in their environment. The reason behind this is; IDPs have shallow energy landscapes with multiple local minima without any global energy minimum compared to ordered proteins which possess global minima (Shown in Figure 1.1.3). The presence of multiple local minima in IDPs is because of different parts of an IDP have their own local energy minimum and each minimum reacts to environmental changes in its own manner (Babu, 2016; Uversky, 2013b).

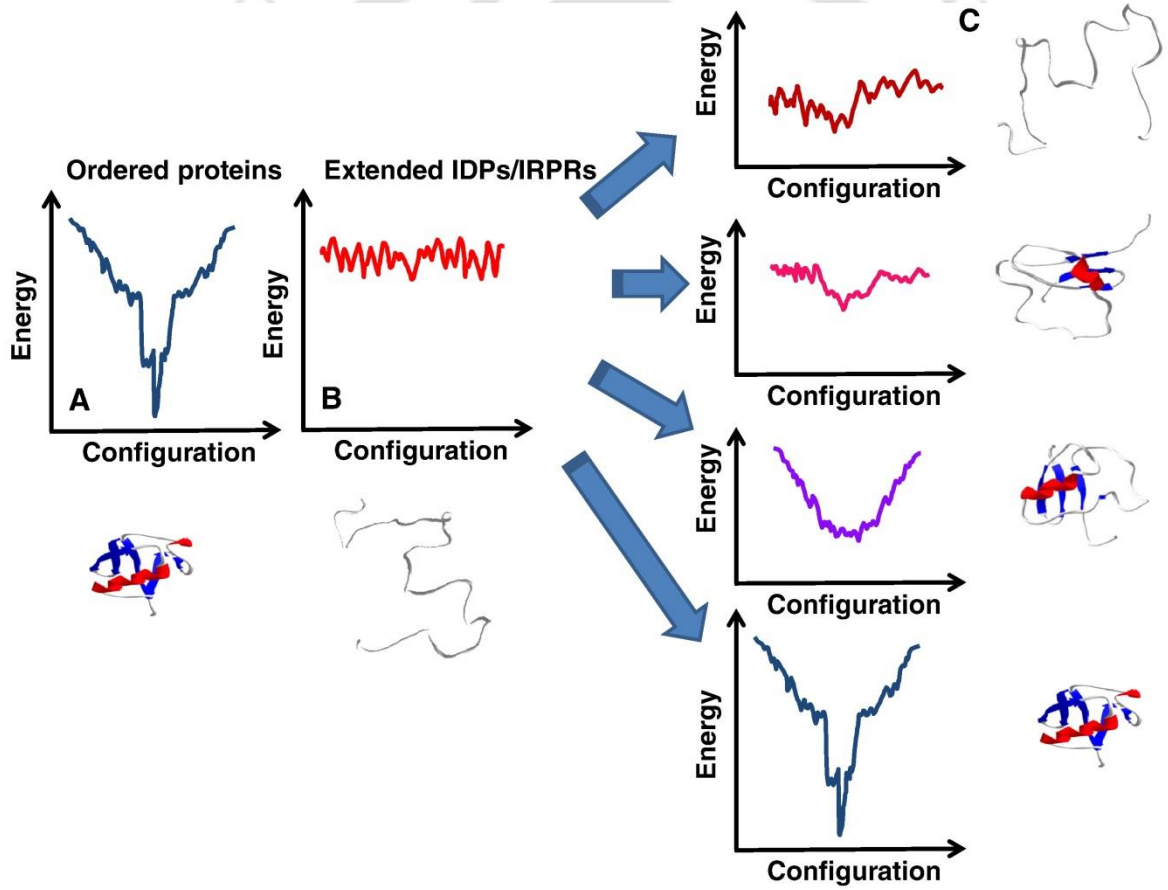

Figure 1.1.3: Energy landscape of ordered proteins and IDPs. A diagram showing the folding energy landscapes of a typical globular protein **[A]** and of a typical natively unfolded protein in the absence **[B]** or presence of different binding partners **[C]**. These landscapes are depicted schematically in one-dimensional cross-section. Illustrative examples of corresponding structures are also shown. Adapted from (Uversky, 2013b).

Some of the characteristics features of IDPs to change in their environment are discussed below.

1.1.3.1 Effect of pH

Extreme change in pH cause folding of the IDPs (Uversky, 2002) contrary to ordered proteins, which get denatured during extreme pH change (Dill and Shortle, 1991). The reason for this pH induced folding of IDPs again lies in the peculiarity of their amino acids composition. At neutral pH, IDPs possess high net charge and strong electrostatic repulsion and extreme change in pH (increasing or decreasing) causes neutralization of charge localized on amino acids side chain. This decrease in the charge of amino acids side chains decreases the electrostatic repulsion between amino acids and promotes hydrophobic residue driven folding of IDPs (Konno et al., 1997; Lynn et al., 1999; Uversky, 2009).

This "turned out" response and folding of IDPs with extreme change in pH have been reported for α-synuclein (Uversky, 2003; Uversky et al., 2001a; Uversky et al., 2001b; Uversky et al., 2001c), ProTa (Uversky et al., 1999), thymosin-β4 (Tβ4) (Watts et al., 1990), myelin basic protein (MBP) (Thomas et al., 1977) and Histidine rich protein II (Lynn et al., 1999).

1.1.3.2 Effect of temperature

Boiling of ordered protein usually causes exposure of hydrophobic patches to the solvent which leads to its precipitation. However, IDPs shows resistance to the boiling temperature and remain soluble in aqueous medium. This temperature induced folding of IDPs arises due to the presence of high charge and low hydrophobic amino acids content in their sequence. Elevated temperature increases the strength of intramolecular hydrophobic interaction and lead to the partial folding of IDPs through hydrophobic driving force (Dunker et al., 2001; Uversky et al., 2000a). This unusual behavior of IDPs has been utilized in their purification (Csizmok et al., 2006; Kalthoff, 2003; Kim et al., 2000).

This folding at higher temperature have been seen in many IDPs such as α-synuclein (Weinreb et al., 1996), calpastatin (Hackel et al., 2000), stathmin (Belmont and Mitchison, 1996), epsin (Kalthoff et al., 2002), p21Cip1 (Kriwacki et al., 1996), protein phosphatase

inhibitor 1 (Nimmo and Cohen, 1978) and group 2 LEA proteins ERD10 and ERD14 (Kovacs et al., 2008).

1.1.3.3 Effect of counter ions

Extreme change in the pH causes folding of IDPs because of charge neutralization and reduced electrostatic repulsion among the amino acids. Similar behavior is shown by IDPs in presence of counter ions. Binding of oppositely charged ions with IDPs can cause charge neutralization and reduced electrostatic repulsion between its amino acids. This decrease in net mean charge and mean hydrophobicity ultimately leads to partial folding of IDPs (Fink et al., 1994; Goto et al., 1990; Johansson et al., 1998). This counter ion stimulated folding has been reported in many IDPs such as α-synuclein (Uversky et al., 2001b), human peptide LL-37 (Johansson et al., 1998) and Human Prothymosin α (Uversky et al., 2000b).

1.1.3.4 Effect of binding partners

It has been experimentally found that the unbound form of the IDPs remain disordered and they show disorder to order transition upon binding with the various binding partners such as different membranes, metal ions, osmolytes, macromolecules like, DNA, RNA, proteins and under macromolecular crowding agents. Even in the bound form many IDPs displays some disordered regions (Burgi et al., 2016; Dunker et al., 2001; Plaxco and Gross, 1997; Uversky et al., 2000a; Uversky and Narizhneva, 1998; Wright and Dyson, 1999). This disorder to order transition of IDPs can be described by influence of binding partners on their mean hydrophobicity and/or mean net charge. Interactions of IDPs with their natural binding partner can change its mean hydrophobicity and/or mean net charge in such a way that these values approaches close to those of ordered protein. This ligand-induced folding in IDPs has been established in many in vitro studies (Gatewood et al., 1990; Horiuchi et al., 1997; Stellwagen et al., 1972; Uversky et al., 2000a; Warrant and Kim, 1978).

1.1.3.5 Effect of osmolytes

Osmolytes are known to be protecting the cells of animals, plants and certain microorganism under the harsh environmental conditions, by stabilizing and shielding the intracellular proteins (Baskakov et al., 1998; Burg, 1995; Yancey et al., 1982). The effect of natural osmolytes on the structure and functions of various IDPs have been studied. For example, unstable proteins have been shown to gain their structure and functional activity in presence of osmolyte, TMAO (trimethylamine-N-oxide) (Baskakov and Bolen, 1998; Bolen, 2001; Kumar et al., 2001). Osmolytes may cause folding of IDPs due to osmophobic effect, which arise due to unfavorable attraction between polypeptide backbone and the osmolyte.

Study on transactivation domain AF1, in presence of different osmolytes, such as methylamines (sarcosine), polyols (sorbitol) and certain amino acids (proline) has been shown to gain its structure and enhanced affinity for specific binding proteins, such as CREB-binding protein, TATA box-binding protein and steroid receptor coactivator-1 (Kumar et al., 2007).

1.1.4 Techniques for recognizing and characterizing of IDPs

As already discussed that the structural properties of IDPs/IDRs are quite different from the normal ordered proteins in several manners, it would be a mistake to study them using normal techniques utilized for characterization of globular proteins (Dunker et al., 2001; Gianni et al., 2016; Liu and Huang, 2014; Uversky, 2013a; Uversky et al., 2000a; Uversky et al., 2009). Some of the important techniques utilized for characterizations of IDPs/IDRs are briefly discussed.

- The traditional technique, X-ray crystallography has been extensively used to determine the structure of ordered proteins. In many protein structures, repeatedly missing electron density was observed which may be an indication for presence of disordered region. The disordered regions possess more flexible atoms which lead to non-coherent X-ray scattering, this makes them unobserved in X-ray crystallography (Bloomer et al., 1978; Dunker et al., 2001; Worbs et al., 2000). Other techniques are

required to confirm that missing regions in proteins (identified by X-ray crystallography) are disordered.

- The heteronuclear multidimensional NMR (Nuclear magnetic resonance) is a solution based complement of X-ray crystallography. This is an immensely powerful technique to characterize protein dynamics and for determination of protein 3D structures in the solution. Structure of several IDPs/IDRs and unstructured parts of folded proteins have been resolved by this technique (Alexandrescu et al., 1994; Bracken, 2001; Habchi et al., 2014; Hershey et al., 1999; Showalter, 2014).

- Near-UV Circular dichroism (CD) is another useful technique to determine the overall tertiary structure of proteins. Near-UV CD spectra in the region of 250-290 nm reveal information about protein tertiary structures (Adler et al., 1973). Secondary structure content in the IDPs can be determined by various spectroscopic techniques such as far-UV CD in the region of 240-190 nm (Adler et al., 1973; Kelly and Price, 1997; Uversky et al., 2000a), optical rotary dispersion, Fourier transform infrared spectroscopy (Uversky et al., 2000a), deep UV Raman spectroscopy and Raman optical activity (Smyth et al., 2001).

- Degree of compactness in the IDPs/IDRs polypeptide chain can be determine by knowing their hydrodynamic parameters using different techniques such as dynamic and static light scattering, small angle X-ray scattering, small angle neutron scattering, gel-filtration chromatography and viscometry (Ptitsyn, 1995a; Uversky, 1993; Uversky, 1994).

- Additional knowledge about local structure and dynamic of IDPs can be obtained using different fluorescence techniques such as steady state fluorescence emission spectra, fluorescence anisotropy, fluorescence quenching, time-resolved fluorescence lifetime and anisotropy decay. Further, 3D distance information across IDPs can be determined using Förster Resonance Energy Transfer (FRET) (Jeganathan et al., 2006; Tompa, 2010). Overall these fluorescence techniques reveal information about conformational details of polypeptide chain (Beechem and Brand, 1985; Brand and Gohlke, 1972; Forster, 1948; Lakowicz, 2006; Schmid, 1989; Stryer, 1978; Weber, 1952).

Several other biophysical and biochemical methods have been employed to characterize and extract structural information about IDPs and IDRs. Each method gives a valuable piece of information about the disordered state in the protein.

1.1.5 Advantage of protein being disordered

The conformational plasticity and flexibility in IDPs/IDRs provides them extensive range of extraordinary functional advantages over the functional mode of structured proteins and domains (Brown et al., 2002; Burgi et al., 2016; Dunker et al., 1998; Fox and Kannan, 2017; Gianni et al., 2016; Liu and Huang, 2014; Uversky et al., 2009). Some of these advantages are discussed here:

- The ability to overcome steric restriction: Highly flexible structure and increased surface area per residue of IDPs enable them to interact with their binding partners (ligand/protein/DNA/RNA) more easily than the ordered proteins.
- Achieving high specificity with low affinity: The unfavourable conformational-entropy changes and high complementary binding interfaces results into high specificity with low affinity. This property of IDPs helps them in rapid association and dissociation with their binding partners during signalling.
- Conformational flexibility of IDPs provides them high exposure and accessibility of sites targeted for post-translational modification.
- Increase binding rate: Kinetic advantage of being disorder protein is high binding rate with their binding partner due to presence of larger capture radius. IDPs show about two to three times faster binding rate than ordered protein with the same affinity.
- Presence of high net charge and low hydrophobic content in the sequence of IDPs allow them to prevent aggregation by favourable interaction with water.
- Unusual amino acid sequence and lack of structure in IDPs provide them to resistance against extreme non-native conditions.

- Allowing compatibility with more available sequences: The sequence space of IDPs/IDRs is about five times more than larger than that of compact ordered proteins.

Finally, the newly discovered concept of IDPs can be considered as a novel, ground breaking and radical shift in the idea of protein structure-function relationship that helps in solving many of the seemingly unsolvable problems in protein science. Knowledge of the IDPs/IDRs is helpful in giving a new boost and a different directionality to the development of protein science. An extensive analysis of the structure, function and dynamics of such disordered proteins/regions pave the way towards better understanding of the mechanism(s) through which they specifically recognize and bind to their targets. Such understanding is necessary for deciphering the elaborate physiological control of IDP functions and how such controls might fail in human diseases. Keeping all these recent advancements in the field of IDPs, we have chosen an IDP (**Human c-Myc PEST region**) which has small size (78 amino acids long) and predicted to be highly disordered (greater than 90% of total length of the protein). It contains a single cysteine residue; we have incorporated a tryptophan residue in the protein to facilitate Trp-Cys FRET studies.

1.2 Human c-Myc PEST region:

The human c-Myc oncoprotein is a basic helix-loop-helix leucine-zipper (bHLH-LZ) transcription factor which plays a critical role in various processes like cell growth, proliferation, differentiation and programmed cell death (Henriksson and Luscher, 1996; Marcu et al., 1992). The c-Myc acts as an activator as well as the repressor of transcription (Grandori et al., 2000). The c-Myc expression is suppressed by growth-inhibitory signals and is induced by mitogenic signals. Constitutive expression of c-Myc prevents differentiation and inhibits exit from the cell cycle (Henriksson and Luscher, 1996; Marcu et al., 1992). Moreover, in the absence of growth factors c-Myc activity is enough to drive quiescent cells into the cell cycle, but it can also, induce programmed cell death when survival factors are missing (Eilers et al., 1991). Thus, to maintained viability of normal cells, stringent controlled activity of c-Myc is very essential. The c-Myc activity is controlled by post-translational modification like phosphorylation and glycosylation (Chou

et al., 1995; Dang, 1999) and its function is also influenced by the expression of its binding partner proteins such as Max (Blackwood and Eisenman, 1991).

Structural organization of human c-Myc (shown in Figure 1.2) resembles with the sequence specific DNA binding transcriptional regulator. At N-terminus end, c-Myc has glutamine and proline residues enriched transcriptional activation domain (TAD), which act as a transcriptional activator upon binding with heterologous DNA binding domain (Kato et al., 1990). This transcriptional activation domain like many TADs remains disordered in absence of its binding partner (Andresen et al., 2012). At C-terminus end, c-Myc has about 100 amino acids long basic helix-loop-helix-leucine zipper (BR-HLH-LZ) region which acts as DNA-binding domain (Blackwell et al., 1990; Prendergast and Ziff, 1991). At physiological concentrations, c-Myc form a heterodimer with another basic helix-loop-helix-leucine zipper, Max protein. This c-Myc-Max dimerization is driven by the leucine zipper which leads to extended coiled coil formation between these two proteins. This heterodimer creates a core DNA-binding module and binds with DNA consensus sequence "CACGTG," which is called as "Enhancer box" (E-box). Dimer formation of c-Myc with Max protein play critical role in c-Myc regulation (Grandori et al., 2000).

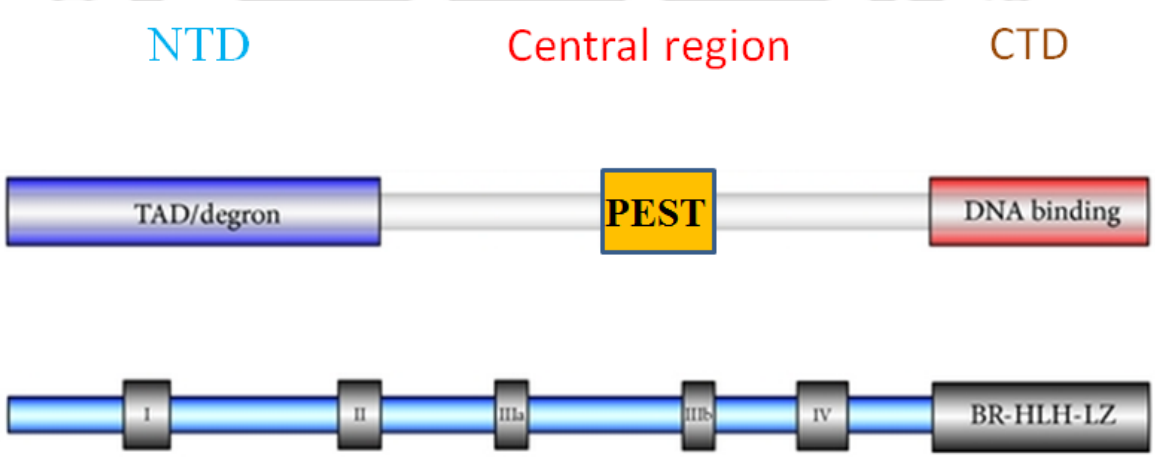

Figure 1.2.: Schematic representation of the human c-Myc protein. The image at the top shows a generic representation of a human c- Myc protein, indicating its N-terminus (transcriptional activation domain), the central region (PEST region), and the C-terminus (DNA binding domain) which involved in DNA binding via interaction with Max Protein. Below is a representation of conserved sequences (I, II, IIIa, IIIb, IV and BR-HLH-LZ) present in human c-Myc protein. Modified from (Tansey, 2014).

Contrary to amino and carboxy terminus, the central region of c-Myc is poorly understood and more systematic analysis is required to gain essential information about the structure and function of the central region of c-Myc. The sequence analysis reveals that central region of c-Myc possesses a number of significantly conserved sequences that are important for its function. The c-Myc has six conserved regions: five are known as Myc Boxes—MbI, MbII, MbIIIa, MbIIIb and MbIV and sixth one is a BR-HLH-LZ motif. The MbI and MbII lies within the transcriptional activation domain (TAD). MbI is a primary interaction point for p-TEFb protein and required for cellular transformation (Eberhardy and Farnham, 2002). The Myc box-MbII is most well studied and is essential for its ability to promote cellular transformation *in vitro* (Stone et al., 1987), to repress (Herbst et al., 2005) and activate (Zhang et al., 2006) the transcription *in vivo* and to drive tumorigenesis (Hemann et al., 2005). Central portion of c-Myc contains three conserved sequences known as MbIIIa, MbIIIb and MbIV (Kurland and Tansey, 2008). Contrary to MbI and MbII, very less is known about the other Myc boxes. Recent studies on Myc MbIIIb show that it interacts with WDR5 protein and this interaction is essentially required for Myc to bind with chromatin (Thomas et al., 2015).

The c-Myc expression is strongly regulated at several levels such as initiation of transcription and attenuation, post transcriptionally at a level of mRNA stability, translation and protein stability (Marcu et al., 1992; Spencer and Groudine, 1991). Overexpression or deregulation of c-Myc expression causes a broad spectrum of cancers such as leukemia and lymphoma, as well as solid tumors including breast, colon, ovarian and lung cancer (Spencer and Groudine, 1991).

Another mechanism utilized by the cell for controlling the c-Myc expression is at a level of protein degradation. Like many other transcription factors such as c-Myb (Bies and Wolff, 1997), c-Fos (Stancovski et al., 1995), c-Jun (Treier et al., 1994), E2F (Campanero and Flemington, 1997) and p53 (Maki et al., 1996), c-Myc is a highly labile protein and normally degrades very rapidly via ubiquitin-proteasome pathway with a typical half-life of around 20 to 30 minutes (Gregory and Hann, 2000). The significance of fast c-Myc degradation to normal cellular growth is highlighted by stabilization of c-Myc in some

tumors (Bahram et al., 2000; Gregory and Hann, 2000; Salghetti et al., 1999). This suggests that enhanced c-Myc stability is responsible for its activation in cancer.

The central portion of c-Myc has a "PEST-region" from amino acid 201 to 268. The PEST sequences are known as a classical protein degradation signals which are enriched in disorder-promoting amino acids [proline (P), glutamic acid (E), serine (S), and threonine (T)] (Rogers et al., 1986). Due to enrichment in disorder promoting amino acids, PEST regions are expected to be intrinsically disordered. PEST sequences were first detected in eukaryotic intracellular proteins which show short half-life and rapid degradation. The presence of PEST region were believed to be the reason behind this fast degradation of proteins (Rechsteiner and Rogers, 1996; Rogers et al., 1986). To determine the role and importance of PEST region in the protein stability, different experiments were performed such as transfer, deletion and mutation of PEST sequences in the PEST containing proteins (Lin et al., 1996; Liu et al., 1997; Yaglom et al., 1995). Transfer of PEST region from mODC to a stable Trypanosaoma ODC converts it into an unstable protein and enhances its degradation (Ghoda et al., 1989). In many cases, PEST region serve as a conditional proteolytic signal. For example, phosphorylation in the PEST regions of *Drosophila* Cactus and IκBα by casein kinase II (CKII) promotes their degradation (Lin et al., 1996; Liu et al., 1997). The PEST region mediates protein degradation via two main pathways, such as the ubiquitin-proteasome degradation and calpain cleavage (Bordone and Campbell, 2002; Gregory and Hann, 2000). Proteome-wide investigation reveals the following observations about the PEST regions: 1) in eukaryotic proteomes, about 25% of proteins contains PEST region; 2) huge fraction of the unstructured proteome in fully sequenced eukaryotes contains PEST region, 3) functionally, PEST containing proteins are frequently involved in the regulation and rarely in the metabolism and 4) PEST region did not show any preference to be confined in the C-terminus of proteins (Singh et al., 2006).

The c-Myc PEST region is predicted to lack a stable tertiary structure and is responsible for rapid degradation of the c-Myc oncoprotein. Like c-Myc, other PEST region containing proteins (Fos, Jun, p53, ODC etc.) also have very short half-life and undergo rapid degradation (Rogers et al., 1986). Deletion study of PEST region show increased stability of c-Myc without changing its ubiquitylation, this suggests that PEST region is necessary

for rapid degradation of c-Myc but not for ubiquitination (Gregory and Hann, 2000). The possibility for that may be: 1) PEST region may contribute to ubiquitin independent turnover of c-Myc or 2) PEST region promotes the turnover of ubiquitylated c-Myc or 3) PEST region serves a structural role within the protein, ensuring the accurate organization of degron and acceptor lysines or 4) PEST region act as initiator sites for proteolysis (Prakash et al., 2004). The PEST region of c-Myc has Casein kinase II phosphorylation site and its degradation could be regulated by phosphorylation where PEST region may serve as a conditional proteolytic signal (Bousset et al., 1993; Luscher et al., 1989).

The exact mechanism of PEST recognition and targeting of PEST containing proteins for degradation via proteasome is poorly understood (Bordone and Campbell, 2002; Gregory and Hann, 2000). Structural analysis of PEST region can provide better insights to understand their functional mechanism. The X-ray structure analysis of several PEST containing proteins are available but unfortunately, the structural information of PEST region in most of the proteins are missing (Rechsteiner and Rogers, 1996; Singh et al., 2006), including the PEST region of c-Myc. Further investigations are required to establish functional consequences of PEST region in the c-Myc degradation.

This thesis work is an attempt to understand the structural and disorder properties of human c-Myc PEST region. The aims of our study are to investigate structure and dynamics of c-Myc PEST region and explore the consequences of change in its milieu (like pH, heat and salt concentration) on its structure and dynamics. These studies on c-Myc PEST region will enable a better understanding of its function including how PEST sequences serve as recognition element and targets for degradation.

1.3 Objectives for the thesis work:

1. Purification and characterization of c-Myc PEST fragment and its mutant, PEST M1.

2. To investigate the effect of pH and salt (NaCl) on the structure and dynamics of c-Myc PEST fragment and its mutant.

3. To unravel the properties of c-Myc PEST fragment dimer and its mutant dimer.

4. To probe the structural transitions in PEST fragment and its mutant by Protein Charge Transfer Spectra (ProCharTS).

Towards this end, the human c-Myc region from amino acid 201 to 268 (PEST Wt) and its mutant (PEST M1) were cloned in pET21b expression vector between the Nde1 and Xho1 restriction sites, encoding the PEST Wt and PEST M1 residues with a hexahistidine tag fused with C-terminus. ***The cloning was carried out in Dr. Rashna Bhandari (Laboratory of Cell Signalling, Centre for DNA Fingerprinting and Diagnostics, Hyderabad) Lab by Dr. Padmavathi Lolla (Postdoc student from Dr. Rashna Bhandari's research group) and clones were gifted to our lab.***

As described in Chapter 3, PEST Wt and PEST M1 were successfully purified using Ni-NTA agarose beads. The amino acid composition profile, various disorder prediction plots, charge hydropathy plots and hydrophobic cluster analysis were carried out using online available tools to predict the disorderness in c-Myc PEST fragment. Further, to gain knowledge about the disorder characteristics of PEST; heat resistance, Stokes radius, 8-Anilinonaphthalene-1-sulfonic acid (ANS) binding assay and effect of 2,2,2-Trifluoroethanol (TFE) on the structure of PEST was studied. Steady state fluorescence and anisotropy, fluorescence lifetime, time-resolved anisotropy measurements of c-Myc PEST tryptophan were done to investigate its structure and dynamics. Further, the secondary structure content in PEST fragment was analyzed by circular dichroism.

In Chapter 4, we monitored the effect of pH and salt (NaCl) on structure and dynamics of PEST M1 using steady state fluorescence and anisotropy, fluorescence lifetime and time-resolved anisotropy measurements of its tryptophan (present at C-terminus end). To extract the information of PEST M1 tryptophan accessibility at different pH; fluorescence quenching experiments were done. Further to gain structural information about N-terminus of PEST Wt and PEST M1; fluorescence of dansyl-labeled cysteine was measured at various pH. To analyze overall structural changes in PEST fragment at different pH; FRET, ANS binding assay and circular dichroism analysis were carried out.

In Chapter 5, the dimeric properties of PEST fragment were revealed using different biophysical techniques like reducing and non-reducing SDS-PAGE, DTNP assay and mass spectrometry. Further, the structural information of PEST dimer was extracted using various fluorescence techniques and circular dichroism.

Finally, the lack of intrinsic spectral probe like tryptophan/tyrosine and richness of charged amino acids in PEST Wt limited its structural analysis to a very few techniques like circular dichroism and NMR. Moreover, the presence of tryptophan in PEST M1 could only provide us the local information in the vicinity of the indole ring. With such tryptophan mutant 3D distance across the protein can be determined by FRET, which required an additional extrinsic probe (acceptor). This imposes severe restrictions on monitoring the structural transitions in IDPs in a label-free approach using UV-Vis spectroscopy. To overcome these restrictions, there is thus a demanding requirement for alternative intrinsic chromophores to probe the structure and dynamics of IDPs. This led us to explore a new label-free, simple and inexpensive method to investigate the conformational changes in IDPs. In Chapter 6, we exploit the richness of charged amino acid population in IDPs to sense their structural transitions using Protein Charge Transfer Spectra (ProCharTS).

It would be important to highlight the types of electronic spectra and traditional chromophores present in the proteins before discussing the Protein Charge Transfer Spectra.

1.4 Types of electronic spectra:

Molecules undergo electronic transitions such that their electrons are promoted from lower to higher molecular orbitals, when excited by higher energy radiation in the UV (200—400 nm) and visible (400—800 nm) range of the electromagnetic spectrum. Different types of possible electronic transitions are mentioned below:

1.4.1 Transitions involving π, σ, and n electrons

Valence electrons exist in any of the three molecular orbital: single, or σ, bonding orbitals; double or triple bonds (π bonding orbitals); and non-bonding orbitals (lone pair electrons). Hence, from bonding orbital to anti bonding orbital, various electronics transitions can take place (Leermakers and Vesley, 1964).

π-π* and n-π* transitions are the most common transitions in biomolecules. The σ-σ* and n-σ* transitions have large energy gap and thus such transitions are reflected in the far ultraviolet region. The n-π* and π-π* transitions mainly involve molecules with unsaturated centers and occur at longer wavelengths as compared to σ* anti-bonding orbitals. Thus, in UV-Vis spectrum, only π-π* and n-π* transitions are reflected (Nilapwar et al., 2011).

Solvents do have an effect on the absorption spectrum of biological molecules (Homocianu, 2011). Increasing solvent polarity shifts n-π* transitions peaks to shorter wavelengths (blue shift) (McConnell, 1952) as the energy of the lone pair of n orbital decreases by increased solvation. But, the reverse (i.e. red shift) is predominant in π-π* transitions (Homocianu, 2011). Attractive polarization forces between the solvent and the absorber is the main reason behind this. It lowers the energy level of the excited state more as compared to the ground states, which results in a small red shift.

1.4.2 Transitions involving *d* and *f* electrons:

First and second transition metal series: Cr, Co, Cu and Ni and ions of lanthanide and actinide elements belong to the *d* and *f* electronic transitions, respectively (Cotton, 2006). The d-d transitions involve the electronic transitions in the filled and unfilled d-orbitals and absorb broad bands of visible region (Crosby, 1975). They are of weak intensity as they are Laporte forbidden. It means, if a molecule is centro-symmetric, transitions within a given set of *p* or *d* orbitals are forbidden (Laporte and Meggers, 1925). But due to vibronic coupling, they are weakly allowed (Sridharan, 2016). These transitions emit visible light upon relaxation and that is why many transition metal complexes are brightly coloured. The color intensity is dependent mainly on: the metal, its oxidation state and the number of metal d-electrons (Reddy et al., 2012). On the other hand, *f*-electrons transitions are narrower with well-defined characteristic peaks (Gschneidner, 1994).

1.4.3 Transitions involving charge-transfer electrons:

Charge-transfer (CT) transitions are quite prevalent in many inorganic species by forming charge-transfer complexes. One of its components of such complex must have electron donating properties (donor) and the other must be able to accept electrons (acceptor). Absorption of radiation involves the transfer of an electron from the donor to the acceptor orbital. Generally metal-ligand complexes show absorptions through charge transfer transitions (Balzani et al., 2007). It is generally categorized into two categories: ligand-to-metal charge-transfer (LMCT) bands (Eg. $KMnO_4$) or metal-to-ligand charge-transfer (MLCT) bands (For e.g. $[Ru(bpy)_3]Cl_2$) (Campagna et al., 2007). Bands arising from such transitions have specific position on the absorption spectra which depend on the nature of the metal ion and ligand and also on the relative ease of oxidation/reduction propensity of the complex (Reddy, 2007).

Biological systems also show Charge transfer transitions and they are quite prevalent (Mason, 1959; Schuster, 2000). Several metalloenzymes Ni (II), Cu (II) and Co (II) metal ions show distinct bands of such transitions. Blue copper proteins are one of the most popular examples of such transitions and its color arises from ligand to metal charge transfer (Pierloot et al., 1998). In some cases, a distorted tetrahedron of two sulfur atoms

and two nitrogen atoms surrounds copper ions, which constitute such transitions and Azurin (Tennent and McMillin, 1979), Plastocyanin and Stellacyanin (McMillin and Morris, 1981) are examples of it. In this case, transition occur from π-bonding orbitals on Cys residue's sulfur atom to the empty t_2* orbitals on Copper which give strong spectral bands in wavelengths ranging from 470-830 nm (Janes and Moore, 2004).

Charge transfer transitions are also quite predominant in various photosynthetic reaction centers in bacteria and plants (King et al., 1997). Two species of purple bacteria (*Rhodobacter sphaeroides* and *Rhodopseudornonavsi ridis*) are the best studied reaction centers where charge transfer transitions occur between two bacterial chlorophylls. Many more examples of such transitions are reported and one of them is Cytochrome C which shows a broad CT band near 700 nm. Electronic transitions take place from the methionine axial ligand to the heme Fe (Green and Parson, 2004) and any changes that disturb the structure and separate the methionine from heme causes disappearance of CT.

1.5 Chromophores in Proteins:

The phenomena of UV light absorption by proteins has been proposed as a structural probe since the early days of molecular biology (Zaccai et al., 2017). But, since absorption of water itself is strong below 170 nm (Quickenden and Irvin, 1980), absorption studies on biological macromolecules are restricted to above 170 nm. In general, three classes of chromophores are predominant in proteins.

1.5.1 Peptide bond

In proteins, the electronic transitions involving peptide bond occur in the far-UV region. The π electrons of peptide bonds are delocalized over the N, C, and O atoms. Also, near the O atom, a nonbonding, n-orbital electron is present. Such electronic transitions show two distinct peaks: (Hunt and Simpson, 1953) one strong peak (arise due to π-π* transitions) at 190 nm (Ɛ = 7000 $M^{-1}cm^{-1}$) while another peak of a weaker intensity (arise due to n-π* transitions) at about 210–220 nm (Ɛ = 100 $M^{-1}cm^{-1}$) (Ham and Platt, 1952). The n-π* transition is symmetry forbidden, thus having weaker intensity and it just forms a shoulder

on to the π-π* transition peak. At around 175 nm, a third transition can be observed which constitutes an n-σ* transition.

The secondary structural changes in protein can influence the absorption of peptide bond. Both poly-L-glutamic acid (Imahori and Tanaka, 1959) and poly-L-lysine shows changes in absorption intensities with conformational changes. The random coil or β-conformation of peptide shows increased absorption intensity as compared to α-helical conformation (Rosenheck and Doty, 1961).

1.5.2 Aromatic amino acids

All charged amino acids (Asp, Glu, Asn, Gln, Arg and His) have relatively weak electronic transitions at around 210 nm because they are masked by the more intense absorption of peptide bond in proteins. The absorption of the peptide bond in the region of 220 nm has been used in the quantification of proteins but it interferes considerably with many other compounds at this wavelength and thus subsequently cannot be justified as a gold standard for estimation. Thus, only the absorptions involving side chain optical properties occurring at wavelengths longer than 230 nm are of importance, where peptide absorption is insignificant. Only the aromatic amino acids: Trp, Tyr and Phe absorb significantly in the near-UV region because of the aromatic moiety and thus serve the limitation stated earlier.

Among the three aromatic amino acids, Trp shows the strongest absorption in the near-UV region (Ɛ = 5,600 $M^{-1}cm^{-1}$ at 280 nm) (Bent and Hayon, 1975b). This complex absorption arises from the indole side chain of Trp. It basically comprises two major peaks; one near 220 nm (Ɛ = 36,000 M^{-1} cm^{-1}) and another at 280 nm (Ɛ = 5,600 M^{-1} cm^{-1}) (Creed, 1984a). At least two independent electronic transitions are known to comprise the spectra of Trp in the 260-310 nm, with π-π* transition being one of them.

Tyrosine is another aromatic residue with appreciable absorption in the near-UV region and its electronic transitions occur at 275 nm (Ɛ = 1400 $M^{-1}cm^{-1}$) and 222 nm (Ɛ = 9000 $M^{-1}cm^{-1}$) (Longworth et al., 1971), the 275 nm absorption band arises due to π-π* transition. At alkaline pH, the tyrosine side chain OH group deprotonates (pK_a = 10.07) (Grinspan et al., 1966) and the resulting tyrosinate ion ($Tyr\text{-}O^-$) shows a red-shift in the absorption profile as

compared to tyrosine, with absorption maxima at 240 nm (Ɛ = 1100 $M^{-1}cm^{-1}$) and 290 nm (Ɛ = 2300 $M^{-1}cm^{-1}$) (Antosiewicz and Shugar, 2016a; Creed, 1984b). Titration of Tyr residues in proteins or the separate determination of Tyr and Trp contributions to an observed absorption spectrum uses this peculiar pH sensitivity of Tyrosine absorption profile (Antosiewicz and Shugar, 2016b). As far as the pH sensitivity is concerned, the Tyr absorbance is more sensitive than that of Trp.

Phe shows two absorption bands: one low intensity absorption band (Bent and Hayon, 1975a) (π-π* transition) around 257 nm (Ɛ = 200 $M^{-1}cm^{-1}$) (Wetlaufer, 1963) and another band at around 205 nm (Ɛ = 9600 $M^{-1}cm^{-1}$). Change in pH has no such impact in the spectrum of Phe (Longworth et al., 1971). Apart from these three aromatic amino acids, Cys and Met, which are basically sulphur containing amino acids show low absorption bands in 230-240 nm range (Wetlaufer, 1963). But, these transitions interfere with the absorption band from peptide bond and are not easily measurable in proteins. However, the disulphides (cystine) have longer-wavelength transitions with λ_{max} values between 250-270 nm (Ɛ = 300 $M^{-1}cm^{-1}$) as compared to cysteine (Otey and Greenstein, 1954) and occurs in high proportions in many proteins. Thus, the disulphides absorption spectra is also taken into account for the near- UV absorption in proteins.

The imidazole group of His in its side chain also absorbs appreciably between 185- 220 nm (Ɛ = 6000 M^{-1} cm^{-1} at 212 nm) (Wetlaufer, 1963) but not as much as the other amino acids which absorb much more strongly in this region.

1.5.3 Prosthetic groups and Co-Enzymes

Various proteins possess tightly bound non-protein part namely, prosthetic groups (For e.g. heme, flavin, carotenoid) which are vital for many biological activity. Such metal–protein complex (for e.g. Azurin, Xanthine oxidase) along with many important coenzymes of proteins such as FAD, NADH and NAD^+ displays strong UV-Vis absorption. FAD absorbs at 450 nm (Ɛ = 11,300 $M^{-1}cm^{-1}$) (Aliverti et al., 1999), NADH at 340 nm (Ɛ = 6220 $M^{-1}cm^{-1}$) and NAD^+ at 259 nm (Ɛ = 16,900 $M^{-1}cm^{-1}$) (Dawson et al., 1969). Heme, which contains a porphyrin ring shows a very intense absorption in the visible region at 404 nm (Ɛ = 1,70,000 $M^{-1}cm^{-1}$) (Karnaukhova et al., 2014), and thus their absorption spectra can be

monitored to follow kinetics of the protein. The light absorption properties of chromophore in proteins are of direct biological relevance as in retinal in vision and chlorophyll in photosynthesis. Apart from the peptide bond, aromatic amino acids, disulphide bond and the prosthetic groups, the absorption spectrum of a protein is expected to be optically negligible beyond 315 nm and practically no absorption signals in this spectral region is expected.

1.6 Protein Charge Transfer Spectra (ProCharTS):

Several year ago, work from our lab reported that aqueous solution of L-Lysine.HCl at high concentrations (0.5-1.0 M) (Homchaudhuri and Swaminathan, 2001) and dilute solutions of lysine rich proteins like poly-L-lysine/human serum albumin (HSA), shows UV-Vis spectra in the region of 270-350 nm, but origin of the unusual absorption spectra remained unexplained (Homchaudhuri and Swaminathan, 2004).

Recently both computational and experimental investigation from our group on α_3C, a synthetic protein that is rich in charged amino acids (Lys and Glu) and devoid of aromatic amino acids, has explained that such UV-Vis absorption spectra in the 250—800 nm region arise from charge transfer transitions. Origin of ProCharTS is accounted by photoinduced charge transfer from: polypeptide backbone to NH_3^+ in lysine; COO^- in glutamate to polypeptide backbone; and COO^- in glutamate to NH_3^+ in lysine (Prasad et al., 2017). The absorption intensities in ProCharTS at wavelengths 250—800 nm are dependent on 3D spatial proximity between charges in Lys-Lys, Glu-Glu and Lys-Glu side chain headgroup pairs across the protein. Thus while close proximity (~3 Å) of like charges in Lys-Lys and Glu-Glu pairs enhanced ProCharTS intensity at longer visible wavelengths, it diminished the same for oppositely charged Lys-Glu pair. However, moderate spatial separation (~6 Å) between oppositely charged Lys-Glu pair, enhanced ProCharTS intensity and extended its presence to longer wavelengths. The protein α_3C which has several such pairs of Lys/Glu in favorable proximity displays intense ProCharTS (Prasad et al., 2017). Recently, computational studies from our collaborator group demonstrates a new UV-visible photoinduced charge transfer transitions in naturally charged amino acids (Lys, Glu, Arg, Asp and His) and phosphorylated amino acids (Tyr, Thr and Ser) (Mandal et al., 2018). As

c-Myc PEST fragment contains about 35% charged amino acids with abundance of His, Lys and Glu. It will be worthy to utilize the ProCharTS as new label free spectroscopic marker to monitor the structural transitions in PEST fragment.

Chapter 2

Experimental Techniques, Materials and Methods

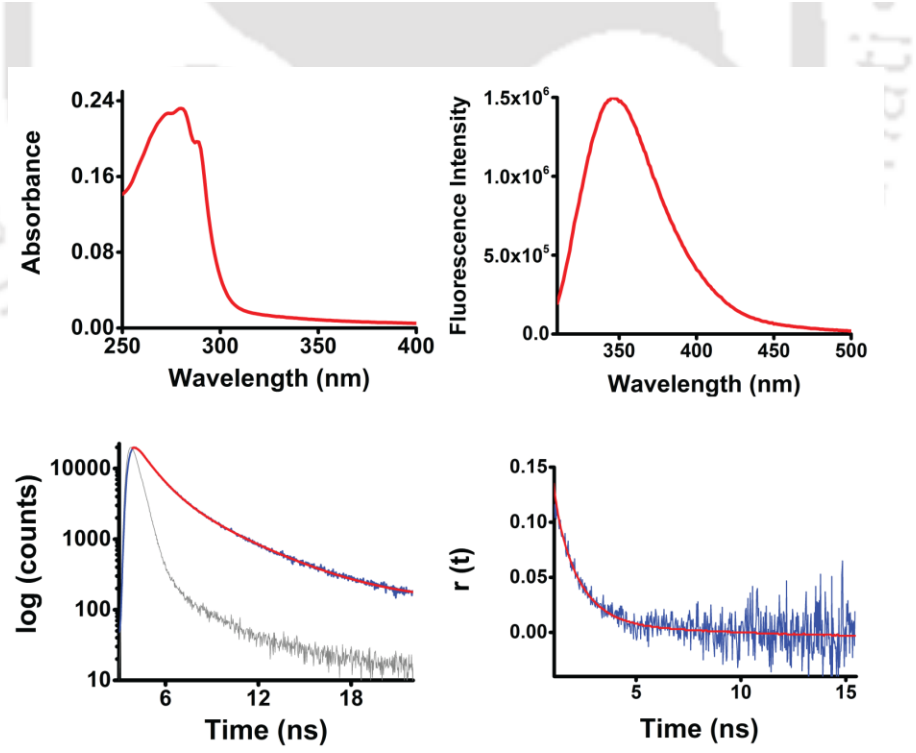

2.1 Experimental techniques:

In this thesis, different spectroscopic techniques were used to accomplish the various experiments. The principles of some important techniques have been explained here.

2.1.1 Absorbance:

When a molecule interacts with electromagnetic radiation, there is an induction of dipoles within the system and this induction of dipoles can be represented as

$$\mu_{ind} = \tilde{\alpha} \, . E \qquad 2.1$$

Here, μ_{ind} denotes induced dipole moment, $\tilde{\alpha}$ represents the polarizability of the molecule and E denotes the electric field of the light. Both E and μ_{ind} fluctuates with time.

Absorption of light causes change in the energy state of molecules. If a molecule initially present in state A will change to state B upon interaction with light. The probability of transition from state A to state B is described by the transition dipole moment (μ_{ba}). μ_{ba} can be calculated by integration $\int \psi_b^* \tilde{\mu} \, \psi_a d\tau$ and can also be written as $\langle \psi_b | \tilde{\mu} | \psi_a \rangle$. Here the wavefunction of two states A and B is represented as Ψ_a and Ψ_b, respectively. The wavefunction in the presence of light can be expressed as

$$\psi \, (t) = \, C_a(t) \psi_a e^{-iE_a t/\hbar} + C_b(t) \psi_b e^{-iE_b t/\hbar} \qquad 2.2$$

Here, the probabilities of system whether it will be present in state A or B relate with coefficients C_a and C_b, energies of states A and B are denoted by E_a and E_b, respectively.

In the presence of light, Hamiltonian can be expressed as

$$\hat{\mathrm{H}}' = \hat{\mathrm{H}} + V(t) \qquad 2.3$$

Here $V\,(t)$ denotes the effect of light on the system. This interaction energy between light and molecule is describe as

$$V(t) = \tilde{\mu} . E_0 e^{i\omega t} \qquad 2.4$$

The probability that the system present in state B at time t can be expressed as

$$P_b = |C_b(t)|^2 \qquad 2.5$$

The absorption intensity can be determined by the rate at which energy is taken up by the molecules from incident light. Transition rate can be described as

$$dP_b/dt = B_{ab}I(\nu) \qquad 2.6$$

Here, B_{ab} is the transition rate per unit energy density and $I(\nu)$ denote the energy density incident on the molecule. B_{ab} can be written as

$$B_{ab} = (2/3)(\pi/\hbar^2)|\langle\psi_b|\tilde{\mu}|\psi_a\rangle|^2 \qquad 2.7$$

The molar extinction coefficient is one of the most important factors in light absorption. When the light with intensity I_0, incident on the sample containing the chromophores in a layer sufficiently thin (dl), the fraction of incident light absorbed by chromophores in the sample is given by,

$$-dI/I = C\varepsilon' dl \qquad 2.8$$

Here, I is the intensity of transmitted light, C is the molar concentration of the absorbing molecule, l is the path length in cm traveled by the light in solution and ε' is a proportionality constant known as the molar extinction coefficient ($M^{-1}cm^{-1}$). When equation 2.8 integrated for entire sample we obtain,

$$\ln(I_0/I) = C\varepsilon' l \qquad 2.9$$

Converting equation 2.9 to log base 10, we have the common Beer-Lambert law:

$$A(\lambda) \equiv \log(I_0/I) = C\varepsilon(\lambda)l \qquad 2.10$$

Where, $\varepsilon = \varepsilon'/2.303$ and A denotes the optical density or absorbance.

The molar extinction coefficient is related to the Einstein coefficient for stimulated absorption as

$$B_{ab} = (1{,}000c/N_0h)\int(\varepsilon'/\nu)d\nu \qquad 2.11$$

Where, N_0 is the Avogadro's number and c is velocity of light with frequency ν

Using equation 2.11 and equation 2.7, and converting ε' to ε, we get the following relation

$$D_{ab} \equiv |\langle\psi_b|\tilde{\mu}|\psi_a\rangle|^2 = 9.180 \text{ x } 10^{-3} \int (\varepsilon/\nu) d\nu \quad \text{(debye)}^2 \quad 2.12$$

Where, D_{ab} is known as the dipole strength. By integrating the area under an absorption band D_{ab} can be calculated. After knowing the D_{ab}, one can measure the strength of the transition dipole.

Another important measure is the oscillator strength, f_{ab}, which compares the intensity of absorption to that expected from a three-dimensional harmonic oscillator. This can be written as

$$f_{ab} = (8\pi^2 mc/3h\nu) D_{ab} = 4.315 \text{ x } 10^{-9} \int \varepsilon(\nu) d\nu \text{ (dimensionless)} \quad 2.13$$

Here, m denotes the mass of the electron. f_{ab} can have the value from 0.1 to 1, for a strongly allowed transition.

2.1.2 Fluorescence:

Fluorescence is a process in which emission of visible or ultraviolet light accompanying a transition of electrons from excited singlet state (S_1) to ground singlet state (S_0) occurs. In the fluorescence, emitted light has longer wavelength compared to absorbed light because of energy loss via vibrational relaxation and other non-radiative processes. Properties of biological molecules like its dynamics and interaction with other molecules revealed by emitted light is quite different in comparison with properties revealed by absorption of light. The reason for this is, the emission process is occurs at much slower timescale (~ nanosecond) than absorption (~femtosecond). Due to slower timescale, emission spectrum is influenced by perturbations and wide range of interactions.

2.1.2.1 Factors that affect fluorescence intensity:

2.1.2.1.1 Internal Conversion

In the process of internal conversion, fluorophore quickly fall from the higher vibrational energy levels (S_1 or S_2) to the lowest vibrational energy level of S_1 through loss of energy by collision with solvent or other molecules or through internal vibrational modes. Internal conversion takes place within 10^{-12} seconds or less. The process of internal conversion and vibrational relaxation cause increase in temperature of solvent. The rate of internal conversion (k_{ic}) depends on temperature and increase with increase in temperature. As a result, increase in temperature causes decrease in observed fluorescence. Monitoring macromolecular conformation changes induced by heat becomes complicated because of this intrinsic temperature dependence.

2.1.2.1.2 Quenching

Any process that causes decrease in the fluorescence intensity of a fluorophore called as fluorescence quenching. Collision or complex formation between quencher (Q) and fluorophore results in deactivation of excited-state. Different molecules like oxygen, amines, halogens and acrylamide can act as collisional quenchers and depopulate the excited state of fluorophore.

Collisions rate of quenchers are limited by diffusion. If quenching is occurring due to collision it can be a bimolecular process.

$$S_b + Q \xrightarrow{k_q} S_a + Q + \text{Heat} \qquad 2.14$$

Where S_a and S_b stands for ground and excited state energy level of a molecule, Q is the quencher and k_q is the bimolecular quenching constant. The observed rate is pseudo first order because quencher concentration is excessive in comparison with population of S_b. By varying the quencher concentration [Q] value of k_q can be measured.

2.1.2.1.3 Intersystem crossing

The fluorophore in the excited singlet state (S_1) can undergo a spin conversion to the excited triplet state (T_1). This conversion of spin from S_1 to T_1 is known as intersystem crossing. Excited triplet state can convert to ground singlet state (S_0) through the process like phosphorescence or internal conversion. Emission from T_1 has longer wavelength and lower energy as compared to S_1. If vibrational levels of the two states overlaps then probability of intersystem crossing increases. Because transition from triplet to singlet state is spin forbidden, average lifetime of triplet state is much longer (~ 10^{-3} s) in comparison with 10^{-9} second average lifetime of an excited singlet state. Heavy atom containing molecules are frequently phosphorescent. The presence of heavy atoms facilitates intersystem crossing by spin orbit coupling.

Due to occurrence of non- radiative process (internal conversion and intersystem crossing) at the same time scale as fluorescence, the observed fluorescence lifetime (τ_F) can be defined as

$$\tau_F = \frac{1}{k_r + k_{isc} + k_{ic} + k_q[Q]} \qquad 2.15$$

k_r, k_{isc}, k_{ic} and k_q denote the rate of decay by fluorescence, intersystem crossing, internal conversion and fluorescence quenching respectively. [Q] is the quencher molar concentration.

The above equation can be simplified as

$$\tau_F = \frac{1}{k_r + k_{nr}} \qquad 2.16$$

k_r and k_{nr} represents rate constant of radiative decay and rate constant of all non-radiative decay.

The quantum yield (ϕ_F) or fluorescence efficiency can be expressed as follow

$$\phi_F = \frac{k_r}{k_r + k_{isc} + k_{ic} + k_q[Q]} = \frac{k_r}{k_r + k_{nr}} \qquad 2.17$$

Fluorescence lifetime in absence of non-radiative process is known as intrinsic or natural lifetime (τ_n) and is a reciprocal of k_r. Theoretically, τ_n can be calculated from absorption spectrum.

$$\tau_n = \frac{1}{k_r} \qquad 2.18$$

Relationship between fluorescence lifetime and quantum yield can be defined as

$$\phi_F = \frac{\tau_F}{\tau_n} \qquad 2.19$$

Above equation show the interdependence of fluorescence lifetime and quantum yield. And this shows that decrease in quantum yield can cause decrease in fluorescence lifetime.

Fluorescence measurements of excited sample can be carried out either by steady-state or time- resolved techniques.

2.1.2.2 Steady state fluorescence:

Measurements of fluorescence can be broadly categorized into two types: steady-state and time-resolved measurements. In steady-state fluorescence measurements, sample is irradiated with continuous beam of light and subsequently fluorescence intensity or emission is recorded. In steady state, equilibrium is generated between the population of fluorophore in the excited states and ground state. This method is used to measure fluorescence intensity as a function of wavelength and also can be used to calculate quantum yield of fluorophore. Steady state method can be used to study different fluorescence properties like steady state anisotropy, resonance energy transfer, quenching etc. However, the steady state fluorescence intensity gives time averaged information of fluorophore present in excited state. Variations in fluorescence intensity and emission maximum can be utilized to studies many important biological phenomena. Fluorescence spectrum can also reveal information about the solvent exposure and degree of polarity around fluorophore.

2.1.2.3 Steady-state fluorescence anisotropy:

Fluorescence anisotropy technique gives information about the rotational motion, shape and size of fluorophore. Anisotropy is utilized to study protein-protein interaction, protein aggregation, protein folding and membrane fluidity. In fluorescence anisotropy, sample is illuminated with vertically polarized light and sample may emit polarized or unpolarized light. Fluorescence anisotropy (r) is measured by monitoring the extent of polarization of emission.

Steady-state anisotropy (r_{ss}), is an average of anisotropy decay time over the intensity decay of the fluorophore and reveals the information about the overall rotational motion of molecules.

$$r_{ss} = \frac{\int_0^\infty r(t)I(t)dt}{\int_0^\infty I(t)dt} \qquad 2.20$$

Intrinsic or extrinsic probe attached with macromolecules shows both local rotational and global rotational motion due to tumbling of the macromolecule through Brownian motion. Depolarization of excited state occurs because the tumbling of molecule in solution.

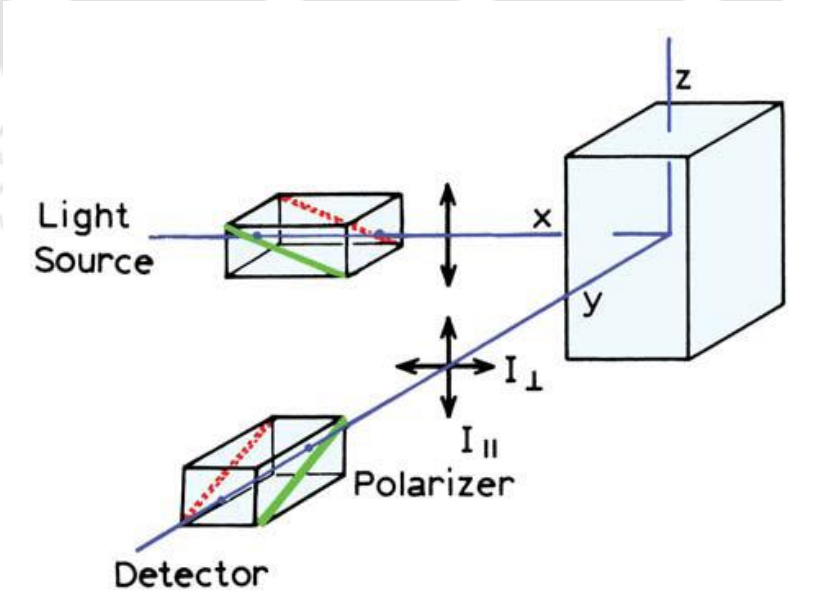

Figure 2.1.2.3: Figure above showing the schematic of fluorescence anisotropy (Adapted from Principle in Fluorescence Spectroscopy by J. R. Lakowicz, third edition, 2006).

Fluorophore in the homogeneous solution are randomly oriented in their ground state. When samples are excited with polarized light, molecules have the higher probability of excitation if its absorption transition dipole are oriented parallel to the electric vector of the excited light. This process is termed as photoselection. In the period of fluorophore excited state (~ 10^{-9} s), extent of polarization changes because of Brownian rotational motion of molecule. This extent of depolarization depends on rate of rotational diffusion and can be measured in term of anisotropy. If fluorophore have fluorescence lifetime comparable to its rotational rate it shows non-zero anisotropy. Anisotropy value is close to zero for fast tumbling fluorophore.

Anisotropy can be expressed by the following equation

$$r_{ss} = \frac{I_{\parallel} - GI_{\perp}}{I_{\parallel} + 2GI_{\perp}} \qquad 2.21$$

Here r_{ss} denotes steady-state anisotropy, $I_{\parallel}$ represents the fluorescence emission intensity when emission and excitation polarizers are vertically align and $I_{\perp}$ denotes the fluorescence emission intensity when emission polarizer aligns perpendicular to the excitation polarizer. Schematic of fluorescence anisotropy measurement is shown in Figure 2.1.2.3. G is known as geometry factor (G-factor) and defined as the ratio of monochromator and detector sensitivity to intensity of vertically and horizontally polarized light.

$$G = \frac{I_{HH}}{I_{HV}} \qquad 2.22$$

The value of G factor depends on the emission wavelength and bandpass of the monochromator. Anisotropy is a dimensionless quantity and does not depend on the concentration of fluorophore in absence of any artifacts, like scattering.

2.1.2.4 Time-resolved fluorescence decay:

In time-resolved fluorescence, sample is excited with a pulse of light and subsequently decay of fluorescence intensity is analyzed as a function of time. Time-resolved measurements can be studies by two methods such as time domain method and frequency domain method. In time domain, sample is excited with pulse of light for ultra-short

duration. Whereas in frequency domain sample is excite by intensity modulated light. Time-domain method is mentioned here briefly.

In time domain fluorescence, sample is illuminated by a pulse of light with a very short pulse width typically in sub-nanosecond or picosecond range. The pulse width should be as short as possible and ideally far shorter than decay time (τ) of fluorophore.

After exciting the sample with short pulse of light, time dependent fluorescence intensity decay of fluorophore is measured using a technique known as Time Correlated Single Photon Counting (TCSPC). From the slope of log $I(t)$ versus t plot, fluorescence decay time (τ) is measured. To avoid the effects of anisotropy or rotational diffusion on the fluorescence intensity decay, the fluorescence intensity decay is generally collected at 54.7° through a polarizer. Set up for fluorescence time-resolved measurements is shown Figure 2.1.2.4.

If the fluorophore has single lifetime, intensity decay equation can be expressed as

$$I(t) = I_0 exp\ (-t/\tau) \qquad 2.23$$

Here $I(t)$ denotes intensity at any time t, I_0 denotes the initial intensity of fluorophore and τ is the fluorescence lifetime of fluorophore.

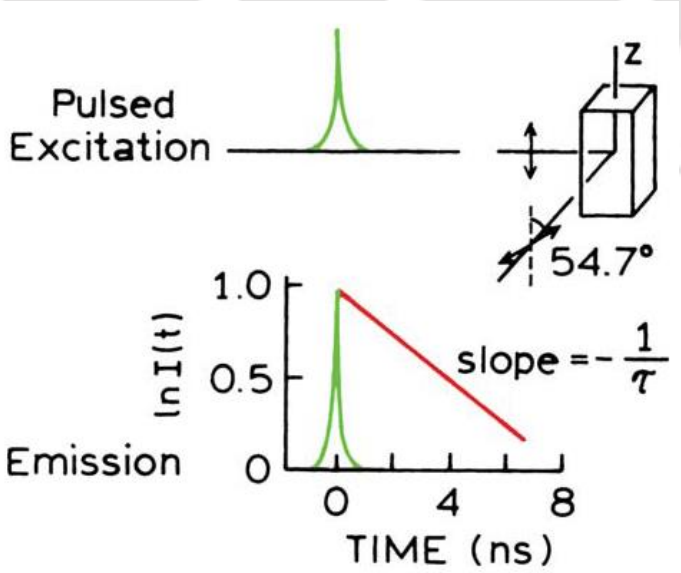

Figure 2.1.2.4: Schematic for Time-domain fluorescence lifetime measurements (Adapted from Principle in Fluorescence Spectroscopy by J. R. Lakowicz, third edition, 2006).

The fluorescence lifetime is a measure of average amount of time a fluorophore stays in its excited state before emission of a photon. Fluorescence lifetime for a single exponential decay can be measured by averaging the time *(t)* over intensity decay of the sample.

$$< t >= \frac{\int_0^\infty tI(t)dt}{\int_0^\infty I(t)dt} = \frac{\int_0^\infty t\,\exp(-t/\tau)dt}{\int_0^\infty \exp(-t/\tau)dt} \qquad 2.24$$

By solving above equation, the average time of a fluorophore stay in the excited state is measured to be equal to fluorescence lifetime τ.

$$< t >= \tau \qquad 2.25$$

The sample shows multi-exponential decay if fluorophore present in different environments or due to presence of more than one fluorophore. Time-dependent intensity for a multi-exponential decay can be expressed as

$$I(t) = \sum_i \alpha_i\, exp(-t/\tau_i) \qquad 2.26$$

Here τ_i and α_i represents the i^{th} fractional lifetime and i^{th} fractional amplitude respectively for the decay component. Addition of fractional amplitude is equals to unity and can be written as

$$\sum_i \alpha_i = 1 \qquad 2.27$$

By using the above equation, mean lifetime τ_m can be measured as

$$\tau_m = \sum_{i=1}^{n} \alpha_i\, \tau_i \qquad 2.28$$

τ_m is directly proportional to area under the intensity decay curve. As steady-state measurement gives an average of the time-resolved event over the fluorescence intensity decay of the fluorophore, it is important to know the relationship between steady-state and time-resolved fluorescence. If a fluorophore display a single decay time *(τ)* its intensity decay can be described as

$$I(t) = I_0\, e^{-t/\tau} \qquad 2.29$$

Relationship between decay time and steady-state intensity (I_{ss}) can be describe as

$$I_{ss} = \int_0^{\infty} I_0\, e^{-t/\tau} dt = I_0\, \tau \qquad 2.30$$

Time-resolved measurement has many advantages in comparison with steady-state. Some important advantages of time-resolve method are: 1) it does not dependent on the fluorophore concentration, 2) tells about the microenvironment around fluorophore by revealing multiple lifetimes and 3) explain about the type of quenching like Static or dynamic quenching.

2.1.2.5 Time-resolved fluorescence anisotropy decay:

Time-resolved fluorescence anisotropy technique is used to reveal the rotational dynamics of the molecule. Time-resolved anisotropy give two type of information about the rotational motion of a molecule: 1) segmental or localized motion, arising due to the independent rotation of fluorophore attached covalently to macromolecule with fast rotation and short rotational correlation time and 2) global motion, arising due to the tumbling of whole macromolecule in the solution with a slow rotation and long correlation time (Figure 2.1.2.5).

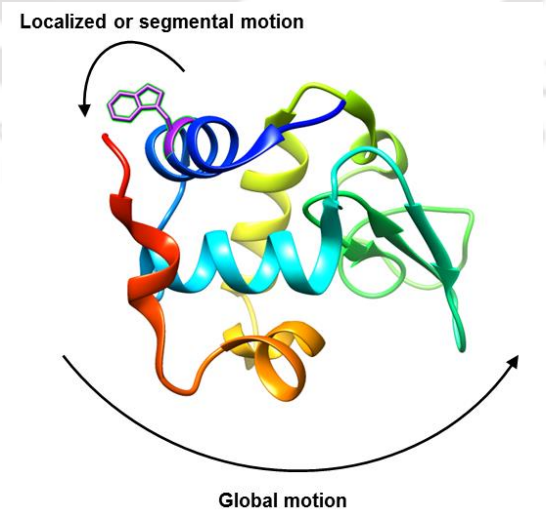

Figure 2.1.2.5: Illustration of the global and localized motion in the protein.

Fast rotational motions in macromolecules can be studied by time-resolved fluorescence and depolarization on the time scales of nanosecond and sub-nanosecond. Information about shape, size and flexibility of macromolecules can be revealed by time-dependent anisotropy *r(t)* (Steiner, 1991).

After exciting the sample with short pulse of light, the anisotropy decay of spherical body rotating in the solution is given by

$$r(t) = r_0\, e^{-t/\theta} = r_0\, e^{-6Dt} \qquad 2.31$$

Here r_0 is initial anisotropy at time (t) = 0, D denotes as the rotational diffusion coefficient and θ indicates the rotational correlation time of molecules rotating freely in the solution. The value of rotational correlation time (θ), depends on temperature (T), viscosity (η) and hydrodynamic volume (V) of the molecule. Rotational correlation time (θ), can be explained by the Stokes-Einstein equation.

$$\theta = \frac{\eta V}{RT} \qquad 2.32$$

Steady-state anisotropy (r_{ss}) for the single-exponential intensity decay can be obtained by Perrin equation.

$$r_{ss} = \frac{r_0}{1 + \frac{\tau}{\theta}} \qquad 2.33$$

Here r_0 denotes initial anisotropy, θ is the rotational correlation time of the molecule and τ represents the lifetime of the fluorophore.

Initial anisotropy (r_0) of a molecule can be written as

$$r_0 = \frac{2}{5}\left(\frac{3 < cos^2\,\beta > -1}{2}\right) \qquad 2.34$$

The value 2/5 comes from the principle of photo-selection for randomly orientated fluorophore in solution. The angle between emission and absorption dipoles is given by β. r_0 is also known as fundamental anisotropy.

If a sample consists of different emitting species, average anisotropy $\bar{r}$ can be explained as

$$\bar{r} = \sum_i f_i \, r_i \qquad 2.35$$

Here r_i denotes anisotropy of each species and f_i express fractional amplitude of each species and $\sum_i f_i = 1$.

For a system containing multiple fluorophore or single fluorophore showing multiple rotational times, anisotropy decay at time t will be multi-exponential and can be expressed as

$$r(t) = r_0 \sum_i \beta_j \exp(-t/\theta_j) \qquad 2.36$$

Here θ_j is the correlation times of individual species and β_j is the fractional amplitudes of each correlation times.

Time-resolved anisotropy is frequently used to study protein-protein and protein-nucleic acid interaction (Hill and Royer, 1997; Rusinova et al., 2002). Stryer and co-workers analyzed the rotational motion in the antibody labeled with dansyl probe. Dansyl labeled antibody exhibit two type of rotational motion: 1) Slow rotation motion (global motion) about 168 ns arising due to the tumbling of whole antibody and 2) Fast rotation motion (segmental motion) about 33 ns arising due to the movement in F_{ab} (Yguerabide et al., 1970).

Baired and co-workers studied the anisotropy decays of IgE in its free state and when it is bound to a receptor in membrane. When IgE bound to the receptor, it shows a long correlation time around 438 ns, while IgE free in solution, exhibits two, 48 and 125 ns correlation times (Holowka et al., 1990).

Molecules may display multiple rotational correlation times because of non-spherical symmetry. Rate of rotation will be different around each axis for non-spherical molecules. For non-spherical molecules two types of ellipsoid of revolution 1) prolate and 2) oblate are used to explain anisotropy decays. Theoretically, non-spherical molecules can display five

correlation times (Belford et al., 1972) but in practice only three correlation times are possible because the magnitude of other two correlation time will be very close and will not resolved easily (Small and Isenberg, 1977).

2.1.2.6 Time-resolved intensity decay analysis:

Time-resolved fluorescence data collected through TCSPC are quite complex and simple graphical methods cannot be used to evaluate the data. Intensity decay curve contains three curves; Instrument Response Function (IRF) [$L(t_k)$], measured intensity decay $N(t_k)$ and calculated (fitted) intensity decay $Nc(t_k)$. The measured intensity decay profile $N(t_k)$ is a convolution of the IRF $L(t_k)$ with actual intensity decay of the sample, $Nc(t_k)$. These functions are in term of discrete time (t_k) because the counted photons are collected into channel each with known width (Δt) and time t_k.

The instrument response function (IRF) [L(tk)] also known as the lamp function is an instrument response to sample with zero fluorescence lifetime. This decay show the shortest time that can be detected by TCSPC. The IRF can be collected by diluted non-fluorescence scattering solution like colloidal silica or $Mg(OH)_2$ in absence of any emission filter. The intensity decay of sample measured by TCSPC is called as measured intensity decay $N(t_k)$. The measured intensity decay $N(t_k)$ contains significant contribution from IRF. This has to be analyzed to determine the actual lifetime of the sample. The mathematical approach used to extract the intensity decay data from measured intensity decay is known as iterative reconvolution

The impulse response is observed if IRF is a δ-function. The concept of convolution can be represent as

$$I_k(t) = L(t_k)I(t - t_k)\Delta t \ (t > t_k) \qquad 2.37$$

The impulse response started at $t=t_k$ because of this term (t-t_k) appears. It is considered that there is no emission prior to excitation (at $t=t_k$).

The measured intensity decay $N(t_k)$ can be defined as the sum of impulse response formed by all the individual δ-function excitation pulses appearing until t_k.

$$N(t_k) = \sum_{t=0}^{t=t_k} L(t_k)\, I(t - t_k)\Delta t \qquad 2.38$$

Above equation can be represented as an integral, for small value of Δt.

$$N(t_k) = \int_0^t L(t')\, I(t - t')dt' \qquad 2.39$$

According to the above expression the measured intensity at time *t* is a sum of the intensities presumed for all the δ-function excitation pulses that appears until time *t*. The new intensity decays are generated in the sample until there is nonzero intensity in $L(t_k)$.

Several methods like non-linear least square analysis (NLLS), the maximum entropy method, the method-of-moments, Laplace transformation and phase-plane method etc. are used to analyze TCSPC data. The Marquardt's algorithm based non-linear least square analysis (NLLS) is broadly used to analyze the complex intensity decay.

A least square analysis starts with a model that is expected to be the best representation of the data.

The guess values of I_0 and τ is assumed for a mono-exponential decay $I(t) = I_0\, exp^{-t/\tau}$. To know the value of calculated or fitted decay, $Nc(t_k)$ these value convoluted with the IRF. Further, this fitted decay $Nc(t_k)$ is compared with experimentally resolved decay $N(t_k)$. The minimized value of goodness of fit parameter χ^2 is calculated to judge the goodness of fit. The χ^2 can be expressed as

$$\chi^2 = \sum_{k=1}^{n} \frac{1}{\sigma_k^2} [N(t_k) - N_c(t_k]^2 \qquad 2.40$$

$$= \sum_{k=1}^{n} \frac{[N(t_k) - N_c(t_k]^2}{N(t_k)} \qquad 2.41$$

The χ^2 is not convenient to interpret as it depends upon numbers of data points. Hence another parameter is used known as reduced χ^2 (χ_R^2) and can be represent as

$$\chi_R^2 = \frac{\chi^2}{n-p} = \frac{\chi^2}{\upsilon} \qquad 2.42$$

Here, n represents the number of data points, p denotes the number of floating parameters, and υ is the number of degree of freedom.

If calculated and experimentally obtained decay data are closely matched then value of χ_R^2 will be close to unity. If the data does not fit properly then value of χ_R^2 will be higher than 1. In this case new set of parameters are selected by modifying the older parameters. Until the value of χ_R^2 does not reach close to unity, process of matching and convolution are repeated iteratively. This operation is termed as iterative reconvolution.

Another parameter to judge the quality of fit is known as deviation plots or distribution of residuals.

The difference between measured and fitted function yields the deviation (D_k). Deviation plot is obtained by plotting standard deviation at each data point against time. The deviation (D_k) can be expressed as

$$D_k = \frac{I(t_k) - I_c(t_k)}{\sqrt{I(t_k)}} \qquad 2.43$$

Goodness of the fit can be judge by checking the randomness of residual distribution. An improper fitting of decay indicates a distinct pattern in the distribution of residual.

2.1.2.7 Time-resolved Anisotropy decay analysis:

The time-resolved anisotropy decays data was analyzed on the basis of equations given below

$$I_{\parallel}(t) = \frac{1}{3} I(t)[1 + 2r(t)] \qquad 2.44$$

$$I_{\perp}(t) = \frac{1}{3} I(t)[1 - r(t)] \qquad 2.45$$

$$r(t) = r_0 \sum_i g_i exp(-t/\theta_i) \quad i = 1 \; or \; 2 \qquad 2.46$$

Here, r_0 denotes the initial anisotropy, amplitude of ith rotational correlation time θ_i is denoted as g_i and $\sum_i g_i = 1$. $I_{\parallel}(t)$ and $I_{\perp}(t)$ represents the sample intensity decay measured with the polarizers in the parallel and perpendicular orientations, respectively.

If biomolecules shows the biexponential $r(t)$ then θ_{fast} and θ_{slow} reveals the information of the local motion of the labeled probe and global motion (overall tumbling) of the biomolecules, respectively. To extract the best value for g_i and θ_i, a non-linear least square fitting model based on Marquardt algorithm (Bevington and Robinson, 1992) is executed. The measured instrument response function (IRF) is used to analyze the $I_{\parallel}$ and $I_{\perp}$.

The values collected in the above fitting analysis were used to yield the steady-state anisotropy r_{ss} (Swaminathan et al., 1994).

$$r_{ss} = \frac{r_0 \sum_i \sum_j \alpha_i \; g_j \left(\frac{1}{\tau_i} + \frac{1}{\theta_j}\right)^{-1}}{\sum_i \alpha_i \tau_i} \qquad 2.47$$

Further, the calculated steady-state anisotropy values were compared with the steady-state anisotropy values measured independently by using spectrofluorometer, to cross verify the fitted values of θ_i, g_i and r_0.

2.1.2.8 Fluorescence quenching:

Quenching is a phenomenon which results in decrease of fluorescence intensity of fluorophore. Various processes can cause quenching of fluorophore like energy transfer, molecular rearrangement, excited state reactions, collision with quencher and ground state complex formation. Various atoms and molecules act as quenchers. Oxygen on collision with excited state fluorophore promotes the intersystem crossing because of its paramagnetic nature. Heavy atoms such as iodide cause quenching by spin-orbit coupling. Quenching can be categories into two type 1) static quenching and 2) dynamic quenching.

2.1.2.8.1 Static quenching

Static quenching occurs due to non-fluorescent complex formation between quencher and the fluorophore in the ground state. Static quenching results decrease in concentration of fluorophore which is undergoing excitation and eventually lead to a decrease in fluorescence intensity. *Schematic representation of static quenching is given below*

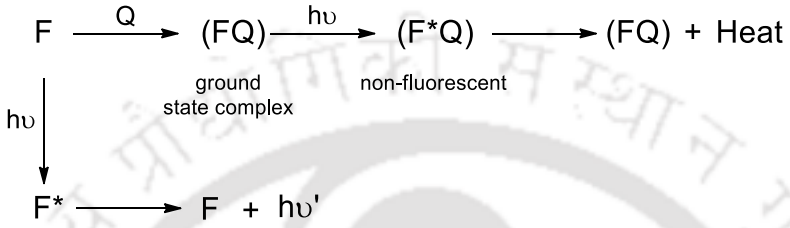

Here, *F* denotes the fluorophore, *Q* represents the quencher and (*FQ*) represents the non-fluorescent ground state complex formed due to interaction between quencher and fluorophore present in the ground state.

Lifetime of fluorophore remains unchanged in static quenching. The fluorophore present in free form exhibits normal excited state properties and gives normal fluorescence after excitation. Static quenching does not depend upon molecular collision or diffusion.

2.1.2.8.2 Dynamic or collisional quenching

Dynamic quenching arises due to collision of quenchers with excited state fluorophore and results in depopulation of excited state. Energy of excited state fluorophore is released in the form of heat. Two form of quenching can be differentiated by measuring the lifetime of the fluorophore. In dynamic quenching, collision of quencher with excited state fluorophore lead to decrease in lifetime of fluorophore by hastening the decay of excited state fluorophore. However, in the static quenching, quencher form a complex with fluorophore present in ground state and the lifetime of un-complexed fluorophore remain unchanged. Hence $\tau_0 / \tau = 1$ in the static quenching and dynamic quenching shows $\tau_0 / \tau > 1$. τ_0 and τ are the lifetime of fluorophore in absence and presence of fluorophore, respectively.

Schematic representation of dynamic quenching is given below

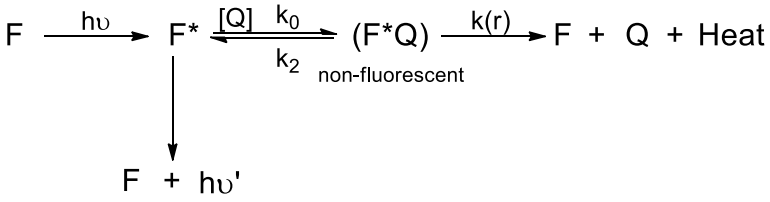

In the above scheme, k_o is the bimolecular rate constant for the formation of *(F-Q)**. k_2 represent the rate constant for breakdown of *(F-Q)** into *F** and *Q*. $k_{(r)}$ denotes rate constant for breakdown of *(F-Q)** into *F* and *Q*. Quenching efficiency E_Q can be describe as

$$E_Q = \frac{k_{(r)}}{k_2 + k_{(r)}} \qquad 2.48$$

Dynamic or collisional quenching can be described by Stern-Volmer equation

$$\frac{\tau_0}{\tau} = \frac{F_0}{F} = 1 + k_q \tau_0 [Q] = 1 + K_{SV} [Q] \qquad 2.49$$

Here, F_0 and F are the fluorescence intensity of fluorophore in absence and presence of quencher, respectively. τ_0 denotes the lifetime of fluorophore in absence of quencher, k_q represents the bimolecular quenching constant and *[Q]* shows the quencher concentration in moles litre^{-1}.

From above equation Stern-Volmer quenching constant (K_{SV}) can be represent as

$$K_{SV} = k_q \tau_0 \qquad 2.50$$

K_{SV} can be determined from the slope of F_0/F verses *[Q]* plot. The bimolecular quenching rate constant k_q reveals about the quenching efficiency. The value of k_q is around $1x10^{10}$ M^{-1} s^{-1} in a diffusion controlled quenching reaction and it is the maximum possible value of k_q in the solution. Less k_q value represents a low quenching efficiency or the shielding of the fluorophore.

2.1.2.9 Förster Resonance Energy Transfer (FRET):

Resonance Energy Transfer (RET) is an important process which occurs in the excited state. RET occurs when there is an overlap between emission spectrum of a fluorophore (donor) and the absorption spectrum of a chromophore (acceptor). FRET is an important tool, utilized for studying the protein-protein interaction, protein folding and protein aggregation. FRET is an electrodynamic process; involve transfer of excited state energy from excited state donor (D) to ground state acceptor (A) molecule. Transfer of energy occurs via non-radiative dipole-dipole interaction between the donor and acceptor. Rate of energy transfer depends upon; a) spectral overlap between donor emission spectrum and the acceptor absorption spectrum, b) orientation of transition dipoles between the donor and acceptor, c) the quantum yield of donor and d) distance between donor and acceptor molecules. Efficiency of energy transfer is very sensitive to the Förster radius (R_0) ranging from 10 to 100 Å. Förster radius can be defined as the distance at which efficiency of energy transfer is 50%. The value of R_0 depends upon the spectral properties of donor and acceptor fluorophore. Förster radius (R_0) can be expressed as

$$R_0^6 = 8.79 \times 10^{23} \left[\kappa^2 n^{-4} Q_D J(\lambda)\right] (\text{Å}) \qquad 2.51$$

Here, κ^2 denotes dipole orientation factor, η represents refractive index, Q_D denotes quantum yield of donor in absence of acceptor and $J(\lambda)$ denotes integral spectral overlap. $J(\lambda)$ can be expressed as

$$J(\lambda) = \int_0^\infty F_D(\lambda)\, \varepsilon_A(\lambda)\, \lambda^4 d\lambda\, M^{-1} cm^3 \qquad 2.52$$

Here, ε_A represents the extinction coefficient of acceptor and F_D denotes fluorescence emission intensity of donor as a fraction of the total integrated intensity.

The rate of energy transfer $k_T(r)$ is expressed as

$$k_T(r) = \left(\frac{1}{\tau_D}\right)\left(\frac{R_0}{r}\right)^6 \qquad 2.53$$

Here, r is the distance between the donor and the acceptor, R_0 denotes the Förster radius and τ_D is the life time of the donor in absence of acceptor.

For a single donor-acceptor pair at a fixed distance, the efficiency of energy transfer can be expressed as

$$E = \frac{R_0^6}{R_0^6 + r^6} \qquad 2.54$$

The transfer efficiency is calculated by taking the relative fluorescence intensity of the donor, in the absence of acceptor (F_D) and presence of acceptor (F_{DA}) and expressed as

$$E = 1 - \left(\frac{F_{DA}}{F_D}\right) \qquad 2.55$$

The transfer efficiency can also be calculated from the lifetimes of donor, in absence and presence of acceptor.

$$E = 1 - \left(\frac{\tau_{DA}}{\tau_D}\right) \qquad 2.56$$

Here, τ_{DA} is the lifetime of donor in presence of acceptor and τ_D is the lifetime of donor in absence of donor.

2.1.3 Circular Dichroism:

Circular Dichroism (CD) is a powerful technique to detect the conformations of proteins and nucleic acids in solution. For display the CD signal, chromophore should have chirality or present in the asymmetric environment.

Parameter collected in the CD is the net difference in absorbance between right and left handed circularly polarized component of plane polarized light. Difference in absorbance can be represent as

$$\Delta A = A_L - A_R \qquad 2.57$$

Where A_L and A_R are the left and right handed circularly polarized light, respectively.

As the shape of CD and absorption bands are usually similar, CD spectrum can be predicted from absorption spectrum by calculating the area under each CD band and noting sign. These quantities together are known as the rotational strength (R_{0a}) for state 0 to state a transition. The rotational strength is equivalent to the dipole strength used as a measure of absorption intensity.

$$R_{0a} = (3hc/8\pi^3 N_0) \int \{[\theta(\lambda)]/\lambda\}\, d\lambda \qquad 2.58$$

Where, *h* denotes Planck's constant and *c* is the speed of light.

Rotational strength can be determined from principles of quantum mechanical and knowledge of ground (ψ_0) and excited (ψ_a) states wavefunction of an asymmetric molecule.

$$R_{0a} = imaginary(\langle\psi_0|\tilde{\mu}|\psi_a\rangle \cdot \langle\psi_a|\tilde{m}|\psi_0\rangle) \qquad 2.59$$

Where, $\tilde{\mu}$ denotes an electric dipole operator and $\tilde{m}$ magnetic dipole operator.

As CD is one of the absorption techniques, chromophores that show the CD spectrum also display absorption spectrum. When plane polarized light pass through the optically active sample, one of the circular component absorbed more than the other. Instead of plane polarized light, elliptically polarized light is obtained by the recombination of unequally absorbed components. Practically, CD instrument separately detect the two component instead of recombined them. Relationship between Circular Dichroism and ellipticity can be expressed as

$$[\theta] = 3300\ \Delta\varepsilon \qquad 2.60$$

Here, *[θ]* represent the molar ellipticity and most of circular dichroism measurements are based on ellipticity determinations.

The far-UV CD spectra basically reveal the information about the secondary structure content in the protein like α-helix, β-sheet, β-turn and random coil. In the region of 240 to 190 nm, light is majorly absorbed by the peptide bond and exhibits a strong π to π^* (~ 190 nm) and weak but broad n to π^* transition (210-220 nm).

Near-UV CD spectra reveal information about the tertiary structure of the protein. CD spectra in the region of 250 to 290 nm basically arises by absorption of aromatic amino acid side chain such as Phe, Tyr and Trp. Folding of polypeptide chain can locate side chain of aromatic amino acids in the chiral environment. This enables the CD spectra to provide a characteristic fingerprint of folded protein.

2.1.4 Dynamic Light Scattering:

Dynamic Light Scattering (DLS), also called as photon correlation spectroscopy (PCS), is a very powerful technique to detect the aggregation of protein, size of nucleic acids and protein on the basis of their diffusion behavior in solution. John Tyndall described one of the earliest light-scattering phenomena known as Tyndall effect, in which light was scattered from the colloidal suspensions and wavelength of the incident light was shorter than particles present in the colloidal solution (Tyndall, 1868). Soon after, scattering of light from particles smaller than the wavelength of light was described by Lord Rayleigh (Rayleigh scattering). Rayleigh scattering explained both that the blue color of sky is due to scattering of light by atmospheric particles and refractive index of the medium plays an important role in scattering of light (Strutt, 1871a; Strutt, 1871b). Gustav Mie in 1908 described a theory known as Mie theory, in comparison to Rayleigh theory. Mie theory describe the scattering of light by absorbing and non-absorbing particles that are larger than the wavelength of incident light, with taking into account shape of particle and difference of refractive index between the particles and medium in which particles are present (Mie, 1908). Peter Debye in 1915 suggests scattering can be studied independently of assumptions on particles mass, size, or shape as a function of angle (Debye, 1915).

In DLS instruments, when laser strikes macromolecules present in the sample it scatters in all directions as a function of size and shape of macromolecules and intensity of scatter light is detected by detector. In static light scattering, by the measurement of scattered light intensity as time-averaged intensity, information regarding molecular weight and radius of gyration of macromolecules can be revealed. On the other hand, by analyzing the fluctuation in the intensity of scattered light (due to Brownian motion of macromolecules in solution), diffusion coefficient (D_τ) can be obtained. The motion of macromolecules in the

solution depends upon their size, temperature and viscosity of the medium (Harding and Jumel, 1998).

Fluctuations in the intensity of scattered light leads to either constructive or destructive interference, which reveals information about the time dependent movement of the macromolecules. Traces of macromolecules can be fitted with an autocorrelation function. Decay of this correlation is directly related to D_τ of macromolecules, motion of macromolecules and their dimensions. The value of D_τ can be extract by numerical methods.

The size distribution of the dissolved macromolecules is extracted by using the time autocorrelation function of the scattered light. The first order electric field correlation function of scattered light can be expressed as

$$G_\tau = 1 + \beta exp^{-2D_\tau q^2 \tau} \qquad 2.61$$

Here, β is a constant and depends upon geometry and optics of instrument, D_τ denotes the translational diffusion coefficient of the macromolecules, τ represents the decay time and q is a scattering vector which can be expressed as

$$|q| = \frac{4\pi\eta_0}{\lambda_0}\sin(\theta/2) \qquad 2.62$$

Here, η_0 denotes the refractive index of the medium, λ_0 represents the wavelength of light in vacuum and θ represents the angle of scattering.

In the case of spheres, the relation between D_τ and hydrodynamic radius (R_h) of the particles can be explained through the Stokes– Einstein equation

$$D_\tau = \frac{k_B T}{6\pi\eta R_h} \qquad 2.63$$

Here, k_B is Boltzmann's constant (1.381 x 10^{-23} J/K), T denotes absolute temperature, viscosity of medium is denoted by η and R_h represents the hydrodynamic radius of macromolecules.

2.2 Materials:

Chemicals/Reagents: Ampicillin (A8351); Isopropyl β-D-1-thiogalactopyranoside (I5502); Benzamidin (12072); Trypsin inhibitor from glycine max (T9128); Nickel Affinity gel (H0537); Triton X-100 (T9284); β Mercaptoethanol (63689); Tris(2-carboxyethyl)phosphine (C4706); Glycine (50046); Sinapic acid (85429); $CaCl_2$ (C8106); Gel loading buffer (G2526); Bovine serum albumin (A3059); Trifluoroacetic acid (T6508); 2,2,2-Trifluoroethanol (T8132) Acetonitrile (34998); Blue dextran (D4772); Alcohol dehydrogenase (A8656); Carbonic Anhydrase (C7025); 1,4-Dithiothreitol (D0632); Guanidine Hydrochloride (G3272); 8-Anilinonaphthalene-1-sulfonic acid (A3125); Acrylamide (A3553); N-acetyl tryptophan amide (A6501); 2,2′-Dithiobis(5-nitropyridine) (158194); L-Cysteine (168149); Ammonium persulfate (A3678); N,N,N′,N′-Tetramethylethylenediamine (A7024); and Hen Egg-white Lysozyme (L6876) protein were purchased from Sigma Aldrich Chemicals Pvt. Limited, Bengaluru, India. The IAEDANS (1,5-IAEDANS, 5-((((2-Iodoacetyl)amino)ethyl)amino)Naphthalene-1-Sulfonic Acid) (I14) was purchased from Invitrogen (Carlsbad, California, USA). The Luria Broth (M1245); Luria Agar (M557); $MgCl_2$ (TC186) and Imidazole (GRM1864) were procured from HiMedia Laboratories, India. The PD-10 desalting column (17-0851-01) was purchased from GE Healthcare. The Tris (Hydroxy methyl amino methane) (93315); Citric acid monohydrate (100244); Sodium acetate (17952); di-Sodium hydrogen Phosphate (17549); Sodium chloride (40731); Dimethylformamide (17754); Dimethyl sulfoxide (61857); SDS (184190); and Potassium chloride (91635) were purchased from Merck India Limited. All chemicals used were analytical grade with purity ≥98%.

Amino acid sequences of PEST Wt and M1 employed in the study are shown in Figure 2.2 and Uniprot ID of human c-Myc PEST region (residues 201-268) is P01106.

The mutant PEST M1 was constructed to study its structure and dynamics by monitoring the intrinsic fluorescence of tryptophan. The PEST contains a single cysteine residue; incorporation of tryptophan in PEST was utilized to facilitate Trp-Cys FRET studies. This mutant, PEST M1 was used to observe whether the insertion of tryptophan alters the ProCharTS absorption spectrum of PEST Wt.

[A] **PEST Wt [77]** (Mass: 8342 Da)
MDSSSPKSCA SQDSSAFSPS SDSLLSSTES SPQGSPEPLV LHEETPPTTS
SDSEEEQEDE EEIDVVSVEL EHHHHHH

[B] **PEST M1 [78]** (Mass: 8528 Da)
MDSSSPKSCA SQDSSAFSPS SDSLLSSTES SPQGSPEPLV LHEETPPTTS
SDSEEEQEDE EEIDVVSVEW LEHHHHHH

Figure 2.2: Amino acid sequence of [A] PEST Wt and **[B]** PEST M1 are shown. Charged and aromatic amino acids are highlighted in bold using black and red coloured fonts, respectively.

2.3 Methods:

2.3.1 Amino acid composition and disorder prediction plots:

Analysis of the amino acid of Human c-Myc PEST Wt and its Tryptophan mutant (PEST M1) was carried out using Composition Profiler tool server (*http://www.cprofiler.org/index.html*). SwissProt version 51 protein database was used as a background data set to compare amino acid composition of PEST Wt and M1 (Vacic et al., 2007). Intrinsic disorder prediction plots for PEST Wt and PEST M1 was performed using Genesilico MetaDisorder server (*http://iimcb.genesilico.pl/metadisorder/index.htm*) (Kozlowski and Bujnicki, 2012). Genesilico MetaDisorder server predicts the disorderness in proteins by using different available disorder predictors, like IUPred, RONN, Pdisorder, MetaDisorderMD and VSL2.

2.3.2 Charge hydropathy plot and hydrophobic cluster analysis:

Charge Hydropathy plots (CH Plots) for PEST Wt and PEST M1 was made using the PONDR server (http://www.pondr.com/). The value of hydrophobicity <*H*> and the mean net charge <*R*> was calculated using the PONDR server as described by Uversky and co-workers in 2000 (Uversky et al., 2000a). The charge hydropathy plot is divided in two regions such as intrinsically disorder protein region and ordered protein region, respectively by a line. Equation used to divide CH plot by a line can be expressed as $< H >_{boundary} = (< R > +1.151)/2.785$ (Uversky et al., 2000a).

Hydrophobic cluster analysis (HCA) of PEST Wt and PEST M1 was performed using the program DRAWHCA 1.0.2 as described by Callebaut and co-workers in 1997 (*http://mobyle.rpbs.univ-paris-diderot.fr/cgi-bin/portal.py#forms::HCA*) (Callebaut et al., 1997).

2.3.3 Cloning, Expression and Purification of PEST Wt and PEST M1:

2.3.3.1 Cloning of PEST Wt and PEST M1

The human c-Myc region from amino acid 201 to 268 (PEST Wt) and its mutant (PEST M1) were cloned in pET21b expression vector between the *Nde*1 and *Xho*1 restriction sites, encoding the PEST Wt and PEST M1 residues with a hexahistidine tag fused with C-terminus. 5'-TGACTCATATGGACAGCAGCTCGCCCAAGTC-3' was used as forward primer. 5'CATGACTCGAGTTCCACAGAAACAACATCG3' and 5'CATGACTCGAGC CATTCCACAGAAACAACATCG-3' was used as reverse primers for PEST Wt and PEST M1, respectively. The recombinant PEST Wt had three extra residues at positions 1, 70 and 71 other than the hexahistidine, while the mutant M1 had four at positions 1, 70, 71 and 72.

2.3.3.2 Preparation of competent cells

E. coli BL-21 (DE3) competent cells were prepared for protein expression. Either a single bacterial colony was picked up from a Luria Agar plate or a very small volume of inoculum from previously prepared competent cell was taken and inoculated into 5 mL of LB medium. The culture was allowed to grow in a shaking incubator at 37 °C and 180 rpm for overnight. 500 µL (1% of the final culture volume) overnight grown culture was used to inoculate in 50 mL of LB medium. This culture was allowed to grow at 37 °C at 180 rpm till the A_{600} of the culture reached approximately to 0.3 or 0.4. Subsequently, culture was incubated at 4 °C for 10 minutes and cells were collected by centrifugation at 3000 rpm for 10 minutes at 4 °C. After discarding the supernatant, cells were resuspended gently by pipetting or inverting in 15 mL of ice cold 80 mM $MgCl_2$+ 20 mM $CaCl_2$ solution. Cells were centrifuged again at 3000 rpm for 10 minutes at 4 °C. The supernatant was discarded and collected pellet was re-suspended in 900 µL of 0.1 M $CaCl_2$ and 100 µL of glycerol. The cells were kept as aliquots of 100 µL in microcentrifuge tubes. The competent cells

were stored at -80 °C until further use. All the materials were autoclaved and all the steps were carried out in laminar air flow to maintain proper sterile conditions.

2.3.3.3 Transformation

The *E. coli* BL-21 (DE3) Competent cells taken out from -80 °C and were thawed in ice for 10 minutes. In the aliquot of the competent cells about 1-2 µL of the plasmid containing gene of interest was added and subsequently incubated for 30 minutes in ice. One aliquot of the competent cells served as negative control in which no plasmid was added. After 30 min of incubation, heat shock was given to the cells at 42 °C for 90 seconds and immediately transferred to ice and incubated for 2-3 minutes. 800 µL of sterile LB media (without any antibiotic) was then added to the cells and was incubated in a shaking incubator at 37 °C and 180 rpm for 45 minutes. The cells were then harvested by centrifugation at 6,000 rpm for 10 minutes. After discarding supernatant the collected pellet was resuspended in 100 µL of fresh LB media. The pellet was then plated on an Ampicillin containing LB agar plate. The LB agar plate was inverted and kept in an incubator at 37 °C for 12 hours. All the materials were autoclaved and all the steps were carried out in laminar air flow to maintain proper sterile conditions.

2.3.3.4 Expression and purification of PEST Wt and PEST M1

Isolated colony of transformed *E. coli* BL21 (DE3) cells was picked up from the LB agar plate and was used for over expression of PEST Wt and PEST M1. The cultures were grown in LB media, containing 100 µg/mL ampicillin (at 37 °C, 180 rpm) in a shaking incubator. At A_{600} of 0.6-0.7, cultures were induced with Isopropyl β-D-1-thiogalactopyranoside (IPTG, 1 mM) at 37 °C for 3 hours. Induced cells were centrifuged at 5000 rpm for 15 minutes at 4 °C to collect the pellet. The collected pellets were resuspended in ice cold lysis buffer (25 mM Tris.HCl (pH 8.0); 100 mM NaCl; 2 mM benzamidine; 10 µg/mL soybean trypsin inhibitor) and incubated at 4 °C for 10 minutes. Subsequently, resuspended cells were disrupted by sonication at 33% power output with cycles of 4 seconds on and 10 seconds off for 30 minutes at 4 °C. To remove the cell debris, cell lysates were centrifuged at 12000 rpm for 30 minutes at 4 °C. Supernatants were filtered with 0.45 µm filter. The filtered supernatants were mixed with 2 mL Ni-NTA

agarose beads (for 1 L culture) pre equilibrated with binding buffer (25 mM Tris.HCl (pH 8.0); 100 mM NaCl) and incubated for 4-5 hours with gentle shaking at 4 °C. Ni-NTA beads bound with lysate were washed with wash buffer A (25 mM Tris.HCl (pH 8.0); 600 mM NaCl; 0.1% Triton-X-100), wash buffer B (25 mM Tris.HCl (pH 8.0); 600 mM NaCl; 0.1% Triton-X-100; 7.5 mM Imidazole) and wash buffer C (25 mM Tris.HCl (pH 7.4); 100 mM NaCl). The recombinant PEST fragment proteins were eluted with elution buffer (25 mM Tris.HCl (pH 7.4); 100 mM NaCl; 150 mM Imidazole).

Purity of proteins was checked by SDS polyacrylamide gel electrophoresis (15% Acrylamide). The fractions containing pure proteins were pooled and dialyzed against dialysis buffer (25 mM Tris.HCl (pH 7.4); 25 mM NaCl) to remove Imidazole. Purified proteins were further analyzed by mass spectrometry to ascertain the identity and purity of purified proteins.

2.3.4 Sodium dodecyl sulfate polyacrylamide gel electrophoresis (SDS-PAGE):

Reducing SDS-PAGE was performed according to the protocol reported in Sambrook and Russel, Molecular Cloning-A laboratory manual (Sambrook et al., 1989) to check the purity of purified protein. Resolving gel (15% acrylamide) was used for running all the purified protein samples. Composition of SDS-PAGE is given in appendix. Protein sample was mixed with the gel loading buffer in 4:1 ratio and subsequently allowed to boil at 95 °C for 5 minutes. Samples were separated on vertical Mini-PROTEAN^{R} Tetra Electrophoresis System (Make: Bio-Rad). All protein samples were run at 80 Volts for 2 hours. After running the samples, gels were removed from electrophoresis apparatus and stained with colloidal Coomassie stain for 4 hours. After proper staining, the gels were placed in de-staining solution (see appendix) for overnight to allow the de-staining of gel. Standard molecular markers were used to determine the approximate molecular weight of protein in the gel.

2.3.5 Protein estimation:

The Lowry method was used to determine the protein concentration (Lowry et al., 1951). The standard curve was made using BSA protein. Various dilutions of BSA ranging from 0.05 mg/mL to 1 mg/mL were prepared from freshly prepared stock of BSA (1 mg/mL) in deionized water. 200 µL of PEST Wt, PEST M1 and each dilution of BSA, were added to the aluminium foil wrapped test tubes. All the samples were taken in duplicates. Deionized water was used as blank. Subsequently 2 mL of Reagent I (see Appendix) was added to each of the tubes and vortex thoroughly. After proper vortexing, all tubes were incubated for 10 minutes at room temperature. After incubation, 200 µL of Reagent II (see Appendix) was added to all tubes and mixed properly. Now all the tubes were incubated in the dark for 30 minutes at room temperature. Subsequently, absorbance of each sample was measured at 650 nm to determine the protein concentration. The approximate concentration of PEST Wt and M1 was calculated from the slope of BSA concentration verses absorbance plot.

Concentration of PEST Wt and PEST M1 was further cross verified by measuring the absorbance in far-UV region. To determine the protein concentration in far-UV region following equation was used (Waddell, 1956).

$$Protein\ concentration\ (\mu g/mL) = 144\ (A_{215} - A_{225}) \qquad 2.64$$

Here, A_{215} and A_{225} represent the absorbance at 215 nm and 225 nm, respectively.

2.3.6 Mass Spectrometry analysis:

Mass of PEST fragments were determined by using MALDI-TOF mass spectrometer (Daltonics Bruker, Germany). Matrix was prepared by saturating solution of Sinapic acid in TA-30 solvent. 0.1% Trifluoroacetic acid and acetonitrile was mixed in 7:3 ratios for preparing TA-30 solvent. Further, saturated solution of Sinapic acid was sonicated for 30 minutes followed by centrifugation at 12000 rpm at room temperature (25 °C) for 15 minutes. Collected supernatant was mixed with protein samples in 2:1 ratios and spotted on the target plate and subsequently allowed to dry at room temperature for 2 hours. Data acquisitions of all samples were done in Linear Mode with flexControl and analysis was done with flexAnalysis software from Bruker Daltonics.

Mass of PEST monomer was determined under reducing environment by dissolving the protein in deionized water containing 6 mM β Mercaptoethanol. While sample of PEST dimer, for mass determination was prepared under non-reducing condition by solubilizing the PEST dimer in deionized water.

2.3.7 Size exclusion chromatography:

Size exclusion chromatography was performed by using ÄKTApurifier™ FPLC (GE Healthcare) chromatography system. HiLoad™ 16/600 Superdex™ 200 pg **(**GE Healthcare, 28-9893-35) size exclusion column was used to determine molecular weight of PEST fragment. This column has fraction limits of 10-600 kDa and 120 mL of bed volume. Column was washed with 2 column volume of deionized water to remove any contaminant from the column. Subsequently, column was equilibrated with 2 column volumes of equilibration buffer (25 mM Tris.HCl (pH 7.4); 25 mM NaCl). Void volume of column was calculated by running blue dextran (2,000 kDa) through the column and calculated void volume of column was 45.34 mL. The standardization of the column was done by using proteins: alcohol dehydrogenase (150 kDa), albumin bovine serum (66 kDa), carbonic anhydrase (29 kDa), and hen egg-white lysozyme (14.3 kDa). All standards were run in elution buffer (25 mM Tris.HCl (pH 7.4); 25 mM NaCl). After running all the standards, column was equilibrated with the sample elution buffer (25 mM Tris.HCl (pH 7.4); 25 mM NaCl; 6 mM DTT). DTT in elution buffer was used to avoid any dimer formation of the PEST fragments. Approximately, 300 μM (1mL) of PEST Wt/M1 was load on the column and eluted with elution buffer (25 mM Tris.HCl (pH 7.4); 25 mM NaCl; 6 mM DTT). All samples and standards were allowed to run with flow rate of 1 mL/minute throughout the experiment. All buffers were carefully filtered and degassed to avoid any air bubble formation in the size exclusion column.

To separate the PEST Wt and M1 dimer from monomer, column equilibration and elution of samples was done with the non-reducing buffer (25 mM Tris.HCl (pH 7.4); 25 mM NaCl). All other conditions were same as describe above.

To know the molecular weight of the sample, standard curve was made by plotting partition coefficient (K_{av}) against logarithm of relative molecular weight. K_{av} can be expressed as

$$K_{av} = \frac{V_e - V_o}{V_t - V_o} \qquad 2.65$$

Here, V_e is the measured elution volume, V_o is the measured void volume and V_t is the total column volume.

2.3.8 Dynamic Light Scattering measurements:

Dynamic Light Scattering measurements were performed using Zetasizer Nano ZS 90 (Malvern instruments) equipped with thermal controlled micro sampler. Scattering of the sample was done with 633 nm laser and scattered light coming from the sample was collected at 90° angle. All samples were thermally equilibrated for 120 seconds by using inbuilt temperature control for cuvette. Each measurement was performed with 20 sub-runs with 20 second duration. All the measurements were performed at least three times to ensure better reproducibility of the data and were performed at room temperature (25 °C). Before the measurements, all samples were centrifuged at 12,000 rpm for 10 minutes and subsequently filtered through 0.22µm syringe filter (GE healthcare life sciences Whatman™ Cat no.9908-2502) to remove large dust particles which can interfere with the sample measurements.

To measure the hydrodynamic radius of PEST fragment, approximately 1.5 mg/mL of PEST Wt/M1 protein was dissolved in the reducing buffer containing 25 mM Tris.HCl (pH 7.4); 25 mM NaCl; 1 mM Tris (2-carboxyethyl) phosphine.HCl (TCEP). To avoid any dimer formation in PEST fragment TCEP was used. To analyse the hydrodynamic radius of PEST dimer, around 1.5 mg/mL PEST Wt/M1 dimer (separated from size exclusion chromatography) was dissolve in non-reducing buffer (25 mM Tris.HCl (pH 7.4); 25 mM NaCl). All DLS measurements were done as describe above. All the data analysis was carried out with the software provided by Zetasizer Nano ZS 90 instrument.

2.3.9 UV-Visible absorption spectra:

The absorption spectrum of PEST Wt and M1 was recorded using double beam Lambda-25 UV-Vis Spectrophotometer (Perkin Elmer, USA) at room temperature (25 °C). UV transmissible quartz cuvette of 10 mm path length (Hellma; Z600210) was used for all absorption measurements. The absorption spectra were acquired with multiple scans (3—5) between 250 nm and 800 nm (1 nm bandwidth; 480 nm/minute scan speed) and averaged subsequently. All spectra shown are averages of at least two independent measurements. For measuring the molar extinction coefficients, PEST Wt/PEST M1 was dissolved in deionized water. PEST samples always contained 5 mM TCEP in all absorption measurements. Blanks were identical to the sample in all respects with the exception that they contained no protein.

For recording pH dependent absorption spectra, PEST fragment was dissolved in different buffers (25 mM) as described under circular dichroism measurements. To monitor the effect of salts on absorption spectra, PEST fragment was dissolved in 250 mM KCl or NaCl.

To probe the temperature dependence of absorption spectra, PEST fragment was dissolved in deionized water. Temperature of protein samples were maintained using a circulating water bath (Julabo; FPW50-HL). The cuvette containing the sample was sealed with parafilm and incubated in water bath for at least 20 minutes at chosen temperature prior to collecting spectra. Initially absorption spectra were measured at 25 °C. Subsequently, absorption spectra were collected by heating the sample to 85 °C. As the sample cooled, absorption spectra were recorded at 65 °C, 45 °C and 25 °C, respectively. All spectral acquisition parameters were kept identical for each temperature.

2.3.10 Labeling of PEST fragment with dansyl probe:

Labeling of single cysteine in the PEST fragment with the IAEDANS (1,5-IAEDANS, 5-((((2-iodoacetyl)amino)ethyl)amino)naphthalene-1-sulphonic acid) was carried out as recommended by Molecular Probe with slight modifications (Wiederschain, 2011). 60 mM stock of IAEDANS was prepared by solubilizing the probe into the DMF. 300 μM of PEST

Wt/M1 was dissolved in 1 mL labeling reaction buffer (25 mM Tris.HCl (pH 9); 25 mM NaCl; 5 mM TCEP). 50 µL of 60 mM IAEDANS in DMF was added (final concentration of IAEDANS was 3 mM) to 1 mL of 300 µM PEST Wt/M1. This reaction mixture was incubated at room temperature (25 °C) for three hours with continuous stirring at 150 rpm. On completion of the reaction, the free dye was removed from the dansyl labeled protein by using pre-equilibrated PD-10 desalting column with 25 mM Tris.HCl (pH 9); 25 mM NaCl. Concentration of protein and dye was measured by using absorbance at 280 and 337 nm, respectively. The molar extinction coefficient of conjugated probe with protein at 337 nm is 6100 $M^{-1}cm^{-1}$ (Hudson and Weber, 1973).

2.3.11 Steady state fluorescence and anisotropy measurements:

All steady state fluorescence and anisotropy measurements were performed using Fluoromax-4 Spectrofluorometer (Jobin-Yvon Horiba Inc., USA) equipped with motorized polarizers. For all tryptophan steady state fluorescence intensity measurements of PEST M1, samples were excited at 295 nm (slit width = 1 nm) and emission was collected between 310 nm to 500 nm (slit width = 5 nm). For acquiring tryptophan steady state anisotropy of PEST M1; all samples were excited at fixed 295 nm (slit width = 1 nm) and emission was collected at fixed 345 nm (slit width = 5 nm).

For acquiring steady state fluorescence intensity of dansyl; labeled with cysteine of PEST Wt and M1, all samples were excited at 340 nm (slit width = 1 nm) and emission was collected between 355 nm to 670 nm (slit width = 5 nm). For collecting steady state anisotropy of dansyl; labeled with cysteine of PEST Wt and M1, all samples were excited at fixed 340 nm (slit width = 1 nm) and emission was collected at fixed 505 nm (slit width = 5 nm). All steady state anisotropy data were G-factor corrected and each anisotropy measurement was an average of 10 independent measurements.

The background intensity from buffers and Raman scatter were insignificant (<5%) in comparison with fluorescence intensity of samples under the identical conditions. However, these were subtracted from emission spectra of sample. All steady state fluorescence measurements were repeated at least three times at room temperature (25 °C) in 700 µL quartz cuvette with a 10 mm pathlength [Hellma (Z802875)].

To study the effect of pH on structure of PEST fragment, 20 μM of PEST M1; 10 μM of dansyl labeled PEST Wt and M1 were dissolved in different 25 mM buffers (pH 3-11), containing 25 mM NaCl and 5 mM TCEP. For monitoring the unfolding of PEST at various pH (3-11), 20 μM of PEST M1; 10 μM of dansyl labeled PEST Wt and M1 were incubated overnight at room temperature in different 25 mM buffers, containing 6 M Gdn.HCl; 25 mM NaCl and 5 mM TCEP.

For monitoring the effect of pH on structure of PEST with higher salt concentration, 20 μM of PEST M1 was dissolved in different 25 mM buffers (pH 3-11), containing 250 mM NaCl and 5 mM TCEP.

To investigate the effect of high salt (NaCl) concentration on structure of PEST M1, 20 μM of PEST M1 was dissolved in buffer 25 mM Tris.HCl (pH 7.4), containing 5 mM TCEP and series of NaCl concentration ranging from 25 to 500 mM.

For acquiring steady state fluorescence intensity and anisotropy of dimeric PEST M1 tryptophan, 10 μM of PEST M1 dimer was dissolved in a non-reducing buffer (25 mM Tris.HCl (pH 7.4); 25 mM NaCl).

Steady state fluorescence of tryptophan derivative, N-acetyl tryptophan amide (NATA) was also monitored as a control under identical conditions for all experiments.

To maintain constant pH, Citric acid monohydrate (pH 3); Sodium acetate (pH 5); Tris.HCl (pH 7; 7.4 and 9) and Sodium phosphate dibasic (pH 11) buffers were used.

2.3.12 ANS binding assay:

To study the binding of 8-Anilinonaphthalene-1-sulfonic acid (ANS) with PEST fragment, stock of ANS (1mg/mL) was prepared in deionized water. Stock concentration of ANS was confirmed by using extinction coefficient of 4,950 $M^{-1}cm^{-1}$ at 350 nm. 10, 25 and 50 μM of PEST Wt/M1 (dissolved in 25 mM Tris.HCl (pH 7.4); 25 mM NaCl; 5 mM TCEP) was mixed with constant 10 μM of ANS.

To analyse the binding of ANS with PEST Wt/M1 at various pH, 30 μM of PEST Wt/ PEST M1 (dissolved in different 25 mM buffers (pH 3-11), containing 25 mM NaCl and 5

mM TCEP) was mixed with 10 μM ANS. To maintain constant pH, Citric acid monohydrate (pH 3; 3.5; 4 and 4.5); Sodium acetate (pH 5); Tris.HCl (pH 7; 7.4 and 9) and Sodium phosphate dibasic (pH 11) buffers were used.

Binding of ANS with PEST fragment was monitored by measuring the steady state fluorescence intensity of ANS. All samples were excited at 380 nm (slit width = 5 nm) and emission was collected between 400 nm to 700 nm (slit width 10 nm). The background intensity from buffer and Raman scatter were negligible (<5%) in comparison with fluorescence intensity of sample under the identical condition. However, these were subtracted from emission spectra of sample. All ANS fluorescence measurements were done in triplicate at room temperature (25 °C).

2.3.13 Time-resolved fluorescence and anisotropy measurements:

All time resolved fluorescence intensity decay and anisotropy decay measurements were done by time-correlated single photon counting (TCSPC) instrument, using the 'Delta-Pro™, equipped with motorized polarizer, supplied by Horiba Scientific, UK. To measure the fluorescence lifetime and anisotropy decay of PEST M1 tryptophan, all samples were excited with pulsed light source, 295 nm DeltaDiode™ having about 0.81 ns Instrument response function (IRF) FWHM and a 20MHz repetition rate. Emission of tryptophan was collected with 320 nm longpass filter (WG320) to block the excitation light. Total peak counts were collected up to 20,000 counts and fluorescence intensity decay was collected in 2202 channel (in 0 to 61.66 ns time range) with temporal resolution of 0.028 ns/ channel.

To measure the fluorescence intensity and anisotropy decay of dansyl, labeled with cysteine of PEST Wt and M1, all samples were excited with pulsed light source, 340 nm DeltaDiode™ having about 0.80 ns IRF FWHM and a repetition rate of 20MHz. Emission of dansyl was measured with 370 nm longpass filter (KV370) to cut the excitation light. Total peak counts were measured up to 20,000 and fluorescence intensity decay was collected in 3995 channel (in 0 to 223.72 ns time range) with temporal resolution of 0.056 ns/channel. Emission of all samples were measured at magic angle position of 54.7° with emission polarizer. IRF was collected using scattering solution of colloidal silica, without

emission filter for each of the sample. All lifetime and anisotropy measurements were done at room temperature (25 °C) and at least three independent measurements were recorded.

All time-resolved anisotropy experiments was performed with the emission polarizer oriented perpendicular ($I_{\perp}$) and parallel ($I_{\parallel}$) to the excitation polarizer. DAS6 v6.8 decay analysis software provided by *HORIBA Scientific* was employed to obtain lifetime of tryptophan from intensity decay data for all conditions. Lifetime of dansyl, labeled with cysteine of PEST Wt and M1; was obtained using *exp 2* decay analysis software (kindly provided by Dr. N. Periasamy, Tata Institute of Fundamental Research (TIFR), Mumbai, India) for all conditions. Rotational correlation times of dansyl (for all conditions) and tryptophan in PEST M1 and its dimer at pH 7.4 were extracted from *tani* software kindly provided by Dr. N. Periasamy, TIFR. DAS6 v6.8 software was used to extract the rotational correlation time of PEST M1 tryptophan at different pH (3-11) under various conditions. The goodness of fit was evaluated by analysing the reduced χ^2 and randomness of residuals.

All sample preparation was same as those described for the *steady state fluorescence and anisotropy* experiments.

2.3.14 Quenching of tryptophan with acrylamide:

Quenching of PEST M1 tryptophan at various pH was done with acrylamide. The fluorescence lifetime of PEST M1 tryptophan was measured by TCSPC. All lifetime measurements were done at room temperature (25 °C).

Tryptophan fluorescence lifetime of 20 μM PEST M1 (dissolved in 25 mM buffer, containing 25 mM NaCl and 5 mM TCEP) was monitored at various pH (3-11) in the absence and presence of a series of acrylamide concentration ranging from 0 to 50 mM.

Quenching of PEST M1 tryptophan was also done in presence of 6 M Gdn.HCl at pH (5; 7 and 9). To ensure complete unfolding, 20 μM PEST M1 was dissolved in different 25 mM buffers (pH 5-9), containing 6 M Gdn.HCl; 25 mM NaCl; 5 mM TCEP and incubated overnight at room temperature prior to the experiment. To maintain constant pH, Citric acid monohydrate (pH 3; 4 and 6); Sodium acetate (pH 5; 5.3 and 5.6); Tris.HCl (pH 7; 8 and 9); Glycine (pH 10) and Sodium phosphate dibasic (pH 11) buffers were used.

Quenching of a tryptophan derivative, N-acetyl tryptophan amide (NATA) was also monitored by measuring its fluorescence lifetime under identical conditions. All measurements were done at least three times to ensure better reproducibility of the data. The bimolecular quenching constant (k_q) was calculated using the Stern-Volmer equation 2.49 (Lakowicz, 1983).

2.3.15 Intramolecular Förster Resonance Energy Transfer (FRET) measurements:

Intramolecular distance in PEST M1, between the tryptophan (present at 70th position) and cysteine (present at 9th position) labeled with dansyl was measured at various pH (3-11). To calculate the distance between tryptophan and cysteine at different pH, fluorescence lifetime of tryptophan, in absence of acceptor (τ_D) and in presence of acceptor (τ_{DA}) was monitored, respectively. The fluorescence lifetime of tryptophan was collected by TCSPC. The tryptophan was excited with pulsed light source, 295 nm DeltaDiode^{TM} and subsequently emission of tryptophan was collected with 330-355 nm bandpass filter (ET340/40X) supplied by *CHROMA*, to avoid the excitation light and emission light coming from the dansyl. Total peak counts were measured up to 15,000 and fluorescence intensity decay was collected in 2202 channel (in 0 to 61.66 ns time range) with temporal resolution of 0.028 ns/channel. All lifetime measurements were done at room temperature and for each samples at least three independent lifetime measurements were recorded.

For acquiring pH dependent lifetime of PEST M1 tryptophan with and without acceptor, 20 μM of unlabelled/labeled PEST M1 was dissolved in different 25 mM buffers (pH 3-11), containing 25 mM NaCl; 5 mM TCEP. For complete unfolding of PEST M1, 20 μM of labeled/unlabelled PEST M1 was soaked overnight at room temperature in different 25 mM buffers (pH 3-11), containing 6 M Gdn.HCl; 25 mM NaCl and 5 mM TCEP. To maintain constant pH, Citric acid monohydrate (pH 3 and 4); Sodium acetate (pH 5); Tris.HCl (pH 7 and 9) and Sodium phosphate dibasic (pH 11) buffers were used.

Förster distance (R_0) 22 Å, for tryptophan-IAEDANS pair was used (Wu and Brand, 1994). FRET efficiency (E) was calculated from mean lifetime of donor alone (τ_D) and in presence of acceptor (τ_{DA}) by using equation 2.56.

2.3.16 Circular Dichroism analysis:

CD spectra of PEST Wt and M1 were recorded on a CD spectrometer (Make: Jasco, Model J-1500, Jasco Inc., Maryland, USA), equipped with a Peltier thermoregulator. For acquiring pH dependent CD spectra, 20 μM of PEST Wt/M1 were dissolved in different 5 mM aqueous buffers. PEST proteins contained 1 mM TCEP, to prevent disulphide linked dimer formation. To maintain constant pH, Citric acid monohydrate (pH 3; 4; 4.3; and 4.6); Sodium acetate (pH 5); Sodium phosphate (pH 7 and 7.4); Tris.HCl (pH 9) and Sodium phosphate dibasic (pH 11) buffers were used.

To measure the CD spectra of PST Wt and M1 dimer, protein samples were prepared under non-reducing conditions by dissolving the 20 μM of PEST Wt/M1 in 5 mM Sodium phosphate buffer (pH 7.4).

For monitoring the effect of 2,2,2-trifluoroethanol (TFE) on structure of PEST fragment, CD spectra was recorded. 20 μM of PEST proteins (dissolved in 5 mM Sodium phosphate (pH 7.4); 1 mM TCEP) were mixed and incubated at least for 5 minutes with the increasing concentration of TFE (10-50% (v/v) to the final concentration) prior to collecting the CD spectra.

For measuring CD spectra at various temperatures (25—85 °C), 20 μM of PEST proteins were mixed in deionized water containing 1 mM TCEP. All samples were incubated at least for 5 minutes at each temperature prior to collecting the CD spectra. All CD spectra were collected from 190 to 260 nm, at a scan speed of 100 nm/minute, bandwidth of 2 nm and data pitch of 0.1 nm. All spectra were collected using 2 mm quartz cuvette (Starna Scientific Ltd). The contribution of deionized water and respective buffers were subtracted from the acquired spectra during data acquisition. For each protein sample at least three independent scans were carried out. CD spectra from 190 to 260 nm were analyzed using DichroWeb server. The CDSSTR program was used to calculate secondary structure content with reference set 7 and the experimental curves were well superimposed on reconstructed curves (Lobley et al., 2002; Sreerama and Woody, 2000; Whitmore and Wallace, 2004; Whitmore and Wallace, 2008).

2.3.17 Estimation of free thiol:

To know the concentration of free thiol in the PEST fragment, 2,2'-dithiobis(5-nitropyridine) (DTNP) was allow to react with the PEST fragment. Due to uncharged nature of pyrimidine derivative, it can react with buried thiol in the protein. Hence, DTNP was selected to react with PEST fragment over most popular benzoic acid derivative (DTNB), which has two negative charges and cannot access the buried thiol in the protein (Kumar et al., 2008; Riener et al., 2002). A 6 mM stock of DTNP was prepared by dissolving the DTNP in the DMSO. 50 μM of DTNP was mixed with the 10, 20 and 30 μM of PEST Wt/PEST M1 dissolved in the reaction buffer (25 mM Tris.HCl (pH 7.4); 25 mM NaCl). The reaction mixture was incubated in a shaking incubator for 15 minutes at room temperature. Formation of yellow colour product, 5-nitropyridine-2-thione was confirmed by monitoring the characteristic absorbance peak at 387 nm where the reactant (DTNP) has negligible absorption. A standard plot was generated by using the known concentration of L-cysteine amino acid (0-100 μM) under identical condition. Concentration of free thiol in the PEST Wt and M1 was calculated by calibrating the absorbance at 387 nm with standard plot of L-cysteine.

For calculating the concentration of free thiol in PEST Wt/M1 in presence of 6 M Gdn.HCl, 10, 20, 30 μM PEST Wt/M1 was mixed with buffer (25 mM Tris.HCl (pH 7.4); 6 M Gdn.HCl; 25 mM NaCl) and incubated overnight at room temperature. Overnight incubated PEST samples in 6 M Gdn.HCl were used to determine free thiol and all other experimental conditions were identical as describe above.

Chapter 3

Purification and characterization of human c-Myc PEST fragment and its mutant

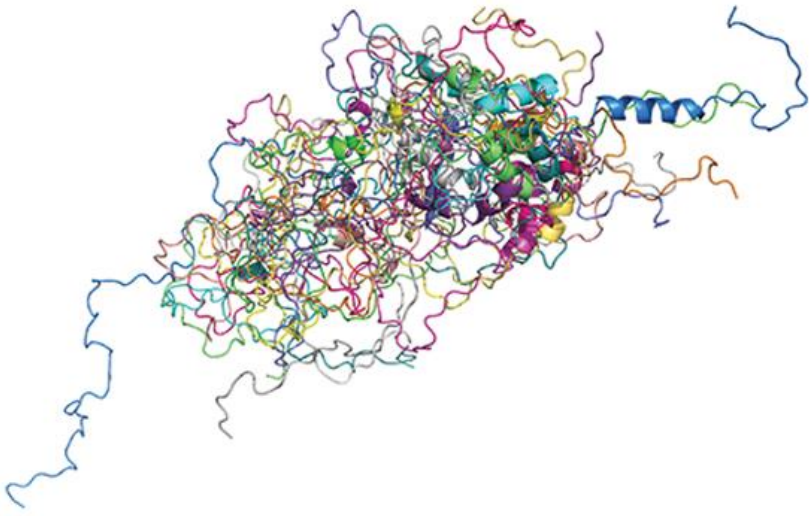

3.1 Introduction:

The discovery of Intrinsically Disordered Proteins (IDPs)/ Intrinsically Disordered Regions (IDRs) is contrary to the traditional protein structure-function paradigm. IDPs remain functionally active without having a well-defined 3D structure. Under the physiological conditions, IDPs lack the stable tertiary and/ or secondary structures (Weinreb et al., 1996; Wildegger et al., 1999). However, this unfolded structure is essential for the function of IDPs. IDPs are extremely abundant in biology and they involved in various important cellular processes like replication, transcriptional and translational regulation, cell cycle control, molecular recognition, signaling, etc. (Dunker et al., 2008; Dyson and Wright, 2005; Tompa, 2005; Tompa, 2010).

Bioinformatics analysis revealed, about one third of the proteins present in eukaryotes is intrinsically disordered (Fink et al., 2005). IDPs are different from ordered globular proteins in many aspects like their amino acid composition, net charge, hydrophobicity, hydrodynamic properties, binding promiscuity and resistance to heat (Csizmok et al., 2006; Dunker et al., 2001; Kalthoff, 2003; Romero et al., 2001; Uversky et al., 2000a; Uversky et al., 2000b). Presently, IDPs are under intense investigation because of their role in normal cellular processes as well as in abnormal protein folding, which lead to many diseases (Dunker et al., 2002a).

The Human c-Myc oncoprotein is a transcription factor which plays an important role in various processes like cell growth, proliferation, differentiation and programmed cell death (Henriksson and Luscher, 1996). Its centrally located highly acidic PEST region is rich in Proline (P), Glutamic acid (E), Serine (S) and Threonine (T). This region is responsible for rapid degradation of the c-Myc oncoprotein (Gregory and Hann, 2000). This PEST region is disordered as it carries abundant negatively charged amino acids. However, the structural information and characterization of the disordered properties of c-Myc PEST region are yet to be done.

The human c-Myc PEST fragment was purified to understand its structural and disorder properties. The detailed studies of structure, dynamics and disordered behavior of PEST fragment was carried out using different computational, biochemical and biophysical techniques. Our computational prediction and experimental results shows, full length of PEST fragment is highly disordered. Structural analysis of PEST fragment displays a random coli-like structure.

3.2 Results and Discussion:

3.2.1 Amino acid composition profile and disorder prediction plots

To gain insights into disorder propensity of wild type human c-Myc PEST fragment (PEST Wt) and its tryptophan mutant (PEST M1), we analyzed their amino acid composition profile using composition profiler tool. Figure 3.2.1A shows the relative enrichment in amino acid composition of PEST Wt, PEST M1 and an ordered protein (Barstar) compared with SwissProt version 51 protein databases. The analysis of amino acid composition revealed enrichment of PEST Wt and M1 in disorder promoting amino acids (Pro, Ser and Glu) and substantially depleted in order promoting residues, including bulky hydrophobic residues (Ile, Leu and Val) and aromatic amino acids (Phe, Tyr and Trp). Amino acid composition profile of PEST Wt and M1 point towards their intrinsic disordered nature as, they are enriched in charged amino acids (Glu, Asp and His) and deficient in hydrophobic amino acids, which generally involve in hydrophobic core formation of folded globular proteins (Dunker et al., 2001; Romero et al., 2001).

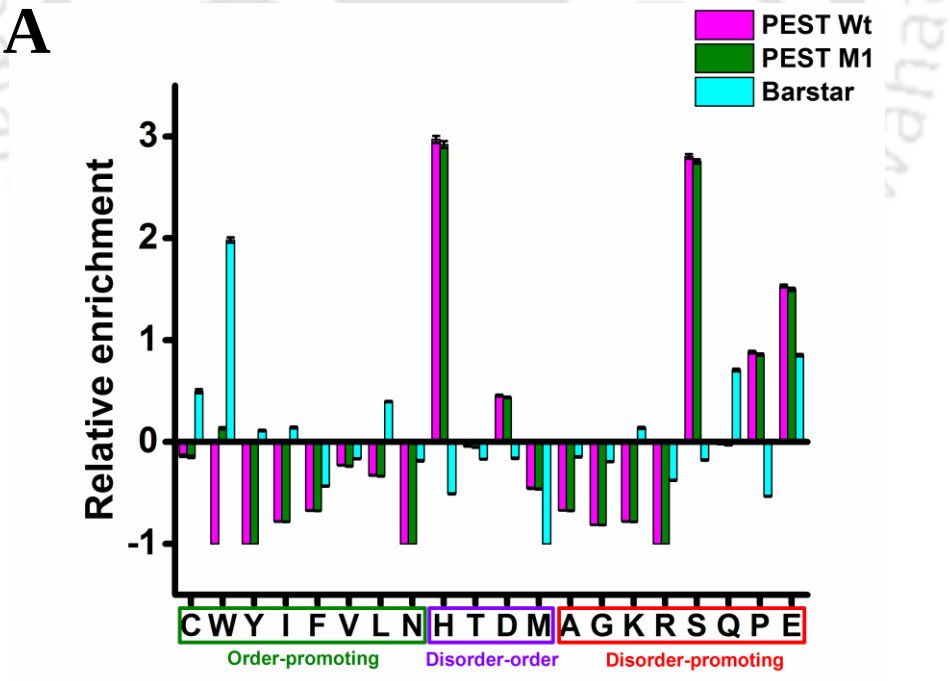

Figure 3.2.1A: Comparison of amino acid composition profile of PEST Wt and its mutant PEST M1 with ordered protein (barstar).

Further, the intrinsic disorder prediction profiles of PEST Wt and M1 were analyzed using Genesilico MetaDisorder server. Figure 3.2.1B, C and D, depicts the disorder prediction plot of PEST Wt, PEST M1 and barstar, respectively using different disordered predictors like IUPred, RONN, Pdisorder, MetaDisorderMD and VSL2. Every amino acid of PEST Wt and M1 shows disorder tendency value more than 0.5. The disorder prediction plots of PEST Wt and M1 are similar but not identical. The PEST M1 shows minor decrease in the value of disorder tendency near the tryptophan vicinity. A detailed inspection of sequences, using different disorder predictor tools clearly predicted that full length of both PEST Wt and M1 is highly disordered.

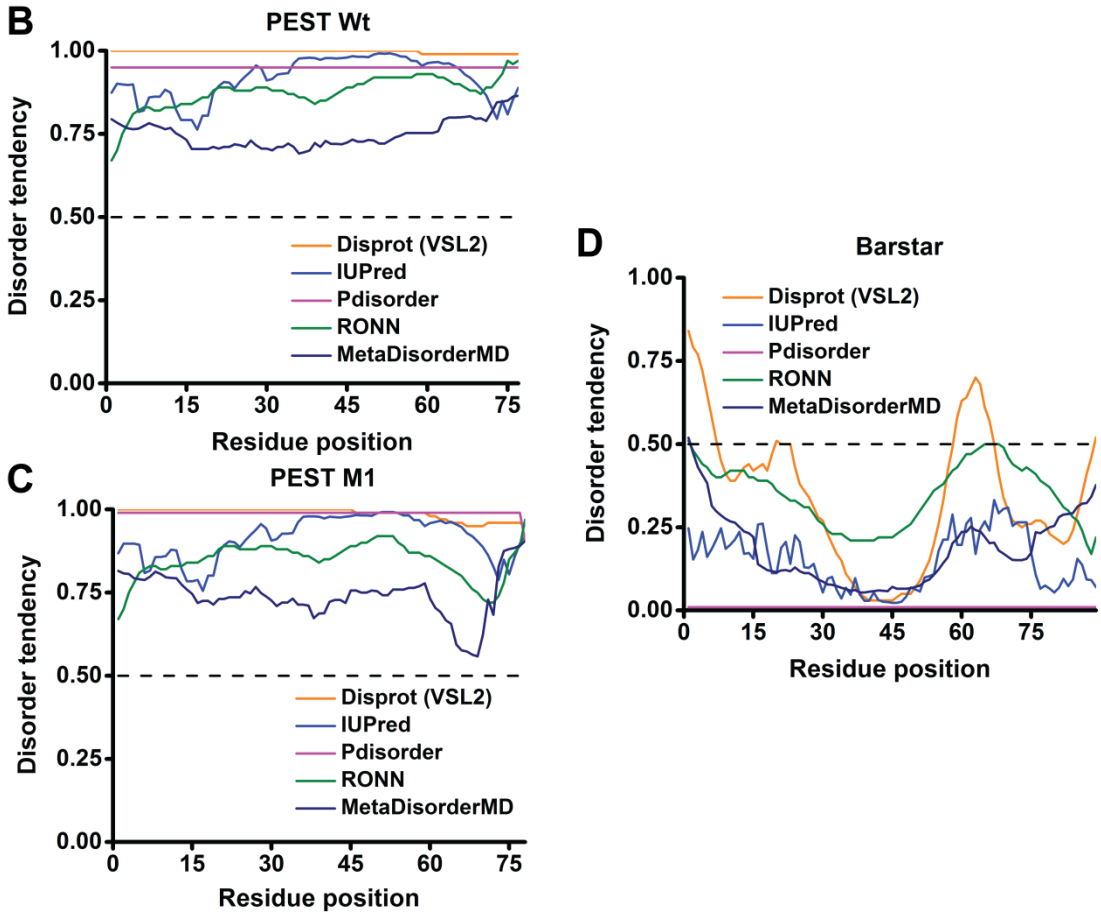

Figure 3.2.1: Comparison of intrinsic disorder prediction plots of **[B]** PEST Wt and **[C]** PEST M1 with ordered protein **[D]** barstar as obtained by various predictors.

3.2.2 Charge hydropathy plot and hydrophobic cluster analysis

To explore the structural disorderness in the PEST fragment, the mean net charge <*R*> and hydrophobicity <*H*> was calculated using PONDR server. Figure 3.2.2A shows the charge hydropathy plot of PEST Wt and M1. The charge hydropathy plot is divided into two phases by a boundary. On the right hand side of boundary a set of folded proteins (squares) are present, which have low net charge and high hydrophobicity. On the left hand side of boundary a set of Intrinsically Disordered Proteins (IDPs) (empty circles) are present, which have high net charge and low hydrophobicity. PEST Wt and M1 appear on the left hand side of the boundary and have high net charge and low hydrophobicity. The combination of high net charge and low hydrophobicity in PEST Wt and M1 signifies the intrinsically disordered nature of PEST fragment as described before (Uversky et al., 2000a; Uversky et al., 2000b).

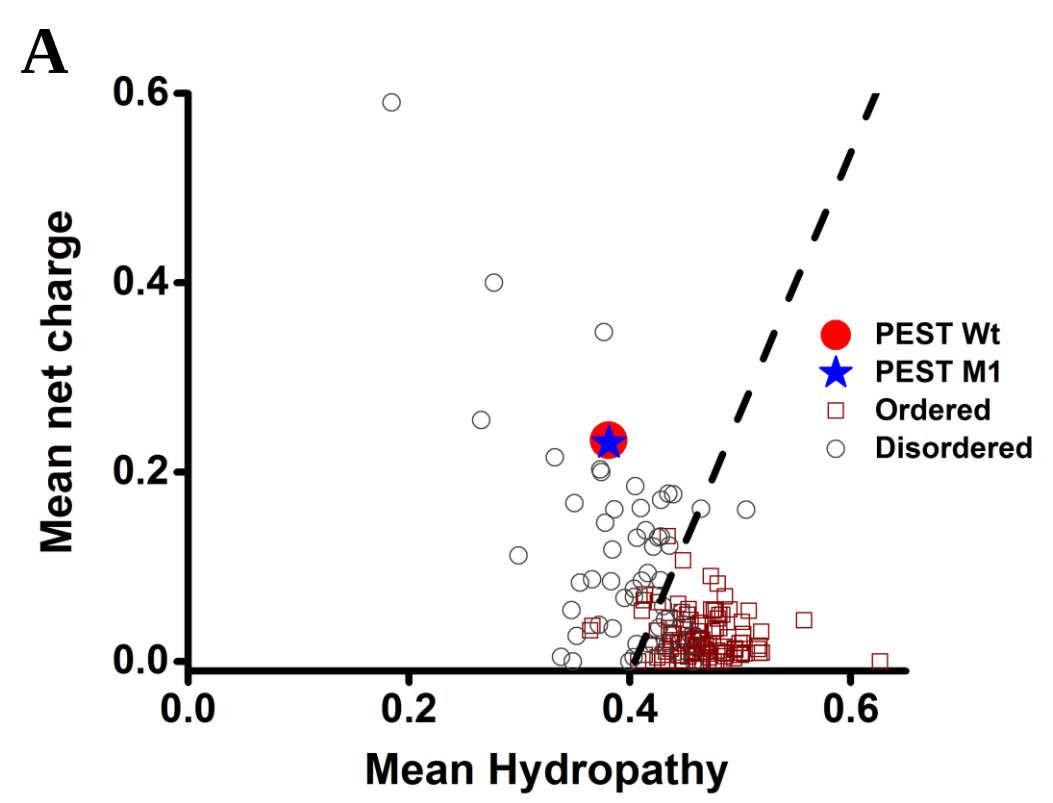

Figure 3.2.2A: Charge hydropathy plot of PEST Wt and PEST M1 as obtained by PONDR server. The black line represents a boundary between the disordered and ordered proteins.

Further, the hydrophobic cluster analysis (HCA) was carried out using DRAWHCA 1.0.2 program for visual illustration of hydrophobic patches present in PEST Wt and M1. Figure 3.2.2B, C and D represent the HCA plots of PEST Wt, M1 and barstar, respectively. The HCA plot investigation reveals the depletion of hydrophobic clusters in PEST fragment. The PEST M1 displays a minor increase in hydrophobic patch between amino acid 60 to 70, in comparison with PEST Wt. The HCA plot is well correlated with charge hydropathy plot, as it also shows low hydrophobicity in PEST fragment. Depletion of hydrophobic clusters also points out the structural disorder in PEST Wt and M1.

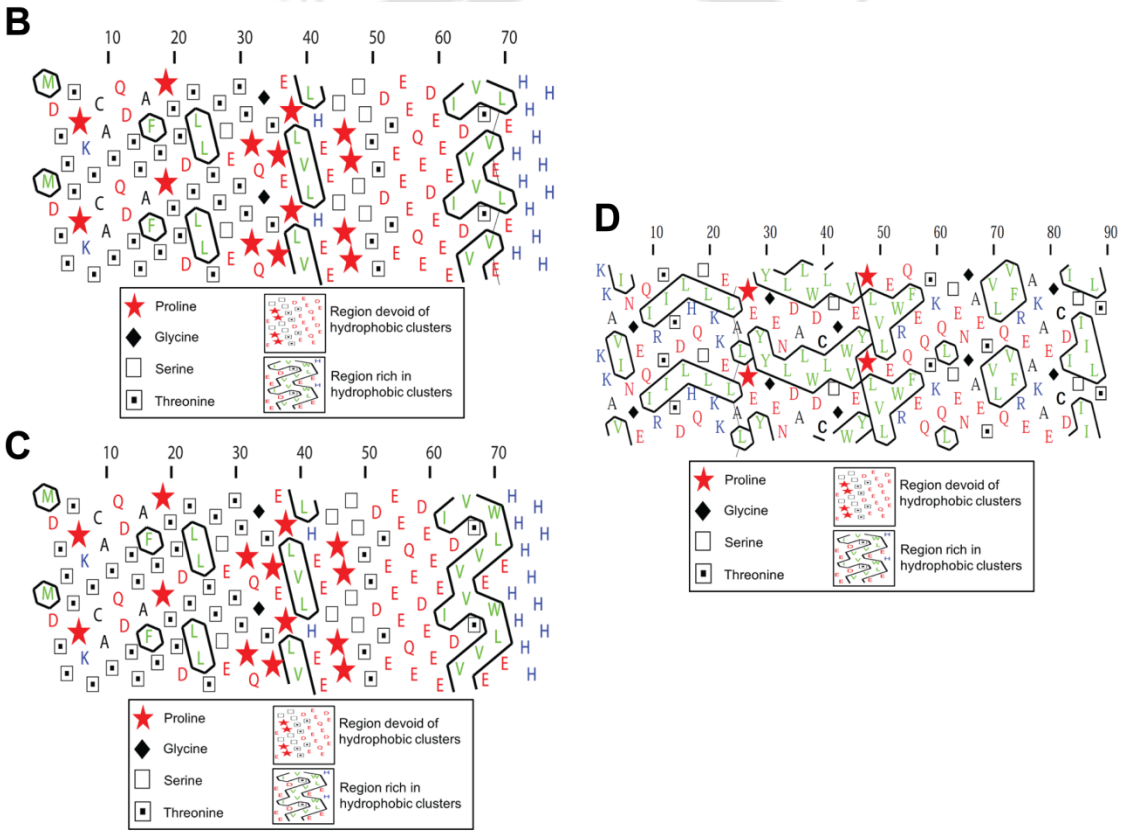

Figure 3.2.2: Comparison the hydrophobic cluster analysis of **[B]** PEST Wt and **[C]** PEST M1 with ordered protein **[D]** barstar determined by using DRAWHCA 1.0.2 program.

3.2.3 Purification of human c-Myc PEST fragment

The PEST Wt and PEST M1 was expressed and purified, to experimentally investigate the structure and various disordered behavior of PEST fragments. The Ni-NTA metal affinity chromatography was performed to purify hexahistidine tag PEST fragments. The purified protein was eluted with 150 mM Imidazole. The purity of protein was checked by reducing SDS polyacrylamide gel electrophoresis (15% acrylamide). Figure 3.2.3A and B shows the single band of purified PEST Wt and M1, respectively on reducing SDS-PAGE. PEST Wt and M1 run on SDS PAGE with an apparent molecular weight of approximately 15 kDa.

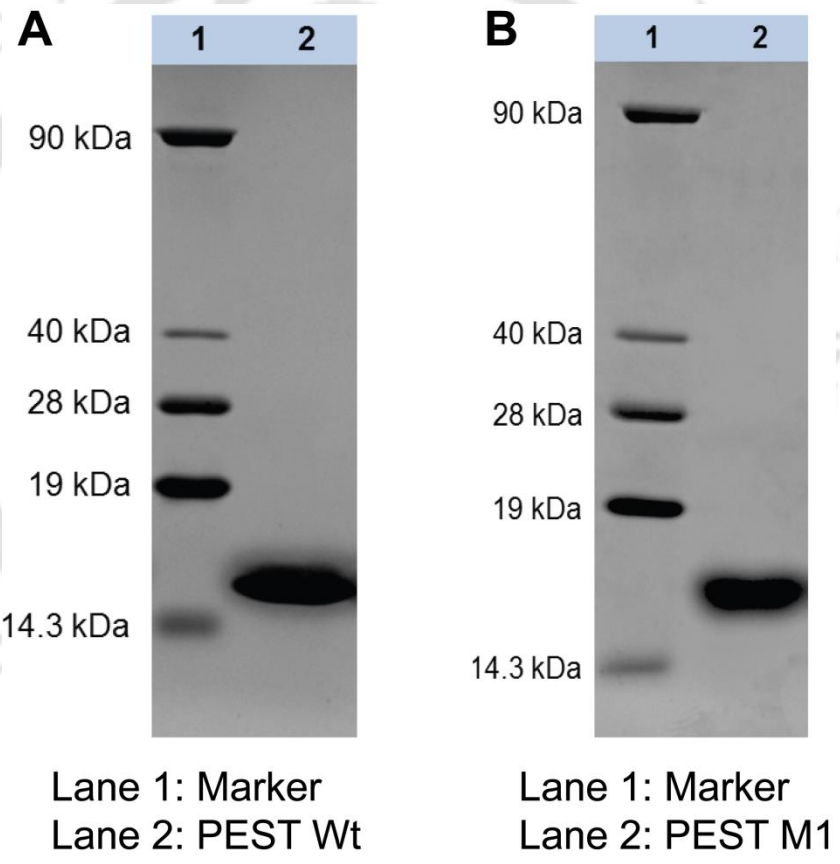

Figure 3.2.3: 15% Reducing SDS-PAGE showing a single band of purified proteins for **[A]** PEST Wt and **[B]** PEST M1.

3.2.4 Mass spectrometry analysis of PEST Wt and M1

Purified PEST Wt and M1 were further analyzed by mass spectrometry to ascertain the identity and purity of purified proteins. Figure 3.2.4A and B display the mass spectra of PEST Wt and M1. Table 3.2.4 display the comparison of PEST Wt and PEST M1 actual Molecular Weight (MW) determined by mass spectrometry with their calculated MW. The MW of PEST Wt and M1 determined by mass spectrometry was 8341.10 and 8525.04 Da, respectively. The actual MW of PEST fragment obtained by mass spectrometry is nearly same as MW calculated from PEST sequence.

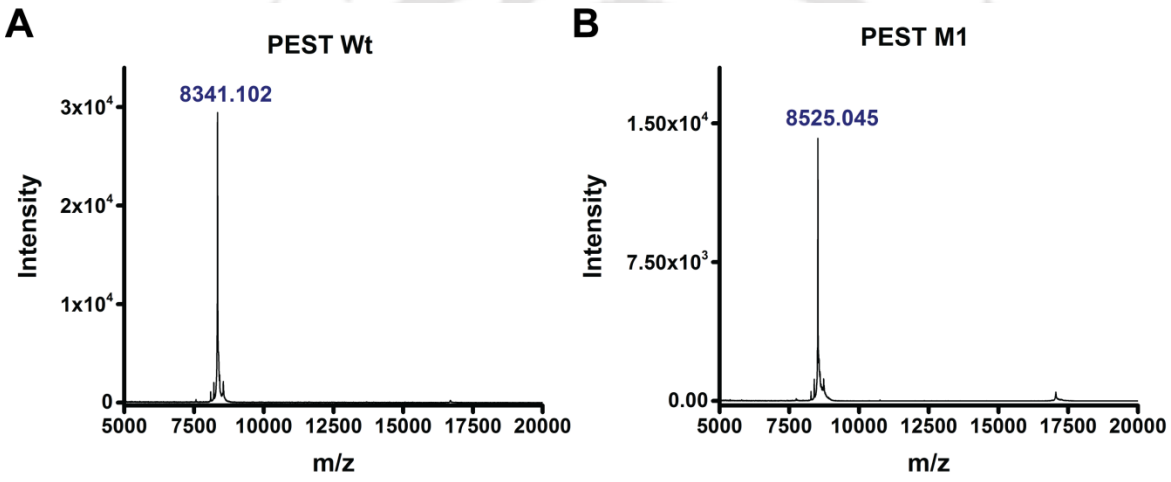

Figure 3.2.4: Mass spectra of **[A]** PEST Wt and **[B]** PEST M1 under reducing condition. The mass calculated from sequence were 8341.61 and 8527.82 Da.

Table 3.2.4: Comparison of PEST fragments molecular weight determined by mass spectrometry with their calculated molecular weight.

Protein name	Observed MW (Da)	Expected MW (Da)
PEST Wt	8341.10	8341.61
PEST M1	8525.05	8527.82

3.2.5 Anomalous SDS-PAGE mobility and heat resistance

Both PEST Wt and M1 display an anomalous behaviour on SDS-PAGE and show slower migration with apparent MW of around 15 kDa (the exact MW confirmed by mass spectrometry is around 8.34 and 8.52 kDa for PEST Wt and M1, respectively). This anomalous mobility arises due to enrichment of negatively charged amino acids in PEST fragment and has been observed in many IDPs (Tompa, 2002). MW of IDPs determined by SDS-PAGE are overestimated by 1.2 to 1.8 times higher than their actual MW, as IDPs bind less with SDS because of high amount of charged amino acids (Tompa, 2002). This 1.8 fold increase in MW of PEST fragment, determined by SDS-PAGE is another indication of intrinsically disordered nature of PEST fragments (Figure 3.2.5).

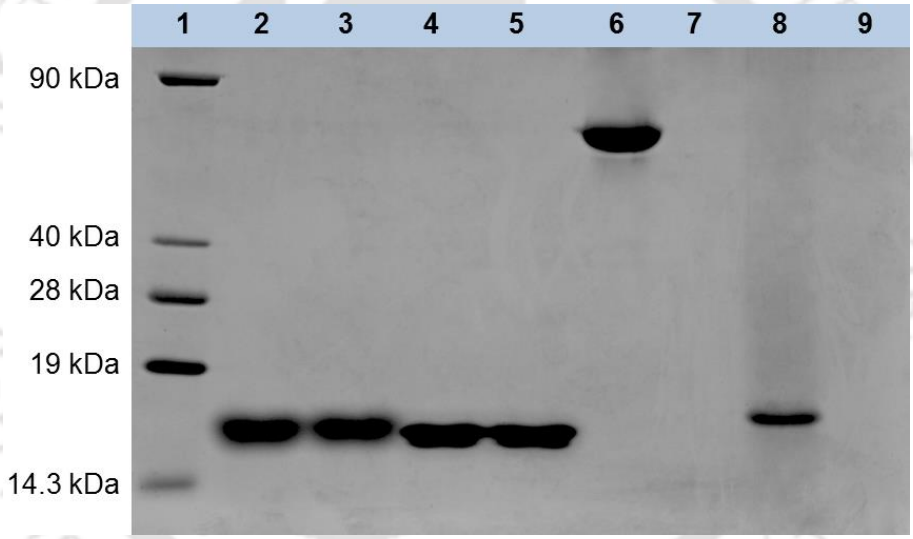

Lane 1: Marker
Lane 2: PEST M1 before boiling
Lane 3: PEST M1 after boiling at 100°C for 10 min.
Lane 4: PEST Wt before boiling
Lane 5: PEST Wt after boiling at 100°C for 10 min.
Lane 6: BSA before boiling
Lane 7: BSA after boiling at 100°C for 10 min.
Lane 8: Soybean trypsin inhibitor before boiling
Lane 9: Soybean trypsin inhibitor after boiling at 100°C for 10 min.

Figure 3.2.5: 15% reducing SDS-PAGE showing anomalous mobility and heat resistance of PEST Wt and PEST M1.

Further, to check the heat resistance properties of PEST fragment, PEST Wt, PEST M1, BSA and soybean trypsin inhibitor were boiled at 100 °C for 10 minutes. After boiling all samples were centrifuged at 12000 rpm for 15 minutes and collected supernatant subsequently loaded on reducing SDS-PAGE. Lane 3 and 5 of Figure 3.2.5 display band of PEST Wt and M1, respectively after boiling. However, the band of BSA and soybean trypsin inhibitor disappears upon boiling in lane 7 and 9, respectively. Hence, both PEST Wt and M1 did not precipitate upon boiling due to enrichment of charged amino acid and low hydrophobicity. While, BSA and soybean trypsin inhibitor (ordered proteins) formed precipitates as their hydrophobic patches exposed, resulting in aggregates at elevated temperature. Survival of proteins at higher temperature has been reported in several IDPs and has been used to purify the recombinant IDPs (Kalthoff, 2003) . Both PEST Wt and M1 remain soluble upon boiling, this behavior points towards their intrinsic disordered nature.

3.2.6 Determination of molecular weight and Stokes radius of PEST fragment by size exclusion chromatography

Size exclusion chromatography of PEST Wt and M1 was performed (using 120 mL GE Healthcare Hiload 200 pg column with fraction limits of 10-600 kDa) to infer their hydrodynamic properties. Elution volume of proteins from gel filtration column was monitored as it depends upon size and shape (folded or extended) of the molecules. To calculate the Molecular Weight (MW) of PEST fragment, standards of known MW was analysed first. The standard proteins: alcohol dehydrogenase (150 kDa), albumin bovine serum (66 kDa), carbonic anhydrase (29 kDa), and hen egg-white lysozyme (14.3 kDa) were eluted with elution volumes of 67.15, 74.61, 87.41 and 102.99 mL, respectively. Further, void volume of column was determined by running blue dextran (2,000 kDa) through the column and calculated void volume was 45.34 mL (Figure 3.2.6A). Figure 3.2.6B shows the elution profile of PEST Wt and M1 and single elution peak clearly show that PEST fragment is highly pure. The PEST Wt and M1 were eluted with elution volume of 82.99 and 83.5 mL, respectively. To determine the MW of PEST Wt and PEST M1, standard curve was plotted between partition coefficient (K_{av}) (calculated using equation 2.65) and logarithmic molecular weight of relative standard proteins (Figure 3.2.6C).

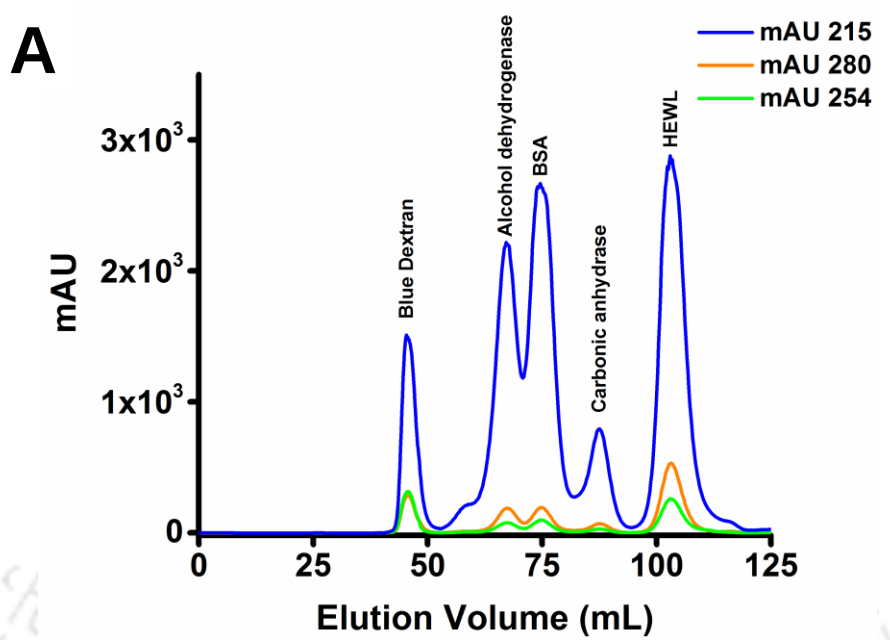

Figure 3.2.6A: Size exclusion chromatography elution profile of standard proteins and blue dextran (used to determined void volume of column) monitored at 215, 254 and 280 nm. All samples were elutes in buffer (25 mM Tris.HCl (pH 7.4); 25 mM NaCl) at room temperature.

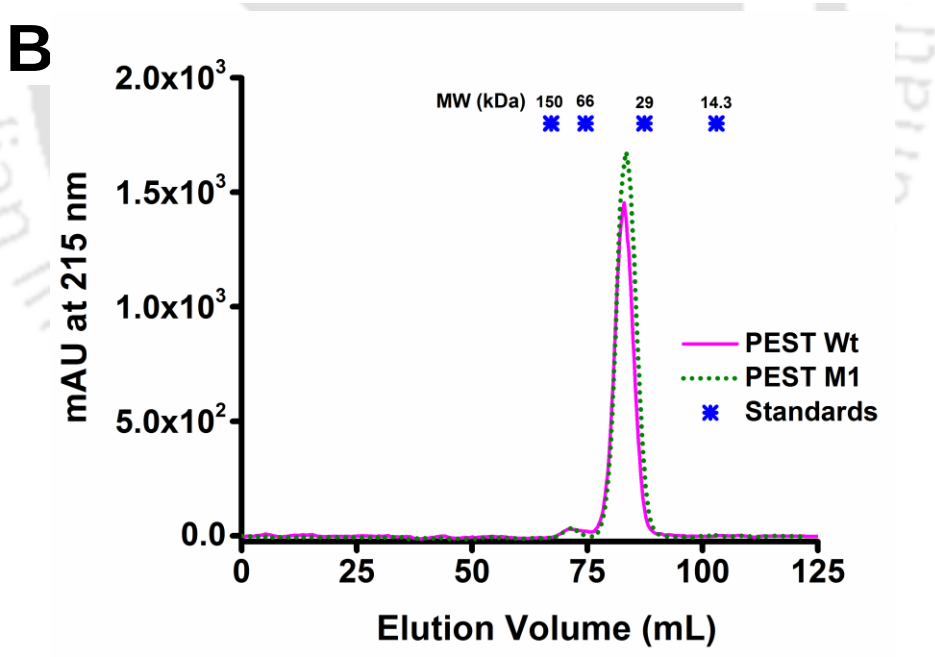

Figure 3.2.6B: Size exclusion chromatography elution profile of PEST Wt and M1, monitored at 215 nm. Both PEST Wt and M1 were eluted with elution buffer (25 mM Tris.HCl (pH 7.4); 25 mM NaCl; 6 mM DTT) at room temperature. Asterisks represent the elution positions of standards.

The apparent MW of PEST Wt and M1 calculated from size exclusion chromatography are shown in Table 3.2.6A. The apparent MW weight was about 5.5 fold higher than its actual MW (determined by mass spectrometry). This increase in apparent MW indicates that PEST fragments do not have compact or globular structure. In IDPs, it has been established that compact molten globule-type protein shows 2 times higher apparent MW, whereas random coil type protein shows 4-6 fold increase in apparent MW from their real value (Csizmok et al., 2006). Hence, a 5.5 fold increase in apparent MW of PEST Wt and M1 hints that PEST fragment may have a random coil type structure.

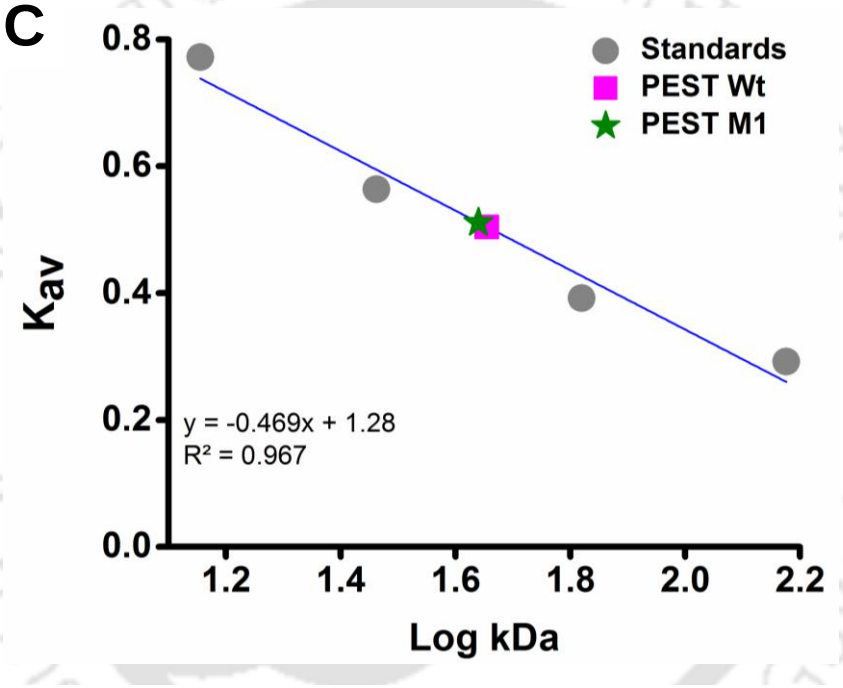

Figure 3.2.6C: Standard curve (partition coefficient (K_{av}) vs. logarithm molecular weight of standard proteins) for calculating the molecular weight of PEST fragments.

Table 3.2.6A: Molecular weight of PEST fragments determined by size exclusion chromatography.

Protein name	Apparent MW (kDa)
PEST Wt	46.54 [1.22][a]
PEST M1	45.98 [2.05]

[a] The numbers in square brackets indicates the standard deviation for n=2—3.

Further, to gain insight about other hydrodynamic behavior, Stokes radius (R_s) of PEST fragment was determined. To calculate the Stokes radius of PEST Wt and M1, standards of known Stokes radii was run from the column and their elution volume was recorded. The standard proteins: alcohol dehydrogenase (R_s = 4.6 nm), albumin bovine serum (R_s = 3.39 nm), carbonic anhydrase (R_s = 2.36 nm), and hen egg-white lysozyme (R_s = 2.0 nm) were eluted with elution volume of 67.15, 74.61, 87.41 and 102.99 mL, respectively (Figure 3.2.6A). Standard curve was plotted between $(-\text{Log } K_{av})^{1/2}$ and Stokes radii of standard proteins to determine Stokes radii of PEST Wt and M1 (Figure 3.2.6D). The observed Stokes radii of PEST Wt and M1 are displayed in Table 3.2.6B. Large value of Stokes radius in comparison to polypeptide chain length reveals a swollen extended coil-like structure for PEST fragments.

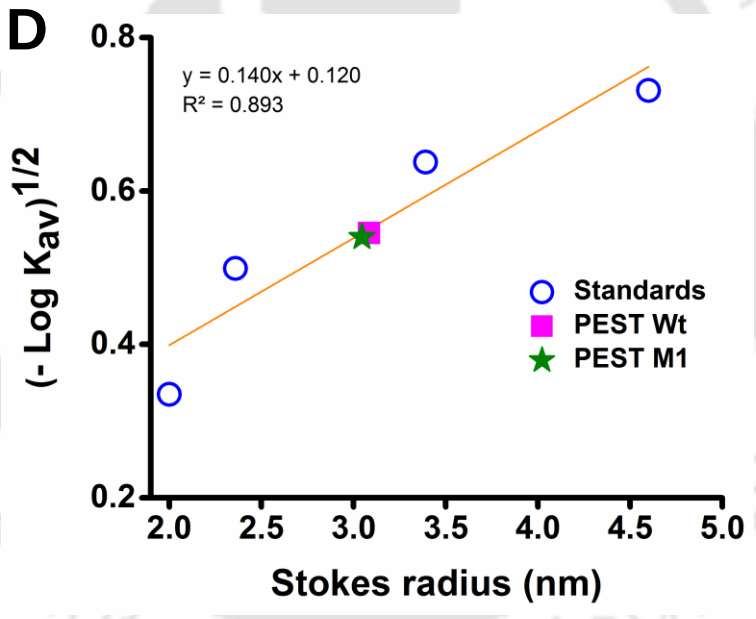

Figure 3.2.6D: Standard curve ($(-\text{Log } K_{av})^{1/2}$ vs. Stokes radii of standard proteins) for calculating the Stokes radii of PEST fragments.

Table 3.2.6B: The Stokes radii of PEST Wt and M1 determined by size exclusion chromatography.

Protein name	Stokes radius (nm)
PEST Wt	3.11 [0.03][a]
PEST M1	3.10 [0.05]

[a] The numbers in square brackets indicates the standard deviation for n=2—3.

3.2.7 Dynamic light scattering measurements of PEST fragment

In view to further validate the calculated Stokes radius of PEST Wt and M1 by size exclusion chromatography, Dynamic Light Scattering (DLS) studies were carried out. Advantage of carrying out DLS study is that it directly determines the Stokes radius while size exclusion chromatography provides only an estimation of the Stokes radius. Figure 3.2.7A shows the size (diameter in nm) of PEST Wt and M1. The Stokes radius of PEST Wt and M1 determined by DLS are presented in Table 3.2.7. Figure 3.2.7B display correlation coefficient of PEST Wt and M1. Fine overlapping of correlation coefficient between PEST Wt and M1; also suggest that both have similar hydrodynamic radii although PEST M1 has one extra tryptophan. The value of Stokes radius calculated by size exclusion chromatography agrees well with value calculated by DLS measurements.

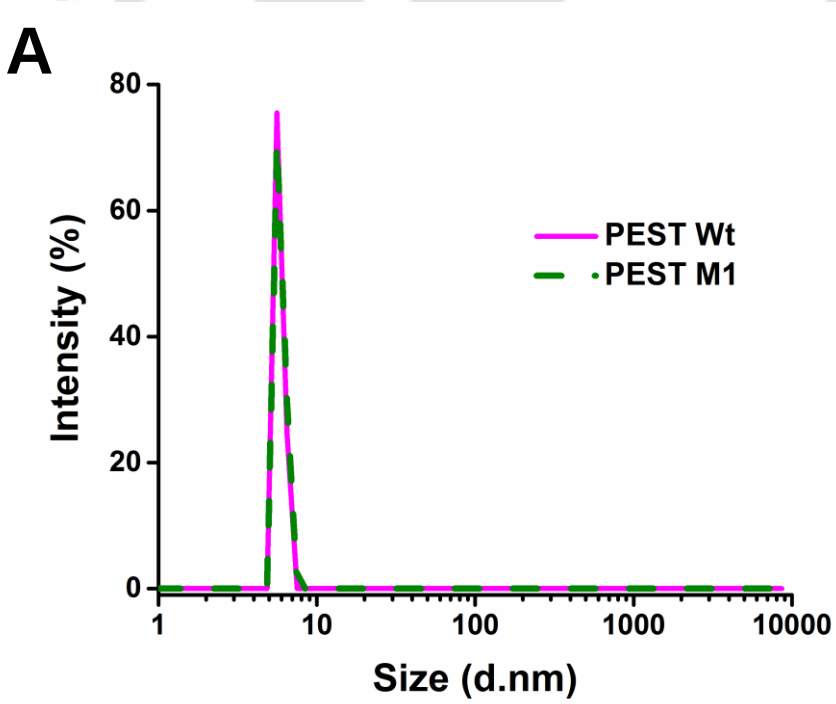

Figure 3.2.7A: Hydrodynamic diameter of 1.5 mg/mL PEST Wt and M1 dissolved in 25 mM Tris.HCl (pH 7.4); 25 mM NaCl; 1 mM Tris (2-carboxyethyl) phosphine.HCl (TCEP) at room temperature.

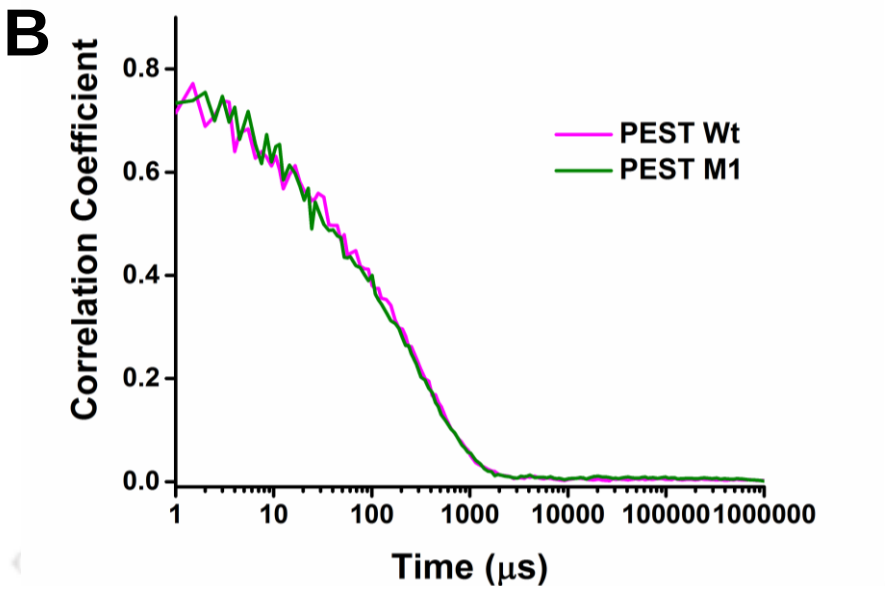

Figure 3.2.7B: Correlation coefficient of PEST Wt and M1 at room temperature. Y-axis denotes correlation function as g (τ) whereas X-axis represents delay time, τ in μs.

Table 3.2.7: The Stokes radii of PEST Wt and M1 determined by dynamic light scattering.

Protein name	Stokes radius (nm)
PEST Wt	3.14 [0.21][a]
PEST M1	3.13 [0.19]

[a] The numbers in square brackets indicates the standard deviation for n=2—3.

3.2.8 Absorption spectra of PEST Wt and M1

The absorption spectra of purified PEST Wt and PEST M1 were recorded to ascertain their identity and purity, spectroscopically. Figure 3.2.8 depicts the absorption spectra of PEST Wt and PEST M1. The PEST Wt contains a single phenylalanine residue and displays a distinct weak absorption profile of phenylalanine. However, the presence of tryptophan in PEST M1 confirmed as it show a distinct strong absorption profile of tryptophan and mask the weak absorption of phenylalanine.

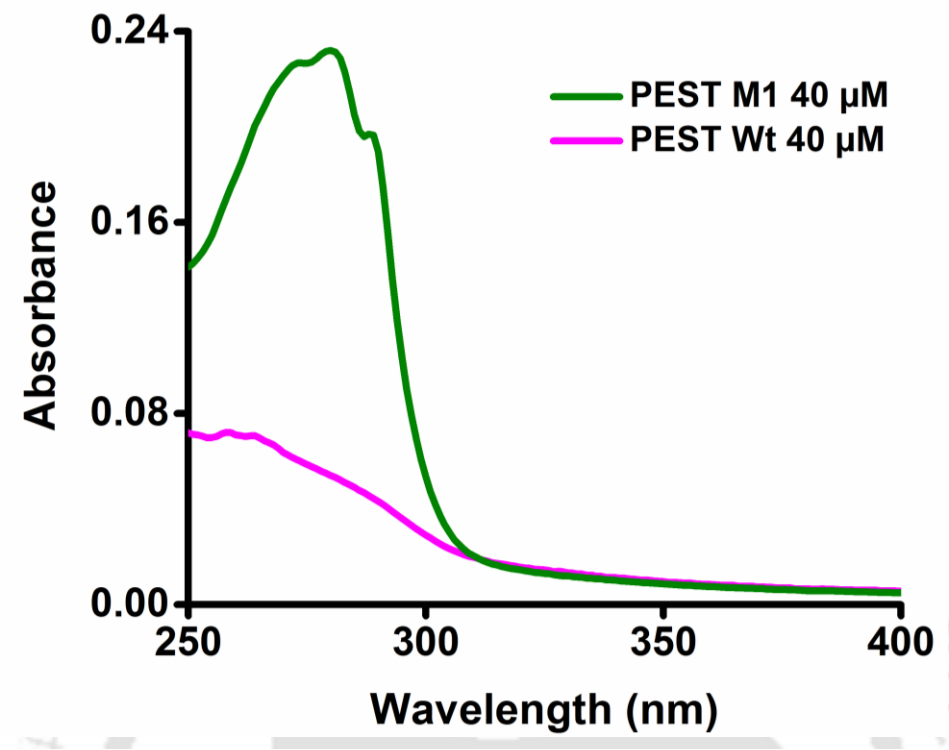

Figure 3.2.8: Absorption spectra of 40 µM c-Myc PEST Wt and its tryptophan mutant PEST M1 dissolved in 25 mM Tris.HCl (pH 7.4) buffer, containing 5 mM TCEP.

3.2.9 Steady state fluorescence and anisotropy analysis of PEST M1

The tryptophan fluorescence has been widely used to study the structure and dynamics of IDPs due to its spectral sensitivity towards the local environment (Beechem and Brand, 1985; Brand and Gohlke, 1972; Jeganathan et al., 2006; Szilvay et al., 2009; Tompa, 2010; Weber, 1952). Tryptophan fluorescence emission shows blue shift when it is buried inside the hydrophobic core of protein and red shifted when it exposed to the aqueous solvent (Lakowicz, 2006; Schmid, 1989). The steady state fluorescence measurements of PEST M1 tryptophan was carried out at pH 7.4 to explore environment around its indole ring. The emission spectra were collected by exciting the samples at 295 nm. Figure 3.2.9 depicts the steady state fluorescence spectra of PEST M1 tryptophan along with a tryptophan derivative known as NATA (N-acetyl tryptophan amide). The observed fluorescence emission spectra of PEST M1 tryptophan display its emission maxima at 346 nm whereas, NATA shows emission maxima at 350 nm, as expected for indole ring that is fully exposed

to aqueous solvent. The maximum fluorescence intensity of PEST M1 at 346 nm clearly suggests predominant exposure of tryptophan to the aqueous solvent.

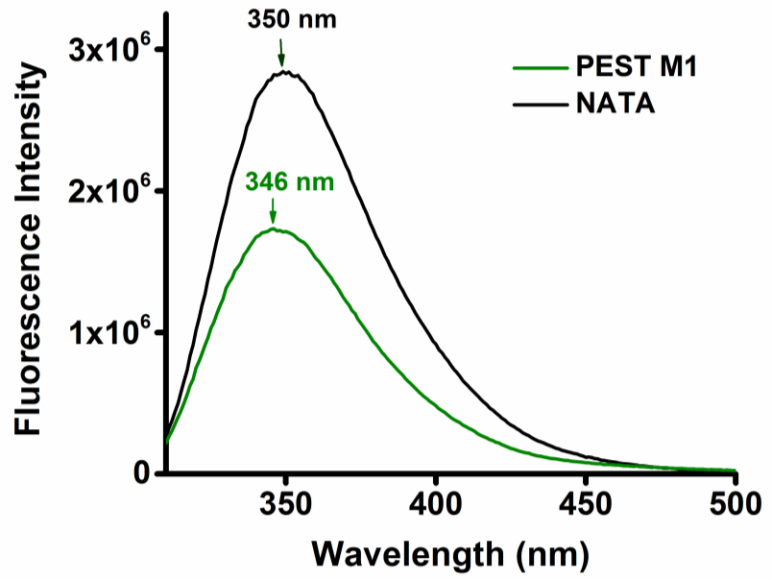

Figure 3.2.9: Steady state fluorescence spectra of 20 µM PEST M1 containing one tryptophan and NATA dissolved in 25 mM Tris.HCl (pH 7.4) buffer, containing 5 mM TCEP. Samples were excited at 295 nm (slit width = 1 nm) and emission was collected with slit width 5 nm.

Further, to gain the information about the structure and rotational dynamics of PEST M1, steady state fluorescence anisotropy (r_{ss}) of its tryptophan was analyzed at room temperature. The steady state anisotropy (r_{ss}) is an excellent technique to investigate rotational dynamics of fluorophore. The steady state anisotropy (r_{ss}) gives the information about the rotational freedom and dynamics of fluorophore in the excited state (Steiner, 1991). The measured anisotropy value of PEST M1 tryptophan (shown in Table 3.2.9), suggests very fast rotation of PEST tryptophan as it can rotate more freely. Very fast rotation of PEST M1 tryptophan and its exposure to aqueous solvent clearly hints at open and loose structure of PEST M1 in the vicinity of tryptophan.

Table 3.2.9: Steady state fluorescence anisotropy of NATA and PEST M1 tryptophan.

Sample	Steady state anisotropy (r_{ss})
NATA	0.004 [0.002][a]
PEST M1	0.054 [0.004]

[a] The numbers in square brackets indicates the standard deviation for n=2—3.

3.2.10 Fluorescence lifetime and time-resolved anisotropy of PEST M1

To extract structural information of PEST M1, nanosecond time-resolved fluorescence lifetime (τ) of its tryptophan was monitored. The fluorescence lifetime is measure of average amount of the time a fluorophore stays in its excited state before returning to ground state. Figure 3.2.10A display the time-resolved fluorescence intensity decay profile of PEST M1 tryptophan in pH 7.4 buffer at room temperature. The lifetime values of PEST M1 tryptophan obtained after fitting the intensity decay profile is given in Table 3.2.10.

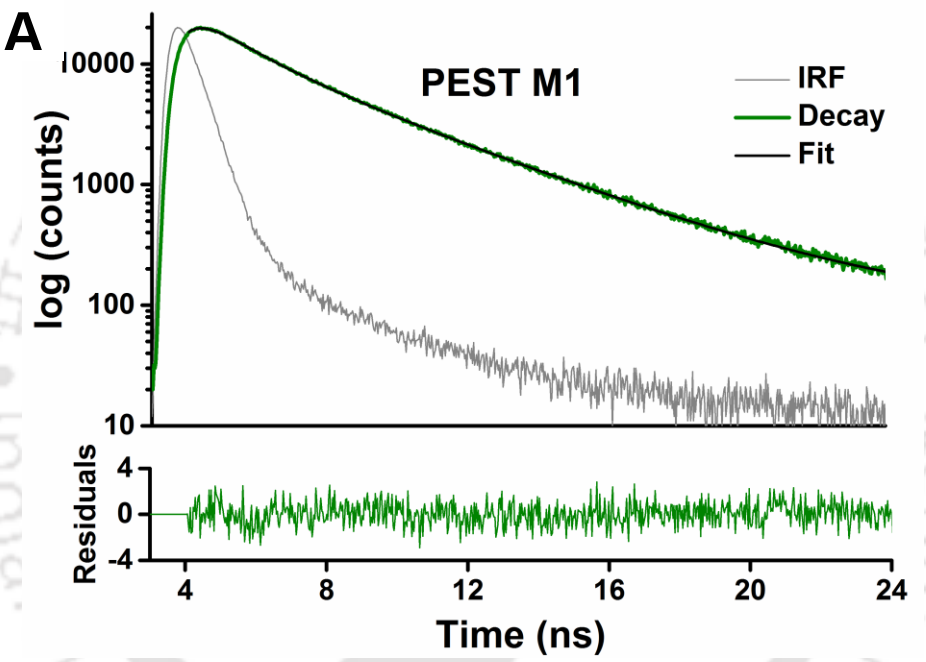

Figure 3.2.10A: Time-resolved fluorescence intensity decay profile (green line in top panel) of 20 μM PEST M1 tryptophan dissolved in 25 mM Tris.HCl (pH 7.4) buffer, containing 5 mM TCEP. Sample was excited using 295 nm DeltaDiode pulsed light source and emission was collected with longpass filter WG320 at magic angle 54.7°. Residual for the fit are shown in bottom panel.

Table 3.2.10: Tryptophan fluorescence lifetime of PEST M1 at pH 7.4.

Sample	$\chi^2_{reduced}$	τ_1 (ns)	α_1	τ_2 (ns)	α_2	Mean lifetime (ns)
PEST M1	1.04	1.46	0.48	4.05	0.52	2.81

The analysis of time-resolved fluorescence decay revealed the presence of two lifetimes. A large component of 4.05 ns with amplitude of 0.52 and a short component of 1.46 ns with amplitude of 0.48 was present. The observed mean fluorescence lifetime of PEST M1 tryptophan was 2.81 ns. The possible origin for two-exponential decay of PEST M1 Trp may be due to presence of Trp rotamers or existence of PEST M1 in two conformation or dynamic processes (including motion of nearby quenching group in protein or spectral relaxation) occurring during the excited-state lifetime.

Further, the time-resolved fluorescence anisotropy decay analysis was performed to calculate rotational correlation time (θ) of tryptophan in PEST M1. Figure 3.2.10B depicts the anisotropy decay profile of PEST M1 in pH 7.4 buffer. The analysis of anisotropy decay profile of PEST M1 reveals two correlation times, a fast correlation time (θ_{fast}) of 0.918 ns with amplitude of 0.759 and a slow correlation time (θ_{slow}) of 6.970 ns with amplitude of 0.241. The fast correlation time (θ_{fast}) measures the local dynamics of tryptophan whereas slow correlation time (θ_{slow}) represents the global motion of PEST M1, arising due to the tumbling of whole PEST fragment in the solution (Steiner, 1991). The dominance of fast correlation time (θ_{fast}) suggests very fast rotation of indole as it is free to rotate due to unfolded structure of PEST M1 in the vicinity of tryptophan. Hence, tryptophan fluorescence measurements reveal that C- terminus of PEST M1 is likely to be disordered.

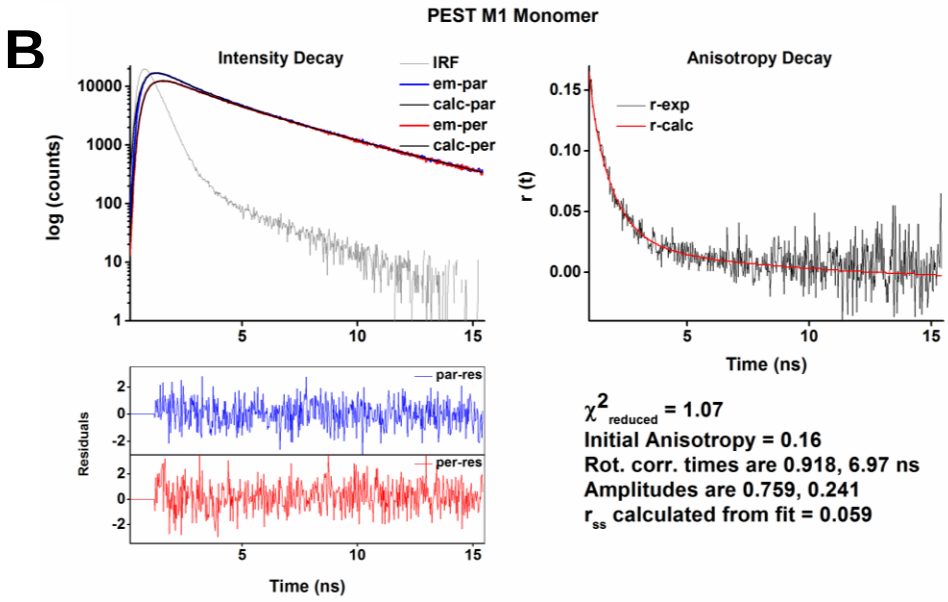

Figure 3.2.10B: Fitted anisotropy decay profile of 20 µM PEST M1 tryptophan. Other conditions are similar to those mentioned in Figure 3.2.10A.

3.2.11 ANS binding assay of PEST Wt and M1

To experimentally confirm the results of hydrophobic cluster analysis (HCA) and charge hydropathy plots, ANS (8-Anilinonaphthalene-1-sulfonic acid) assay of PEST Wt and M1 was carried out. ANS is a non-covalent extrinsic fluorophore, which displays a negligible fluorescence in the water, however its fluorescence dramatically enhances upon binding to hydrophobic patches in the proteins. ANS shows much higher fluorescence intensity in partially folded (molten globule) protein in comparison with fully folded or fully unfolded proteins. This makes ANS, a classic probe to detect the molten globule states of the proteins (Goldberg et al., 1990; Greene et al., 2006; Musci et al., 1985). Figure 3.2.11A and B display the steady state fluorescence spectra of 10 μM ANS with the increasing concentrations (10—50 μM) of PEST Wt and M1, respectively. ANS displays similar fluorescence intensity pattern with both PEST Wt and M1 however, PEST M1 shows slightly higher ANS fluorescence intensity in comparison with PEST Wt. The insignificant increase in fluorescence intensity of ANS with increasing concentration of PEST fragments demonstrated weak binding of ANS due to presence of few hydrophobic patches. This reveals that PEST Wt and PEST M1 have mostly an unfolded structure with very little hydrophobic pockets for ANS to bind.

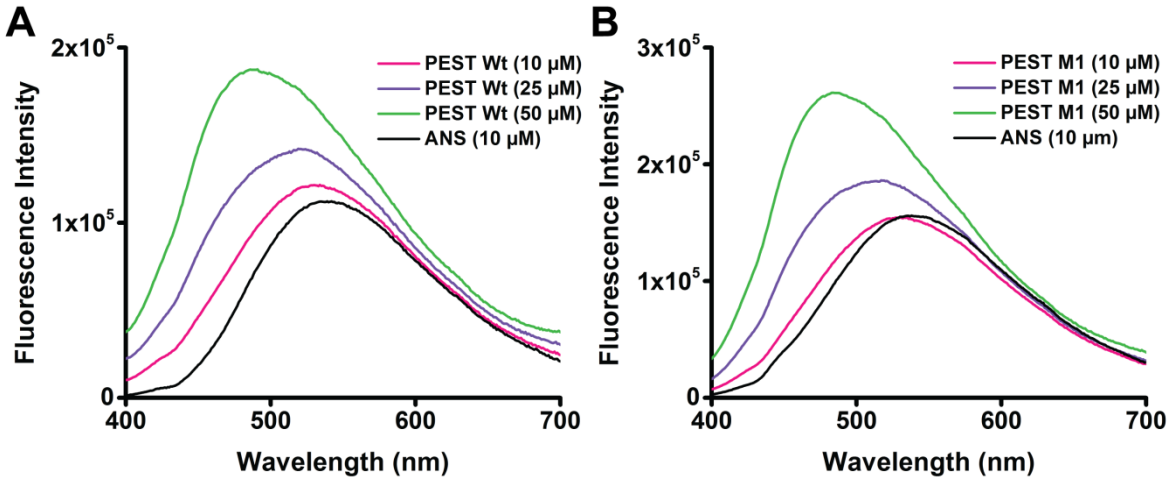

Figure 3.2.11: Fluorescence spectra of 10 μM ANS with 10, 25 and 50 μM of **[A]** PEST Wt and **[B]** PEST M1, dissolved in 25 mM Tris.HCl (pH 7.4) buffer, containing 5 mM TCEP. All samples were excited at 380 nm (slit width = 5 nm) and emission was collected between 400 nm to 700 nm (slit width = 10 nm) at room temperature.

Hence, the result of ANS assay is in agreement with HCA and charge hydropathy plot which also revealed the presence of insignificant population of hydrophobic patches in PEST fragment.

3.2.12 Secondary structure analysis of PEST Wt and M1 by CD

Far-UV Circular Dichroism (CD) spectra of PEST Wt and M1 in the range of 190 to 260 nm were recorded to determine their secondary structure content. Figure 3.2.12A displays the far-UV CD spectra of PEST Wt and M1 in pH 7.4 buffer at room temperature. The PEST Wt and M1 show a negative ellipticity peak at 201 nm; which resembles with the spectrum of disordered proteins. The close overlap in CD spectra of PEST Wt and PEST M1 suggests there is no structural alteration due to incorporation of extra tryptophan in PEST Wt. The CD spectra of PEST Wt and M1 were analyzed using DichroWeb server and CDSSTR program was used to calculate their secondary structure content. The experimental curve was well superimposed on reconstructed curve (fitted CD curves are shown in Figure A1 of appendix). Figure 3.2.12B depicts the secondary structure content in PEST Wt and M1. Both PEST Wt and M1 show highest percentage of unordered content in their secondary structure and clearly point towards the random coil conformation of PEST fragments. This CD analysis further supports the size exclusion chromatography results, which also revealed the presence of random coil structure in PEST fragment.

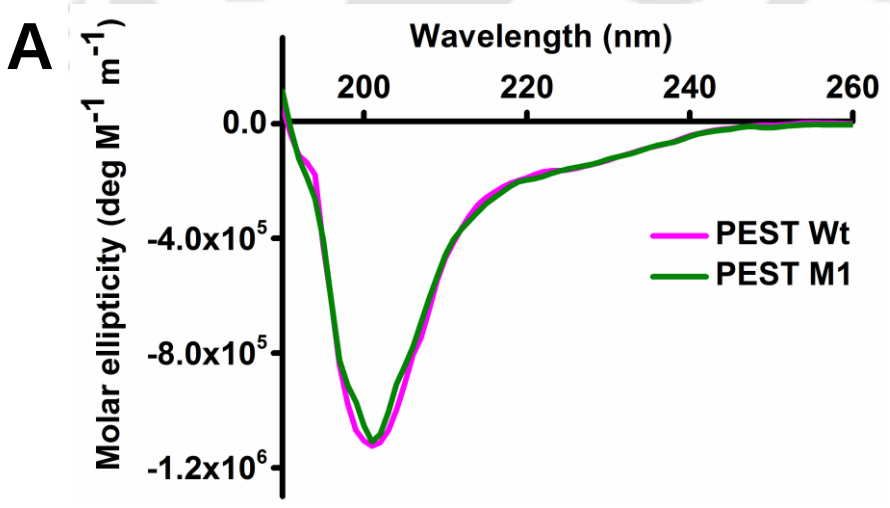

Figure 3.2.12A: Far-UV CD spectra of 20 μM PEST Wt and M1, dissolved in 5 mM sodium phosphate (pH 7.4) buffer, containing 1 mM TCEP recorded at room temperature.

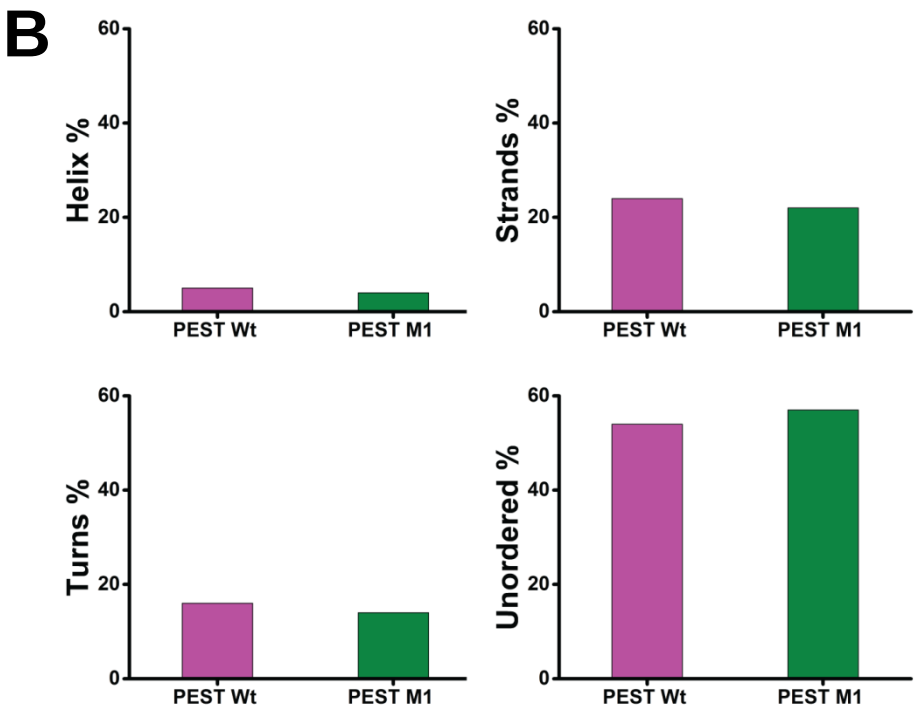

Figure 3.2.12B: Secondary structure content in PEST Wt and PEST M1 at pH 7.4, calculated by CDSSTR program.

3.2.13 Effect of TFE (Trifluoroethanol) on structure of PEST Wt and M1

The another important characteristic of IDPs is to gain its structure upon binding with different metal ions, osmolytes, membranes, macromolecules like- DNA, RNA and proteins (Cortese et al., 2008; Dunker et al., 2008; Dyson and Wright, 2005). In this regard, we examined whether ordered structure can be induced in PEST Wt and M1 in presence of solvent TFE, which mimics the hydrophobic milieu sensed by a protein during protein-protein interaction (Dahlman-Wright and McEwan, 1996; Hua et al., 1998; Sun et al., 2010). To monitor the effect of TFE on structure of PEST Wt and PEST M1, far-UV CD spectra were recorded with increasing concentration of TFE (0-50%). Figure 3.2.13A and B represent the far-UV CD spectra of PEST Wt and M1 with different TFE concentration, respectively. The analysis of CD spectra indicates increase in the negative ellipticity at 222 nm with increasing concentration of TFE (Figure 3.2.13C).

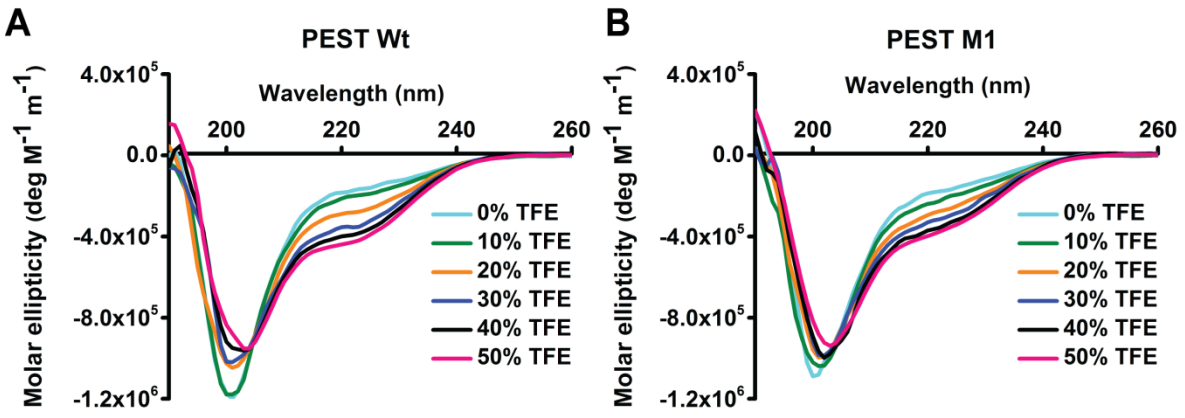

Figure 3.2.13: Effect of TFE on Far-UV CD spectra of 20 µM **[A]** PEST Wt and **[B]** M1 (dissolved in 5 mM Sodium phosphate (pH 7.4) buffer, containing 1 mM TCEP) with the increasing concentration of TFE (10-50% (v/v)). All spectra were recorded at room temperature.

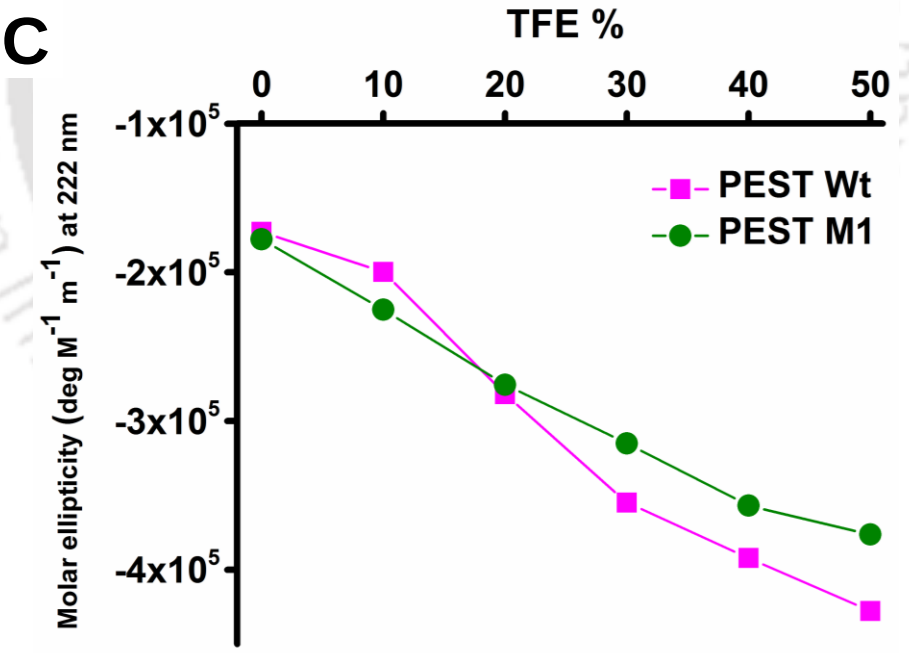

Figure 3.2.13C: Change in the molar ellipticity of PEST Wt and M1 at 222 nm with the increasing concentration of TFE (0-50% (v/v)).

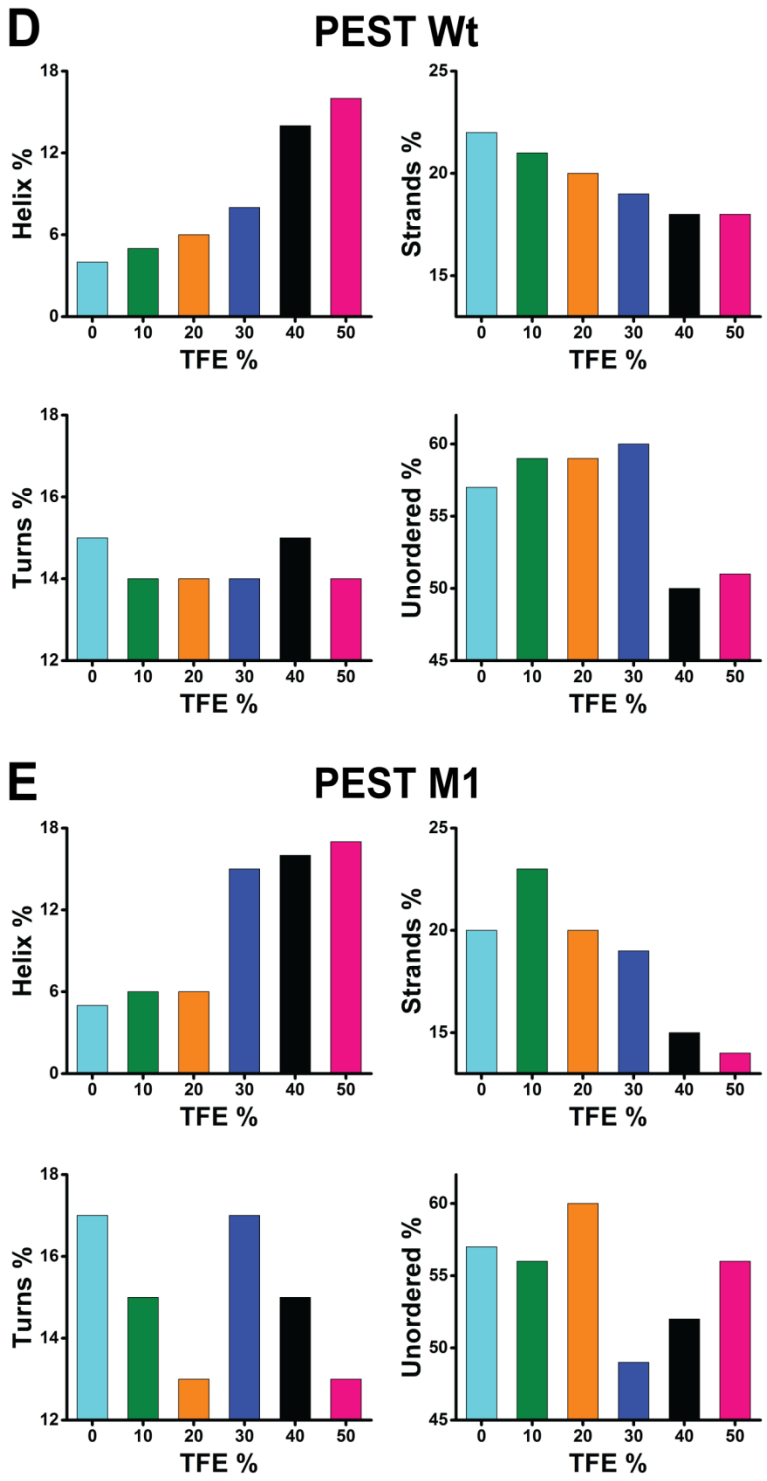

Figure 3.2.13: Change in the secondary structure content in **[D]** PEST Wt and **[E]** PEST M1 with increasing concentration of TFE (0-50%), calculated by CDSSTR program.

The CD spectra of PEST Wt and M1 show similar but not identical behavior with increasing concentration of TFE. PEST Wt depicts higher negative ellipticity at 222 nm in comparison with PEST M1. Figure 3.2.13D and E display the secondary structure content of PEST Wt and M1 with TFE, respectively. A marginal rise in helical content is seen for both PEST Wt and M1 with increase in TFE concentration (0-50%). PEST Wt shows gradual increase in α-helical content with increasing concentration of TFE (0-50%) in comparison with PEST M1, which shows transition in α-helical content between 20-30% TFE concentration. However, both PEST Wt and M1 remain significantly unstructured at 50% TFE. These results clearly demonstrate the increase in the α-helical content of PEST fragments in presence of TFE and also suggest that PEST fragment could fold upon interaction with other proteins.

3.3 Conclusions:

- The amino acid composition profile, charge hydropathy plots and hydrophobic cluster analysis demonstrate that both PEST Wt and PEST M1 are highly disordered and have low hydrophobicity.
- Anomalous mobility on SDS PAGE and heat resistance indicates disorderedness in PEST fragment.
- PEST fragment shows about 5 fold high apparent molecular weight determined by size exclusion chromatography, indicating its random coil structure.
- The fluorescence measurements of PEST M1 indicate free rotation and solvent exposure of its tryptophan due to unfolded structure at the C-terminus.
- The minor increase in ANS fluorescence intensity show presence of insignificant hydrophobic patches in PEST fragment.
- The secondary structure analysis of PEST fragment by circular dichroism reveals its random coil structure.
- About 3.5 fold increases in α-helical content with 50% of TFE, demonstrate folding of PEST fragment and suggest possibility of its interaction with binding partners.

Chapter 4

Effect of pH and salt on structure and dynamics of human c-Myc PEST fragment and its mutant

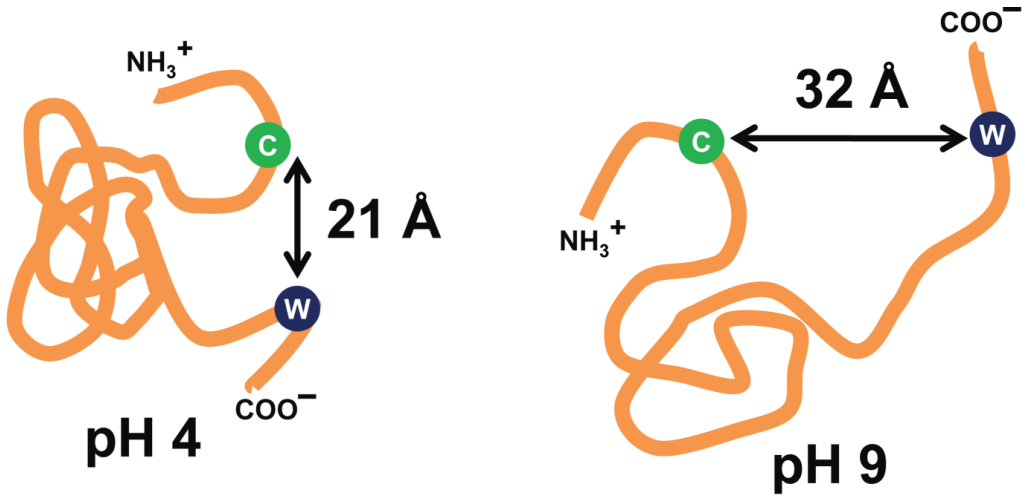

4.1 Introduction:

Intrinsically Disordered Proteins (IDPs)/ Intrinsically Disordered Regions (IDRs) are highly sensitive to change in their milieu. This is because of IDPs/ IDRs have shallow energy landscapes with multiple local minima without any global energy minimum contrary to typical ordered proteins which possess global minima. Each local minimum in their energy landscape arises from different parts of an IDP and each minimum reacts to environmental changes in its own manner. Thus, the heterogeneity and the complexity of the energy landscape define fuzziness of IDPs, where the intrinsic disorderness is preserved even in the bound conformation by some domains/regions in the protein (Uversky, 2013b).

Extreme change in pH usually causes denaturation of ordered proteins but IDPs show resistance to extreme pH. IDPs undergo folding on decrease or increase in the pH due to minimization of high net charge localized on their side chains at neutral pH. This charge minimization causes decrease in electrostatic repulsion and allows hydrophobic driven folding of IDPs (Johansson et al., 1998; Konno et al., 1997; Lynn et al., 1999; Uversky, 2009; Uversky et al., 1999). Addition of excess salt counter ions stabilize the charge localized on the amino acid side chains of IDPs and reduced the strong electrostatic repulsion between the same charges. This has been established that many IDPs show disorder to order transitions on binding with oppositely charged ions (Fink et al., 1994; Goto et al., 1990; Uversky et al., 2001b).

In this chapter we report the effect of pH and excess salt (NaCl) on the structure of human c-Myc PEST fragment. To monitor the effect of pH and salt (NaCl) on structure and dynamics of PEST M1; steady state fluorescence emission, fluorescence anisotropy, fluorescence lifetime and time-resolved fluorescence anisotropy measurements of its single tryptophan^{70} (residue 70, present at C-terminus end) was carried out. To extract the information of PEST M1 tryptophan accessibility at different pH, fluorescence quenching experiment was done. Further, to gain structural information about N-terminus of PEST Wt and PEST M1 at various pH, steady state and time-resolved fluorescence of dansyl probe (labeled with single cysteine) was measured. Finally, to analyze overall structural changes in PEST fragment at different pH (3-11), Förster Resonance Energy Transfer (FRET), ANS

binding assay and Circular Dichroism analysis were carried out. These investigations elucidate the change in structure and dynamics of PEST fragment in presence of extreme pH and high salt concentration (25 mM—500 mM NaCl).

4.2 Results and Discussion:

4.2.1 Steady state fluorescence intensity and fluorescence anisotropy studies of PEST M1 tryptophan

To investigate the effect of pH on structure and dynamics of PEST M1, intrinsic fluorescence of its single tryptophan[70] (residue 70, present at C-terminus) was monitored. Fluorescence emission and steady state fluorescence anisotropy (r_{ss}) of PEST M1 tryptophan was recorded at different pH (3-11), to extract the information about environment around indole ring and its rotational dynamics at various pH. Fluorescence

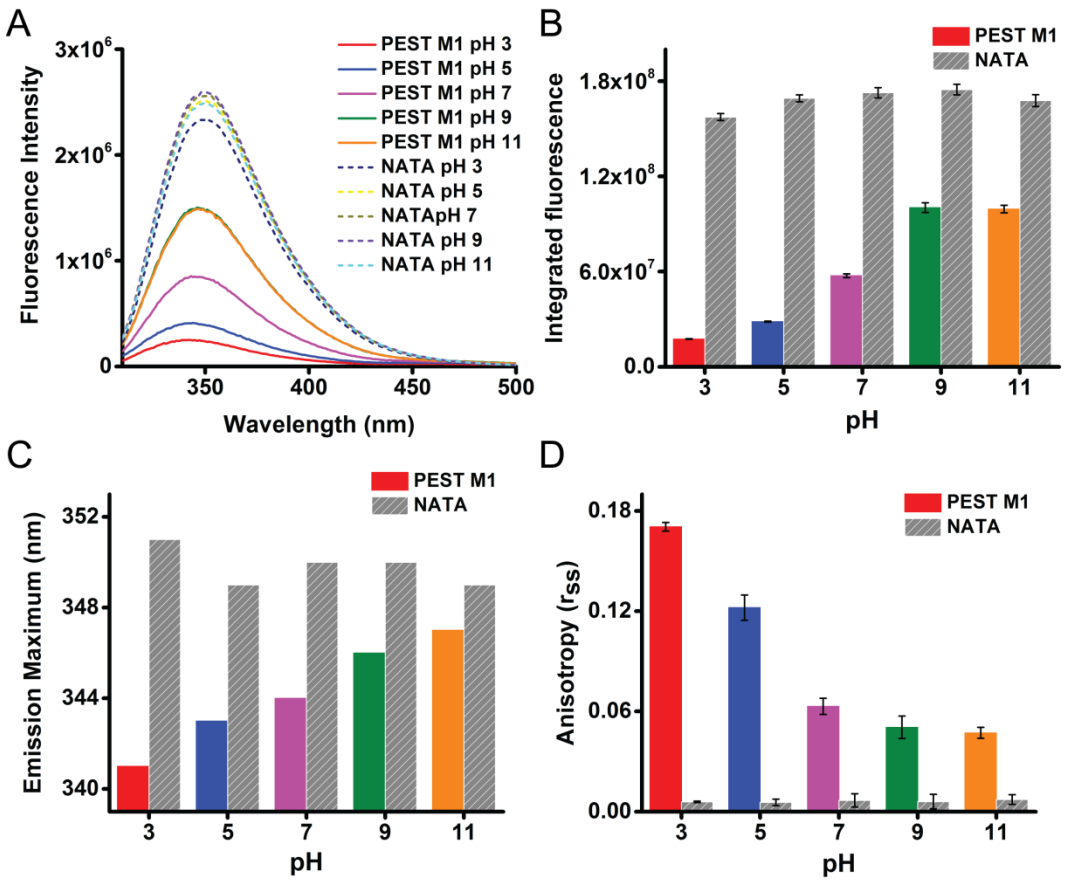

Figure 4.2.1: Effect of pH on steady state fluorescence and fluorescence anisotropy of 20 μM PEST M1 and 20 μM NATA dissolved in different 25 mM buffers (pH 3-11), containing **25 mM NaCl** and 5 mM TCEP. **[A]** Steady state fluorescence spectra; **[B]** integrated fluorescence yield; **[C]** fluorescence emission maxima and **[D]** steady state anisotropy of PEST M1 tryptophan and NATA at different pH.

emission spectra of PEST M1 at different pH (3-11) were collected by exciting the samples at 295 nm. Figure 4.2.1A shows the emission spectra of PEST M1 tryptophan and its derivative known as NATA (N-acetyl tryptophan amide) at different pH (3-11) in presence of 25 mM NaCl. The integrated fluorescence intensity of PEST M1 tryptophan decreases gradually from alkaline pH (11) to the acidic pH (3) (Figure 4.4.1B). The fluorescence emission spectra of PEST M1 tryptophan shows a progressive blue shift in its emission maxima (347 nm to 341 nm) from pH 11 to pH 3 (Figure 4.2.1C). The observed fluorescence emission spectra of NATA display negligible change at different pH (3-11) as it is fully exposed to solvent. The decrease in the tryptophan fluorescence intensity and blue shift in its emission maxima hints that tryptophan of PEST M1 is buried inside the protein core at acidic pH. Figure 4.2.1D depicts the steady state anisotropy (r_{ss}) of PEST M1 tryptophan and NATA at different pH (3-11) in presence of 25 mM NaCl. Substantial increase was observed in the r_{ss} of PEST M1 tryptophan when moving from pH 11 to pH 3. Change in the anisotropy of NATA was insignificant at different pH (3-11). An increase in the anisotropy at acidic pH may be due to hindrance of tryptophan rotation as it buried inside the protein at pH 3. Blue shift in the emission maxima and increase in the r_{ss} value indicates local folding of PEST M1 at acidic pH in the vicinity of tryptophan.

Next, we investigated the effect of pH on structure of PEST M1 in presence of excess salt (250 mM NaCl). Excess salt was used to study involvement of electrostatic interaction in the folding of PEST at lower pH. The charge localized on the side chains of amino acids will be stabilized by introducing excess salt counter ions and could influence the folding of PEST in acidic pH. Steady state fluorescence and anisotropy of PEST M1 tryptophan was monitored to study the effect of pH on its structure and dynamics in presence of excess salt. Figure 4.2.1E, F, G and H depicts the fluorescence spectra, integrated fluorescence yield, fluorescence emission maxima and steady state anisotropy of PEST M1 tryptophan and NATA at different pH (3-11) in presence of 250 mM NaCl. The changes observed in the fluorescence spectra, emission maxima and anisotropy of PEST M1 in presence of 250 mM NaCl at different pH (3-11) was similar to the changes observed in presence of 25 mM NaCl. This similar but not identical change in fluorescence spectra and anisotropy of PEST M1 in presence of 250 mM NaCl indicates the involvement of interactions aside from electrostatics in the folding of PEST at acidic pH.

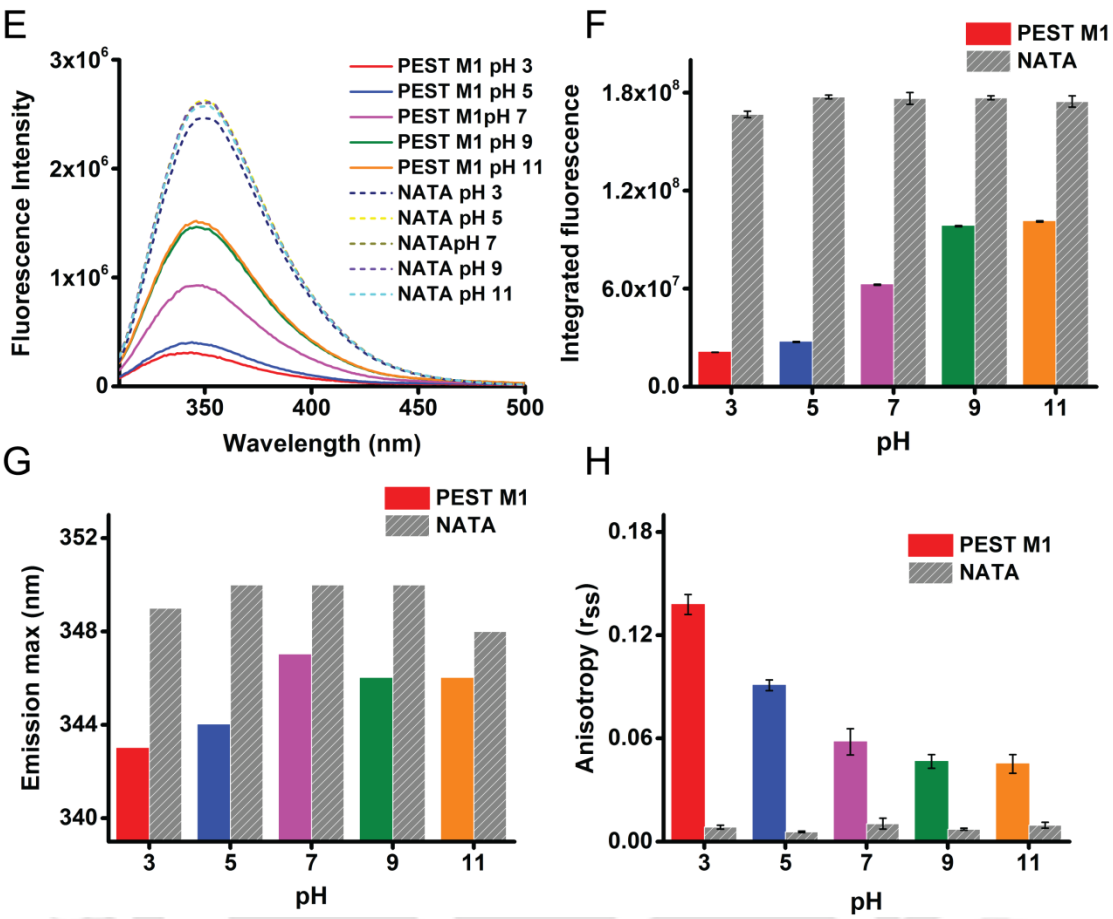

Figure 4.2.1: Effect of pH on steady state fluorescence and fluorescence anisotropy of 20 μM PEST M1 and 20 μM NATA dissolved in different 25 mM buffers (pH 3-11), containing **250 mM NaCl** and 5 mM TCEP. **[E]** Steady state fluorescence spectra; **[F]** integrated fluorescence yield; **[G]** fluorescence emission maxima and **[H]** steady state anisotropy of PEST M1 tryptophan and NATA at different pH.

Further, the fluorescence spectra and anisotropy of PEST M1 tryptophan was monitored in presence of 6 M Gdn.HCl, to completely unfold the PEST fragment at different pH (3-11). Figure 4.2.1I, J, K and L represent the fluorescence spectra, integrated fluorescence yield, fluorescence emission maxima and fluorescence anisotropy of PEST M1 tryptophan and NATA at various pH (3-11) in presence of 6 M Gdn.HCl. In presence of 6 M Gdn.HCl, decrease in fluorescence intensity was minor and change in emission maxima was insignificant at different pH (3-11) as compared with these changes observed in presence of 25 and 250 mM NaCl. The emission λ_{max} of tryptophan ranges from 346-347 nm in comparison to ~343 nm at high salt and ~341 nm at low salt, clearly indicating a more exposed indole ring in presence of 6 M Gdn.HCl. The change in anisotropy values was

marginal in presence of 6 M Gdn.HCl suggesting no major structural alteration occurs in PEST M1 as its tryptophan freely rotates at various pH (3-11) (Figure 4.2.1L). These observations clearly indicate a predominantly unfolded structure of PEST M1 at different pH (3-11) in presence of 6 M Gdn.HCl.

The r_{ss} value depends upon fluorescence lifetime (τ) and rotational correlation time (θ) of the protein. So, change in r_{ss} may be due to change in lifetime of tryptophan or could arise from change in rotational correlation time (θ) of PEST fragment at different pH (3-11). To resolve actual reason, we monitored lifetime of PEST M1 tryptophan at different pH (3-11).

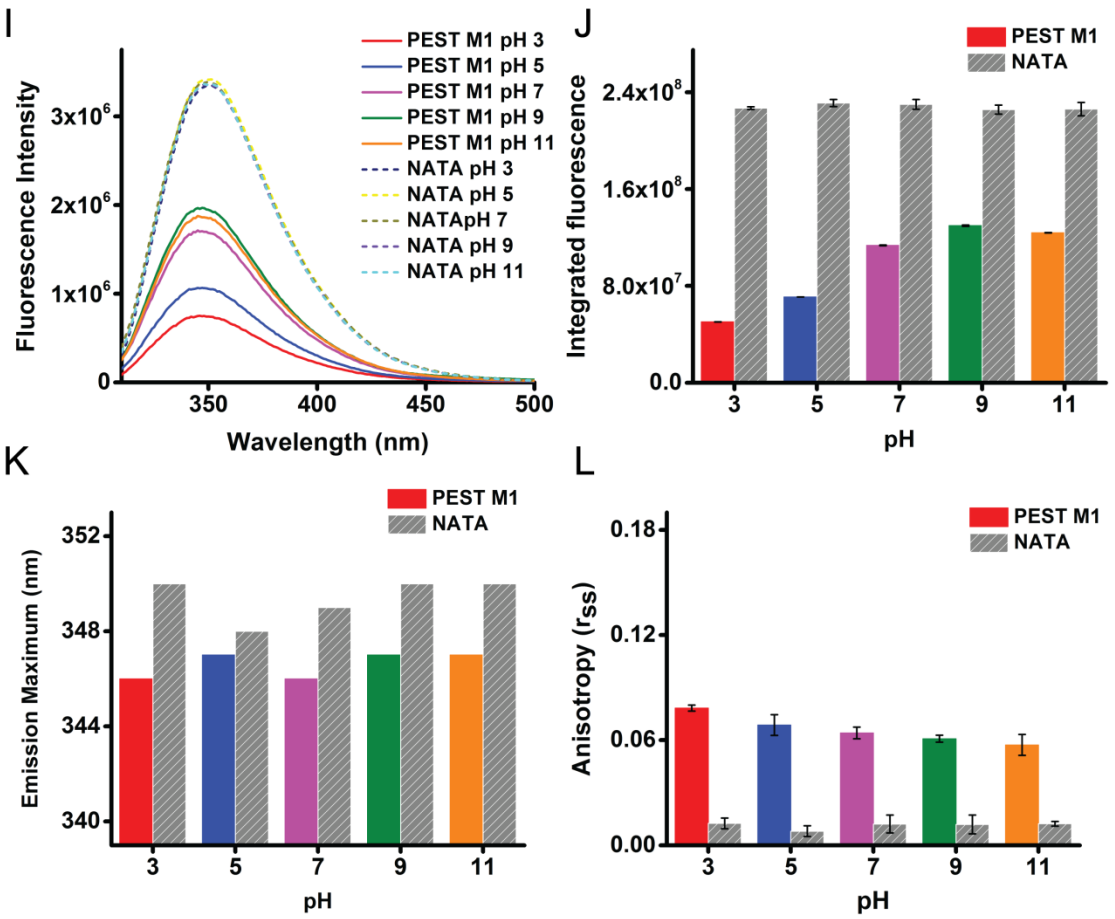

Figure 4.2.1: Effect of pH on steady state fluorescence and anisotropy of 20 µM PEST M1 and 20 µM NATA dissolved in different 25 mM buffers (pH 3-11), containing 25 mM NaCl, **6 M Gdn.HCl** and 5 mM TCEP. **[I]** Steady state fluorescence spectra; **[J]** integrated fluorescence yield; **[K]** fluorescence emission maxima and **[L]** steady state fluorescence anisotropy of PEST M1 tryptophan and NATA at different pH.

4.2.2 Tryptophan fluorescence lifetime analysis of PEST M1

Nanosecond time-resolved fluorescence lifetime (τ) of PEST M1 tryptophan was monitored to analyze the effect of pH (3-11) on its structure. Figure 4.2.2A, B and C display fluorescence intensity decay profile of PEST M1 tryptophan at different pH (3-11) in presence of 25 mM NaCl, 250 mM NaCl and 6 M Gdn.HCl, respectively. Intensity decay in presence of 25 mM NaCl was similar at pH 9 and 11 and gradually increases from pH 9 to 3. Similar trend was observed in intensity decay profile in presence of 250 mM NaCl. However, in presence of 6 M Gdn.HCl intensity decay was same at pH (7, 9 and 11) and minor increase was observed at pH 3 and 5.

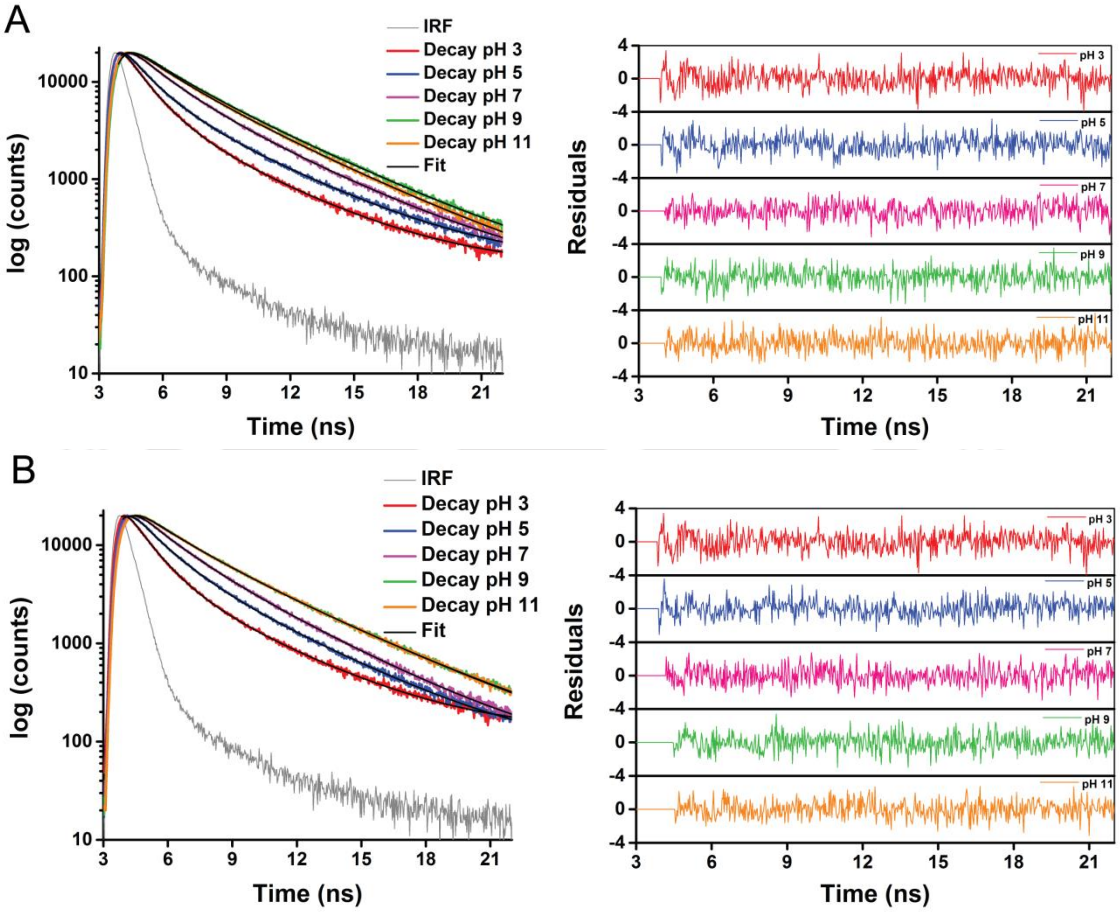

Figure 4.2.2: Fitted time-resolved fluorescence intensity decay profile of 20 µM PEST M1 tryptophan at different pH (3-11) in presence of **[A]** 25 mM NaCl and **[B]** 250 mM NaCl (Left panels). Panels in the right reveal the residual distribution of the fit for each pH condition.

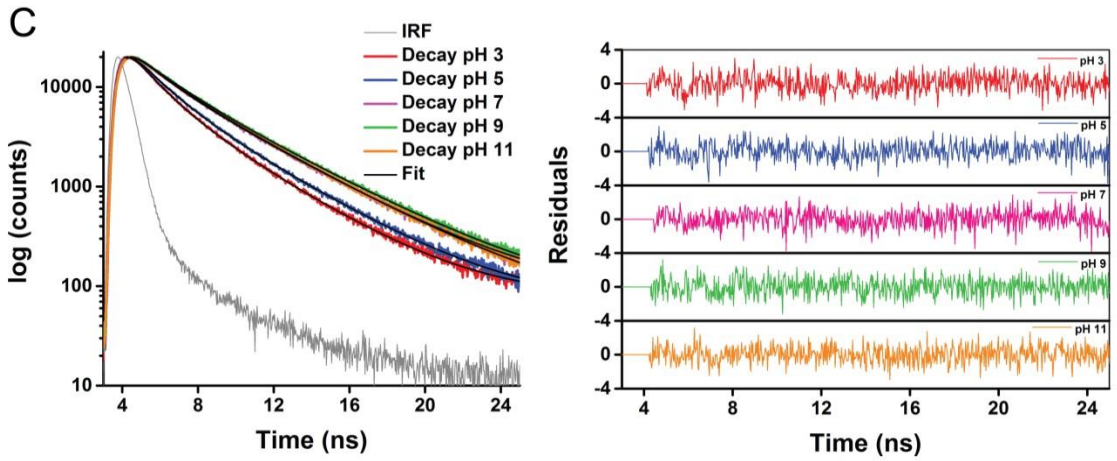

Figure 4.2.2C: Fitted time-resolved fluorescence intensity decay profile of 20 μM PEST M1 tryptophan at different pH (3-11) in presence of 6 M Gdn.HCl (Left panel). Panel in the right reveal the residual distribution of the fit for each pH condition.

Analysis of fluorescence intensity decay of tryptophan at different pH (3-11) shows presence of two lifetimes. A short component of ~2 ns and long component of ~4 ns was present at pH 11 in presence of 25 mM NaCl. Both long and short component values decrease on lowering the pH from 11 to 3. Table 4.2.2A, B and C display the tryptophan lifetime values obtained after fitting the intensity decay profile at different pH (3-11) in presence of 25 mM NaCl, 250 mM NaCl and 6 M Gdn.HCl, respectively.

PEST M1 tryptophan displays a dominant short lifetime component at acidic pH in 25 and 250 mM NaCl. As one moves towards basic pH this lifetime becomes longer while its amplitude decreases, resulting in increased mean lifetime with increasing pH. In presence of 6 M Gdn.HCl, this trend is significantly reduced. It is likely that the short lifetime arises from quenching of tryptophan due to its proximity to a quencher in the polypeptide chain aided by a folded structure.

Table 4.2.2A: Fluorescence lifetime of PEST M1 tryptophan at different pH (3-11) in presence of 25 mM NaCl. Fluorescence lifetime of NATA under same condition is shown in square brackets.

pH	$\chi^2_{reduced}$	τ_1 (ns)	α_1	τ_2 (ns)	α_2	Mean lifetime (ns)
3	1.17 [1.06]	1.14 [2.78]	0.80	3.89	0.20	1.7 [2.8]
5	1.07 [1.06]	1.26 [3.00]	0.70	4.09	0.30	2.1 [3.0]
7	1.02 [1.08]	1.67 [3.03]	0.57	4.19	0.43	2.8 [3.0]
9	1.00 [1.00]	1.78 [3.02]	0.40	4.35	0.60	3.3 [3.0]
11	1.01 [1.05]	1.93 [2.87]	0.46	4.35	0.54	3.2 [2.9]

Table 4.2.2B: Fluorescence lifetime of PEST M1 tryptophan at different pH (3-11) in presence of 250 mM NaCl. Fluorescence lifetime of NATA under same condition is shown in square brackets.

pH	$\chi^2_{reduced}$	τ_1 (ns)	α_1	τ_2 (ns)	α_2	Mean lifetime (ns)
3	1.17 [1.03]	1.14 [2.87]	0.80	3.89	0.20	1.7 [2.9]
5	1.00 [1.00]	1.40 [3.03]	0.68	4.01	0.38	2.2 [3.0]
7	1.08 [1.02]	1.70 [3.08]	0.55	3.98	0.45	2.7 [3.1]
9	1.00 [1.01]	1.93 [3.06]	0.44	4.43	0.56	3.3 [3.1]
11	1.01 [1.08]	2.04 [2.93]	0.46	4.52	0.54	3.4 [2.9]

Table 4.2.2C: Fluorescence lifetime of PEST M1 tryptophan at different pH (3-11) in presence of 6 M Gdn.HCl. Fluorescence lifetime of NATA under same condition is shown in square brackets.

pH	$\chi^2_{reduced}$	τ_1 (ns)	α_1	τ_2 (ns)	α_2	Mean lifetime (ns)
3	1.05 [1.10]	1.39 [2.97]	0.63	3.69	0.37	2.3 [3.0]
5	0.99 [1.09]	1.57 [3.10]	0.58	3.94	0.42	2.6 [3.1]
7	1.04 [1.04]	1.65 [3.06]	0.44	4.27	0.56	3.1 [3.1]
9	1.09 [1.03]	1.98 [3.14]	0.44	4.52	0.56	3.4 [3.1]
11	1.00 [1.04]	1.94 [3.02]	0.44	4.38	0.56	3.3 [3.0]

Figure 4.2.2D, E and F shows the variation of mean lifetime (τ_m) of PEST M1 tryptophan, along with NATA at different pH (3-11) in presence of 25 mM NaCl, 250 mM NaCl and 6 M Gdn.HCl, respectively. Examination of mean lifetime value of tryptophan depicts decrease in lifetime at the acidic pH in comparison with alkaline pH, while NATA remained nearly steady. However, in presence of 6 M Gdn.HCl change in mean lifetime values at different pH (3-11) was less.

These observations hint at presence of a local folded structure near tryptophan which is not stabilized by electrostatic interactions. Addition of Gdn.HCl caused this local structure to become partially unfolded increasing mean lifetime. Changes observed in the mean lifetime of PEST M1 tryptophan at different pH (3-11) under various conditions were well correlated with its steady state emission spectra. As lifetime of tryptophan changed at different pH (3-11), the change in r_{ss} values may be partly due to change in lifetime of Tryptophan with varying pH. In order to determine what is actually happening, next we performed the anisotropy decay analysis to calculate rotational correlation time (θ) of PEST M1 tryptophan.

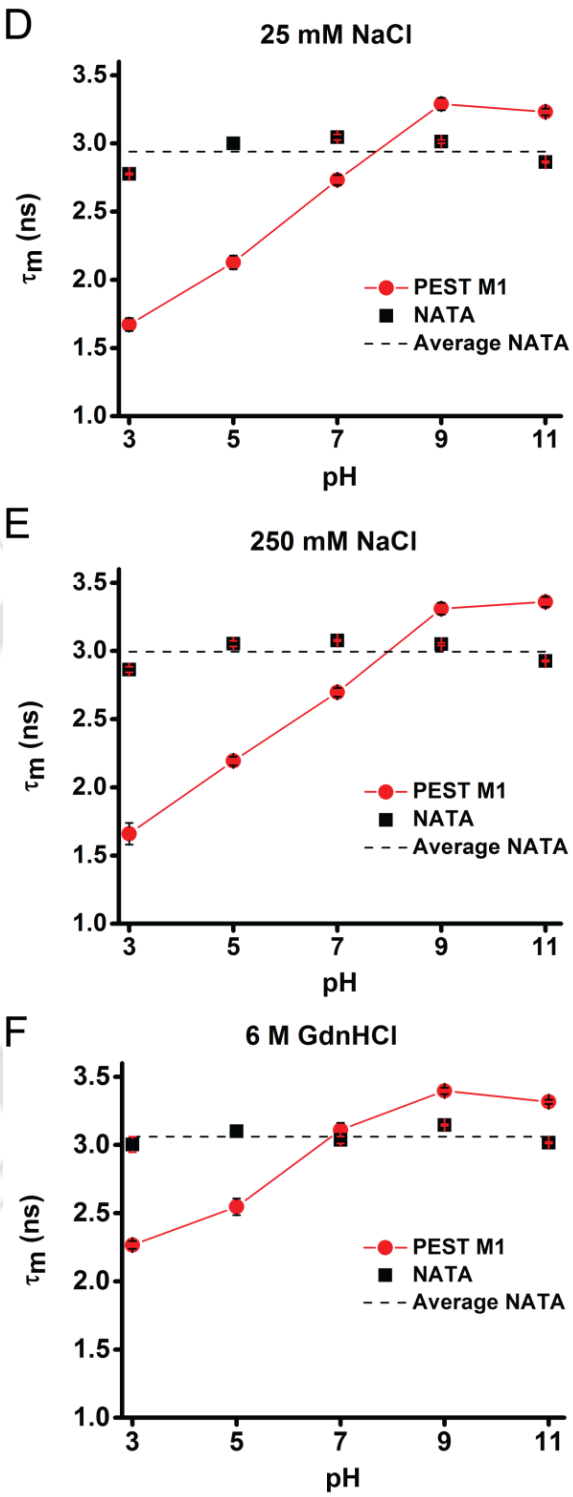

Figure 4.2.2: Comparison the mean lifetime of 20 μM PEST M1 tryptophan and 20 μM NATA at different pH (3-11), in presence of **[D]** 25 mM NaCl; **[E]** 250 mM NaCl and **[F]** 6 M Gdn.HCl.

4.2.3 Time-resolved anisotropy decay analysis of PEST M1 tryptophan

Anisotropy decay of tryptophan in PEST M1 was measured to determine its rotational correlation time (θ) in different pH (3-11) under various conditions like in presence of 25 mM NaCl, 250 mM NaCl and 6 M Gdn.HCl. Figure 4.2.3A, B and C display the anisotropy decay profile of PEST M1 tryptophan at different pH (3-11) in presence of 25 mM NaCl, 250 mM NaCl and 6 M Gdn.HCl, respectively. At pH 11, 9 and 7 (in presence of 25 mM NaCl) anisotropy decay profile display fast decay whereas, moderate and very slow decay was observe at pH 5 and 3, respectively. Comparison of residual anisotropy (r_∞) at different pH (3-5) in various conditions is shown in Figure 4.2.3D. Table 4.2.3 displays the fitted anisotropy parameters and the value of r_∞ at different pH under various conditions. The value of residual anisotropy (r_∞) at pH 11, 9 and 7 was close to zero, however small residual anisotropy (0.056) was present at pH 5 and this value significantly increased to 0.121, at pH 3. Similar but not identical anisotropy decay profile of PEST M1 tryptophan was observed at different pH (3-11) in presence of 250 mM NaCl.

Anisotropy decay analysis hints increased contribution of longer correlation time as it has higher value of r_∞ at acidic pH 3 and 5 whereas at pH 11, 9 and 7 value of r_∞ is ~0.0 depicting the absence of longer rotational correlation time. Presence of residual anisotropy at pH 3 and 5 clearly indicates hindered rotational motion of tryptophan. This hindrance to rotational motion suggests that PEST fragment has folded structure at pH 3 and 5.

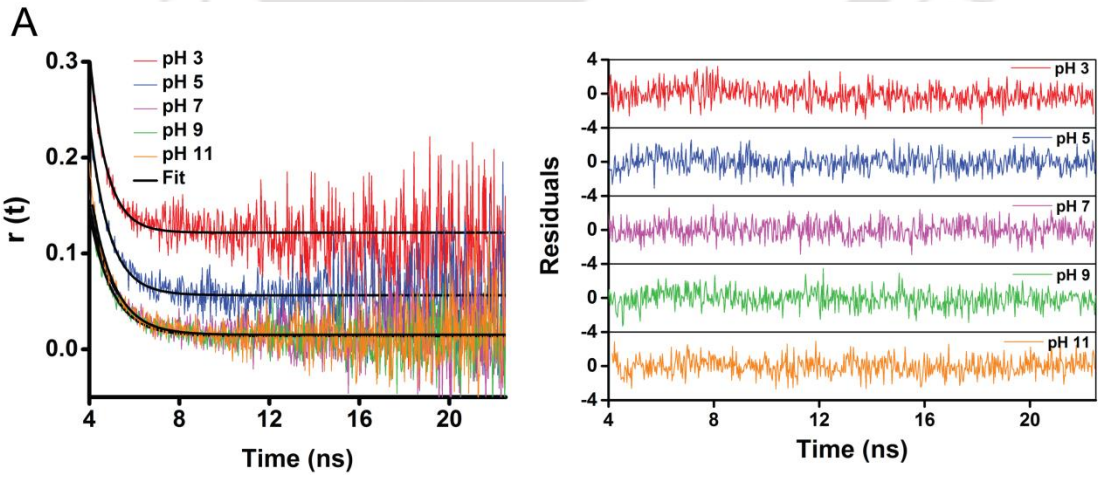

Figure 4.2.3A: Fitted tryptophan anisotropy decay profile of 20 μM PEST M1 at different pH (3-11) in presence of 25 mM NaCl. (left). Residuals for the fit are shown in right panel.

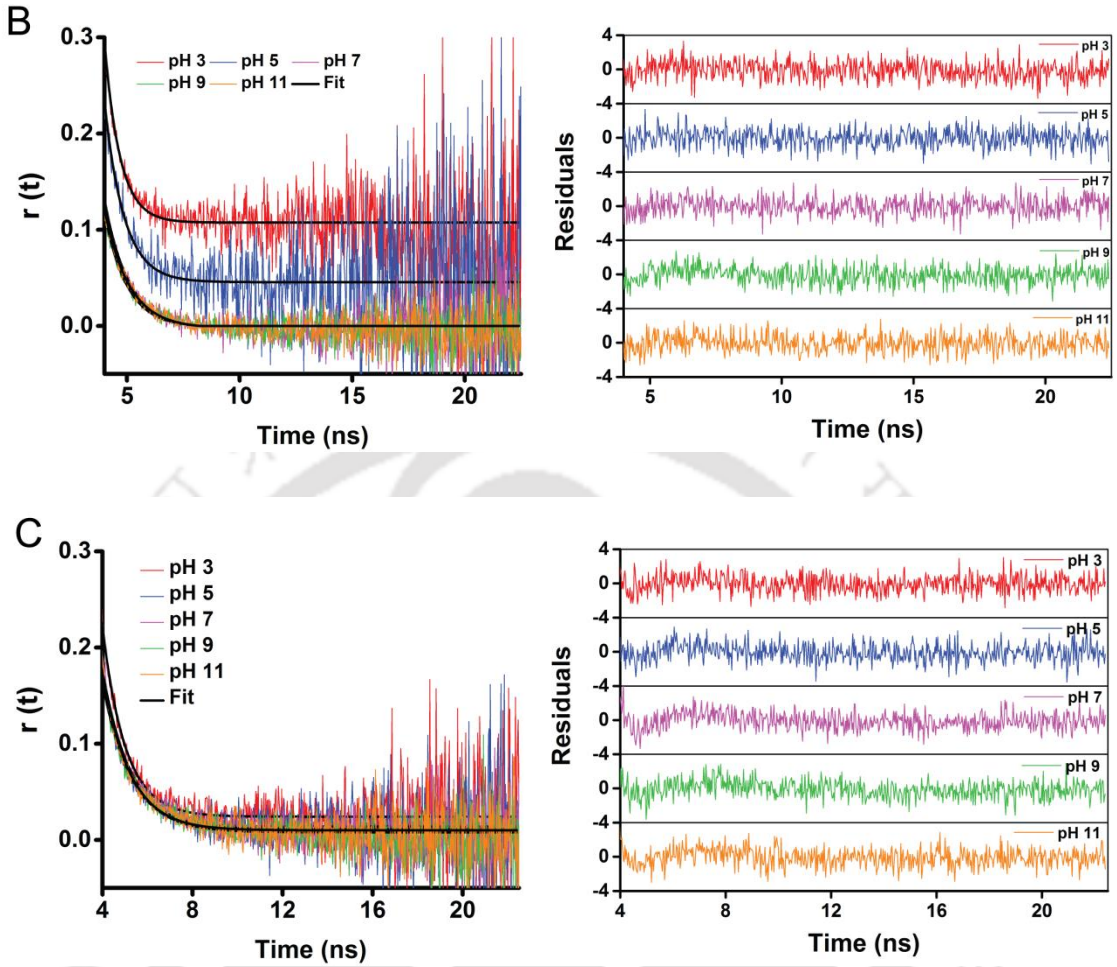

Figure 4.2.3: Fitted tryptophan anisotropy decay profile of 20 μM PEST M1 at different pH (3-11) in presence of **[B]** 250 mM NaCl and **[C]** 6 M Gdn.HCl (left panels). Residuals for the fit are shown in right panels.

However, in presence of 6 M Gdn.HCl tryptophan anisotropy decay profiles showed fast decay at each pH (3-11) and decay profiles appeared similar at every pH (3-11). The calculated value of r_∞ was nearly ~ 0.0 at different pH (3-11) which suggests unhindered rotation of tryptophan. A small and diminished value of residual anisotropy was however seen at pH 3 in presence of 6 M Gdn.HCl. This clearly indicates unfolding of PEST M1 in presence of 6 M Gdn.HCl at different pH (3-11), quite unlike in absence of Gdn.HCl.

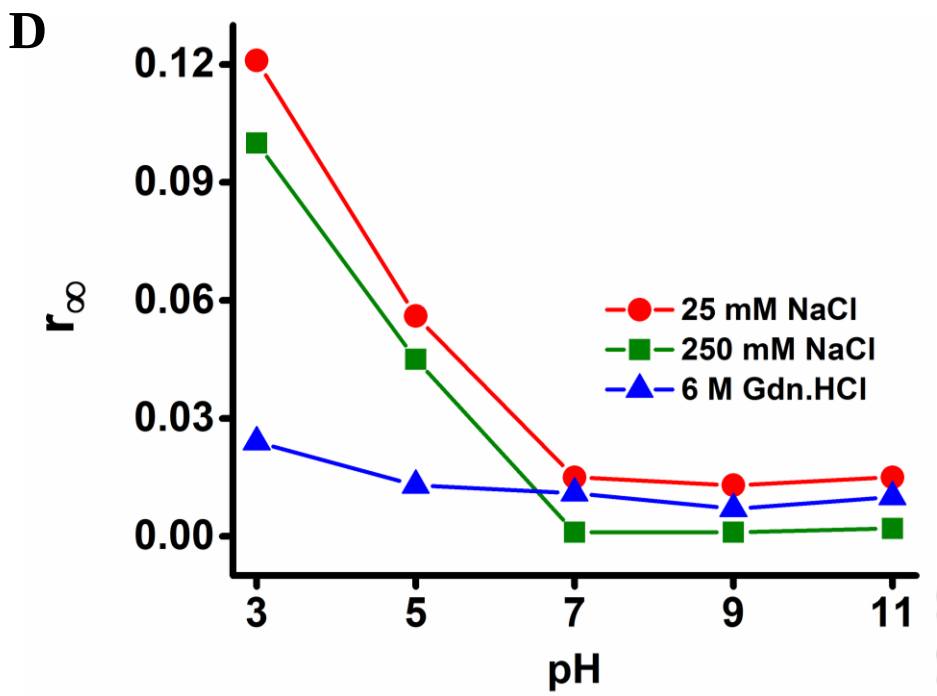

Figure 4.2.3D: Comparison of PEST M1 tryptophan residual anisotropy (r_∞) at different pH (3-11) in presence of 25 mM NaCl, 250 mM NaCl and 6 M Gdn.HCl.

Table 4.2.3: Fitted anisotropy decay data and residual anisotropy (r_∞) of PEST M1 tryptophan at different pH (3-11) in various conditions.

pH	25 mM NaCl			250 mM NaCl			6 M Gdn.HCl		
	$\chi^{2\,a}$	$\phi^{b\,\#}$ (ns)	r_∞	$\chi^{2\,a}$	$\phi^{b\,\#}$ (ns)	r_∞	$\chi^{2\,a}$	$\phi^{b\,\#}$ (ns)	r_∞
3	1.19	0.8	**0.121**	1.12	0.7	**0.10**	1.06	1.0	**0.024**
5	1.06	0.9	**0.056**	1.05	0.9	**0.045**	1.09	1.1	**0.013**
7	1.08	1.1	**0.015**	1.03	1.1	**0.001**	1.02	1.3	**0.011**
9	1.04	1.0	**0.013**	1.06	1.0	**0.001**	1.03	1.3	**0.007**
11	1.03	1.0	**0.015**	1.05	1.1	**0.002**	1.07	1.2	**0.010**

[a] reduced χ^2 for the fit; [b] rotational correlation time(s); [#] the values of rotational correlation time are not reliable to any interpretation as they are not deconvoluted and very close to FWHM of IRF.

4.2.4 Quenching of PEST M1 tryptophan by acrylamide

To gain insights on PEST M1 structure, tryptophan surface accessibility and specifically how deep it is buried inside the protein core, fluorescence quenching of tryptophan with acrylamide was performed at different pH (3-11) by monitoring its fluorescence lifetime. Figure 4.2.4A, B, C and D shows fluorescence intensity decay profile of PEST M1 tryptophan and model compound NATA with increasing concentration of acrylamide from 0—0.05 M at pH 5 and 9, respectively. Quenching of PEST M1 tryptophan was observed at several other pH (3-11), however these are not shown due to space constraints. Decay in fluorescence intensity of tryptophan at pH 5 (Figure 4.2.4A) shows minor change with increasing concentration of quencher as in comparison with its decay profile at pH 9 (Figure 4.2.4B). This clearly indicates more quenching of PEST M1 tryptophan at pH 9 as it is more accessible for diffusional encounter with the quencher compared to pH 5. However, tiny molecule NATA shows similar intensity decay profile at pH 5 and 9 as it is equally available for collision with acrylamide at both pH 5 and 9 (Figure 4.2.4C and D).

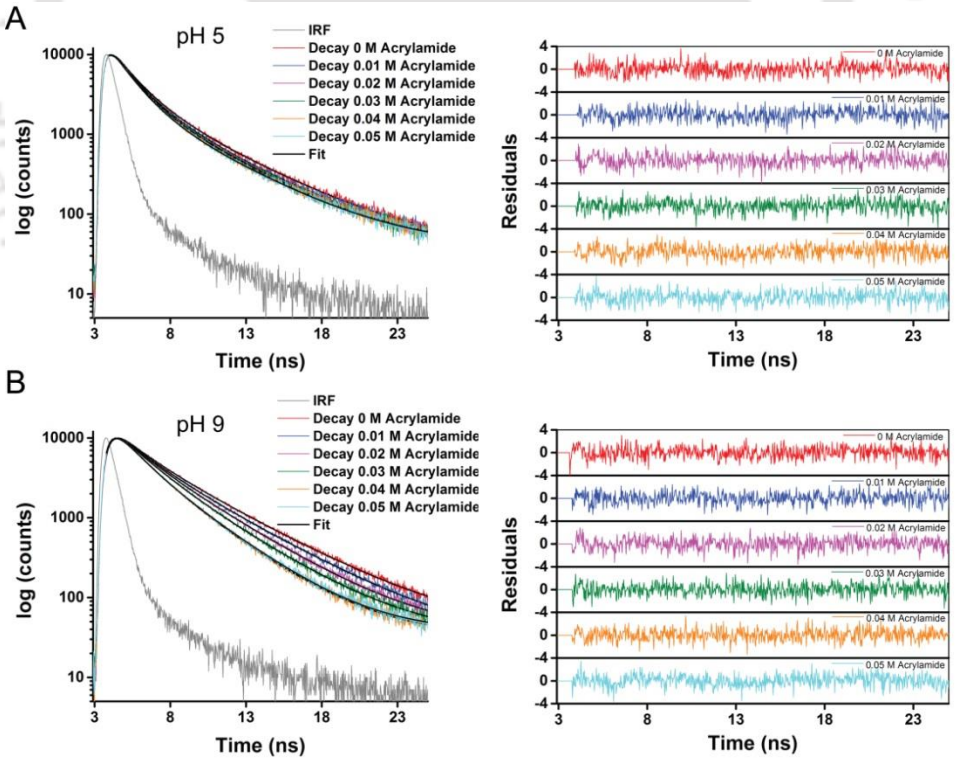

Figure 4.2.4: Fitted fluorescence intensity decay profile of 20 μM PEST M1 tryptophan at **[A]** pH 5 and **[B]** pH 9, in presence increasing concentration of acrylamide (left panels). Residuals for the fit are shown in the right panels.

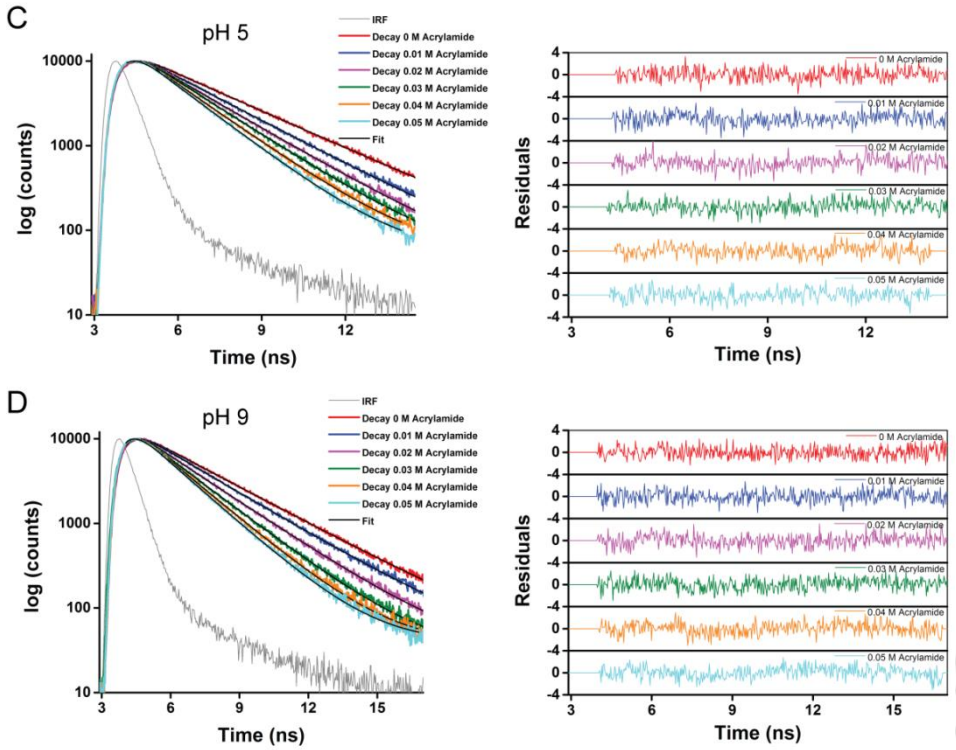

Figure 4.2.4: Fitted fluorescence intensity decay profile of 20 μM NATA at **[C]** pH 5 and **[D]** pH 9, in presence increasing concentration of acrylamide (left panels). Residuals for the fit are shown in the right panels.

Further, to obtained quantitative insights on the quenching of PEST M1 tryptophan and NATA, Stern-Volmer plot was made by plotting of τ_0/τ vs. quencher concentration at different pH in presence of 25 mM NaCl and 6 M Gdn.HCl. Figure 4.2.4 E and F display the Stern-Volmer plot of PEST M1 tryptophan and NATA at different pH (3-11) in presence of 25 mM NaCl and Figure 4.2.4 G and H shows their Stern-Volmer plot in presence of 6 M Gdn.HCl (pH 5-9). All the plots appear linear suggesting a single type of accessible tryptophan population. To determine the extent of quenching in tryptophan and NATA at different pH, Stern-Volmer constant (K_{sv}) was calculated from the slope of the fitted straight line in Stern-Volmer plot. PEST M1 tryptophan display increase in the slope with increasing pH, however minor changes in the slope were observed with NATA at different pH in presence of 25 mM NaCl. This revealed that tryptophan was buried inside the protein core at acidic pH. No change in the slope of PEST M1 tryptophan and NATA was observed at different pH (5-9) in presence of 6 M Gdn.HCl, as tryptophan is probably exposed to the solvent on unfolding of PEST M1 and gets equally quenched at each pH with acrylamide.

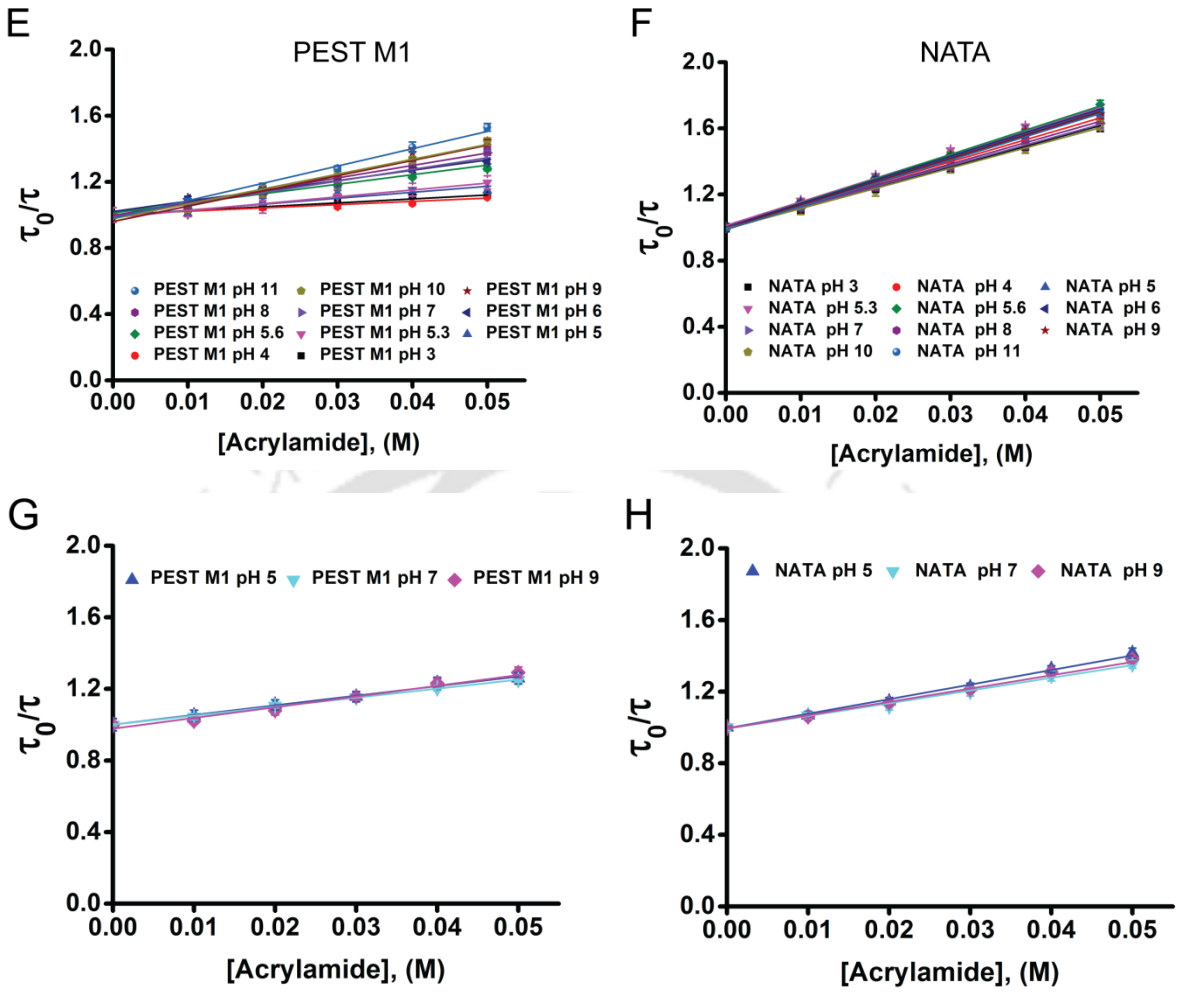

Figure 4.2.4: Stern-Volmer plot depicting the quenching of, **[E]** 20 µM PEST M1 tryptophan, **[F]** 20 µM NATA at different pH (3-11) in presence of **25 mM NaCl**, **[G]** 20 µM PEST M1 tryptophan and **[H]** 20 µM NATA at different pH (5-9) in presence of **6 M Gdn.HCl** .

Stern-Volmer constant (K_{sv}) is dependent on both fluorescence lifetime (τ_0) in absence of quencher and the bimolecular fluorescence quenching rate constant (k_q). As the fluorescence lifetime (τ_0) of PEST M1 tryptophan changes with changing pH, structural changes in PEST M1 due to change in pH cannot be solely determine by values of K_{sv}. In order to obtain molecular insights, bimolecular fluorescence quenching rate constant (k_q) was determined using equation 2.50. Figure 4.2.4I depicts the k_q value of tryptophan and NATA in presence of 25 mM NaCl and Figure 4.2.4J shows k_q values in presence of 6 M Gdn.HCl. The calculated value of K_{sv} and k_q is given in the Table 4.2.4A and B in presence of 25 mM NaCl and 6 M Gdn.HCl, respectively.

The lower value of k_q (1.43x 10^9 M^{-1} s^{-1}) at pH 3 reveals that tryptophan is buried inside the protein whereas, higher k_q value (3.13x 10^9 M^{-1} s^{-1}) at pH 11 demonstrates more quenching of tryptophan residue as it is exposed to the solvent. Further investigation of quenching in presence of 6 M Gdn.HCl discloses higher k_q values in both acidic and alkaline pH which indicates exposure of tryptophan as protein gets unfolded. These experiments established folding of PEST M1 at acidic pH in the vicinity of tryptophan.

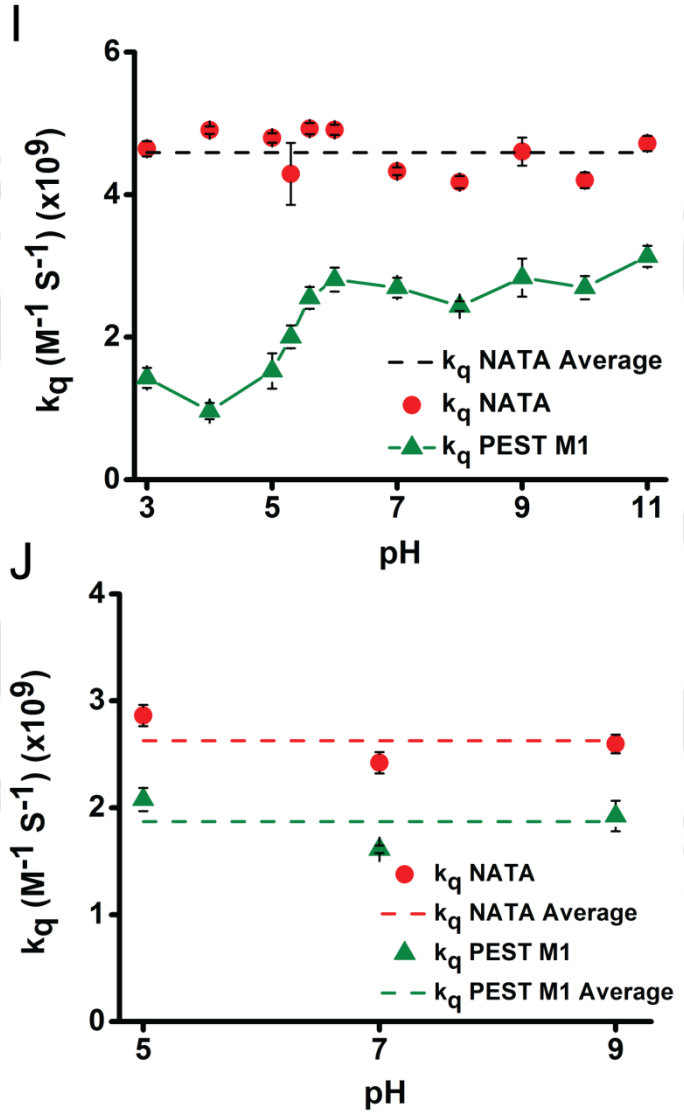

Figure 4.2.4: Bimolecular fluorescence quenching rate constant (k_q) of PEST M1 tryptophan and NATA by acrylamide at different pH in presence of **[I] 25 mM NaCl** and **[J] 6 M Gdn.HCl** at room temperature.

Table 4.2.4A: The τ_0, K_{sv} and k_q values of PEST M1 tryptophan and NATA at different pH in presence of 25 mM NaCl. Average k_q for NATA = 4.59 ± 0.29 x10^9 M^{-1} s^{-1}.

pH	PEST M1			NATA		
	K_{sv} (M^{-1})	τ_0 (ns)	k_q (M^{-1} s^{-1}) (x 10^9)	K_{sv} (M^{-1})	τ_0 (ns)	k_q (M^{-1} s^{-1}) (x 10^9)
3	2.52	1.76	1.43	12.51	2.70	4.64
4	1.88	1.95	0.96	13.31	2.71	4.90
5	3.37	2.21	1.53	14.23	2.97	4.80
5.3	4.10	2.05	2.00	13.04	3.04	4.29
5.6	5.41	2.12	2.55	14.63	2.97	4.93
6	6.23	2.22	2.81	14.02	2.86	4.91
7	7.44	2.76	2.70	12.70	2.93	4.33
8	7.89	3.24	2.44	12.96	3.10	4.18
9	9.41	3.32	2.84	14.14	3.07	4.60
10	9.09	3.37	2.70	12.41	2.95	4.20
11	10.77	3.44	3.13	14.17	3.00	4.72

Table4.2.4B: The τ_0, K_{sv} and k_q values of PEST M1 tryptophan and NATA at different pH in presence of 6 M Gdn.HCl. Average k_q for PEST M1 tryptophan and NATA is 1.87 ± 0.24 and 2.63 ± 0.22 x10^9 M^{-1} s^{-1}, respectively.

pH	PEST M1			NATA		
	K_{sv} (M^{-1})	τ_0 (ns)	k_q (M^{-1} s^{-1}) (x 10^9)	K_{sv} (M^{-1})	τ_0 (ns)	k_q (M^{-1} s^{-1}) (x 10^9)
5	5.38	2.59	2.08	8.39	2.93	2.86
7	5.09	3.16	1.61	7.19	2.97	2.42
9	6.20	3.22	1.92	7.82	3.01	2.60

Tryptophan provides only local structural information around its surroundings and has a short mean lifetime ~3 ns which is insufficient to capture full rotational motion of PEST fragment. For these reasons, another probe is needed at other terminus of PEST fragment and it was decided to label cysteine at N-terminus with dansyl probe.

4.2.5 Steady state fluorescence and anisotropy studies of dansyl

To investigate the effect of pH on structure and dynamics of PEST fragments at N-terminus, the fluorescence emission spectra and steady state anisotropy (r_{ss}) of dansyl probe labeled with single cysteine[9] (residue 9, present at N-terminus) of PEST Wt and PEST M1 was recorded at different pH (3-11). Fluorescence emission spectra of dansyl at different pH (3-11) were collected by exciting the samples at 340 nm. Figure 4.2.5A, B and C display the emission spectra, integrated fluorescence yield and emission maxima of dansyl labeled with PEST Wt at different pH (3-11), respectively.

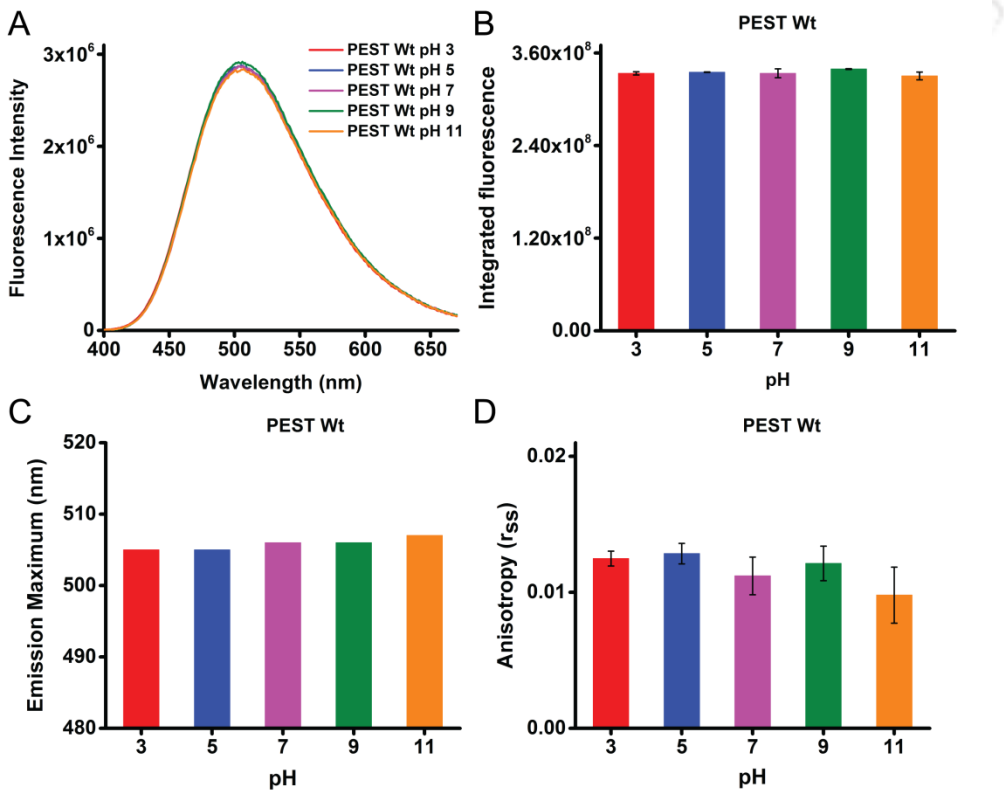

Figure 4.2.5: Effect of pH on steady state fluorescence and fluorescence anisotropy of 10 μM dansyl labeled with 11 μM PEST Wt. **[A]** Shows steady state fluorescence spectra; **[B]** integrated fluorescence yield; **[C]** fluorescence emission maxima and **[D]** steady state anisotropy of dansyl.

Integrated fluorescence of dansyl at different pH (3-11) shows insignificant change. Slight change (507 to 505 nm) in emission maxima of dansyl was observed from pH 11 to 3. Figure 4.2.5D show slight increase in the steady state fluorescence anisotropy (r_{ss}) of dansyl at acidic pH (3-5). Similar trend in fluorescence emission and anisotropy of dansyl that is labeled with the cysteine[9] of PEST M1 was observed at different pH (Figure 4.2.5E, F, G and H). This insignificant change in the integrated fluorescence yield, emission maxima and anisotropy of dansyl probe suggest minor structural alterations in PEST fragment at different pH (3-11) when monitored around cysteine residue.

Further, fluorescence emission and anisotropy of dansyl, labeled with PEST Wt and M1 was collected at different pH (3-11) in presence 6 M Gdn.HCl to completely denature the PEST fragment. As expected, insignificant change in the fluorescence emission of dansyl labeled PEST Wt and M1 was observed. However, a slight trend for anisotropy to decrease with increase pH is noticed in presence of 6 M Gdn.HCl similar to samples in absence of Gdn.HCl (Figure A2 of appendix). These results indicate PEST Wt and M1 are completely unfolded at different pH (3-11) in presence of 6 M Gdn.HCl.

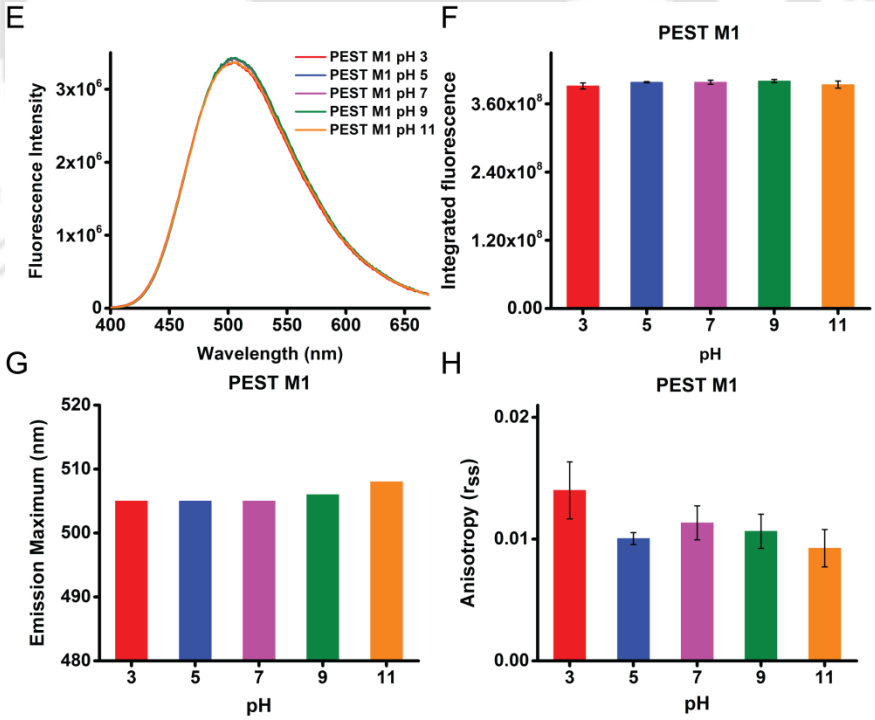

Figure 4.2.5: Effect of pH on steady state fluorescence and anisotropy of 10 µM dansyl labeled with 11 µM PEST M1. **[E]** Shows steady state fluorescence spectra; **[F]** integrated fluorescence yield; **[G]** fluorescence emission maxima and **[H]** steady state anisotropy of dansyl.

4.2.6 Fluorescence lifetime analysis of dansyl labeled PEST Wt and M1

To gain further insights into the effect of pH on structure of PEST fragments, fluorescence lifetime measurement of dansyl labeled PEST Wt and PEST M1 was performed at different pH (3-11). Figure 4.2.6A and B shows intensity decay profile of dansyl labeled PEST Wt and PEST M1 at different pH (3-11), respectively. Insignificant change in the fluorescence intensity decay of dansyl labeled PEST Wt and M1 was observed at different pH (3-11). Analysis of fluorescence intensity decay shows presence of two lifetimes. Mean fluorescence lifetime (τ_m) of dansyl labeled PEST Wt decreased from 12.43 to 11.23 ns whereas; for PEST M1 it has decreased from 12.67 to 10.48 ns with change in pH from 3 to 11. Table 4.2.6A and B display the lifetime values of dansyl labeled PEST Wt and M1 at different pH (3-11) obtained after fitting the intensity decay profile, respectively.

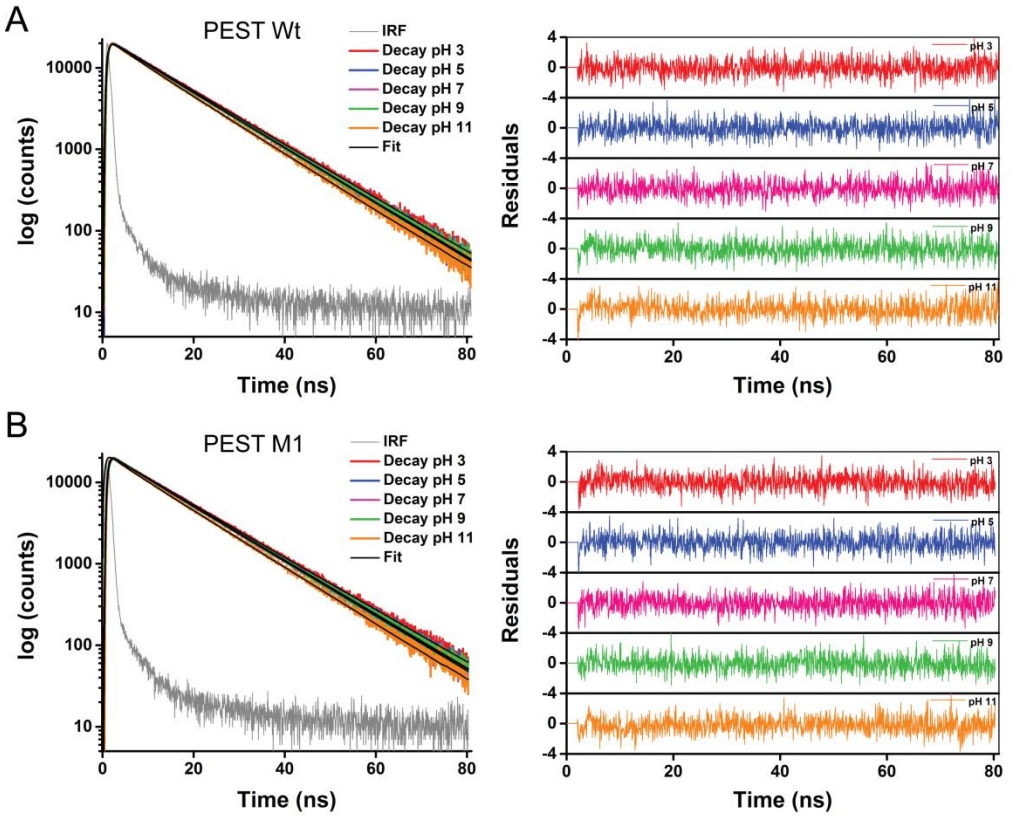

Figure 4.2.6: Fitted time-resolved fluorescence intensity decay profile of 10 µM dansyl labeled with 11 µM of **[A]** PEST Wt and **[B]** PEST M1 at different pH (3-11) (left panels). Residuals for the fit are shown in the right panels.

Table 4.2.6A: Fluorescence lifetime of dansyl labeled PEST Wt at different pH (3-11).

pH	$\chi^2_{reduced}$	τ_1 (ns)	α_1	τ_2 (ns)	α_2	Mean lifetime (ns)
3	1.06	13.2	0.908	4.5	0.092	12.4
5	1.03	12.9	0.907	3.9	0.093	12.0
7	1.04	12.8	0.907	3.2	0.093	11.9
9	1.06	12.9	0.884	4.3	0.116	11.9
11	1.09	12.3	0.857	4.9	0.143	11.2

Table 4.2.6B: Fluorescence lifetime of dansyl labeled PEST M1 at different pH (3-11).

pH	$\chi^2_{reduced}$	τ_1 (ns)	α_1	τ_2 (ns)	α_2	Mean lifetime (ns)
3	1.04	13.6	0.889	5.7	0.111	12.7
5	1.07	13.1	0.904	4.6	0.096	12.3
7	1.08	12.9	0.905	3.7	0.095	12.0
9	1.05	12.9	0.890	4.6	0.110	12.0
11	1.11	12.2	0.795	3.7	0.205	10.5

Further, fluorescence lifetime of dansyl labeled PEST Wt and M1 was monitored at different pH (3-11) in presence of 6 M Gdn.HCl, to unfold the PEST fragment. Figure A3 of appendix display the intensity decay profile of dansyl labeled PEST Wt and M1 at different pH (3-11) in presence of 6 M Gdn.HCl. Both dansyl labeled PEST Wt and M1 shows no change in the intensity decay from pH 3-9, however some increase in the decay was observed at pH 11. This could perhaps account for decrease in r_{ss} at alkaline pH. Dansyl labeled PEST Wt shows much increase in the intensity decay at pH 11 than PEST M1. Table 4.2.6C and D show the lifetime values of dansyl labeled PEST Wt and M1 at

different pH (3-11) in presence of 6 M Gdn.HCl obtained after fitting the intensity decay profile, respectively. A clear decrease in mean lifetime is noticeable at pH 11 compared to other pH values.

Table 4.2.6C: Fluorescence lifetime of dansyl labeled PEST Wt at different pH (3-11) in presence of 6 M Gdn.HCl.

pH	$\chi^2_{reduced}$	τ_1 (ns)	α_1	τ_2 (ns)	α_2	Mean lifetime (ns)
3	1.02	11.2	0.902	5.2	0.098	10.6
5	1.04	11.3	0.889	5.3	0.111	10.7
7	1.08	11.2	0.905	4.2	0.095	10.5
9	1.02	11.1	0.916	3.9	0.084	10.5
11	1.12	9.7	0.747	5.8	0.253	8.7

Table 4.2.6D: Fluorescence lifetime of dansyl labeled PEST M1 at different pH (3-11) in presence of 6 M Gdn.HCl.

pH	$\chi^2_{reduced}$	τ_1 (ns)	α_1	τ_2 (ns)	α_2	Mean lifetime (ns)
3	1.08	11.3	0.920	3.3	0.080	10.6
5	1.03	11.3	0.911	3.8	0.089	10.6
7	1.01	11.2	0.901	4.7	0.099	10.5
9	1.02	11.2	0.887	4.5	0.113	10.5
11	1.09	10.7	0.728	6.4	0.272	9.5

4.2.7 Time-resolved anisotropy decay analysis of dansyl labeled PEST Wt and M1

To obtain deeper insight into the effect of pH on structure and dynamics of PEST fragment at its N-terminus region, time-resolved fluorescence anisotropy decay measurements of dansyl labeled PEST Wt and M1 was performed at different pH (3-11). This was done to determine its rotational correlation time (θ). Figure 4.2.7A and C display the anisotropy decay profile of dansyl labeled PEST Wt and PEST M1 at different pH (3-11), respectively. Inset of Figure 4.2.7A reveals slower anisotropy decay of dansyl labeled PEST Wt at pH 3 as compared to pH 5. However, decay profiles at pH 7 to 11 appear faster. The anisotropy

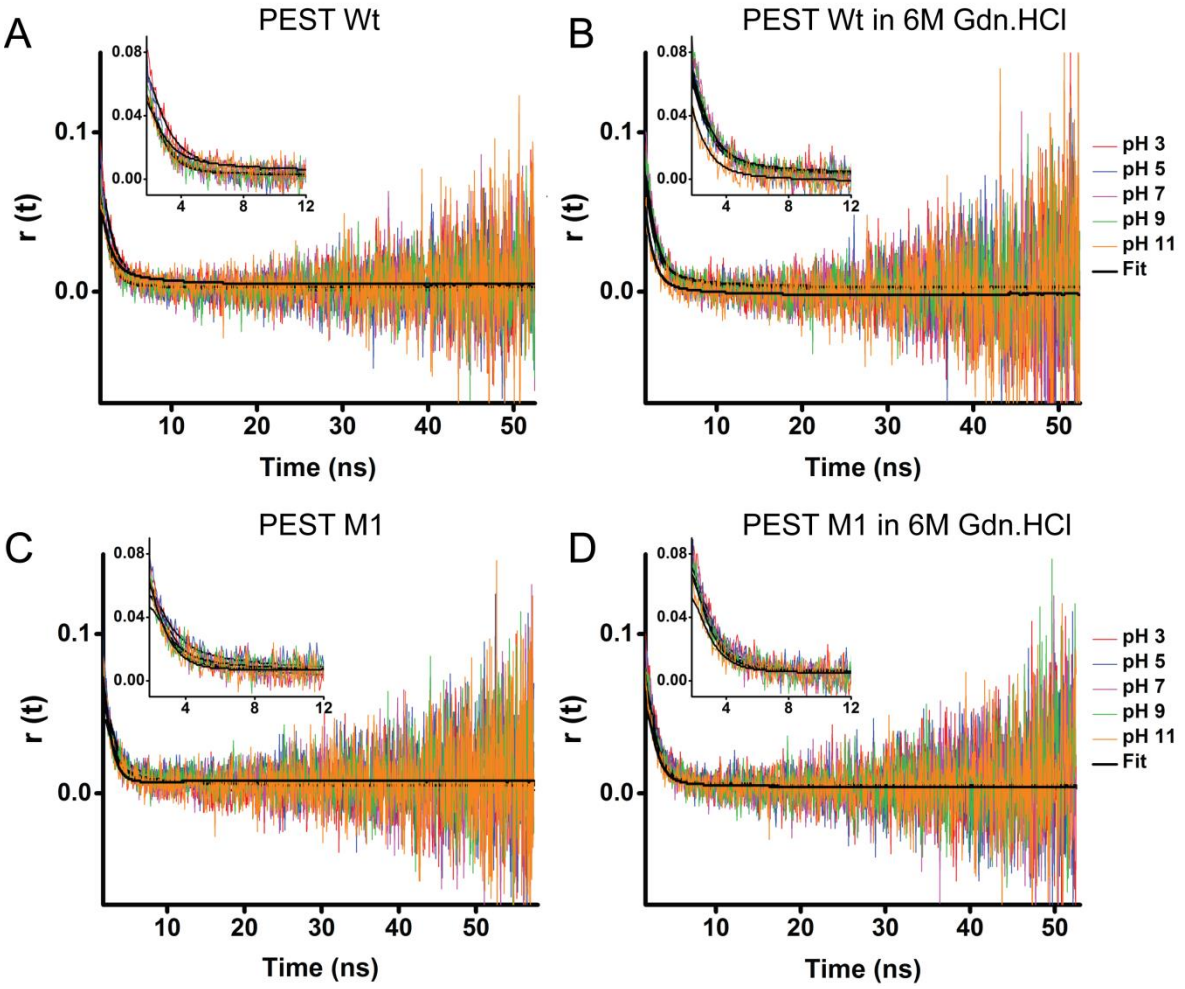

Figure 4.2.7: Fitted anisotropy decay profile of 10 μM dansyl labeled with 11 μM of **[A]** PEST Wt, **[C]** PEST M1 at different pH 3-11, **[B]** PEST Wt and **[D]** PEST M1 at different pH (3-11) in presence of 6 M Gdn.HCl. Insets shows the expanded form of anisotropy decay at shorter time scale.

decay profile of dansyl labeled PEST Wt looks similar from pH 7 to 11. Inset of Figure 4.2.7C shows similar but not identical anisotropy decay profile of dansyl labeled PEST M1 at different pH (3-11). Analysis of anisotropy decay profile shows presence of two correlation time. At pH 3 dansyl labeled PEST Wt shows a fast rotational component of 0.97 ns with amplitude of 0.880 and a slow rotational component of 5.01 ns with amplitude of 0.120. At higher pH (7-11) amplitude of fast rotational component is increased and slow rotational component amplitude diminished. This reduced amplitude for shorter rotational correlation time clearly suggests restricted rotational motion of dansyl probe at pH 3 and pH 5, compared to higher pH (7-11). Table 4.2.7A and B display the detailed analysis of anisotropy decay of dansyl labeled PEST Wt and PEST M1 at different pH, respectively. Dansyl labeled PEST M1 also shows the rotational behavior similar to PEST Wt at different pH. Restricted rotational motion of dansyl probe reveals presence of folded structure of PEST fragment at acidic pH.

Table 4.2.7A: Anisotropy decay data of dansyl labeled PEST Wt at different pH (3-11).

pH	$\chi^{2\,a}$	$r_0{}^b$	$r_{ss}{}^c$	$\phi_1{}^d$ (ns)	$\alpha_1{}^e$	$\phi_2{}^d$ (ns)	$\alpha_2{}^e$
3	1.19	0.13	0.013	0.97	0.880	5.0	0.120
5	1.21	0.13	0.013	0.90	0.902	5.0	0.098
7	1.23	0.11	0.010	0.94	0.960	6.3	0.040
9	1.21	0.14	0.010	0.90	0.998	6.0	0.002
11	1.15	0.13	0.013	0.90	0.966	5.6	0.034

Table 4.2.7B: Anisotropy decay data of dansyl labeled PEST M1 at different pH (3-11).

pH	$\chi^{2\,a}$	$r_0{}^b$	$r_{ss}{}^c$	$\phi_1{}^d$ (ns)	$\alpha_1{}^e$	$\phi_2{}^d$ (ns)	$\alpha_2{}^e$
3	1.20	0.14	0.013	0.93	0.889	5.2	0.111
5	1.27	0.12	0.013	0.90	0.847	5.5	0.153
7	1.14	0.15	0.011	0.90	0.991	5.2	0.009
9	1.23	0.12	0.010	0.91	0.960	6.0	0.040
11	1.32	0.18	0.015	0.90	0.985	5.3	0.015

[a] reduced χ^2 for the fit; [b] initial anisotropy; [c] steady state anisotropy calculated from fit; [d] rotational correlation time(s); [e] fractional amplitude associated with the correlation time.

Further, anisotropy decay of dansyl labeled with PEST fragment was monitored at different pH in presence of 6 M Gdn.HCl to completely unfold the PEST protein. Figure 4.2.7 B and D display the anisotropy decay profile of dansyl labeled PEST Wt and M1 at different pH (3-11) in presence of 6 M Gdn.HCl, respectively. No significant change in the anisotropy decay profiles were observed at different pH in presence of Gdn.HCl. Table 4.2.7C and D display the detailed analysis of anisotropy decay of dansyl labeled PEST Wt and PEST M1 at different pH in presence of Gdn.HCl, respectively. Analysis of anisotropy decay reveals insignificant changes in correlation times of dansyl labeled PEST Wt and M1 at different pH in Gdn.HCl. This clearly demonstrates unfolded structure of PEST fragment at different pH in presence of 6 M Gdn.HCl. Figure (A4-A7), obtained in the process of analyzing anisotropy decays in different conditions are given in the appendix.

Table 4.2.7C: Anisotropy decay data of dansyl labeled PEST Wt at different pH (3-11) in presence of 6 M Gdn.HCl.

pH	$\chi^{2\,a}$	$r_0{}^b$	$r_{ss}{}^c$	$\phi_1{}^d$ (ns)	$\alpha_1{}^e$	$\phi_2{}^d$ (ns)	$\alpha_2{}^e$
3	1.21	0.15	0.014	0.94	0.952	5.5	0.048
5	1.23	0.15	0.014	0.97	0.952	5.5	0.048
7	1.18	0.14	0.015	0.97	0.915	5.1	0.085
9	1.18	0.15	0.016	0.99	0.940	6.0	0.060
11	1.12	0.12	0.014	0.92	0.942	6.5	0.058

Table 4.2.7D: Anisotropy decay data of dansyl labeled PEST M1 at different pH (3-11) in presence of 6 M Gdn.HCl.

pH	$\chi^{2\,a}$	$r_0{}^b$	$r_{ss}{}^c$	$\phi_1{}^d$ (ns)	$\alpha_1{}^e$	$\phi_2{}^d$ (ns)	$\alpha_2{}^e$
3	1.18	0.14	0.016	1.1	0.921	5.7	0.079
5	1.17	0.16	0.015	1.0	0.974	5.3	0.026
7	1.16	0.15	0.014	1.0	0.974	5.1	0.026
9	1.15	0.16	0.014	0.97	0.986	5.1	0.014
11	1.08	0.12	0.012	0.99	0.981	5.2	0.019

[a] reduced χ^2 for the fit; [b] initial anisotropy; [c] steady state anisotropy calculated from fit; [d] rotational correlation time(s); [e] fractional amplitude associated with the correlation time.

So far, we have discussed the structural changes in PEST fragment at different pH (3-11) by monitoring the fluorescence of tryptophan and the dansyl probe. Fluorescence data reveals more pronounced folding of PEST fragment in the vicinity of tryptophan at C-terminus region than its N-terminus region (in the vicinity of dansyl probe labeled with cysteine). However, fluorescence of tryptophan and dansyl is sensitive to its local environment and provides information about local structure and dynamics of protein (Lakowicz, 2006). Next we performed various experiments like FRET, ANS assay and CD measurements, to determine overall structural change in PEST fragment at different pH (3-11).

4.2.8 Förster Resonance Energy Transfer (FRET) analysis

FRET study was carried out to investigate the effect of pH on overall structure and dynamics of PEST fragment. Presence of single cysteine^{9} (9^{th} residue on N-terminus) and single tryptophan^{70} (70^{th} residue on C-terminus) in PEST M1 was utilized for intramolecular FRET measurements. Fluorescence lifetime of PEST M1 tryptophan in presence and absence of acceptor (dansyl labeled with cysteine^{9}) was measured at different pH (3-11). Figure 4.2.8 A and C display the fluorescence intensity decay profile of PEST M1 tryptophan at pH 4 and 9, respectively in presence and absence of acceptor (dansyl). At pH 4 in presence of acceptor, tryptophan show faster decay in the fluorescence intensity as compared with pH 9. This indicates significant energy transfer from tryptophan to the acceptor at pH 4. This suggests tryptophan is more close to the acceptor at pH 4 than pH 9.

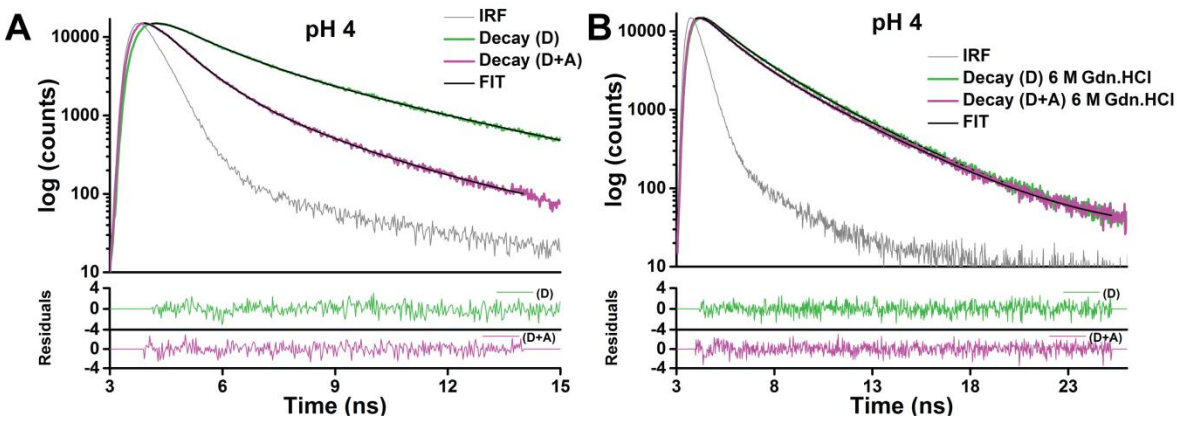

Figure 4.2.8: Fitted time-resolved fluorescence intensity decay profile of 20 μM PEST M1 tryptophan (donor), in presence of **[A]** 25 mM NaCl and **[B]** 6 M Gdn.HCl at pH 4 with and without acceptor (dansyl) (in top panel). Residuals for the fit are shown in the bottom panels.

However, no change in the fluorescence intensity decay of tryptophan was observed at pH 4 and 9 in presence and absence of acceptor with 6 M Gdn.HCl (Figure 4.2.8 B and D). This reveals that close proximity between Cys^{9} and Trp^{70} which existed in absence of Gdn.HCl at pH 4 does not exist in presence of Gdn.HCl perhaps due to unfolding of the protein.

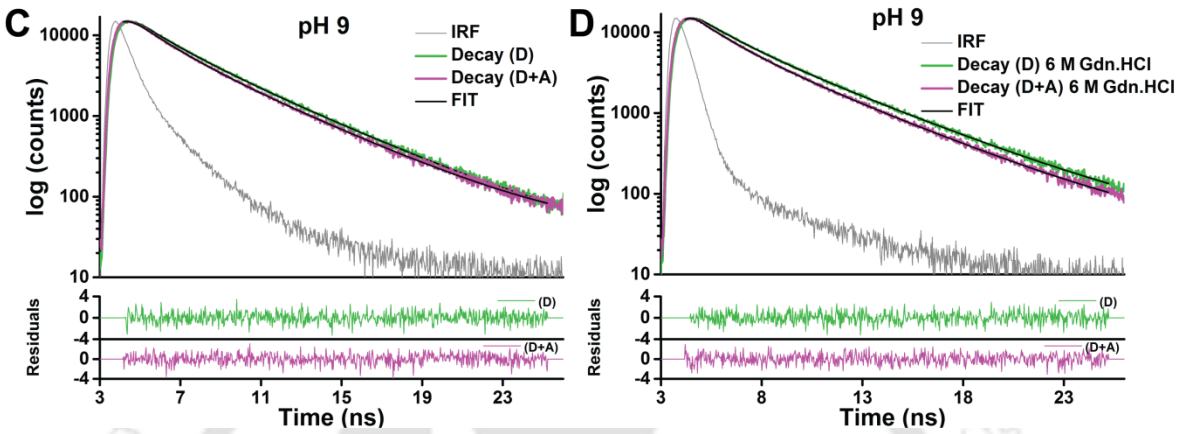

Figure 4.2.8: Fitted time-resolved fluorescence intensity decay profile of 20 µM PEST M1 tryptophan (donor), in presence of **[C]** 25 mM NaCl and **[D]** 6 M Gdn.HCl at pH 9 with and without acceptor (dansyl) (in top panel). Residuals for the fit are shown in the bottom panels.

Further, FRET efficiency and distance between single cysteine^{9} and single tryptophan^{70} of PEST M1 was calculated using equation 2.56 and 2.54, respectively. Figure 4.2.8E display the comparison of FRET distance between cysteine^{9}-tryptophan^{70} in presence of 25 mM NaCl and 6 M Gdn.HCl. Table 4.2.8A and B display the calculated lifetime of tryptophan (in presence and absence of acceptor), FRET efficiency and distance in presence of 25 mM NaCl and 6 M Gdn.HCl, respectively. Distance between cysteine^{9}-tryptophan^{70} has increased (from 24.2 to 31.2 Å) when pH was changed from pH 3 to 11. More interestingly at pH 4, PEST has closest (21.4 Å) distance between cysteine^{9}-tryptophan^{70}. PEST also shows lowest value of bimolecular fluorescence quenching rate constant (k_q = 0.96x 10^{9} M^{-1} s^{-1}) at pH 4. Both FRET distance and k_q value suggest PEST M1 has more folded structure at pH 4 than any other pH value. Further, FRET studies in presence of 6 M Gdn.HCl indicate unfolded structure of PEST, as distance between cysteine^{9}-tryptophan^{70} is more and varied from 30.1 to 33.9 Å at different pH (3-11). The higher error bars at 6 M Gdn.HCl hints at a more fluctuating structural ensemble at that condition in comparison to 25 mM NaCl condition. Figure 4.2.8F depicts the proposed model of PEST fragment at pH 3 and 11.Hence, FRET results established that PEST M1 has folded structure at acidic pH

whereas at alkaline pH it has unfolded structure as distance between cysteine[9]-tryptophan[70] increased.

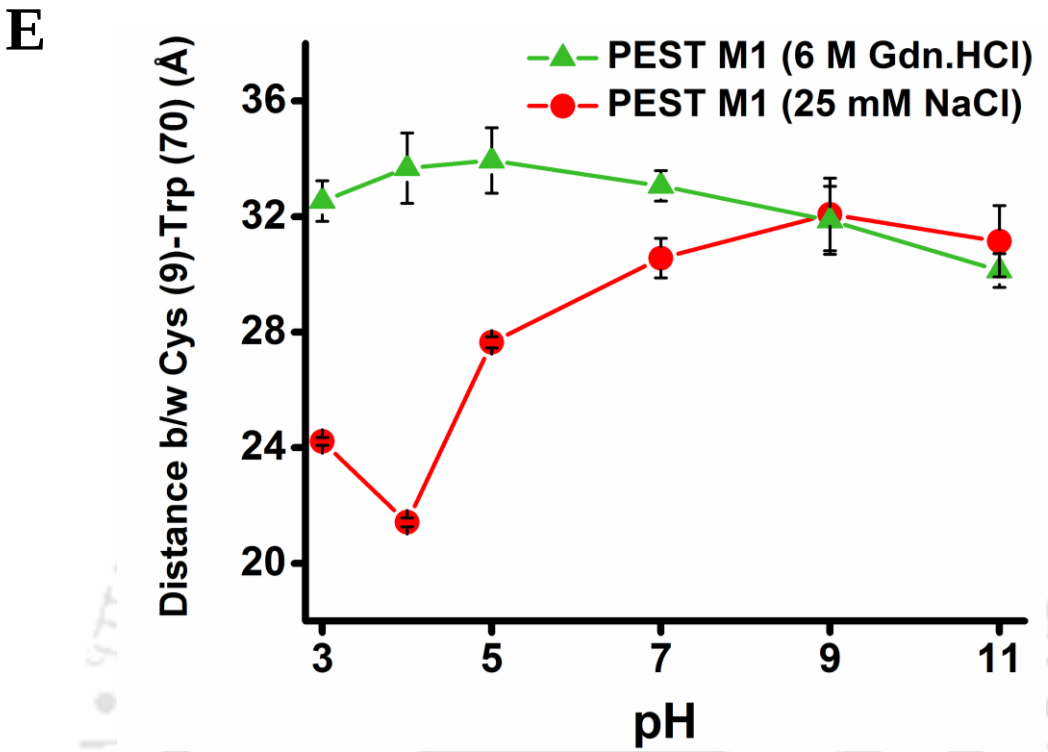

Figure 4.2.8E: Intramolecular FRET distance between tryptophan[70] (donor) and dansyl labeled cysteine[9] (acceptor) of PEST M1 at different pH (3-11).

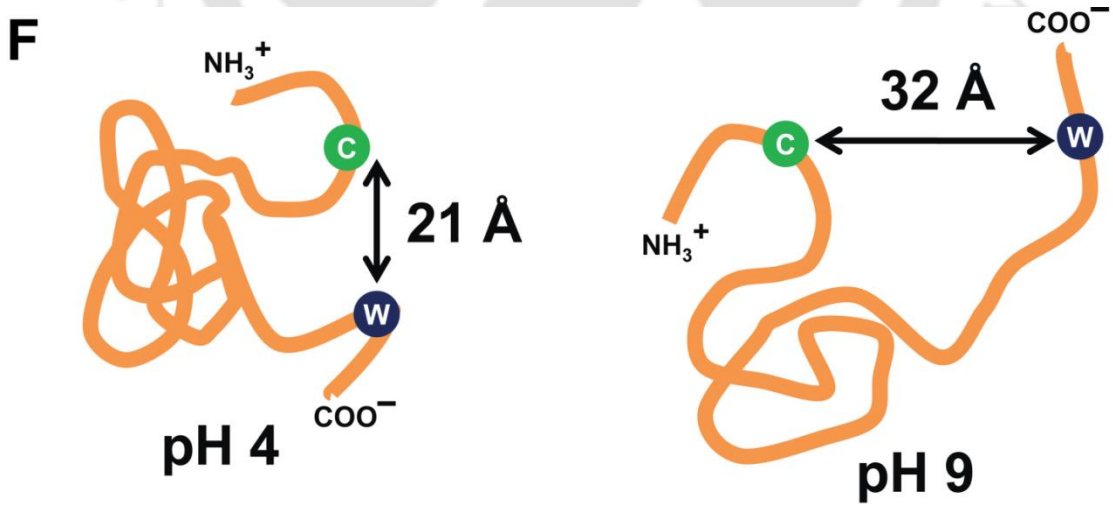

Figure 4.2.8F: The proposed model of PEST fragment at pH 4 and 9.

Table 4.2.8A: Fluorescence lifetime of PEST M1 tryptophan (in presence and absence of acceptor), FRET efficiency and distance between cysteine^{9}-tryptophan^{70} at different pH (3-11).

pH		χ^2 reduced	τ_1 (ns)	α_1	τ_2 (ns)	α_2	τ_m (ns)	Average FRET Efficiency	Average distance b/w Cys^{9}-Trp^{70} (Å)
3	**Donor**	1.10	1.30	0.74	3.71	0.26	1.93	0.36 ± 0.01	24.2 ± 0.1
	Donor+ Acceptor	*1.02*	*0.90*	*0.81*	*2.71*	*0.19*	*1.23*		
4	**Donor**	1.01	1.39	0.70	4.10	0.30	2.21	0.54 ± 0.01	21.4 ± 0.2
	Donor+ Acceptor	*1.05*	*0.82*	*0.88*	*2.60*	*0.12*	*1.04*		
5	**Donor**	1.06	1.26	0.68	3.83	0.32	2.08	0.20 ± 0.01	27.7 ± 0.2
	Donor+ Acceptor	*1.04*	*1.08*	*0.73*	*3.31*	*0.27*	*1.68*		
7	**Donor**	1.07	1.58	0.54	3.93	0.46	2.66	0.12 ± 0.01	30.6 ± 0.7
	Donor+ Acceptor	*1.05*	*1.23*	*0.56*	*3.76*	*0.44*	*2.35*		
9	**Donor**	1.04	1.76	0.44	4.06	0.56	3.05	0.10 ± 0.02	32.1 ± 1.3
	Donor+ Acceptor	*1.02*	*1.68*	*0.51*	*4.01*	*0.49*	*2.83*		
11	**Donor**	1.09	1.87	0.45	4.25	0.55	*3.17*	0.11 ± 0.02	31.2 ± 1.2
	Donor+ Acceptor	*1.04*	*1.57*	*0.47*	*3.97*	*0.53*	*2.85*		

Table 4.2.8B: Fluorescence lifetime of PEST M1 tryptophan (in presence and absence of acceptor), FRET efficiency and distance between cysteine[9]-tryptophan[70] at different pH (3-11) in presence of 6 M Gdn.HCl.

pH		$\chi^2_{reduced}$	τ_1 (ns)	α_1	τ_2 (ns)	α_2	τ_m (ns)	Average FRET Efficiency	Average distance b/w Cys[9]-Trp[70] (Å)
3	**Donor**	1.02	1.46	0.64	3.57	0.36	2.23	0.09 ± 0.01	32.5 ± 0.7
	Donor+ Acceptor	*1.07*	*1.35*	*0.67*	*3.46*	*0.33*	*2.05*		
4	**Donor**	1.04	1.58	0.61	3.56	0.39	2.36	0.07 ± 0.01	33.7 ± 1.2
	Donor+ Acceptor	*1.05*	*1.41*	*0.66*	*3.57*	*0.34*	*2.15*		
5	**Donor**	1.00	1.59	0.58	3.79	0.42	2.51	0.07 ± 0.01	33.9 ± 1.1
	Donor+ Acceptor	*1.01*	*1.53*	*0.62*	*3.75*	*0.38*	*2.38*		
7	**Donor**	1.00	1.80	0.49	4.33	0.51	3.10	0.08 ± 0.01	33.1 ± 0.5
	Donor+ Acceptor	*1.03*	*1.65*	*0.52*	*4.21*	*0.48*	*2.87*		
9	**Donor**	1.08	1.93	0.46	4.57	0.54	3.37	0.10 ± 0.02	31.9 ± 1.2
	Donor+ Acceptor	*1.03*	*1.74*	*0.51*	*4.39*	*0.49*	*3.03*		
11	**Donor**	1.00	1.88	0.43	4.43	0.57	3.33	0.13 ± 0.01	30.1 ± 0.6
	Donor+ Acceptor	*1.03*	*1.61*	*0.52*	*4.17*	*0.48*	*2.84*		

4.2.9 ANS binding assay of at different pH

ANS (8-Anilinonaphthalene-1-sulfonic acid) binding assay was performed to find changes in the hydrophobic patches of PEST Wt and PEST M1 with varying pH from 3 to 11. All ANS fluorescence spectra were collected by exciting samples at 380 nm (slit width = 5 nm) and emission was collected between 400 nm to 700 nm (slit width = 10 nm) at room temperature. Figure 4.2.9A and B depicts the fluorescence spectra, C and D shows integrated fluorescence and E and F display fluorescence emission maxima of ANS in presence of PEST Wt and PEST M1, respectively at different pH (3-11). Fluorescence emission of ANS without PEST fragment (control) was also collected at different pH (3-11). Both PEST Wt and M1 displays progressive increase in the ANS fluorescence spectra with decrease in the pH. Changes observed in the ANS fluorescence intensity with PEST Wt is nearly similar comparison with PEST M1 at different pH. PEST Wt and PEST M1 display pronounced increase in the ANS fluorescence intensity at pH (3 to 5) whereas; insignificant change was observed from pH 7 to 11. The PEST Wt and PEST M1 show ~ 510% and 470% increase in the integrated ANS fluorescence at pH 3 with respect to pH 11, respectively. Fluorescence spectra of ANS with PEST Wt and M1 show blue shift (505 nm to 476 nm) in its emission maxima with decrease in the pH from 11 to 3. This strong increase in the ANS fluorescence intensity and large blue shift in its emission maxima suggest more binding of ANS with PEST Wt and PEST M1 at acidic pH. However, insignificant change in the ANS fluorescence was observed without PEST fragment at different pH.

Significant increase in the ANS fluorescence intensity with PEST Wt and PEST M1 at pH (3 to 5) demonstrated more ANS binding to PEST fragment resulting from the presence of substantial hydrophobic patches. This indicates presence of folded structure of PEST Wt and PEST M1 at acidic pH (3-5). However, poor changes in ANS fluorescence intensity at pH (7-11) suggest less binding of ANS with the PEST fragment as insignificant population of hydrophobic patches is available. This reveals that PEST Wt and PEST M1 have an unfolded structure at pH (7-11).

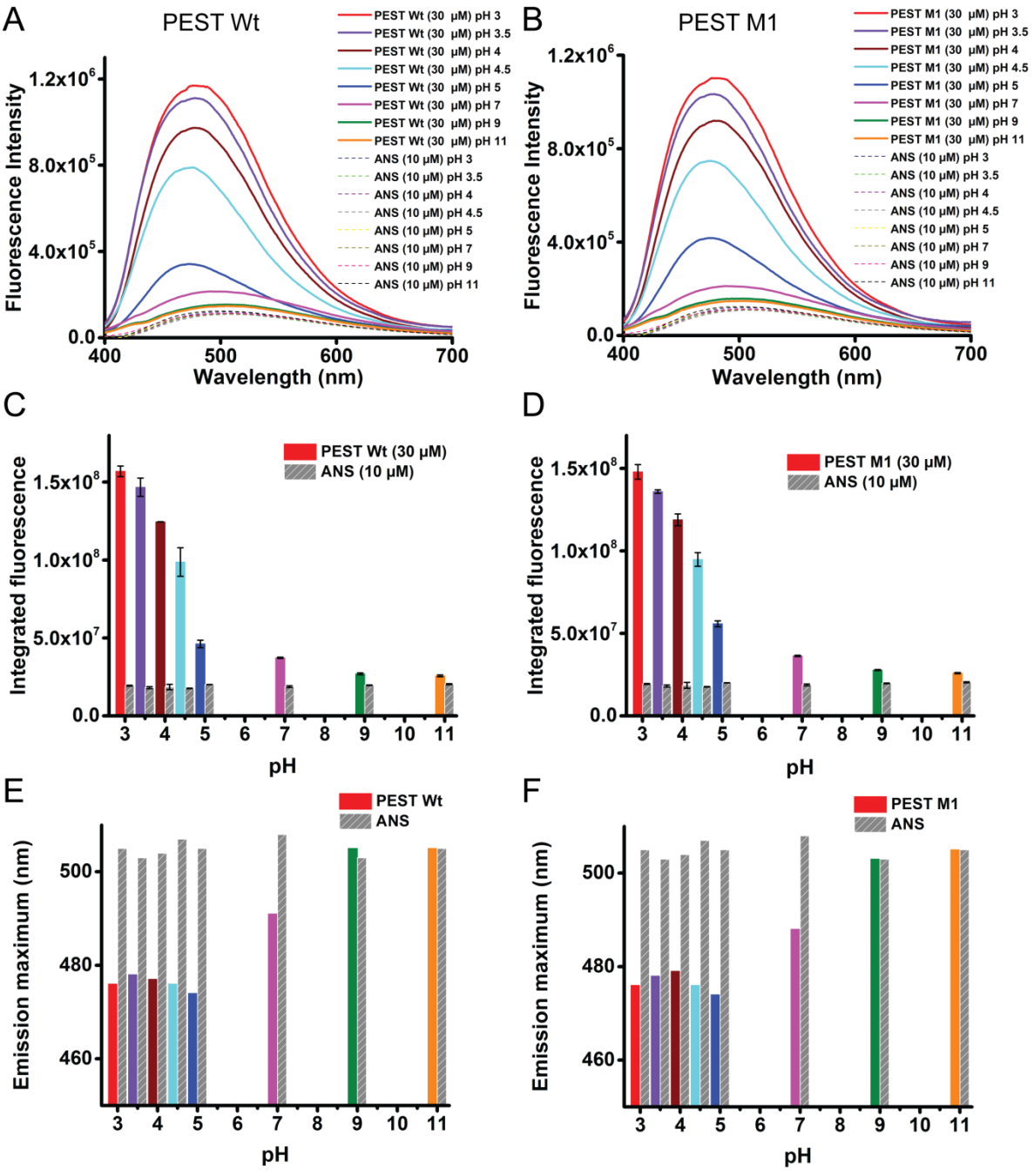

Figure 4.2.9: Effect of pH on ANS fluorescence: [A] and **[B]** display the fluorescence spectra, **[C]** and **[D]** shows integrated fluorescence yield and **[E]** and **[F]** depicts the fluorescence emission maxima of 10 μM ANS in presence of 30 μM of PEST Wt and PEST M1, respectively at different pH 3-11.

4.2.10 Circular Dichroism (CD) analysis

In order to determine the effect of pH on secondary structure content of PEST fragment, Far-UV circular dichroism (CD) spectra of PEST Wt and PEST M1 was collected at different pH (3-11) in the range of 190 to 260 nm. Figure 4.2.10A and B shows the Far-UV CD spectra of PEST Wt and PEST M1 at different pH (3-11), respectively. Both PEST Wt and PEST M1 display similar but not identical CD spectra at different pH (3-11). CD spectra of PEST Wt and PEST M1 show similar negative ellipticity at pH (5-11). CD spectra of PEST Wt and M1 display shift (from 200 nm to 215 nm) in the negative ellipticity at pH (3-4.6). CD spectra of both PEST Wt and PEST M1 are well correlated with the ANS fluorescence emission spectra at different pH (3-11). CD spectra of PEST Wt and PEST M1 depict ample increase in the negative ellipticity at 222 nm at pH (3-4.6) and slight increase at pH 5. Increase in negative ellipticity at 222 nm confirms gain of more α helix and β strand in PEST fragment at acidic pH. However, PEST Wt and M1 display prominent negative ellipticity peak around 200 nm at pH (7-11), which clearly indicate abundance of disordered structure.

To calculate secondary structure content at different pH, CD spectra of PEST Wt and M1 were analyzed using CDSSTR program. Fitted CD curves are shown in the Figure A8 of appendix. Figure 4.2.10C and D depicts the secondary structure content in PEST Wt and M1 at different pH. Both PEST Wt and M1 show increase in the α-helix and β-strands

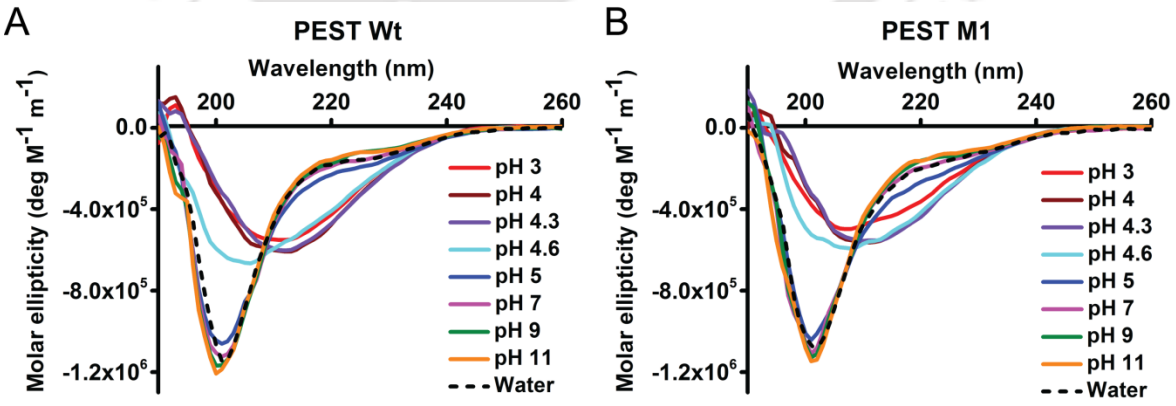

Figure 4.2.10: Effect of pH on CD spectra of **[A]** 20 μM PEST Wt and **[B]** PEST M1, dissolved in water and different 5 mM buffers (pH 3-11). All spectra were recorded at room temperature.

content and decrease in the disorder content at acidic pH (3-4.6). Hence, this secondary structure analysis of PEST fragment also reveals the presence of folded structure at acidic pH. The transition observed in fluorescence quenching is consistent with these results.

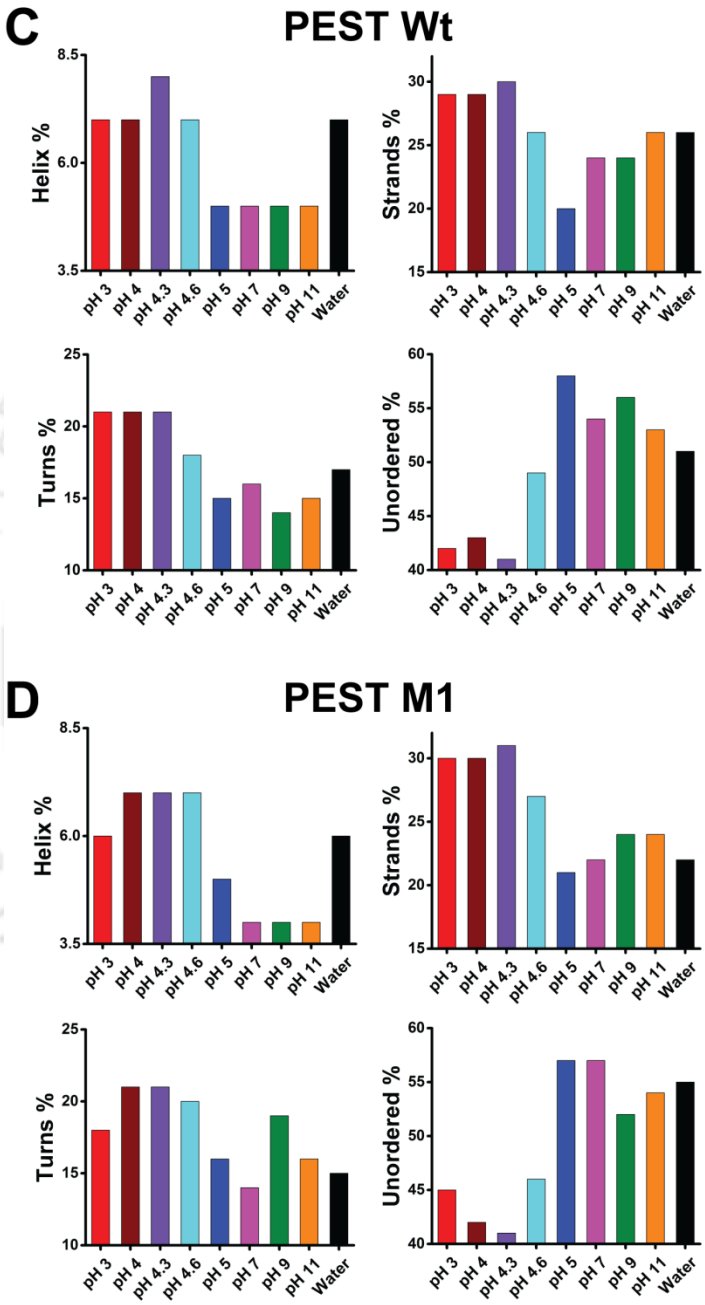

Figure 4.2.10: Change in the secondary structure content in **[C]** PEST Wt and **[D]** PEST M1 at various pH (3-11) and in deionized water.

4.2.11 Effect of salt (NaCl) on PEST fragment

To investigate the effect of excess salt (NaCl) on the structure of PEST fragment, fluorescence emission spectra and steady state anisotropy (r_{ss}) of PEST M1 tryptophan was recorded at pH 7.4 in presence of 25 mM to 500 mM NaCl. Fluorescence emission and anisotropy of tryptophan derivative (NATA) was also recorded under similar conditions. Figure 4.2.11A, B, C and D depicts the fluorescence emission spectra, integrated fluorescence yield, emission maxima and anisotropy of PEST M1 tryptophan and NATA, respectively. No change was observed in the fluorescence spectra, emission spectra and anisotropy of PEST M1 and NATA with increasing concentration of NaCl (25 mM-500 mM). This indicates that introducing the excess salt counter ions to stabilized charge present on PEST fragment does not affect its structure.

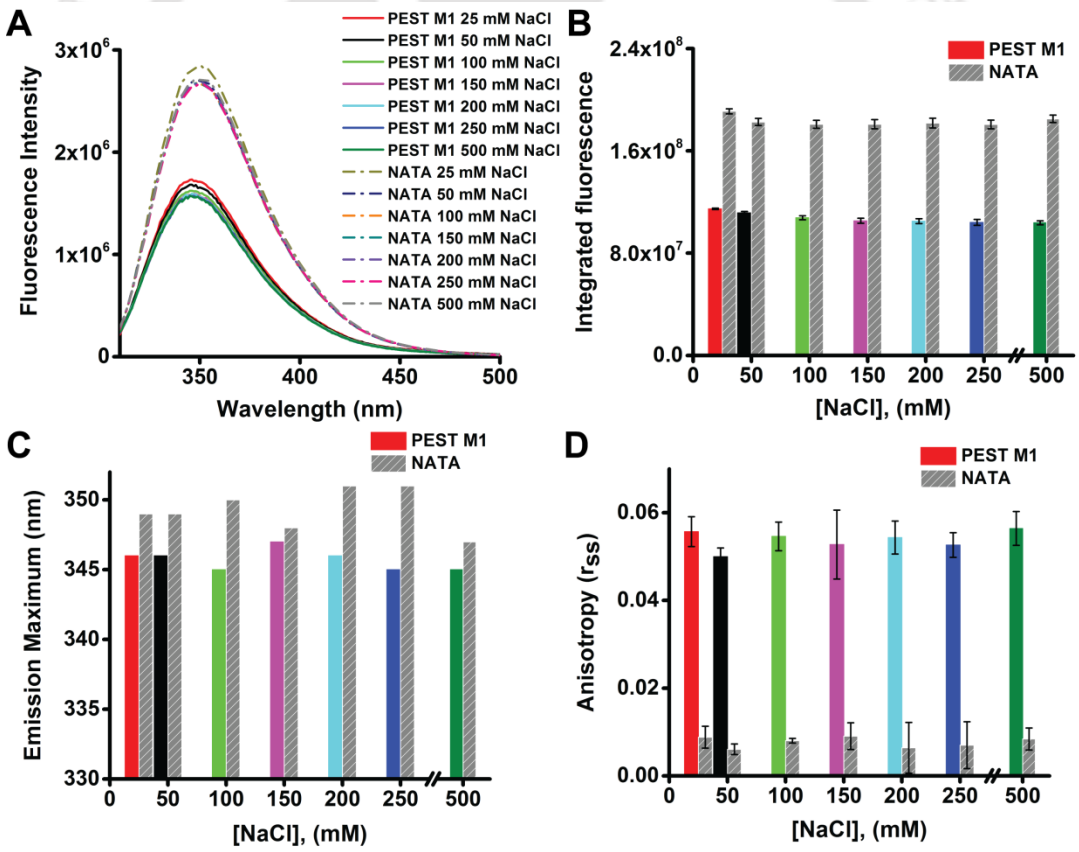

Figure 4.2.11: Effect of excess salt (NaCl) on **[A]** steady state fluorescence spectra; **[B]** integrated fluorescence yield; **[C]** emission maxima and **[D]** steady state anisotropy of 20 μM PEST M1 tryptophan and NATA at pH 7.4 with different NaCl concentrations (25 mM-500 mM).

Further, fluorescence lifetime of PEST M1 tryptophan was monitored with different NaCl concentrations (25 mM-500 mM) at pH 7.4. Figure 4.2.11E and F shows fitted fluorescence intensity decay profile and residuals of PEST M1 tryptophan. No change was observed in intensity decay profile of tryptophan with increasing concentration of NaCl. Table 4.2.11 shows lifetime value of PEST M1 tryptophan with varying NaCl concentration. Analysis of intensity decay reveals insignificant change in the mean lifetime of tryptophan and NATA at different NaCl concentrations (25 mM—500 mM) (Figure 4.2.11G). This time-resolved fluorescence analysis established no structural changes occurred in the vicinity of tryptophan in PEST M1 with increasing concentration of salt (NaCl).

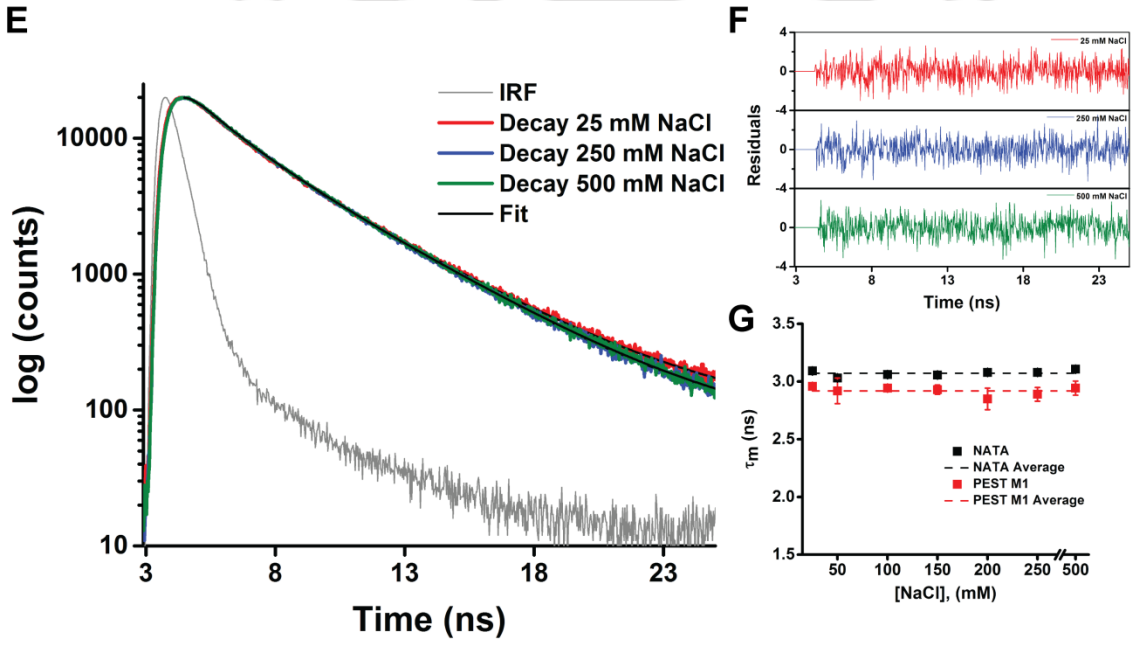

Figure 4.2.11: [E] Fitted time-resolved fluorescence intensity decay profile of 20 µM PEST M1 tryptophan, **[F]** corresponding residuals of the fit and **[G]** mean lifetime (τ_m) of PEST M1 tryptophan and NATA at pH 7.4 with different NaCl concentrations (25 mM-500 mM).

Table 4.2.11: Fluorescence lifetime of PEST M1 tryptophan at pH 7.4 with different NaCl (25 mM-500 mM) concentrations. Average mean lifetime for PEST M1 tryptophan = 2.93 ns ± 0.03 ns.

NaCl Conc. (mM)	$\chi^2_{reduced}$	τ_1 (ns)	α_1	τ_2 (ns)	α_2	Mean lifetime (ns)
25	1.00	1.69	0.50	4.18	0.50	2.95
50	1.07	1.83	0.52	4.21	0.48	2.96
100	1.07	1.77	0.51	4.14	0.49	2.93
150	1.02	1.79	0.53	4.11	0.47	2.89
200	1.01	1.70	0.50	4.10	0.50	2.89
250	1.04	1.79	0.50	4.12	0.50	2.95
500	1.00	1.67	0.47	4.05	0.53	2.93

4.3 Conclusions:

- Steady state fluorescence emission, fluorescence anisotropy (r_{ss}), fluorescence intensity decay and time-resolved anisotropy decay studies of single tryptophan demonstrate more pronounced folding of PEST M1 at C-terminus region in low pH compared to neutral and basic pH as:

  A- Fluorescence mean lifetime of tryptophan increased from 1.7 ns at pH 3 to 3.3 ns at pH 9.

  B- Time-resolved anisotropy decay reveals a significant hindrance to rotational motion of tryptophan at pH 3 and pH 5 as noted from high residual anisotropy (r_∞) values.

  C- The pH dependent effects observed in 25 mM NaCl were greatly diminished in presence of 6 M Gdn.HCl.

- Fluorescence studies of dansyl probe (labeled with single cysteine) revealed less folded form of PEST fragment at N-terminus region in acidic pH.

- A two fold increase in the value of bimolecular fluorescence quenching rate constant (k_q) for tryptophan [1.4 to 3.13 M^{-1} s^{-1} ($X10^9$)] from pH 3 to 11 suggests that tryptophan is buried in protein core at lower pH compared to neutral and basic pH.

- Förster resonance energy transfer studies revealed the distance between cysteine[9] and trytophan[70] was ~21 Å at pH 4 and increased to 32 Å at pH 9. This > 10 Å change in proximity clearly indicates major conformational change in PEST fragment when going from acidic to basic pH.

- Circular Dichroism analysis shows increase in α-helix and β-strands and decrease in disordered structural content in PEST fragment at acidic pH (3—4.6) compared to neutral and basic pH.

- About five-fold increase in integrated fluorescence intensity of ANS at pH 3 with respect to pH 11, reveals presence of significant hydrophobic patches in the PEST fragment at acidic pH.

- Tryptophan fluorescence measurements revealed no structural alteration in PEST fragment at pH 7.4 in presence of excess salt, 25 mM—500 mM NaCl.

Chapter 5

Unravelling the dimeric properties of human c-Myc PEST fragment and its mutant

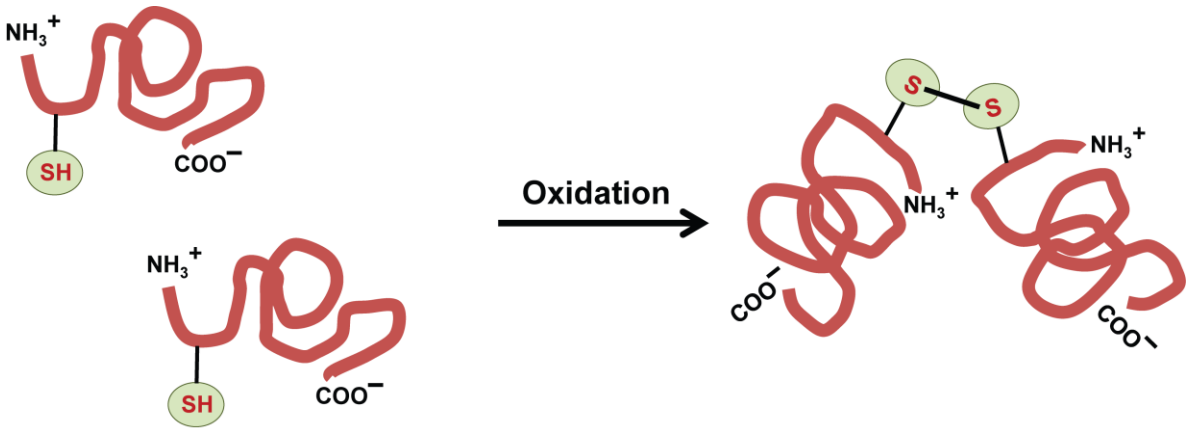

5.1 Introduction:

An exciting feature of many Intrinsically Disordered Proteins (IDPs)/ Intrinsically Disordered Regions (IDRs) is the ability to gain structure upon binding with their specific partners and ligands (like different metal ions, osmolytes, membranes, DNA, RNA, proteins and in the macromolecular crowding). Even in the bound form many IDPs displays some disordered regions (Dunker et al., 2001; Plaxco and Gross, 1997; Uversky et al., 2000a; Uversky and Narizhneva, 1998; Wright and Dyson, 1999). This ligand-induced folding can be described by its influence on the mean hydrophobicity and/or mean net charge of IDPs. Interactions of IDPs with their natural binding partner can change its mean hydrophobicity and/or mean net charge in such a way that these values approaches close to those of ordered protein. This ligand-induced folding in IDPs has been established in many in vitro studies (Gatewood et al., 1990; Horiuchi et al., 1997; Stellwagen et al., 1972; Uversky et al., 2000a; Warrant and Kim, 1978).

We made many unsuccessful attempts to label PEST fragment in non-reducing condition with dansyl probe using IAEDANS (1,5-IAEDANS, 5-((((2-Iodoacetyl) amino) ethyl) amino)Naphthalene-1-Sulfonic Acid) which reacts with the free thiol group of cysteine. But to our surprise, this labeling of dansyl to PEST fragment only happened in reducing environment. This gave us an idea about cysteine being involved in the dimerization of PEST. This motivated us to investigate the structure of PEST dimer and nature of interaction involved in its dimerization.

In this chapter, we investigate the dimeric properties of PEST fragment by using different techniques like reducing and non-reducing SDS-PAGE, DTNP assay and mass spectrometry. Further, the structural and dynamics information of PEST dimer was extracted using different fluorescence techniques. These investigations explore the structural properties of PEST dimer and interactions involved in the dimer formation.

5.2 Results and Discussion:

5.2.1 Estimation of free thiol group

To check for the dimer formation in PEST fragment and nature of interactions involved in the dimerization, estimation of its free thiol group was done using DTNP (2,2′-Dithio*bis*(5-nitropyridine)) assay. Figure 5.2.1A and B display the standard plots for known concentration of L-cysteine in presence of 25 mM Tris.HCl (pH 7.4) and 6 M Gdn.HCl, respectively. Concentration of free thiol group in PEST Wt and PEST M1 was determined by calibrating the absorbance at 387 nm with standard plot of L-cysteine under the identical conditions. Figure 5.2.1C depicts the amount of free thiol group (in percentage) present in different concentrations (10—30 µM) of PEST Wt and M1 in presence of 25 mM Tris.HCl (pH 7.4) and 6 M Gdn.HCl, respectively. Results of DTNP assay reveals that significantly lower amount of free thiol is present in PEST Wt and PEST M1 in presence of 25 mM Tris.HCl (pH 7.4). The reason for this may be due to involvement of free cysteine in the dimer formation of PEST fragment through disulphide bond or free cysteine may not be available to react with DTNP because of its buried nature either inside the protein core or within the formed dimer.

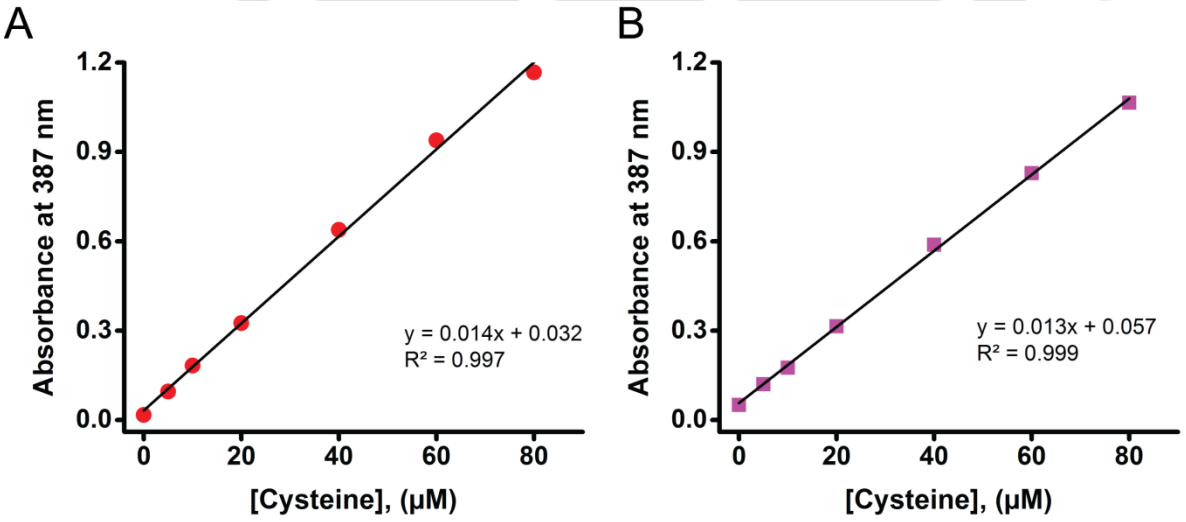

Figure 5.2.1: Standard plot of L-cysteine monitored at 387 nm using 50 µM DTNP in presence of **[A]** 25 mM Tris.HCl (pH 7.4) and **[B]** 6 M Gdn.HCl.

To resolve this, DTNP assay was performed by overnight incubation of PEST Wt and M1, in 6 M Gdn.HCl at room temperature to completely unfold and expose the free cysteine. Even in the presence of 6 M Gdn.HCl, insignificant increase in free thiol of PEST Wt and PEST M1 was observed. This availability of fewer free thiol in PEST Wt and M1 in presence of 6 M Gdn.HCl, clearly suggests involvement of free thiol in the dimer formation of PEST fragment through disulphide bond.

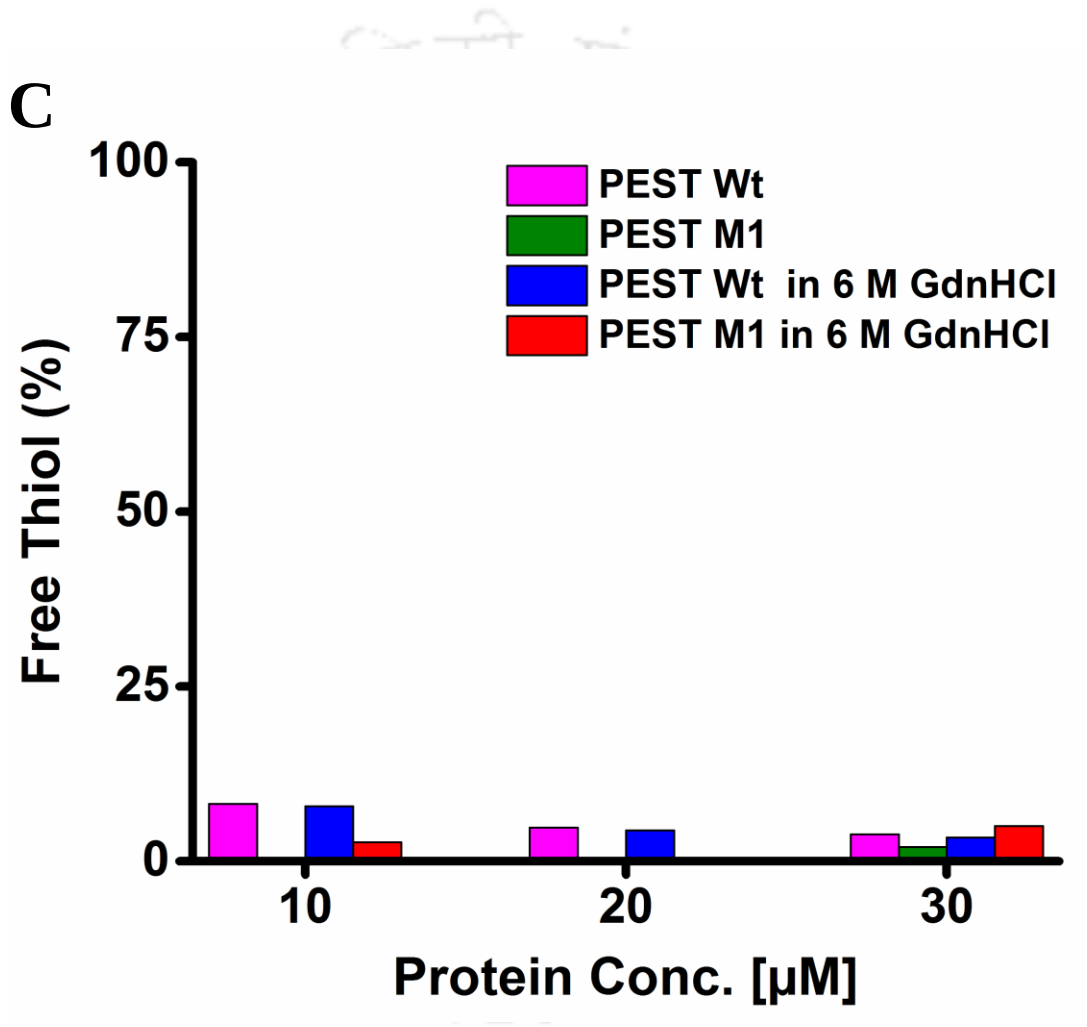

Figure 5.2.1C: Percentage of free thiol group present in 10—30 μM of PEST Wt and PEST M1 in presence of 25 mM Tris.HCl (pH 7.4) and 6 M Gdn.HCl, respectively using 50 μM of DTNP at room temperature is shown.

5.2.2 Non-reducing and reducing SDS-PAGE

To confirm involvement of free cysteine into dimerization of its PEST fragment through disulphide bond formation, 15% non-reducing and reducing SDS-PAGE analysis of PEST Wt and PEST M1 was carried out. Figure 5.2.2A and C displays non-reducing, while B and D depict reducing SDS-PAGE of PEST Wt and PEST M1, respectively. Non-reducing SDS-PAGE shows mixture of both monomeric and dimeric bands. While in reducing SDS-PAGE, presence of reducing agent (β-Mercaptoethanol) caused reduction of disulphide bond (formed between free cysteines) and it displays only monomeric band of PEST Wt and PEST M1. This result clearly indicates dimerization of PEST fragment by disulphide bond formation.

Like monomeric PEST fragment (described in chapter 3), dimer of PEST Wt and PEST M1 also shows anomalous behavior on the non-reducing SDS-PAGE. Dimer of PEST fragment display slower migration on the SDS-PAGE with approximate Molecular Weight (MW) of 28 kDa.

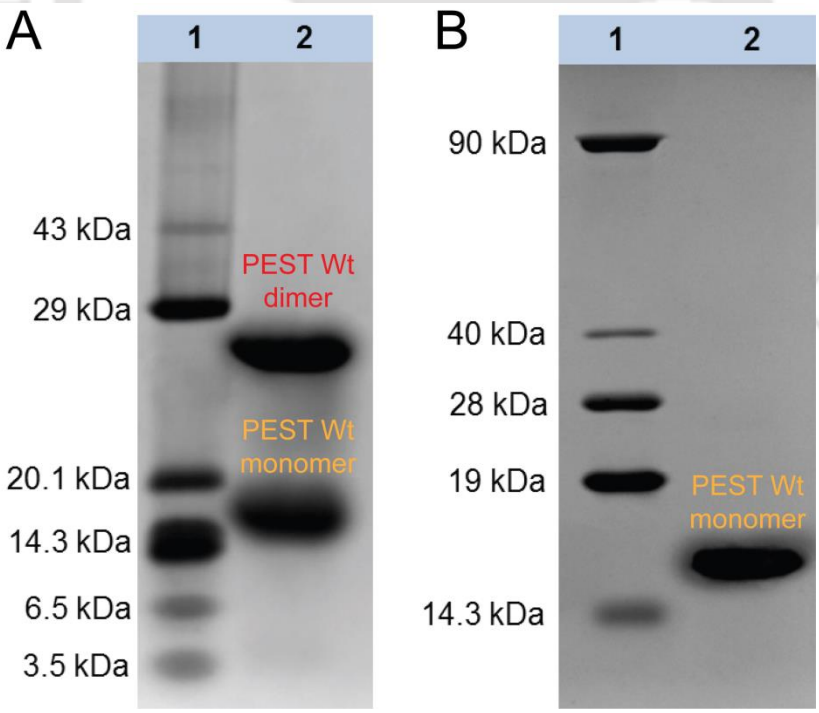

Figure 5.2.2: [A] 15% non- reducing and **[B]** reducing SDS-PAGE of PEST Wt showing monomeric and dimeric bands of purified proteins.

This anomalous nature of PEST dimer on SDS-PAGE hints toward presence of disordered structure.

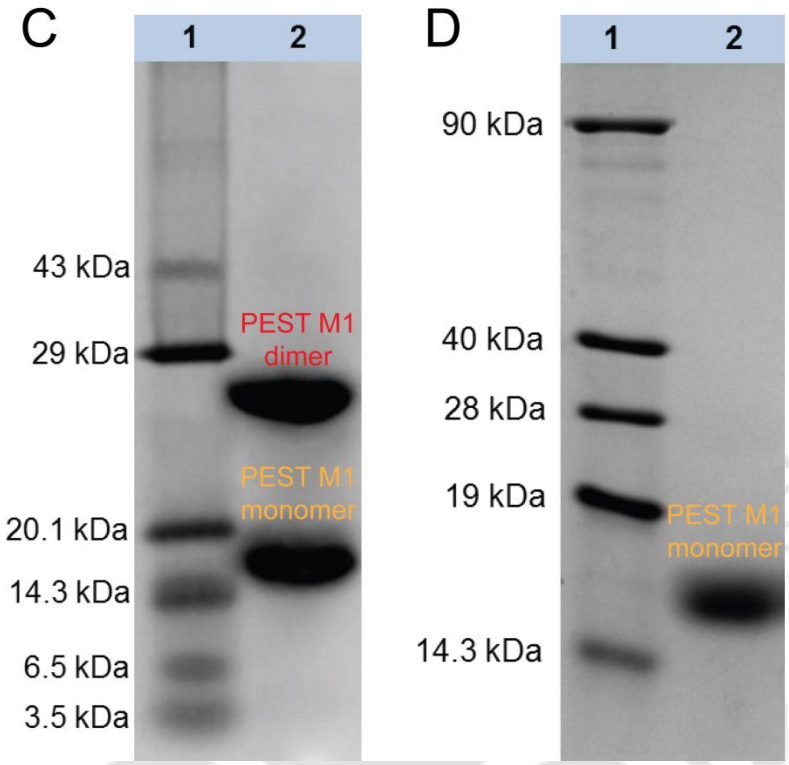

Figure 5.2.2: [C] 15% non- reducing and **[D]** reducing SDS-PAGE of PEST M1 showing monomeric and dimeric bands of purified proteins.

5.2.3 Mass analysis of PEST dimer

To confirm the actual Molecular Weight (MW) of PEST dimer, mass spectra of PEST Wt and PEST M1 were recorded under the non-reducing conditions. Figure 5.2.3 shows mass spectra of PEST Wt and PEST M1 under non-reducing conditions. Analysis of mass spectra explores presence of monomeric and dimeric forms of PEST fragments. However, in the presence of reducing agent (β-Mercaptoethanol) mass spectra of PEST Wt and PEST M1 show only the monomeric forms (shown in Figure 3.2.4 of chapter 3). Table 5.2.3 displays a comparison of PEST Wt and PEST M1 dimer molecular masses with their monomeric PEST fragment. The actual molecular mass of PEST Wt and PEST M1 dimer, determined by mass spectrometry was 16681.43 and 17050.29 Da, respectively. However, PEST dimer shows about 1.7 fold increases in its MW (about 28 kDa), determined by non-reducing SDS-PAGE.

Hence, mass spectrometry investigations establish the dimer formation in PEST fragment by disulphide bond formation and its disordered nature. This dimerization of PEST fragment and its disordered behavior encouraged us further to extract its structural information.

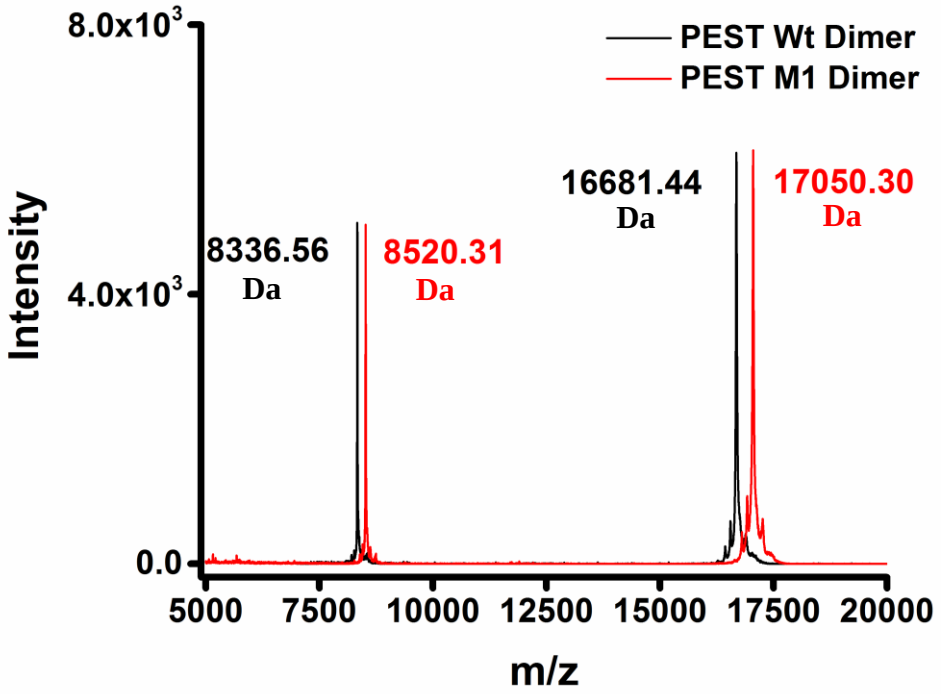

Figure 5.2.3: Mass spectra of PEST Wt and PEST M1 dimer under non-reducing condition, showing mixture of monomeric and dimeric population in both PEST Wt and PEST M1.

Table 5.2.3: Comparison of PEST dimer molecular weight determined by mass spectrometry with monomeric PEST fragment.

Protein name	Observed MW (Da)	Expected MW (Da)
PEST Wt Dimer	16681.44	16681.22
PEST M1 Dimer	17050.30	17053.64
PEST Wt monomer	*8336.56*	*8341.61*
PEST M1 monomer	*8520.31*	*8527.82*

5.2.4 Size exclusion chromatography of PEST Dimer

In order to investigate structural properties of PEST dimer, it was separated from PEST monomer using size exclusion chromatography. Figure 5.2.4A displays the elution profile of PEST Wt and PEST M1 under non-reducing condition. Both PEST Wt and PEST M1 shows separated elution peak for monomeric and dimeric population. PEST Wt and M1 monomer eluted with 82.31 and 82.43 mL whereas, their dimer were eluted with the elution volume of 72.19 and 72.37 mL, respectively. Dimeric and monomeric population of PEST fragment as calculated from their area under elution peak is shown in Table 5.2.4A. PEST M1 has slightly higher dimeric population (63.3%) than PEST Wt dimer (59.1%).

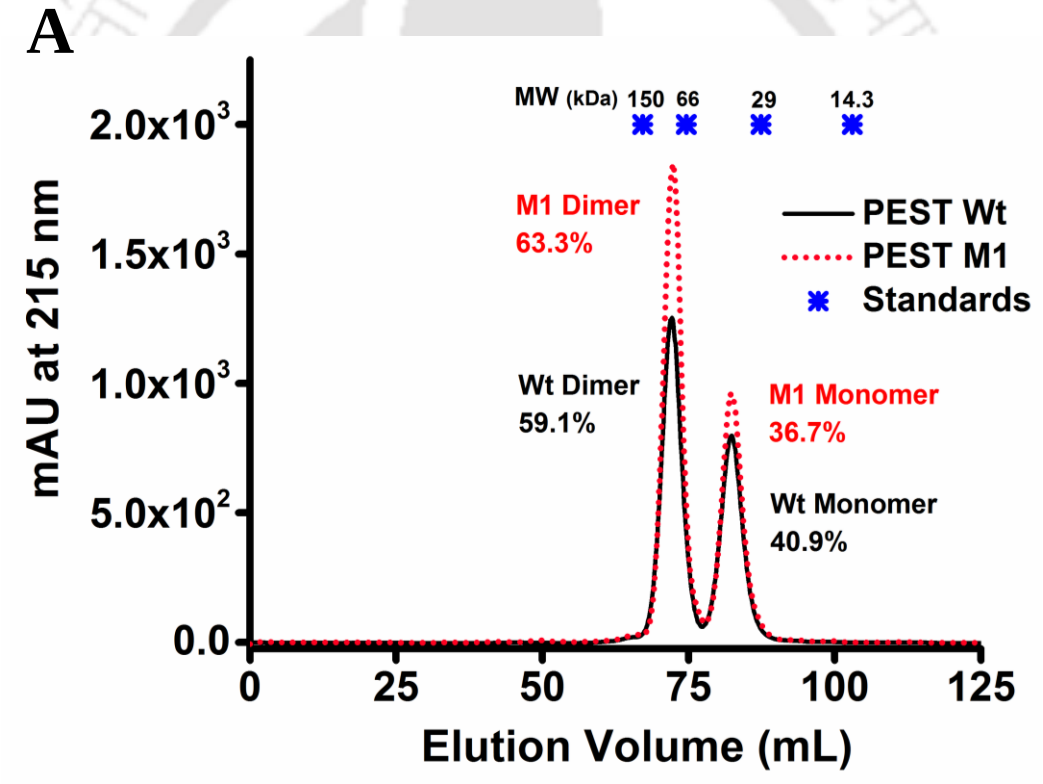

Figure 5.2.4A: Size exclusion chromatography elution profile of PEST Wt and M1; monitored at 215 nm, showing the mixture of monomer and dimer. Both PEST Wt and M1 were eluted with non-reducing elution buffer (25 mM Tris.HCl (pH 7.4); 25 mM NaCl) at room temperature. Asterisks represent the elution positions of standards.

Further, the Molecular Weight (MW) of PEST Wt and PEST M1 dimer was calculated from the standard plot (Figure 5.2.4B), plotted between partition coefficient (K_{av}, calculated using equation 2.65) and logarithmic molecular weight of relative standard proteins (described in section 3.2.6 of chapter 3). Table 5.2.4A shows calculated MW of PEST Wt and PEST M1 dimer using size exclusion chromatography. The apparent MW of PEST Wt and PEST M1 dimer determined by size exclusion chromatography were about 5.5 times higher than its actual MW (calculated by mass spectrometry). Further, the monomer and dimer forms of PEST Wt and mutant M1 both fall in the fitted line (Figure 5.2.4B) suggesting similar shapes. This over estimation in the MW of PEST Wt and PEST M1 dimer determined by size exclusion chromatography reveals random coil structure of PEST dimer.

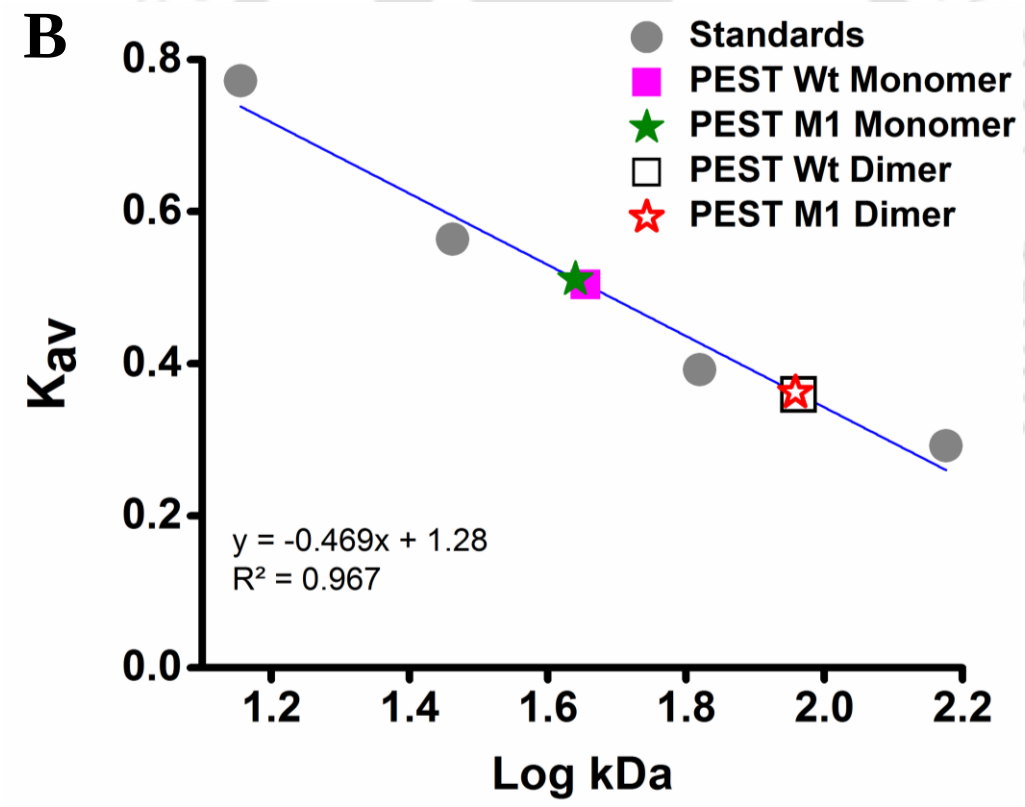

Figure 5.2.4B: Standard curve (partition coefficient (K_{av}) vs. logarithm molecular weight of standard proteins) for calculating the molecular weight of PEST monomer and dimer.

Table 5.2.4A: Comparison of PEST dimers molecular weight and their fractional populations determined by size exclusion chromatography with monomeric PEST fragment.

Protein name	Apparent MW (kDa)	Population in %
PEST Wt Dimer	91.85 [0.04][a]	59.1
PEST M1 Dimer	90.71 [0.12]	63.3
PEST Wt monomer	*46.54 [1.22]*	*40.9*
PEST M1 monomer	*45.98 [2.05]*	*36.7*

[a] The numbers in square brackets indicates the standard deviation for n=2—3.

Additionally, to get more insight about hydrodynamic properties of PEST dimer, its Stokes radii (R_s) was calculated. The Stokes radii of PEST Wt and PEST M1 dimer was determined from the standard plot (Figure 5.2.4C), plotted between $(-\text{Log } K_{av})^{1/2}$ and known Stokes radii of standard proteins (describe in the section 3.2.6 of chapter 3). The calculated

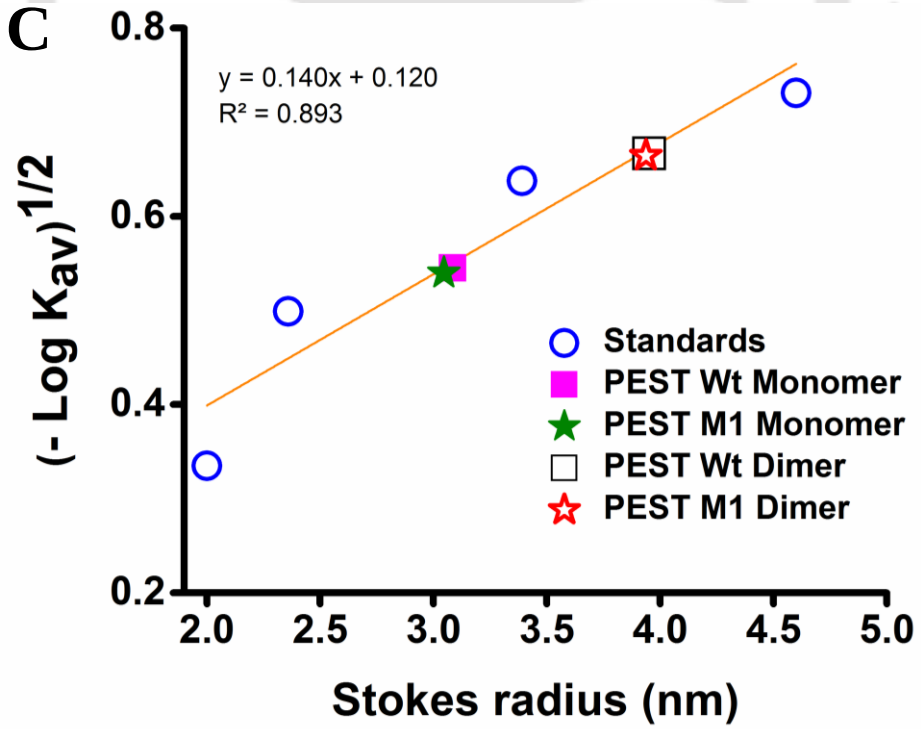

Figure 5.2.4C: Standard curve ($(-\text{Log } K_{av})^{1/2}$ vs. Stokes radii of standard proteins) for calculating the Stokes radius of PEST monomer and dimer.

Stokes radii of PEST Wt and PEST M1 dimer are given in the Table 5.2.4B. The calculated Stokes radii of PEST Wt and PEST M1 dimer were 3.95 and 3.93, respectively. This large Stokes radii value in comparison to polypeptide chain length of PEST Wt and PEST M1 dimer reveals their extended coil-like structure.

Table 5.2.4B: Comparison of PEST Wt and PEST M1 dimers Stokes radii with their monomers determined by size exclusion chromatography.

Protein name	Stokes radius (nm)
PEST Wt Dimer	3.95 [0.001][a]
PEST M1 Dimer	3.93 [0.002]
PEST Wt monomer	*3.11 [0.030]*
PEST M1 monomer	*3.10 [0.052]*

[a] The numbers in square brackets indicates the standard deviation for n=2—3.

5.2.5 Dynamic light scattering studies of PEST Dimer

To directly determine and validate the Stokes radius estimated by size exclusion chromatography, Dynamic Light Scattering (DLS) studies of PEST Wt and PEST M1 dimer were carried out under non-reducing condition. The size (diameter in nm) of PEST Wt and PEST M1 dimer are shown in Figure 5.2.5A. Table 5.2.5 display the comparison of PEST Wt and M1 dimer Stokes radius with PEST monomer. Stokes radius of PEST dimer determined by DLS is closely matching with the value estimated by size exclusion chromatography. Figure 5.2.5B display the comparison of PEST Wt and PEST M1 dimer correlation coefficient with their monomer. Correlogram of both PEST Wt and PEST M1 dimer shows the longer decay time than PEST Wt and M1 monomer, respectively. This is due to larger hydrodynamic size of dimer as compared to monomeric PEST fragment.

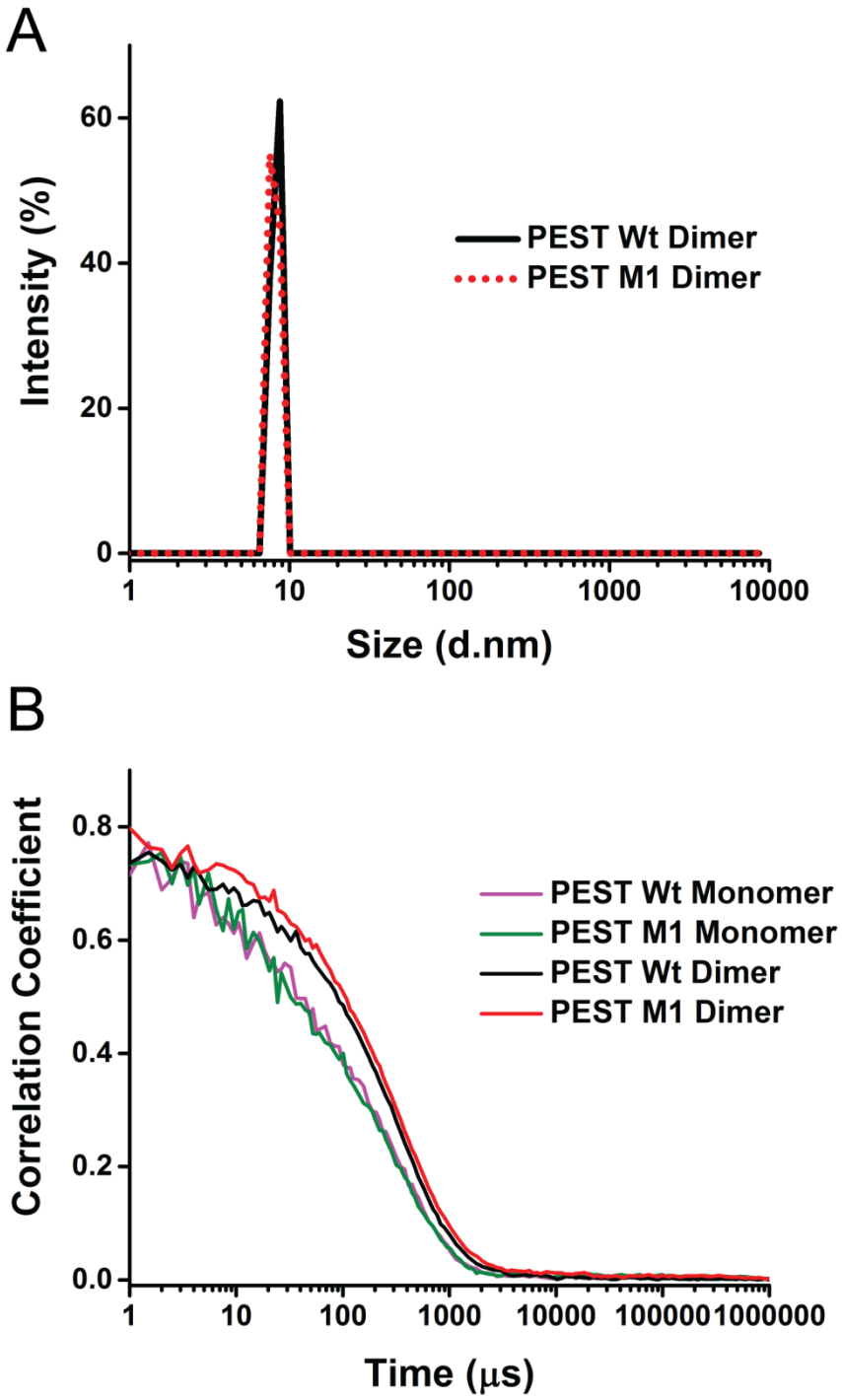

Figure 5.2.5: [A] Hydrodynamic diameter of 1.5 mg/mL PEST Wt and M1 dimer dissolved in non-reducing buffer (25 mM Tris.HCl (pH 7.4); 25 mM NaCl) at room temperature is shown and **[B]** show the comparison of correlation coefficient of monomeric and dimeric PEST Wt and M1, respectively.

Table 5.2.5: Comparison of PEST Wt and PEST M1 dimers Stokes radii with their monomers determined by dynamic light scattering.

Protein name	Stokes radius (nm)
PEST Wt Dimer	4.19 [0.20][a]
PEST M1 Dimer	4.12 [0.08]
PEST Wt monomer	*3.14 [0.21]*
PEST M1 monomer	*3.13 [0.19]*

[a] The numbers in square brackets indicates the standard deviation for n=2—3.

5.2.6 Steady state fluorescence and anisotropy studies of PEST M1 dimer

The tryptophan steady state fluorescence emission of PEST M1 dimer was measured at pH 7.4 in non-reducing environment to explore the environment around its indole ring. The tryptophan emission spectra were collected by exciting the samples at 295 nm. Figure 5.2.6 displays the tryptophan steady state fluorescence spectra in PEST M1 monomer and its dimer along with a tryptophan derivative, NATA (N-acetyl tryptophan amide). Both PEST M1 dimer and monomer display its tryptophan emission maxima at 346 nm whereas, NATA show its emission maxima at 349 nm, as expected for indole ring fully exposed to aqueous solvent. The maximum fluorescence intensity of PEST M1 dimer at 346 nm clearly suggests significant exposure of tryptophan to the aqueous solvent.

Additionally, to gain the information about the structure and rotational dynamics of PEST M1 dimer at the C-terminus region, steady state fluorescence anisotropy (r_{ss}) of its tryptophan was analyzed at room temperature. Table 5.2.6 display the fluorescence anisotropy value of PEST M1 dimer, monomer and NATA. The measured tryptophan anisotropy of PEST M1 dimer was lower than its monomer. This lower anisotropy suggests faster rotation of tryptophan in PEST dimer than monomer due to its unhindered motion.

Free rotational motion of tryptophan clearly indicates more loose structure of PEST M1 dimer in the vicinity of tryptophan than PEST M1 monomer.

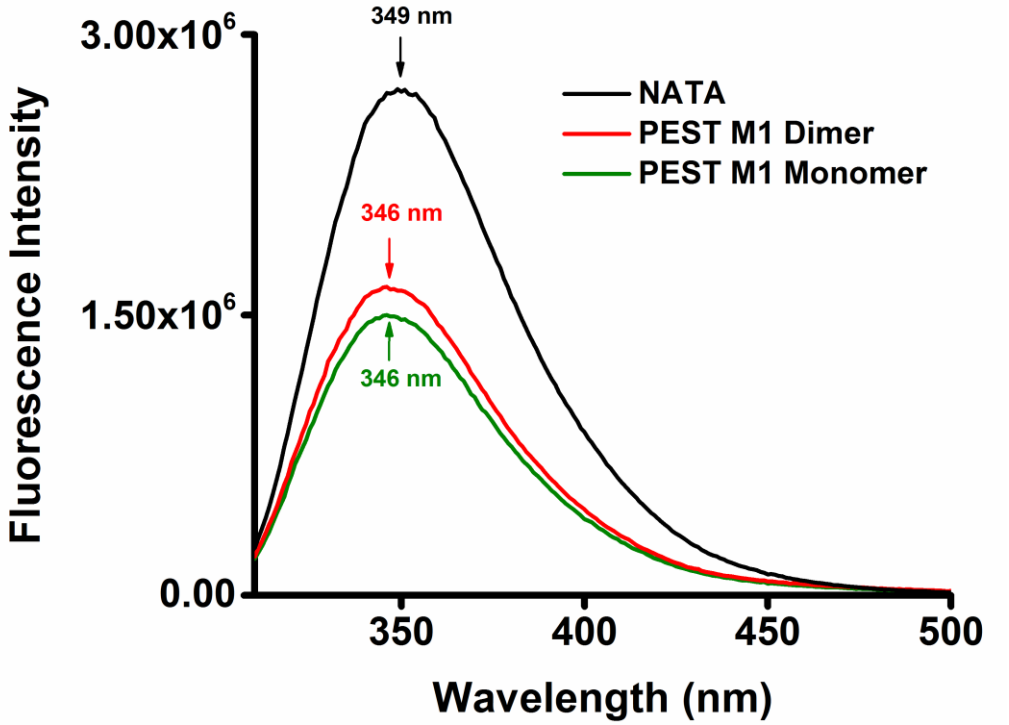

Figure 5.2.6: Tryptophan steady state fluorescence spectra of 20 µM PEST M1 monomer and 10 µM PEST M1 dimer; dissolved in 25 mM Tris.HCl (pH 7.4); 25 mM NaCl; 5 mM TCEP and 25 mM Tris.HCl (pH 7.4); 25 mM NaCl, respectively. Emission spectra of 20 µM NATA is also shown as a control.

Table 5.2.6: Steady state anisotropy of NATA and tryptophan of the PEST M1 dimer and monomer.

Protein name	Steady state anisotropy (r_{ss})
PEST M1 Dimer	0.042 [0.002][a]
PEST M1 monomer	0.051 [0.005]
NATA	0.004 [0.003]

[a] The numbers in square brackets indicates the standard deviation for n=2—3.

5.2.7 Fluorescence lifetime analysis of PEST M1 dimer

To extract more structural insights of PEST M1 dimer, fluorescence lifetime (τ) of its tryptophan was determined at pH 7.4 in non-reducing condition. Figure 5.2.7 depicts the tryptophan fluorescence intensity decay profile of PEST M1 dimer and its monomer. The analysis of tryptophan fluorescence decay revealed the presence of two lifetimes in PEST dimer. A large component of 4.05 ns with amplitude of 0.49 and a short component of 1.71 ns with amplitude of 0.51 was present. No change in tryptophan mean fluorescence lifetime of was observed in PEST M1 dimer (2.84 ns) and its monomer (2.88 ns). The tryptophan lifetime values of PEST dimer and monomer obtained after fitting the intensity decay profile are given in Table 5.2.7.

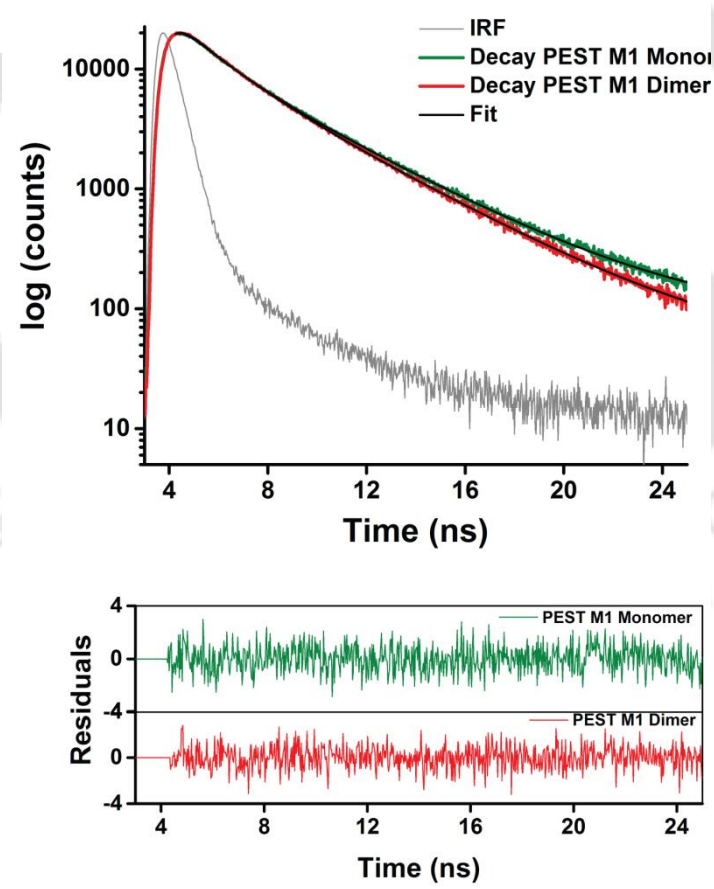

Figure 5.2.7: Tryptophan fluorescence intensity decay profiles of 20 μM PEST M1 monomer and 10 μM PEST M1 dimer at pH 7.4 in reducing and non-reducing condition, respectively are shown in top panel. Residual for fit are shown in bottom panel.

Table 5.2.7: Tryptophan Fluorescence lifetime of PEST M1 dimer and monomer at pH 7.4.

PEST	$\chi^2_{reduced}$	τ_1 (ns)	α_1	τ_2 (ns)	α_2	Mean lifetime (ns)
Dimer	1.00	1.71	0.51	4.05	0.49	2.84
Monomer	1.01	1.59	0.49	4.12	0.51	2.88

5.2.8 Time-resolved anisotropy decay analysis of PEST M1 dimer

To calculate rotational correlation time (θ) of PEST M1 dimer, the fluorescence anisotropy decay of its tryptophan was measured at pH 7.4 in non-reducing condition. Figure 5.2.8A display the tryptophan anisotropy decay profile of PEST M1 dimer and its monomer. PEST M1 dimer shows faster anisotropy decay profile in comparison with PEST M1 monomer. Figure 5.2.8B depicts the fitted anisotropy decay and its corresponding residuals for PEST M1 dimer. The analysis of anisotropy decay profile of PEST M1 dimer shows two correlation times, a fast correlation time (θ_{fast}) of 1.06 ns with an amplitude of 0.85 and a slow correlation time (θ_{slow}) of 6.89 ns with an amplitude of 0.15. The detailed analysis of tryptophan anisotropy decay of PEST M1 dimer and its monomer are shown in Table 5.2.8. PEST M1 dimer reveals higher fractional contribution of fast correlation time (θ_{fast}) than PEST M1 monomer to the decay. The dominance of fast correlation time (θ_{fast}) in PEST M1 dimer suggests free and fast rotation of its indole ring due to more unfolded structure in the vicinity of tryptophan. Hence, tryptophan fluorescence measurements indicate that C-terminus of PEST M1 dimer is likely to be more disordered than PEST M1 monomer.

Table 5.2.8: Tryptophan anisotropy decay data of PEST M1 dimer and its monomer at pH 7.4.

PEST	$\chi^{2\,a}$	$r_0{}^b$	$r_{ss}{}^c$	$\phi_1{}^d$ (ns)	$\alpha_1{}^e$	$\phi_2{}^d$ (ns)	$\alpha_2{}^e$
Dimer	1.00	0.13	0.047	1.06	0.850	6.9	0.150
Monomer	1.07	0.16	0.059	0.92	0.759	7.0	0.241

[a] reduced χ^2 for the fit; [b] initial anisotropy; [c] steady state anisotropy calculated from fit; [d] rotational correlation time(s); [e] fractional amplitude associated with the correlation time.

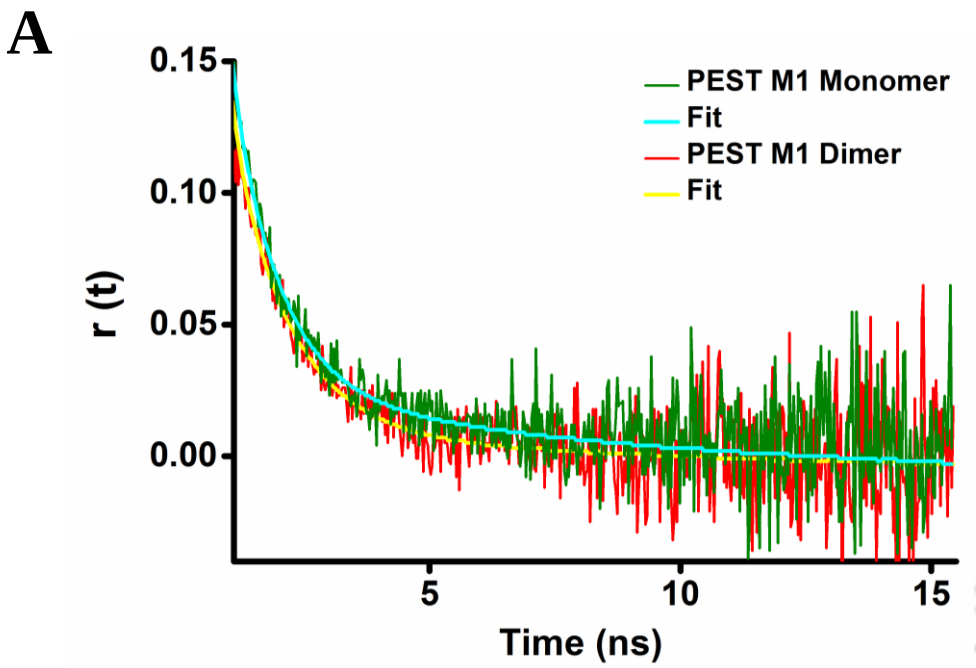

Figure 5.2.8A: Tryptophan anisotropy decay profile of 20 μM PEST M1 monomer and 10 μM PEST M1 dimer at pH 7.4 in reducing and non-reducing condition, respectively.

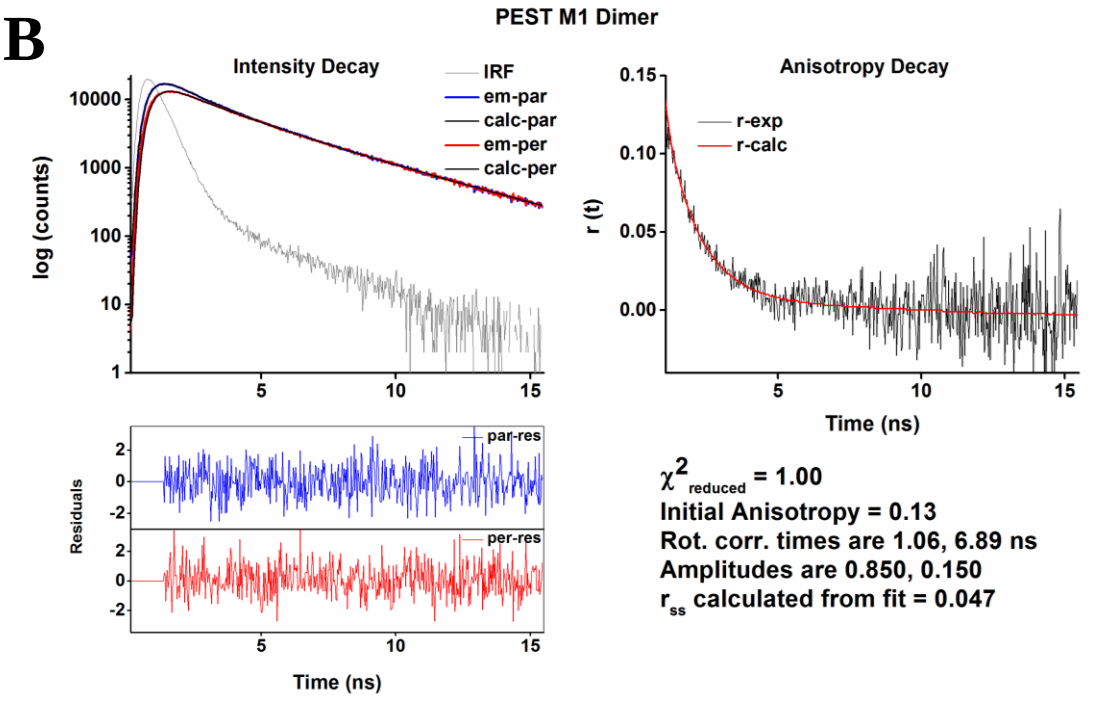

Figure 5.2.8B: Fitted tryptophan anisotropy decay profile of 10 μM PEST M1 dimer; dissolved in non-reducing buffer.

5.2.9 Circular Dichroism analysis of PEST Wt and M1 dimer

To determine the change in the secondary structure content of PEST fragment upon dimerization, Far-UV Circular Dichroism (CD) spectra of PEST Wt and PEST M1 dimer were recorded in the range of 190 to 260 nm at pH 7.4 under non-reducing conditions. Figure 5.2.9A depicts the comparison of Far-UV CD spectra of PEST Wt and PEST M1 dimer with their monomers. Both PEST Wt and PEST M1 monomer shows negative ellipticity peak at 201 nm whereas, PEST Wt and PEST M1 dimer display negative ellipticity peak at 205 and 202 nm, respectively. PEST Wt dimer shows more negative ellipticity at 205 and 222 nm in comparison with PEST M1 dimer. This higher negative ellipticity of PEST Wt dimer at 222 nm suggests gain of more ordered structure than PEST M1 dimer.

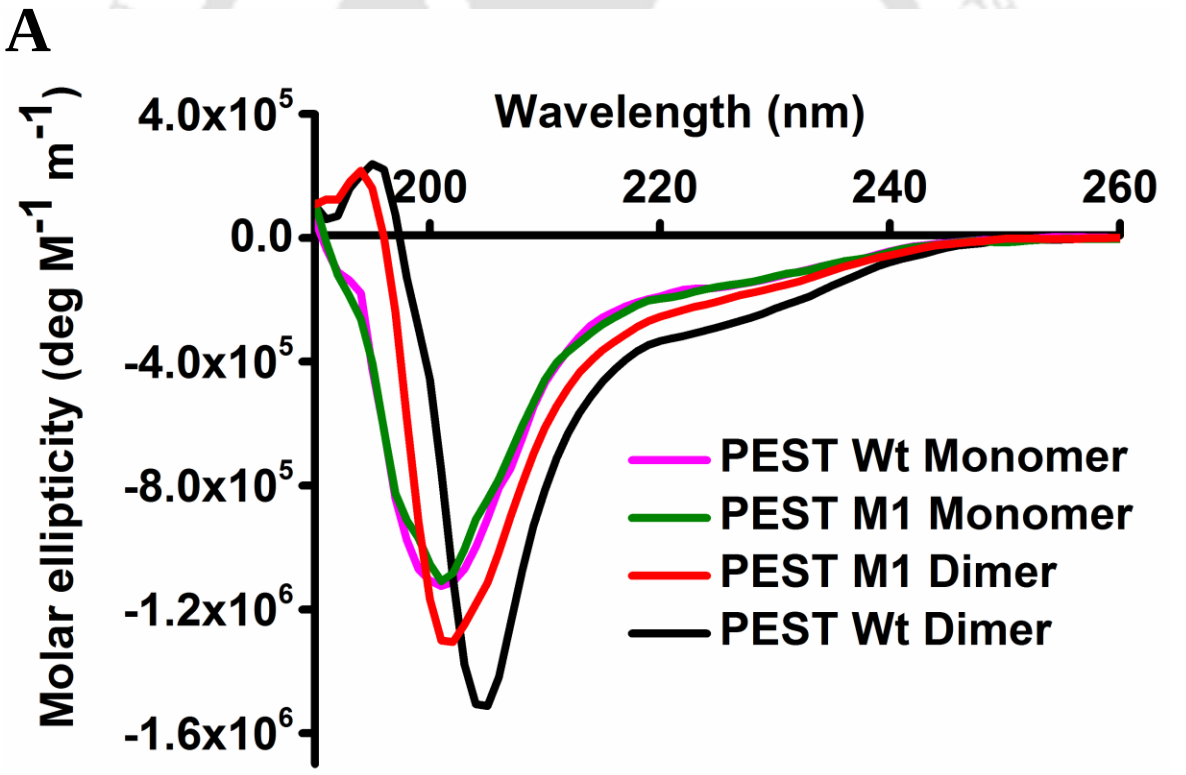

Figure 5.2.9A: Far-UV CD spectra of 20 µM monomeric and 20 µM dimeric PEST Wt and PEST M1, respectively recorded at room temperature. Monomeric PEST fragment was dissolved in 5 mM Sodium phosphate (pH 7.4) buffer, containing 1 mM TCEP and dimeric PEST fragments was dissolved in non-reducing 5 mM Sodium phosphate (pH 7.4) buffer.

Figure 5.2.9B display the comparison of secondary structure content in PEST Wt and PEST M1 dimer with their respective monomers. The secondary structure content in PEST Wt and PEST M1 dimer was calculated using CDSSTR program and reconstructed spectra was well superimposed on experimental spectra (Figure 5.2.9C and D). PEST Wt dimer displays more α-helix content than PEST M1 dimer. Both PEST Wt and M1 dimer shows decrease in their disorder content in comparison with PEST Wt and M1 monomer, respectively. Secondary structure content calculations clearly indicate some structural gain in PEST Wt and PEST M1 dimer as compared to their monomers. However, both PEST Wt and M1 remain significantly disordered after dimerization.

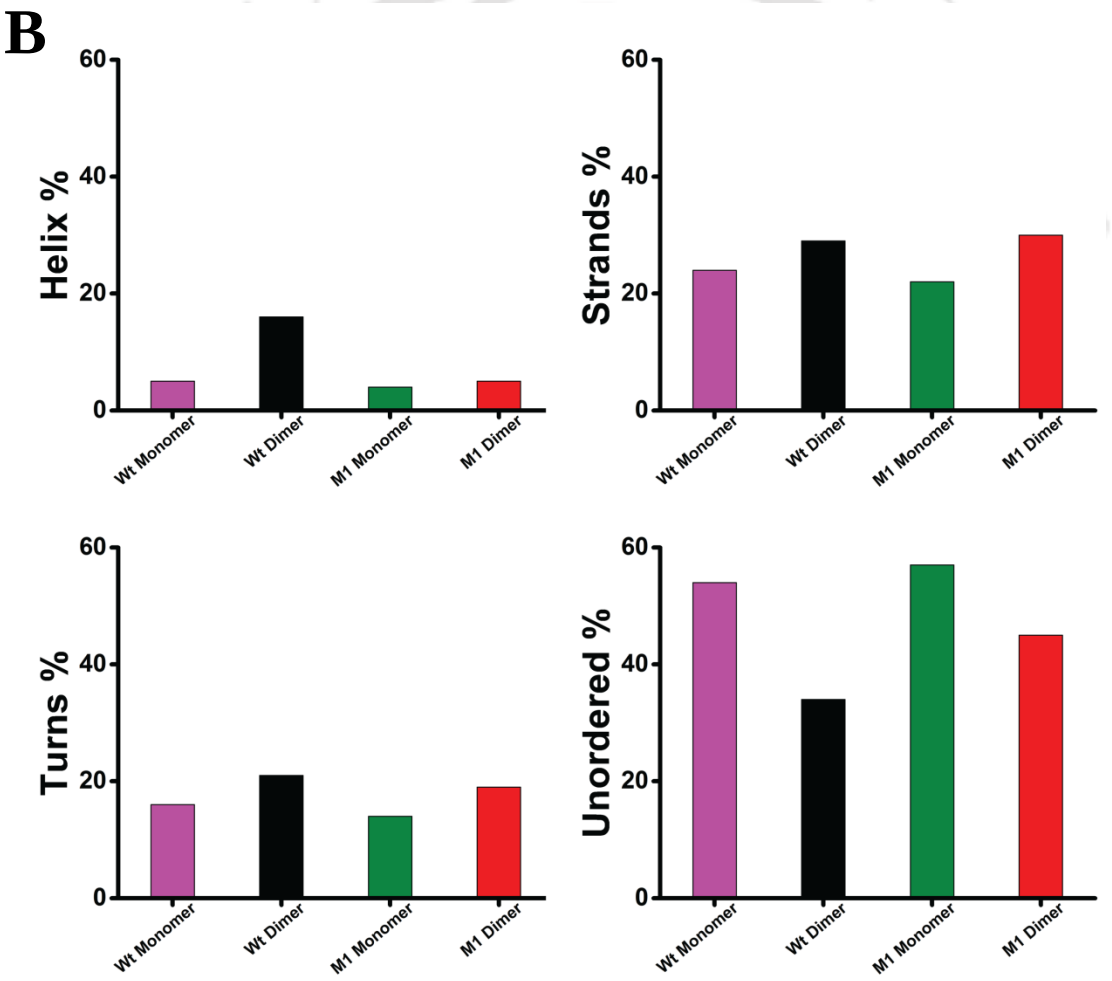

Figure 5.2.9B: Secondary structure content in monomeric and dimeric PEST Wt and PEST M1, respectively at pH 7.4, calculated by CDSSTR program.

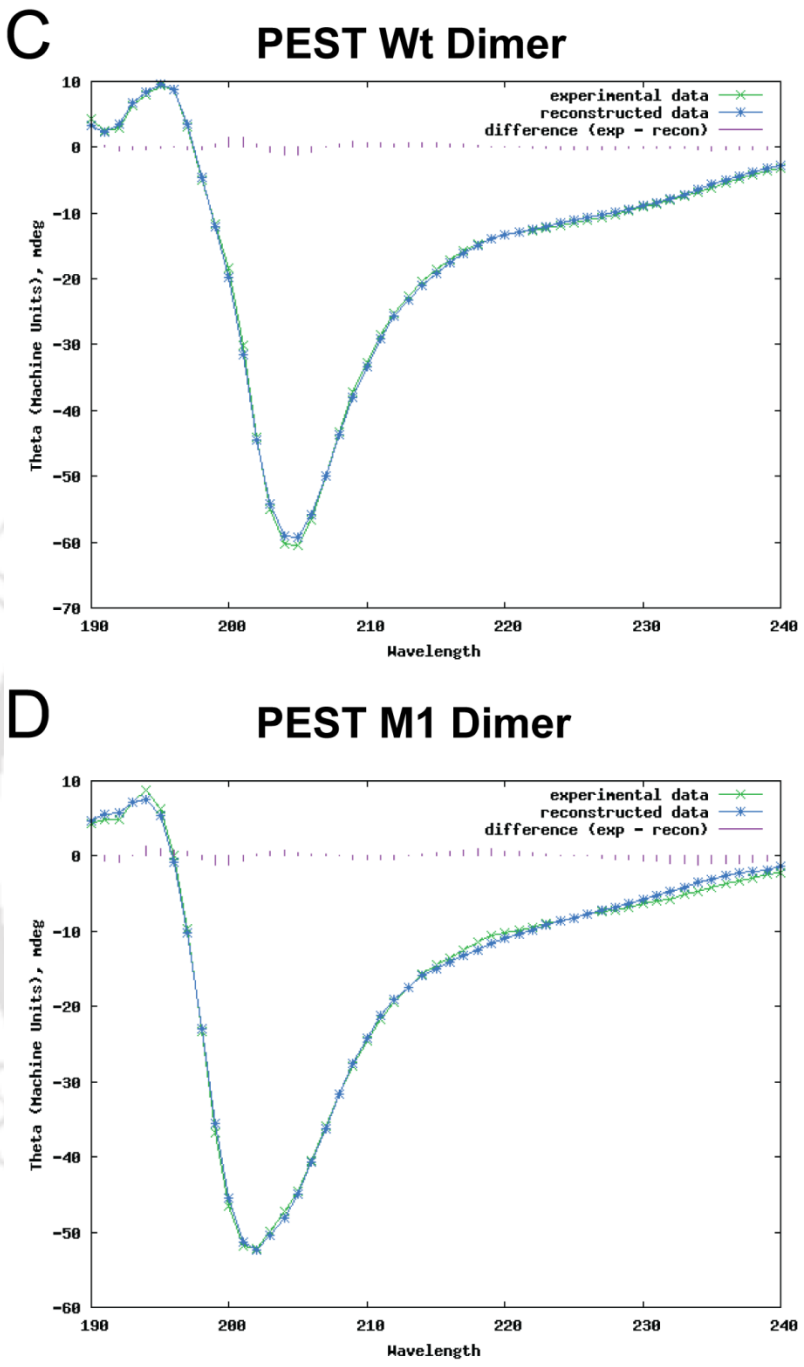

Figure 5.2.9: Fitted CD spectra of **[C]** PEST Wt and **[D]** PEST M1 dimer by using DichroWeb server at pH 7.4.

5.3 Conclusions:

- Estimation of free thiol groups, non-reducing SDS-PAGE and mass spectrum analysis reveals dimerization of PEST fragment through formation of disulphide bond involving sole cysteine residue.
- Anomalous SDS-PAGE mobility of PEST dimer indicates its disordered character.
- About 5 fold high molecular weight of PEST dimer determined by size exclusion chromatography reveals its random coil structure.
- DLS measurements reveal higher Stokes radius for the PEST dimer in comparison to monomer. The DLS Stokes radii appear consistent with the values obtained using size-exclusion chromatography.
- Tryptophan fluorescence studies indicate that dimer of PEST M1 is more disordered in the vicinity of its tryptophan than monomer.
- Fluorescence anisotropy investigations of tryptophan indicate a more free and dynamic indole in the PEST dimer compared to monomer.
- Circular Dichroism studies reveal that dimerization of PEST fragment induces some gain in ordered structure.

Chapter 6

Probing the structural transitions in human c-Myc PEST fragment and its mutant by Protein Charge Transfer (ProCharTS) Absorption Spectra

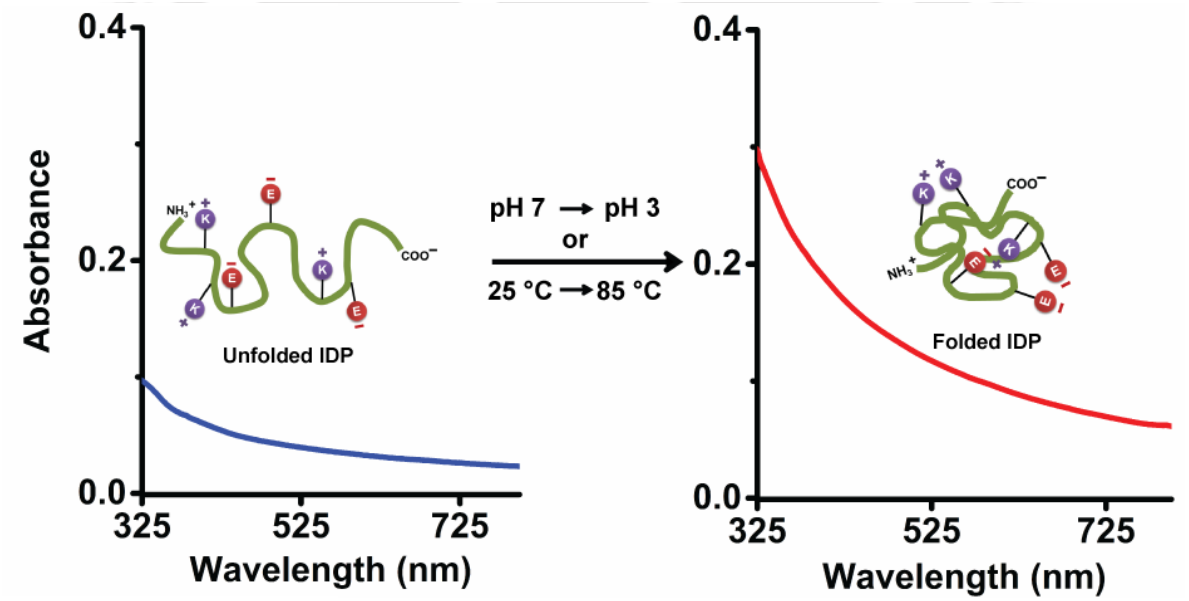

6.1 Introduction:

Protein Charge Transfer Spectra (ProCharTS) originate due to photoinduced electron transfer from: polypeptide backbone to NH_3^+ in lysine; COO^- in glutamate to polypeptide backbone; and COO^- in glutamate to NH_3^+ in lysine. The absorption intensities in ProCharTS at wavelengths 250—800 nm are dependent on 3D spatial proximity between charges in lysine-lysine, glutamate-glutamate and lysine-glutamate side chain headgroup pairs across the protein (Prasad et al., 2017). Intrinsically disordered proteins (IDPs) are rich in charged amino acids but lack structure promoting intrinsic spectral probes like tyrosine or tryptophan in their sequence, making their structural characterization difficult (Dunker et al., 2001; Mateos-Gil et al., 2016; Romero et al., 2001; Uversky, 2011).

As Human c-Myc PEST fragment contains about 35% charged amino acids with abundance of histidine, lysine and glutamate it will be worthy to utilize the ProCharTS as new label free spectroscopic markers to monitor the structural transitions in PEST fragments. In this chapter, we exploit the richness of charged amino acid population in IDPs to sense their structural transitions using ProCharTS. Conformational changes induced in the PEST fragments by altering pH and temperature of aqueous medium was monitored by ProCharTS and confirmed by CD spectra.

Our results revealed that in presence of tryptophan, ProCharTS absorbance was substantially reduced, specifically at wavelengths where absorption by tryptophan was near its maximum. Significant changes in ProCharTS spectrum was observed with changing pH in the range 3—11, which correlated with changes in secondary structure of PEST fragments. ProCharTS intensity was sensitive to temperature induced changes in the secondary structure of PEST fragments between 25—85^{o}C. Presence of 250 mM NaCl or KCl in the medium also altered the ProCharTS spectrum. Taken together, we highlight the utility of ProCharTS as a new label-free intrinsic probe to monitor structural transitions in IDPs.

6.2 Results and Discussion:

6.2.1 Protein Charge Transfer (ProCharTS) Absorption Spectra of PEST

Amino acid sequences of PEST Wt and M1 proteins (shown in Figure 2.2 of chapter 2) reveals that they are rich in charged amino acids with few sparsely distributed aromatic amino acids. Both PEST Wt and PEST M1 are abundant in glutamate, histidine and aspartate. To study the ProCharTS of PEST Wt and the effect of tryptophan insertion on the ProCharTS absorption spectrum of PEST Wt, absorption spectra of PEST Wt and PEST M1 were recorded from 250 to 800 nm. Figure 6.2.1A shows the absorption spectra observed for PEST Wt and PEST M1. The numerical values of molar extinction coefficients observed for PEST Wt and M1 proteins are given in Table 6.2.1. From the inset in Figure 6.2.1A, it is noticeable that influence of tryptophan absorption in PEST M1 is diminished after 315 nm when both Wt and mutant spectra of PEST fragments nearly merge together. It is clear that stronger tryptophan absorption in the mutant can significantly mask the weaker ProCharTS spectrum in same protein between 250 and 315 nm. Thus the absorption intensity arising from ProCharTS can be unambiguously identified only beyond these wavelengths as shown in Figure 6.2.1A when all other amino acid chromophores are silent. Therefore, molar extinction coefficients observed at and beyond 315 nm arise solely from ProCharTS. Both PEST fragments reveals a distinctive broad tail of ProCharTS absorption between 325—800 nm as observed earlier with α_3C (Prasad et al., 2017).

Inset of Figure 6.2.1A reveal that when strong contribution from tryptophan is deducted from PEST M1 spectrum near 250—290 nm using molar extinction coefficients reported previously (Fasman, 1992), a weakened spectrum of ProCharTS is left behind. Further, the weak chromophore in phenylalanine has negligible influence on ProCharTS of PEST Wt (Figure 6.2.1A), highlighting the importance of chromophore strength in this phenomenon. The additional absorption contributed by ProCharTS at 280 nm, if unaccounted, can lead to significant overestimation of protein concentration based on tryptophan absorption. However, at wavelengths beyond 315 nm, the ProCharTS spectra of Wt and mutant PEST appear nearly comparable. This indicates that presence of extra tryptophan in PEST mutant has minimal bearing on the ProCharTS spectrum in this region.

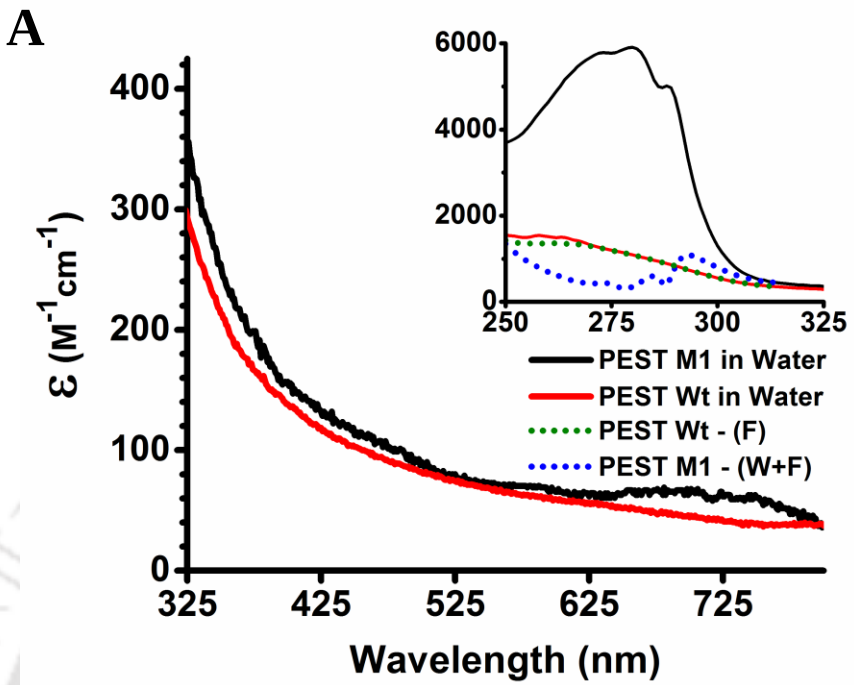

Figure 6.2.1A: Absorption spectra of c-Myc PEST Wt and its mutant PEST M1 in deionized water containing 5 mM TCEP are displayed. Inset shows the absorption spectra at shorter wavelengths in expanded form. Spectrum left behind after subtracting contribution of aromatic chromophore is also shown in the inset. Extinction coefficients reported are an average of multiple concentrations between 25—75 µM for PEST Wt and 20—40 µM for PEST M1.

Table 6.2.1: ProCharTS absorption: Molar extinction coefficients of absorption arising from ProCharTS, among PEST Wt and M1 are displayed. Other conditions are similar to Figure 6.2.1A. The numbers in brackets indicate standard deviations for n = 2—3.

PEST	Charged residue fraction	ε (M^{-1} cm^{-1}) at different wavelengths in nm											
		315	***320***	***325***	***350***	***400***	***450***	***500***	***550***	***600***	***650***	***700***	***750***	***800***
Wt	35%	343 (57)	316 (57)	293 (49)	214 (45)	138 (20)	103 (9)	82 (5)	67 (2)	59 (1)	52 (1)	44 (1)	39 (1)	37 (1)
M1	35%	430 (11)	392 (9)	357 (10)	255 (9)	157 (8)	112 (8)	90 (19)	73 (22)	65 (26)	64 (27)	64 (27)	60 (19)	37 (4)

Further, to investigate contribution of intramolecular or intermolecular interactions in the absorption spectra of PEST fragments, absorbance of PEST Wt and PEST M1 with their increasing concentrations (25—150 μM) was monitored. Figure 6.2.1B and C indicates that the absorbance of PEST fragments (Wt and M1) shows a linear increase with increasing concentrations at different wavelengths. This clearly ruled out the possibilities of ProCharTS spectra arising due to any intermolecular interactions.

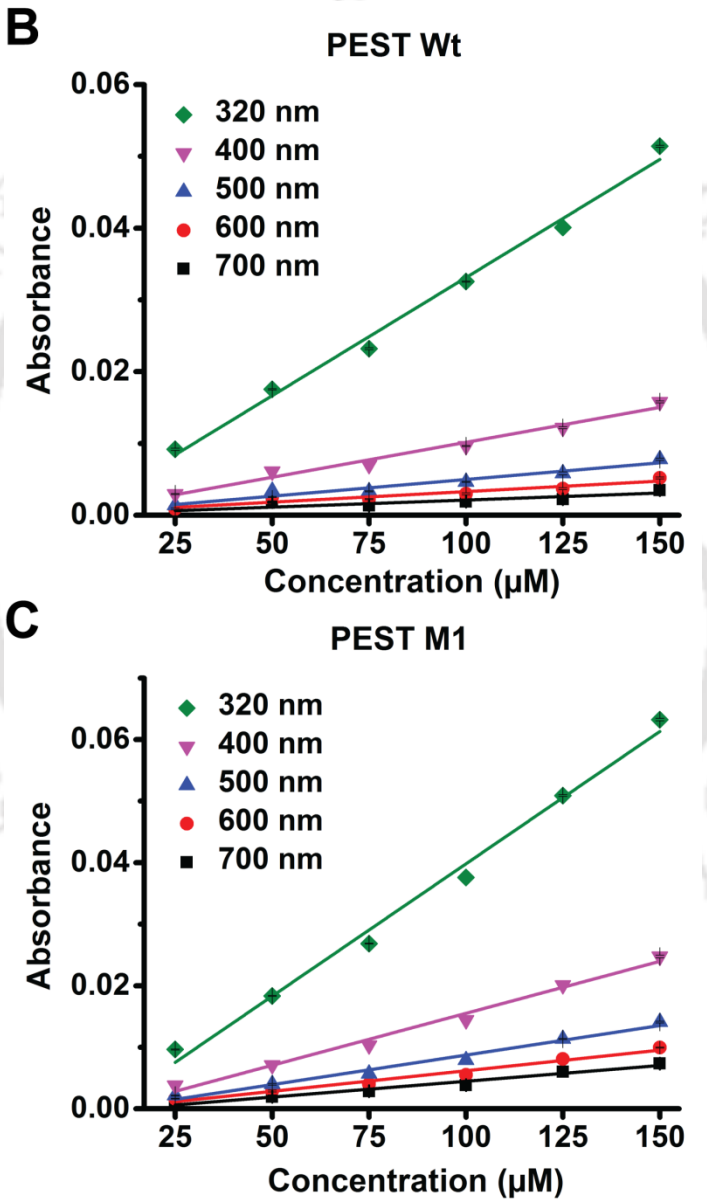

Figure 6.2.1: Variation of ProCharTS absorbance with protein concentration for **[B]** PEST Wt and **[C]** PEST M1 at chosen wavelengths.

6.2.2 Comparison of absorption spectra with simulated Rayleigh Scatter

To assess if the observed spectral features at and beyond 315 nm arise due to Rayleigh scattering, the absorption spectrum of PEST Wt and PEST M1 was compared with simulated Rayleigh scatter. The simulated Rayleigh scatter was obtained by plotting the observed absorption spectrum of PEST Wt and PEST M1 as λ^{-4} dependence using equation 6.1 (Siegel, 2001). If scattering component is present in the sample it will overlap with the simulated Rayleigh scatter profile, which follows ($1/\lambda^4$) dependence (Hulst and van de Hulst, 1957; Rayleigh, 1899).

$$\sigma_s = \frac{2\pi^5}{3}\frac{d^6}{\lambda^4}\left(\frac{\eta^2-1}{\eta^2+2}\right)^2 \qquad 6.1$$

Here, σ_s represents the Rayleigh scattering cross-section, λ is the wavelength of light, d is the diameter of the particles and $\eta = \frac{\eta_{particle}}{\eta_{medium}}$ is the relative refractive index.

Figure 6.2.2A and B display the comparison of absorption spectra of PEST Wt and PEST M1 with simulated Rayleigh scatter profile, respectively. Presence of any scattering artefacts behind the observed spectra of PEST Wt and PEST M1 from 250—800 nm ruled out due to poor overlap of ProCharTS spectra with simulated Rayleigh scattering profile. Presence of ProCharTS in PEST fragment motivated us to check the utility of ProCharTS to detect the structural transitions in IDPs.

To evaluate the sensitivity of ProCharTS spectrum to structural transitions in the PEST fragments, several maneuvers were attempted. In the first, the pH of medium was varied from pH 3 to pH 11, so as to both alter the ionization state of charged amino acid and gently perturb the structure of the protein, as discussed in the next section.

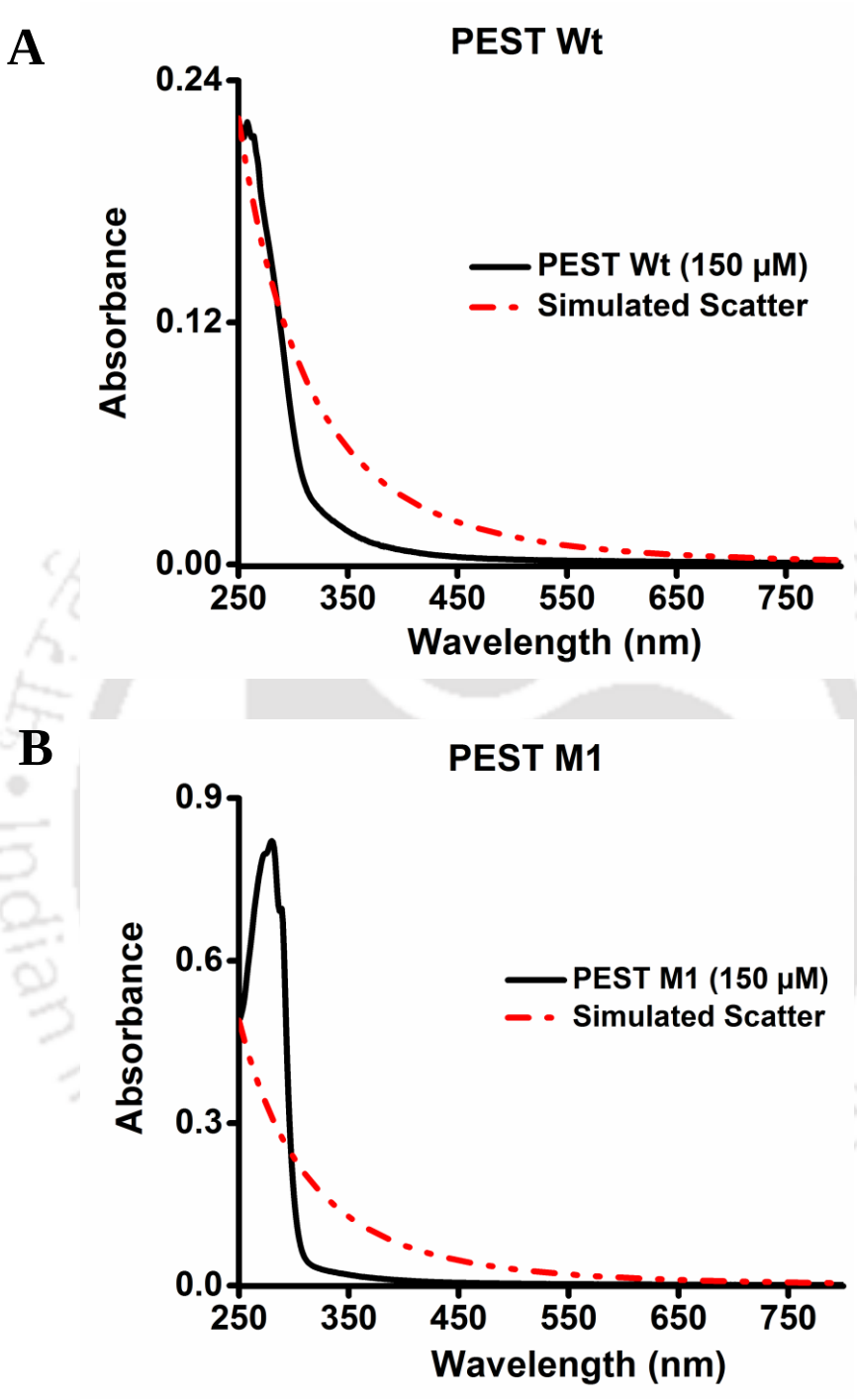

Figure 6.2.2: Comparison of absorbance spectra with simulated Rayleigh scatter (using $1/\lambda^4$ dependence) for **[A]** PEST Wt and **[B]** PEST M1.

6.2.3 Effect of pH on the ProCharTS of PEST fragments

To investigate the effect of pH on the ProCharTS of PEST fragments, the absorption spectra of PEST Wt and M1 were recorded from 250 to 800 nm at different pH (3-11). Figure 6.2.3A and B depict the effect of varying pH (3-11) on the ProCharTS absorption spectra of PEST fragments. Figure 6.2.3C and D shows the percent change in absorption intensity of PEST fragments at different pH (3-11). Comparing the Figure 6.2.3C and D and inset in Figure 6.2.3A and B, it is noticeable that PEST M1 has uniformly higher absorption near 250—290 nm in pH 3, while PEST Wt too displays a consistent but weak increase between 250—270 nm at same pH. The modest increase over and above tryptophan (indole) absorption in PEST M1 must arise from increase in ProCharTS absorption, because tryptophan absorption is only barely sensitive to changes in pH in the acidic range. Further, tryptophan absorption is known to increase between 260—280 nm and decrease between 282—300 nm, with increasing acidity (Fasman, 1992).

The uniform increase observed in absorption of PEST M1 for pH 3 in 250—290 nm wavelength range, runs contrary to this reversal, thus ruling out the role of tryptophan. Figure 6.2.3A, B, C and D show that both PEST Wt and PEST M1 exhibit increased absorbance in pH 3 starting from 325 nm, but PEST M1 has a slightly higher absorption. These results hint at an alternative structure in both PEST fragments in pH 3 and to a lesser extent in pH 5 in comparison to other pH conditions where no significant changes are apparent. The proposed structural change in pH 3 coincides with major changes in far UV CD spectrum for both PEST Wt and M1 in pH 3 (Figure 4.2.10A and B of chapter 4). Minor changes in CD spectrum in pH 5 are also evident, in comparison to remaining pH matching somewhat with observations from ProCharTS. Moving to higher pH, the trends in both PEST Wt and M1 appear nearly similar but not identical. The absorption spectra for pH 7 and 11 are superimposed for Wt PEST, while for PEST M1, pH 7 spectrum is marginally higher compared to pH 11. Spectra in pH 9 and in pure water appear nearly similar for both PEST Wt and M1. Absorption of PEST Wt and PEST M1 in deionized water was however less in comparison with buffers.

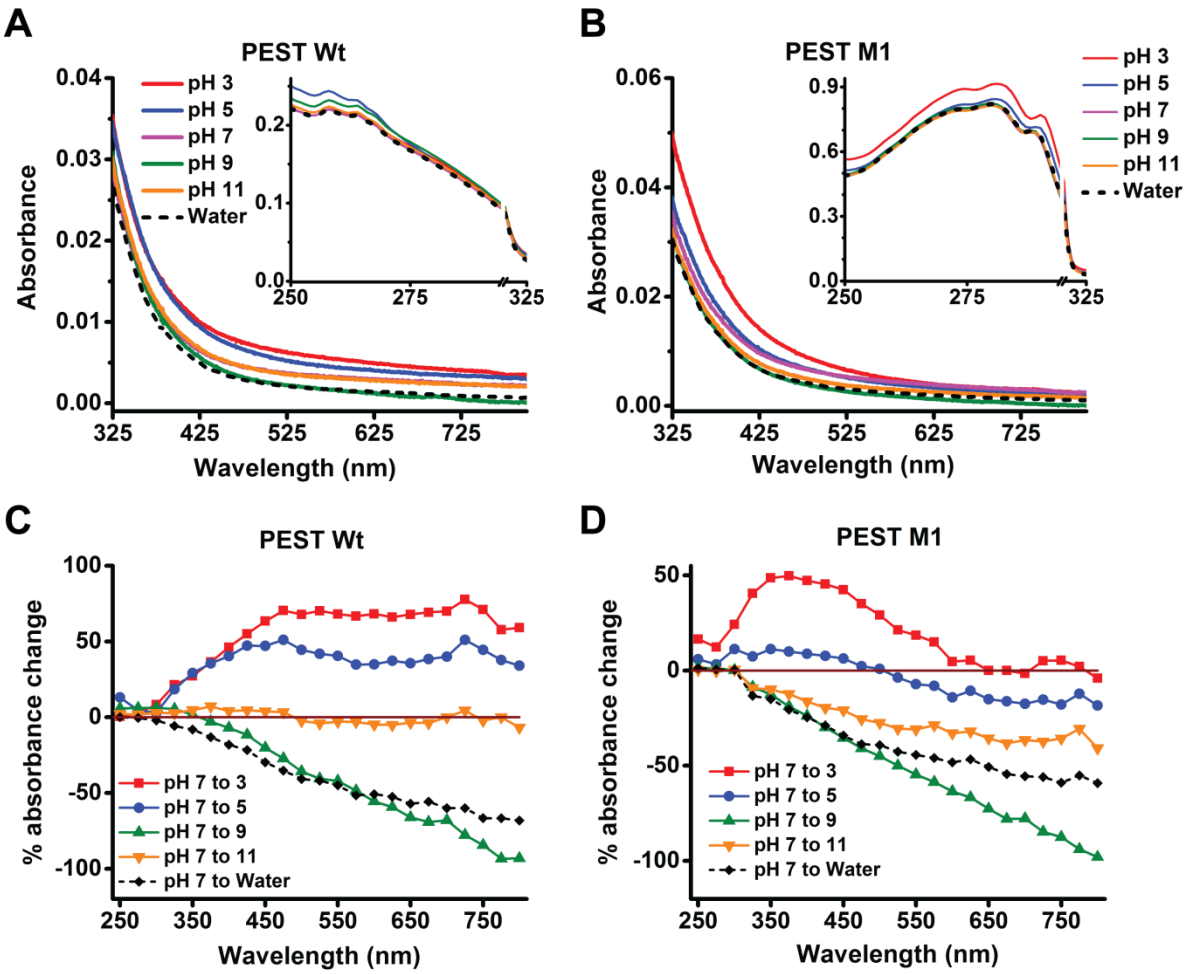

Figure 6.2.3: Effect of pH on ProCharTS: The effect of changing pH on absorption spectra of **[A]** 150 µM PEST Wt and **[B]** 150 µM PEST M1 are shown. Inset shows the absorption spectrum at shorter wavelengths. Inset scales of Figure A and B have a break between 294 and 295 nm. Solid lines and dashed line show spectra in buffer and water, respectively. Percent change in absorption intensity measured every 25 nm at specified pH among the proteins **[C]** PEST Wt and **[D]** PEST M1 with respect to pH 7. The change in absorbance at selected wavelengths were calculated as [(Absorbance at chosen pH – Absorbance at pH 7)/Absorbance at pH 7]×100.

The pH effects observed with ProCharTS (Figures 6.2.3A, B, C and D) can be analyzed collectively to identify common features. At pH 3, the carboxylate groups in both glutamate and aspartate are likely to be protonated and uncharged, so all proteins at this pH are likely to have a net positive charge from histidine, lysine and arginine residues only. This also means that salt bridge interactions between oppositely charged residues cannot exist in pH 3. The higher ProCharTS in PEST fragments (Wt and M1) in pH 3 appears to correlate with

increased helix and strand population along with more ordered structure compared to remaining pH (Figure 4.2.10C and D of chapter 4) as revealed by CD. Interestingly, pH 5, 7 and 9 appear generally healthy and mostly uneventful for ProCharTS in PEST fragments (Figure 6.2.3A and B), perhaps due to rich presence of negative and positive charges in all charged residues in this pH range. As the protonated imidazole side chain of histidine has a pK_a close to 6.0, it is surprising that both PEST Wt and M1, which are rich in histidine residues reveal little change in ProCharTS between pH 5—9. Overall, pH related changes in ProCharTS appear complex due to concomitant changes in: a) ionization state of charged residue; b) protein conformation and c) salt concentration. Interpretation of changes at extremes, like pH 3 and 11, appear easier.

Thus, ProCharTS appears sensitive to pick up pH induced structural transitions as shown for PEST fragment. In the next approach, we raised the temperature of the medium to disrupt the protein structure and proceeded to evaluate its effect on the ProCharTS spectrum.

6.2.4 Effect of temperature on the ProCharTS of PEST fragments

To study the effect of temperature on the ProCharTS of PEST fragments, the absorption spectra of PEST Wt and M1 were recorded from 250 to 800 nm at different temperatures (25—85 °C). Figure 6.2.4A and C (with inset) shows a prompt rise in ProCharTS absorption in PEST Wt and PEST M1, when temperature is raised from 25 to 85 °C. The increase in absorbance is quantitatively more in the PEST Wt protein compared to mutant M1 (Figure 6.2.4E and F).

Further, the proportional rise in absorbance appears non-uniform across the entire spectral range (Figure 6.2.4E and F) for both the PEST Wt and PEST M1, ruling out the possibility of increase in absorbance as a result of evaporation. As the protein samples cool from 85 °C to lower temperatures (65, 45 and 25 °C), the absorbance values come down. At 45 and 25 °C, the spectra appear nearly identical (including the inset). The spectrum after cooling to 25 °C appears almost identical to that at the beginning before heating (Figure 6.2.4E and F), suggesting complete reversibility in the process of regaining the original conformation.

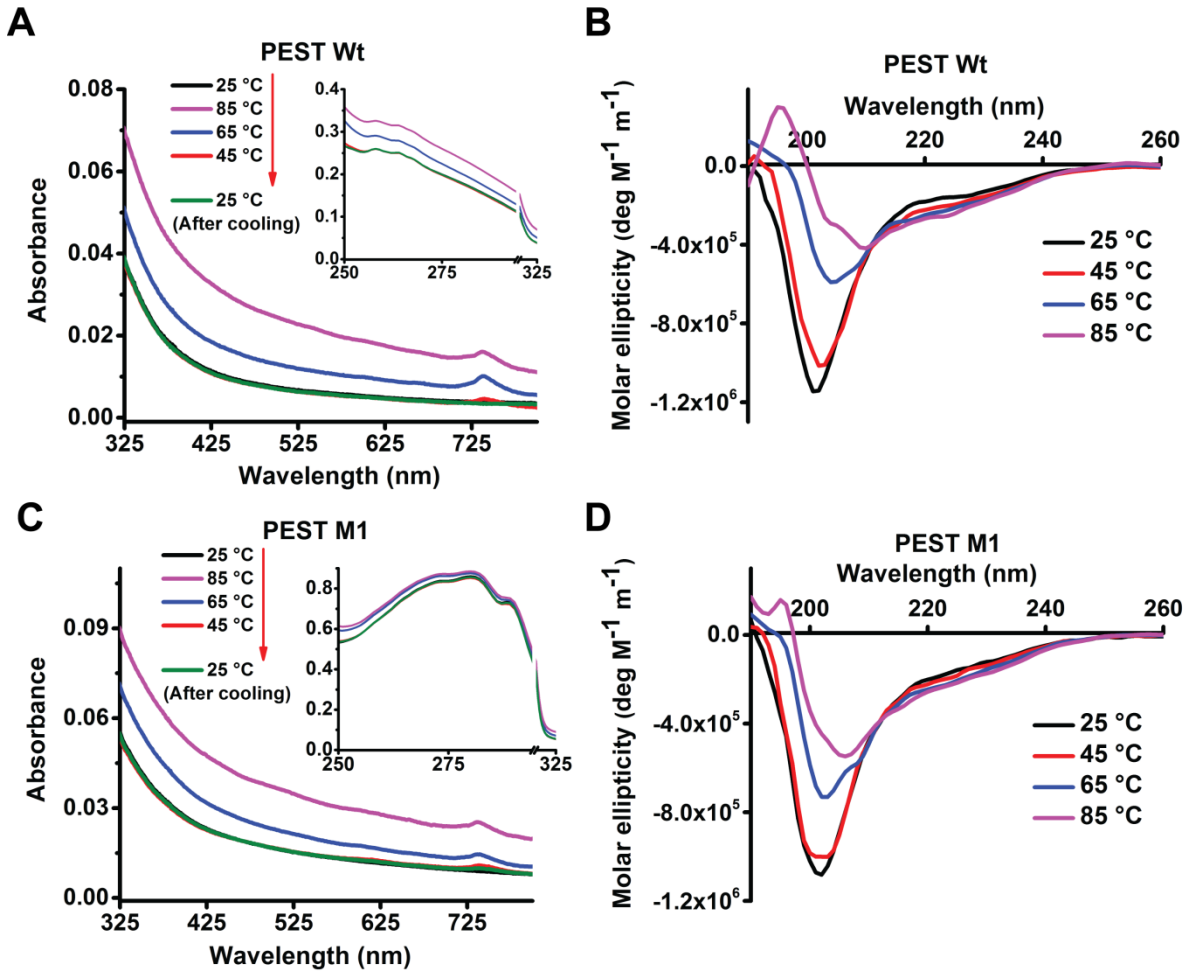

Figure 6.2.4: Effect of temperature on ProCharTS and CD: The effect of temperature on absorption spectra of **[A]** 150 µM PEST Wt and **[C]** 150 µM PEST M1 in water is shown. Inset scales of Figure 6.2.4A and C have a break between 294 and 295 nm. The effect of temperature on CD spectra for **[B]** 20 µM PEST Wt and **[D]** 20 µM PEST M1 at different temperatures is also shown.

Interestingly at all higher temperatures (85, 65 and 45 °C), a significant peak in the tail of the ProCharTS spectrum near ~735 nm is visible for both PEST Wt and M1.

The CD spectrum for PEST Wt and PEST M1 are shown in Figures 6.2.4B and D, respectively. It is observed that for both PEST fragments, the individual CD spectra at 25 and 45 °C is nearly identical, matching the trend in ProCharTS spectrum. At 85 °C, a major change in the CD spectrum is observed in both PEST fragments, while at 65 °C, a moderate change is noticeable compared to spectrum at 25 °C for both PEST fragments. These

structural changes observed in CD spectra almost mirror the changes noticed in the ProCharTS spectra for the same proteins (Figure 6.2.4E and F). Hence, ProCharTS spectra appear truly sensitive to heat induced structural transitions in the PEST Wt and M1 proteins.

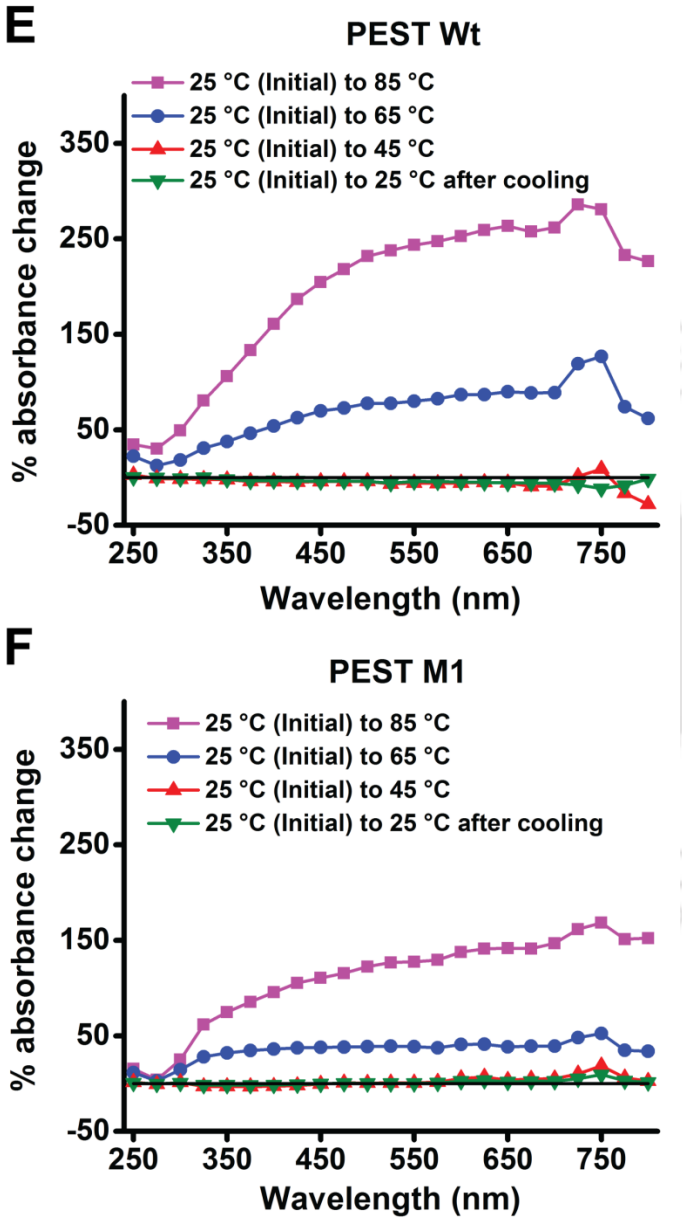

Figure 6.2.4: Percent change in absorption intensity measured every 25 nm at specified temperature among the proteins **[E]** PEST Wt and **[F]** PEST M1 with respect to room temperature (25 ˚C). The change in absorbance at selected wavelengths were calculated as [(Absorbance at chosen temperature – Absorbance at 25°C)/Absorbance at 25 °C]×100.

The effect of increasing temperature (25 to 85 °C) is manifested as increased ProCharTS in PEST Wt and PEST M1 starting from 325 nm and going to higher wavelengths (Figures 6.2.4A, C, E and F). This increase is non-uniform against wavelength, similar to that observed with α_3C (Prasad et al., 2017). The CD spectra (Figures 6.2.4G, H, I and J) reveal increased fraction of α-helix and β-strand population along with ordered structure at 85 °C in comparison to lower temperatures in PEST fragments.

Overall, heat-induced changes monitored using ProCharTS spectra could identify structural transition in both PEST fragments at 85 °C. Taken together, ProCharTS appears sensitive to pick thermally induced structural transitions in charged proteins. It may be added that ProCharTS may be sensitive to subtle changes in tertiary structure which are not discernible by CD. Such changes are however, difficult to verify in absence of 3D structural data.

In the last section we investigate the role of excess salt on the ProCharTS spectrum of the chosen proteins. The objective of this experiment was to perturb the electrostatic interactions between like and opposite charges in the protein by introducing salt counter ions. As the ProCharTS spectrum is dependent on the charges localized on amino acid side chains and their interactions with those in neighboring side chains, stabilizing the charges by introducing excess salt counter ions could influence the spectrum. These changes in ProCharTS spectra could in turn provide insights on the multiple side chain interactions contributing to the spectrum.

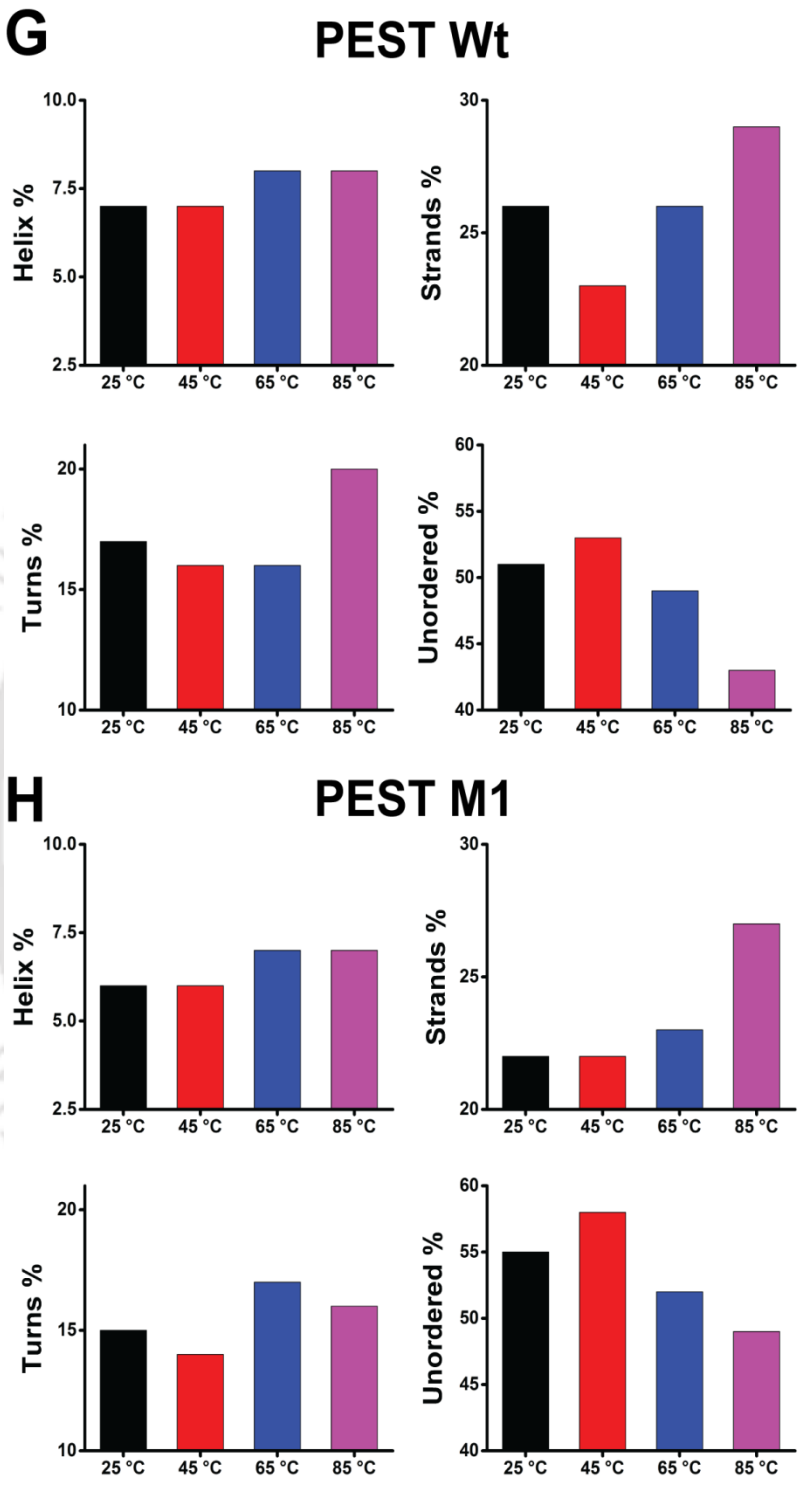

Figure 6.2.4: Change in secondary structure content in **[G]** PEST Wt and **[H]** PEST M1 at different temperatures (25 to 85 °C).

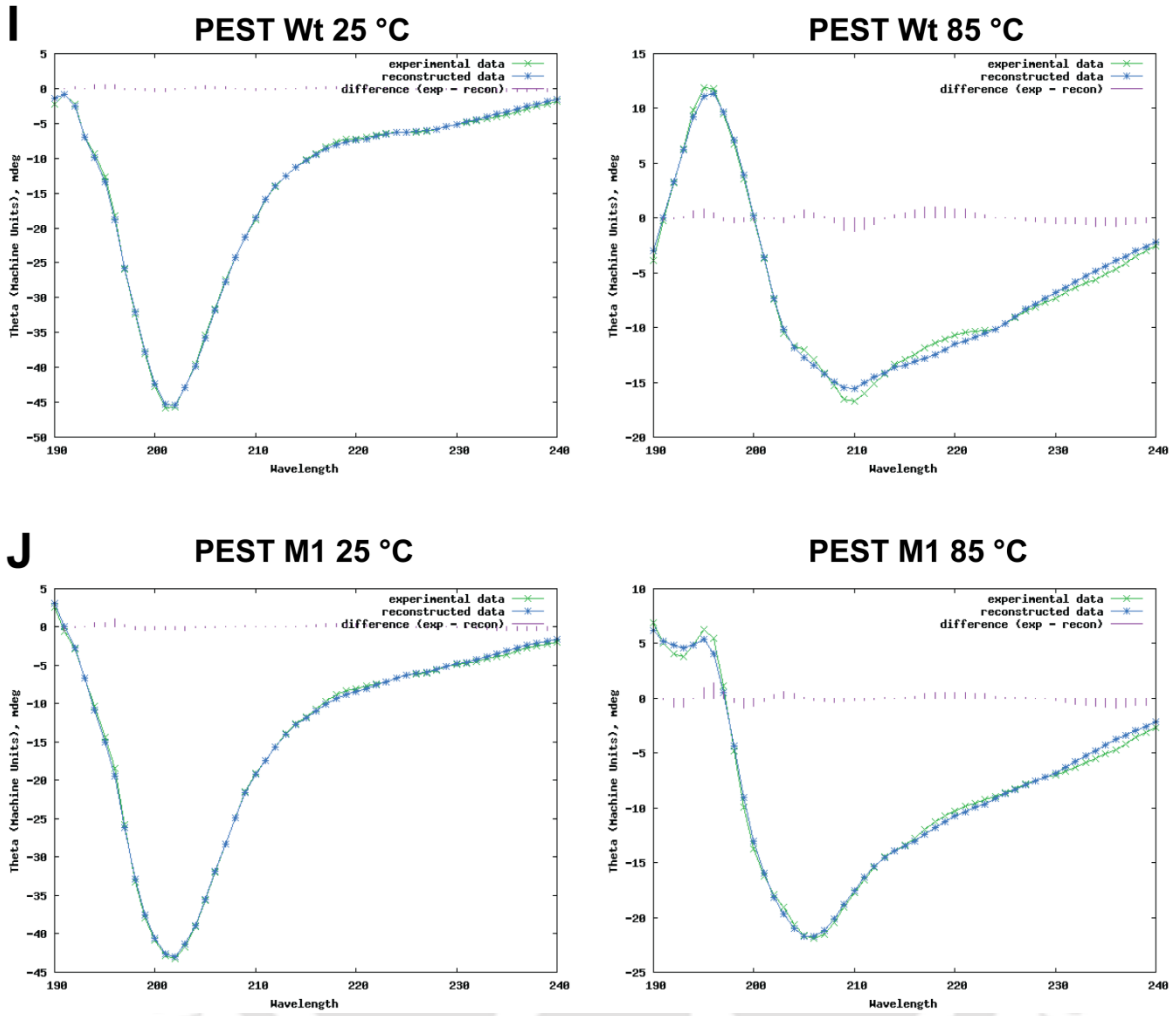

Figure 6.2.4: Fitted CD spectra of **[I]** PEST Wt and **[J]** PEST M1 by using DichroWeb server at 25 and 85 °C are shown.

6.2.5 Effect of salt on the ProCharTS of PEST fragments

To analyze the effect of excess salt on the ProCharTS of PEST fragments, the absorption spectra of PEST Wt and PEST M1 were recorded from 250 to 800 nm in presence of 250 mM NaCl and KCl. In Figures 6.2.5A, B, C and D, the absorption of PEST Wt and M1 are significantly higher in the presence of NaCl and KCl at wavelengths longer than 325 nm. No significant changes are noticed at shorter (250—325 nm) wavelengths (inset of Figures 6.2.5A and B). This trend is consistent with higher ProCharTS observed in presence of buffer salts (Figures 6.2.3A and B) compared to pure water at shorter wavelengths.

Interestingly, the larger potassium ion appears to cause more change in ProCharTS compared to sodium consistently in both the PEST Wt and M1. Overall, the results suggest that salt ions can alter the ProCharTS spectra significantly.

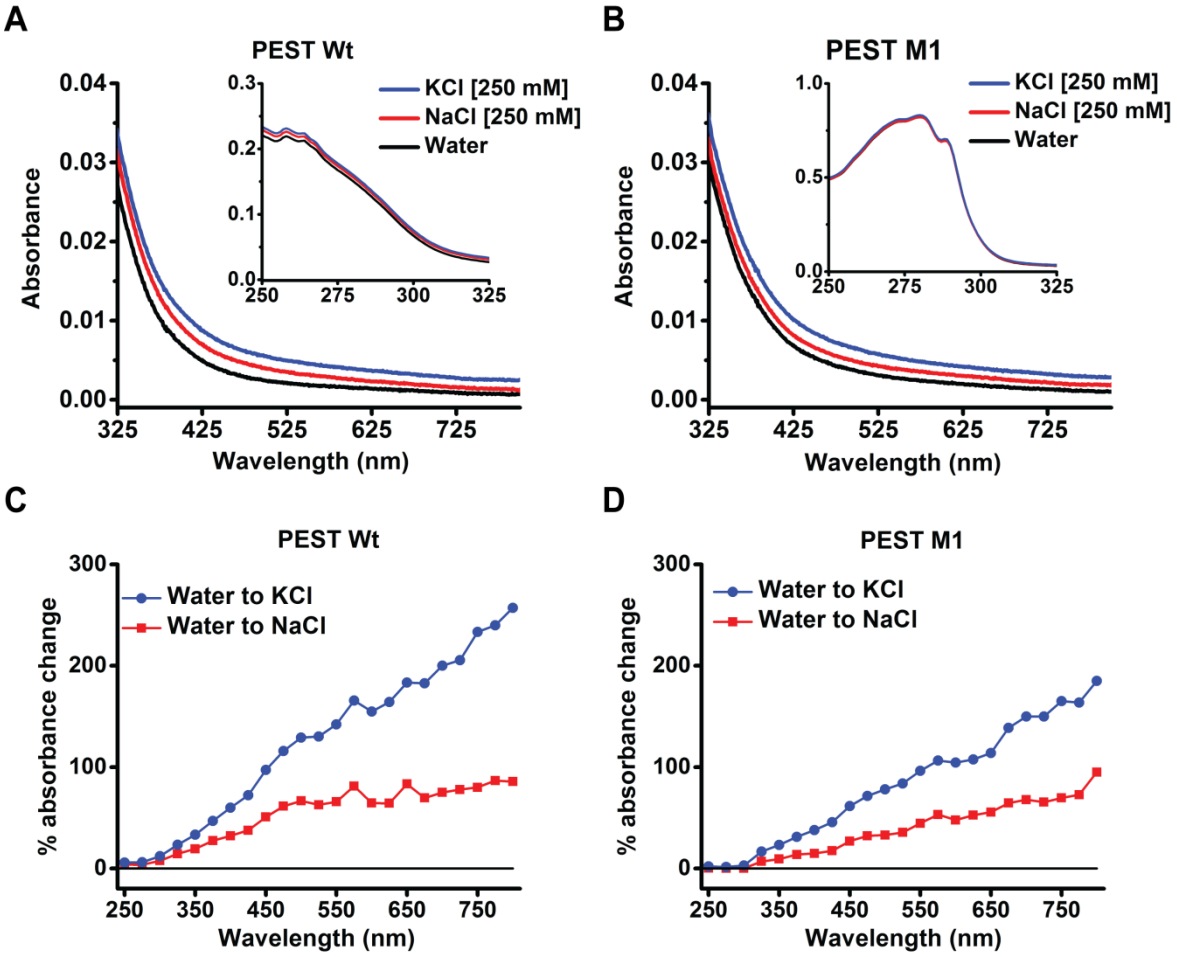

Figure 6.2.5: Effect of excess salt on ProCharTS: The effect of 250 mM KCl and 250 mM NaCl on absorption spectra of **[A]** 150 µM PEST Wt and **[B]** 150 µM PEST M1 dissolved in water is shown. Percent change in absorption intensity measured at 25 nm intervals among the proteins **[C]** PEST Wt and **[D]** PEST M1 in 250 mM NaCl and 250 mM KCl with respect to absorption of proteins in deionized water. The change in absorbance were calculated at selected wavelengths as [(Absorbance in salt – Absorbance in water)/Absorbance in water]×100.

6.3 Conclusions:

- Protein Charge Transfer Spectra (ProCharTS) was distinctly observed from 325—800 nm wavelength range in PEST fragments.
- Interference from strong absorption arising from aromatic amino acids was clearly absent in the 325—800 nm wavelength region, making this a universal absorption band for ProCharTS.
- ProCharTS absorption was sensitive to changes in structure of PEST fragments due to change in pH.
- Increase in ProCharTS intensity with increasing temperature correlated with changes in protein secondary structure as observed by CD.
- ProCharTS intensity was sensitive to presence of salts in the medium.
- ProCharTS absorption serves as an ideal label-free intrinsic probe to monitor structural transitions in IDPs.

Chapter 7

Thesis summary and future perspectives

7.1 Summary:

The highly unstable human c-Myc oncoprotein acts as a transcription factor which involves many vital cell processes and subsequently degrades quickly within 20 to 30 minutes. For the normal cell activity rapid destruction of c-Myc protein is important as its stabilization causes development of tumors. For quick degradation of c-Myc oncoprotein, its centrally located highly acidic PEST region is responsible. However, the exact mechanism of PEST recognition and targeting of PEST containing proteins for degradation via proteasome is poorly understood. The structural information of PEST region can provide better insights to understand their functional mechanism. But unfortunately, structural determination and characterization of disordered properties of human c-Myc PEST region has not been done.

This thesis work presents thorough study of disorder properties of the human c-Myc PEST fragment, analysis of its structure and dynamics and how PEST fragment behaves in different environments using multiple spectroscopic and biophysical techniques. This will enable in better understanding the function of c-Myc PEST fragment. We have predicted highly disordered structure of PEST fragment by different disorder prediction tools and experimentally confirmed various disorder properties of PEST fragment. The structural analysis of PEST fragment revealed its random coil structure. This random coil structure of PEST fragment may be responsible for rapid destruction of c-Myc protein as it will easily be accessible and recognized by proteolytic enzymes. Further, by utilizing steady state and time-resolved fluorescence and other biophysical techniques we found that lowering the pH induces folding in PEST fragment and folding was more pronounced at the C-terminus compared to the N-terminus. This pH triggered folding in PEST fragment suggests a model for stabilization of c-Myc protein in some tumors as it will not be cleaved easily by proteolytic enzymes after folding. We also discovered involvement of sole cysteine residue in dimerization of PEST fragments through disulphide bond formation and this dimer of PEST was also found highly disordered in structure. This dimer formation provides some clue about involvement of PEST fragment's single cysteine in intramolecular disulphide bond formation in c-Myc protein.

In the final part of my thesis work, we exploit the richness of charged amino acid population in IDPs to sense their structural transitions using recently discovered Protein Charge Transfer Spectra (ProCharTS). ProCharTS open a new spectral window to detect the structural transitions in charge rich proteins (like IDPs and histones proteins) beyond 300 nm and can be serves as a new label free intrinsic probe.

7.2 Future perspectives:

Disorder to order transitions in PEST fragment with changing pH from alkaline to acidic, gives a great opportunity to resolve the structure of PEST fragment using X-ray crystallography upon crystallization and exploring its function at acidic pH. The PEST fragment has casein kinase phosphorylation site but its function is not known. The structural analysis of PEST fragment after phosphorylation will provide functional role of phosphorylation and its effect on the stability of c-Myc.

Since we have explored the ProCharTS in detection of structural transitions in IDPs/IDRs, it would be promising to utilize ProCharTS to explore and detect various biological processes like protein-ligand, protein-protein, protein-DNA/RNA interactions and post translational modifications (like phosphorylation, acetylation). Moreover, it would be quite interesting to focus in the emissive properties of ProCharTS. Some of our preliminary studies revealed that these transitions are emissive in nature. The fluorescence emission from such transitions would be far more sensitive than the absorption from ProCharTS. Since, the prerequisite for the Charge-Transfer is the proximity of charged amino acid side chains in a protein, any change or loss of this proximity would be similarly reflected in ProCharTS emission. This speculation could be utilized to study the protein folding and dynamics.

Appendix

Components of SDS-PAGE

Components for 15% (Acrylamide) Resolving Gel

Solutions	Resolving Gel (10 mL)	Stacking Gel (5 mL)
Deionized water	2.3 mL	3.4 mL
30% Acrylamide	5 mL	830 µL
1.5 M tris(hydroxymethyl)aminomethane	2.5 mL (pH 8.8)	630 µL (pH 6.8)
10% SDS	100 µL	50 µL
10% Ammonium persulphate (APS)	100 µL	50 µL
Concentrated N,N,N′,N′ Tetramethylethylenediamine (TEMED)	12 µL	8 µL

Gel loading buffer composition

Gel loading buffer was prepared by mixing, 0.05% (w/v) bromophenol blue, 40% (w/v) sucrose, 0.5% (w/v) SDS and 0.1 M EDTA, pH 8.0.

- **Staining solution**

Staining solution was prepared by dissolving 0.025% (w/v) Coomassie Blue R-250 in a solution of 45% methanol, 45% deionized water and 10% glacial acetic acid.

- **Destaining solution**

Destaining solution was prepared by mixing, 30% of methanol, 10% of glacial acetic acid and 60% of deionized water

Solutions for Lowry method

Solution A (2 % Sodium carbonate in 0.1 % NaOH), 100 mL

NaOH	0.47 g
Na_2CO_3	2 g

Solution B (2.37 % Potassium sodium tartrate in water), 50 mL

$KNaC_4H_4O_6 \cdot 4H_2O$	1.185 g

Solution C (1.56 % Copper sulfate in water), 50 mL

$CuSO_4.5H_2O$	0.78 g

REAGENT I: Prepared by mixing 48 mL of solution A; 1 mL of solution B and 1 mL of solution C

REAGENT II: It was prepared by mixing of equal volume of Folin's reagent and water (Stored in dark)

Both reagents I and II were prepared freshly prior to experiment.

Figure A1: Fitted CD curves of PEST Wt and PEST M1

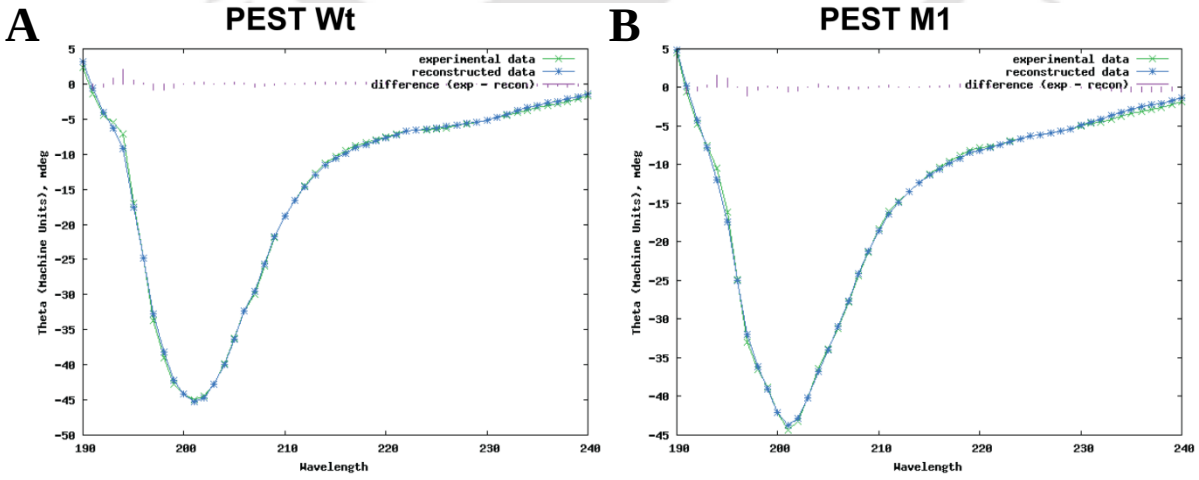

Figure A1: Fitted CD spectra of **[A]** PEST Wt and **[B]** PEST M1 by using DichroWeb server at pH 7.4.

Figure A2: Effect of pH on dansyl at different pH (3-11) in presence of 6 M Gdn.HCl

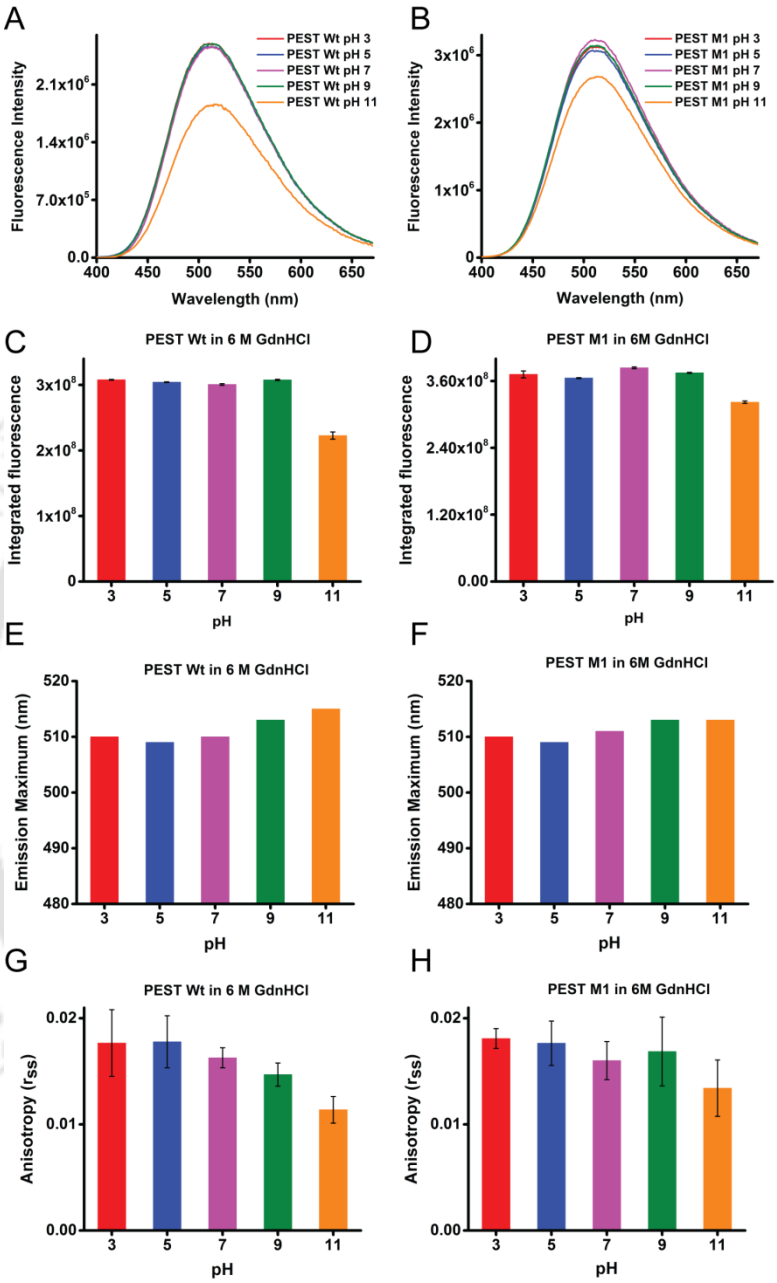

Figure A2: Effect of pH on steady state fluorescence and fluorescence anisotropy of 10 µM dansyl labeled with 11 µM of PEST Wt and M1 in presence of 6 M Gdn.HCl. Steady state fluorescence spectra of **[A]** PEST Wt; **[B]** PEST M1, integrated fluorescence yield of **[C]** PEST Wt; **[D]** PEST M1, fluorescence emission maxima of **[E]** PEST Wt; **[F]** PEST M1, steady state anisotropy of dansyl labeled with **[G]** PEST Wt and **[H]** PEST M1.

Figure A3: Fluorescence intensity decay profile of dansyl labeled PEST Wt and M1 at different pH (3-11) in presence of 6 M Gdn.HCl

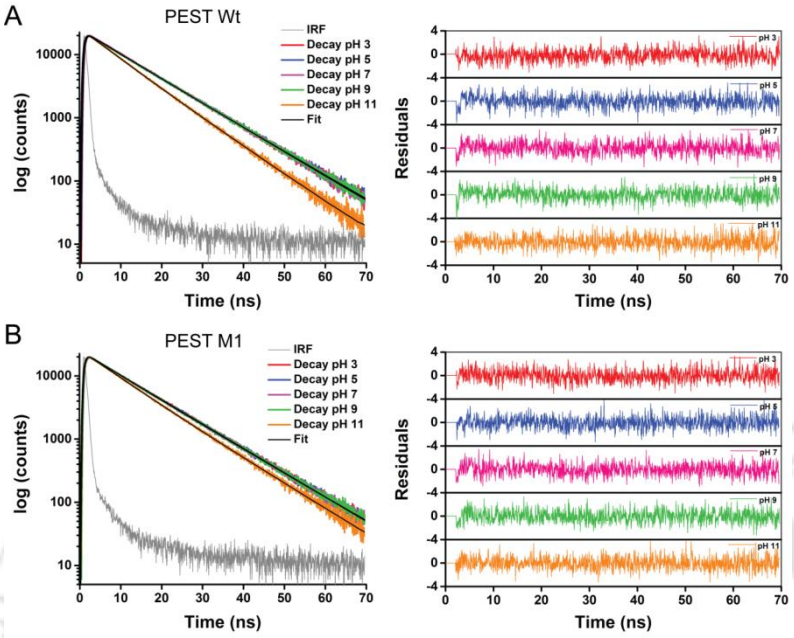

Figure A3: Fitted time-resolved fluorescence intensity decay profile of 10 µM dansyl labeled with 11 µM of **[A]** PEST Wt and **[B]** PEST M1 at different pH (3-11) in presence of 6 M Gdn.HCl (left panels). Residuals for the fit are shown in the right panels.

Figure A4: Fitted anisotropy decay profile of dansyl labeled PEST Wt at pH 3

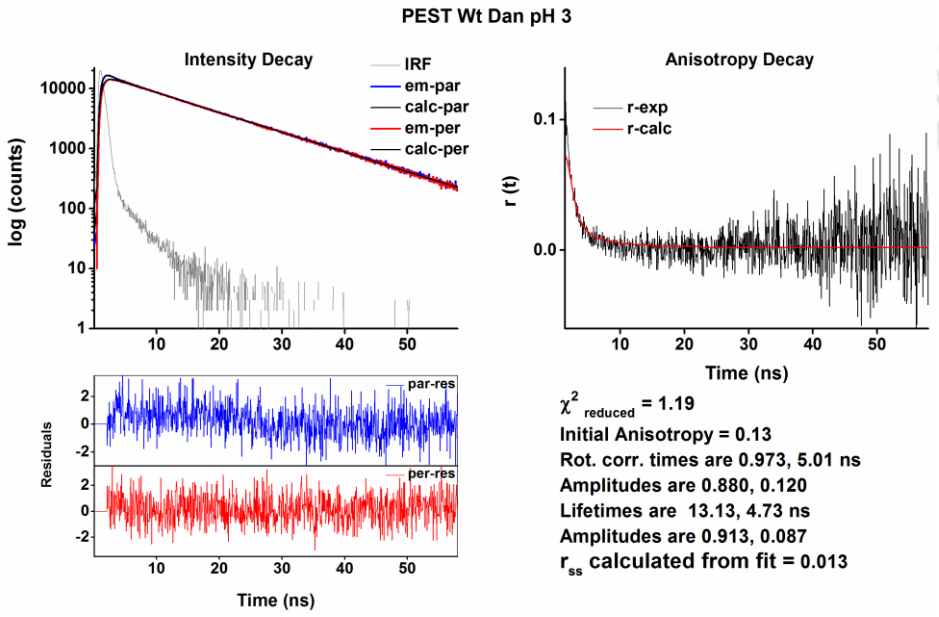

Figure A4: Fitted anisotropy decay profile of 10 µM dansyl labeled with 11 µM of PEST Wt at pH 3.

Figure A5: Fitted anisotropy decay profile of dansyl labeled PEST Wt at pH 9

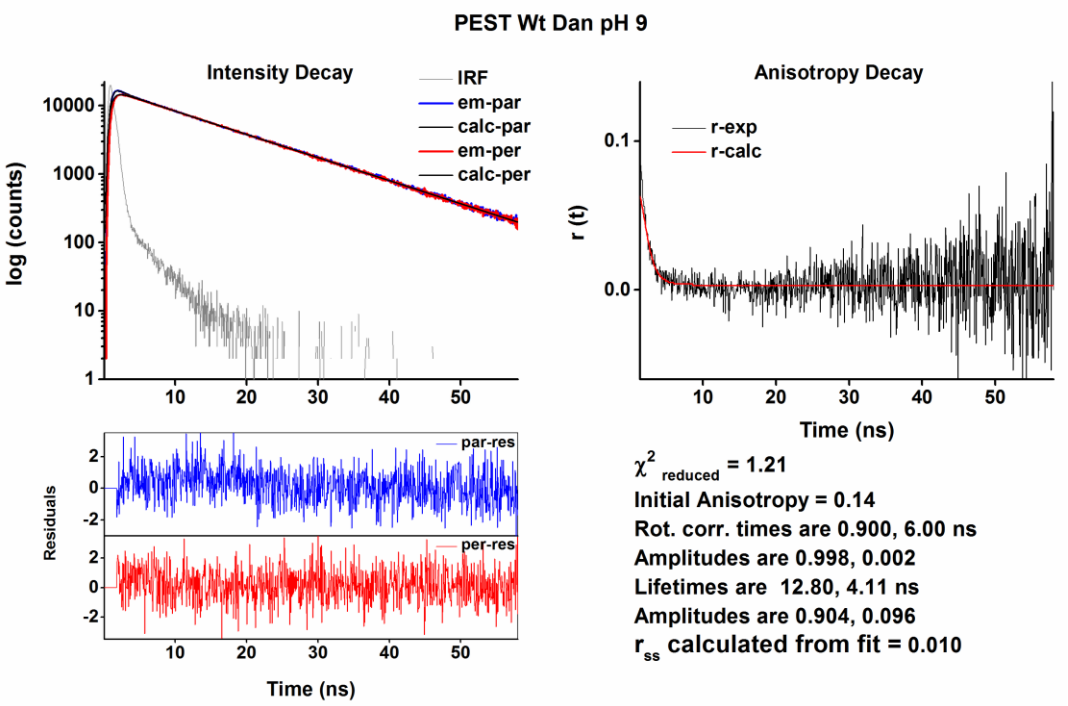

Figure A5: Fitted anisotropy decay profile of 10 µM dansyl labeled with 11 µM of PEST Wt at pH 9.

Figure A6: Fitted anisotropy decay profile of dansyl labeled PEST M1 at pH 3

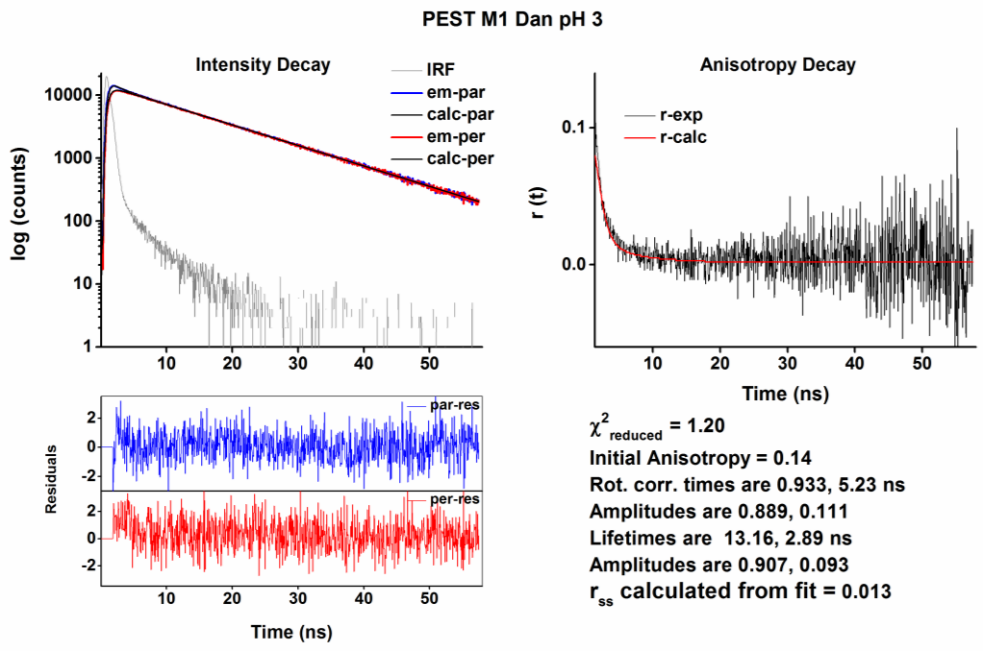

Figure A6: Fitted anisotropy decay profile of 10 µM dansyl labeled with 11 µM of PEST M1 at pH 3.

Figure A7: Fitted anisotropy decay profile of dansyl labeled PEST M1 at pH 9

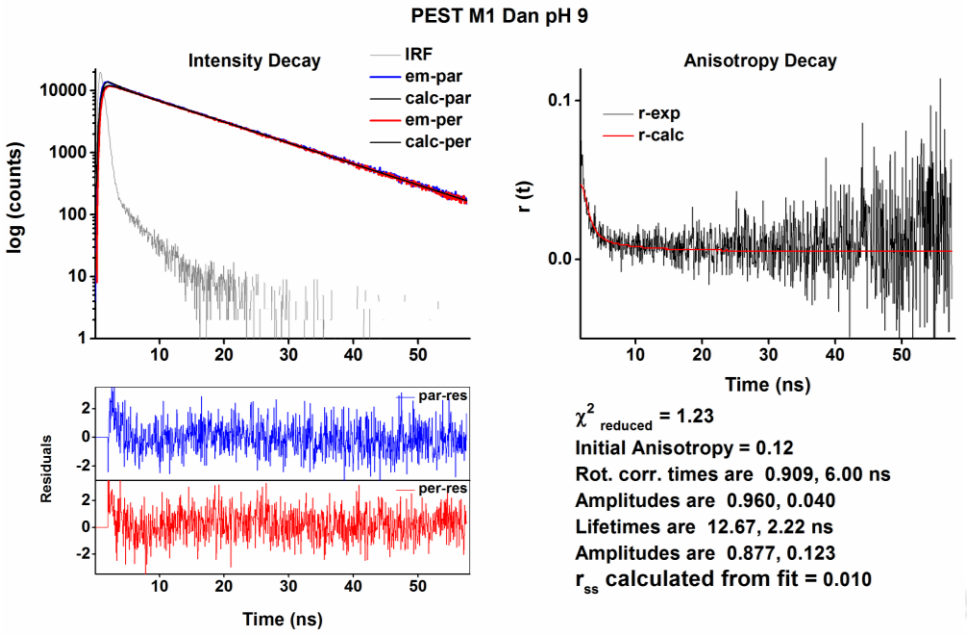

Figure A7: Fitted anisotropy decay profile of 10 µM dansyl labeled with 11 µM of PEST M1 at pH 9.

Figure A8: Fitted CD Spectra of PEST Wt and M1 at various pH

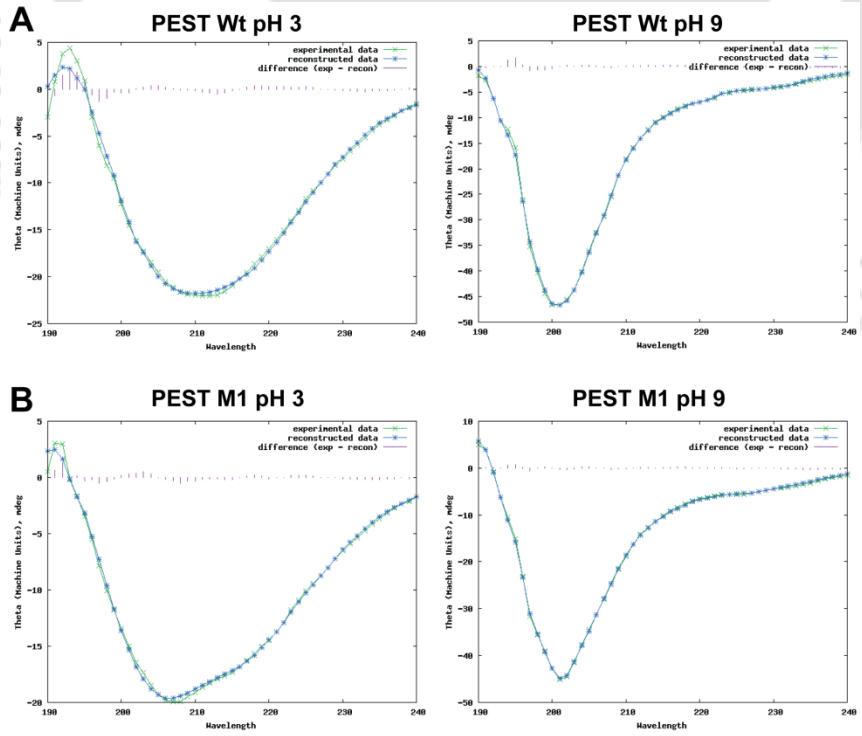

Figure A8: Fitted CD spectra of **[A]** PEST Wt and **[B]** PEST M1 by using DichroWeb server at pH 3 and 9.

LIST OF PUBLICATIONS AND CONFERENCES

LIST OF PUBLICATIONS

1. Ansari, MZ, Kumar, A, Ahari, D, Priyadarshi, A, Lolla, P, Bhandari, R, and Swaminathan, R (2018): Protein charge transfer absorption spectra: an intrinsic probe to monitor structural and oligomeric transitions in proteins. *Faraday Discuss.* **207**, 91-113.

2. Ansari, MZ, Lolla, P, Bhandari, R, and Swaminathan, R,: Unravelling the changes in structure, dynamics and disorder properties of human c-Myc PEST fragment during a pH induced disorder to order transition. (*Manuscript under preparation*).

3. Ansari, MZ, Lolla, P, Bhandari, R, and Swaminathan, R,: Investigating the changes in the structure and dynamics of human c-Myc PEST fragment upon dimer formation . (*Manuscript under preparation*).

Conferences/Workshop

1. Participated and presented a poster in the "**National Conference on Fluorescence and Raman Spectroscopy**" held during 17th - 21st December 2017 at IIT Guwahati, Assam, India.

2. Participated and presented a poster in the "**International Conference on Intrinsically Disordered Proteins: Forms, Functions and Diseases**" held during 9th - 12th December 2017 organized by IISER Mohali, Punjab, India.

3. Participated in Indo-Japan symposium on "**Hope from Herbs: Research-Based Care & Cure Potentials**" held during 8th and 9th May 2017 at IIT Guwahati, Assam, India.

4. Participated in a "**Workshop on Advanced Microscopy and Imaging Techniques"** held during 18th - 20th April 2017 at IIT Guwahati, Assam, India.

5. Participated and presented a poster in the "**Research Conclave**" held during 16th - 19th March 2017 organized by Students' Academic Board, IIT Guwahati, Assam, India.

6. Participated in a **"Workshop on Intellectual Property Rights"** held during 30th November and 1st December 2016 at IIT Guwahati, Assam, India.

7. Participated and presented a poster in International Conference **"Optics Within Life Sciences (OWLS)"** held during 16th - 19th March 2016 organized by TIFR, Mumbai, India.

8. Participated and presented a poster in the "**Research Conclave**" held during 23rd - 26th March 2015 organized by Students Academic Board, IIT Guwahati, Assam, India.

9. Participated and presented a poster in the "**National Symposium on Biophysics and Golden Jubilee of the Indian Biophysical Society**" held during 14th - 17th February 2015 organized by Jamia Millia Islamia, New Delhi, India.

10. Participated in a Workshop on **"Technical Writing"** held during 6th and 7th December 2014 at IIT Guwahati, Assam, India.

References

Adler, AJ, Greenfield, NJ, and Fasman, GD (1973): Circular dichroism and optical rotatory dispersion of proteins and polypeptides: *Methods in enzymology*, Vol. 27. Elsevier, pp. 675-735.

Alexandrescu, AT, Abeygunawardana, C, and Shortle, D (1994): Structure and dynamics of a denatured 131-residue fragment of staphylococcal nuclease: a heteronuclear NMR study. *Biochemistry* **33**, 1063-1072.

Aliverti, A, Curti, B, and Vanoni, MA (1999): Identifying and quantitating FAD and FMN in simple and in iron-sulfur-containing flavoproteins: *Flavoprotein protocols*. Springer, pp. 9-23.

Andresen, C, Helander, S, Lemak, A, Farès, C, Csizmok, V, Carlsson, J, Penn, LZ, Forman-Kay, JD, Arrowsmith, CH, and Lundström, P (2012): Transient structure and dynamics in the disordered c-Myc transactivation domain affect Bin1 binding. *Nucleic Acids Res.* **40**, 6353-6366.

Antosiewicz, JM, and Shugar, D (2016a): UV–Vis spectroscopy of tyrosine side-groups in studies of protein structure. Part 1: basic principles and properties of tyrosine chromophore. *Biophys. Rev.* **8**, 151-161.

Antosiewicz, JM, and Shugar, D (2016b): UV–Vis spectroscopy of tyrosine side-groups in studies of protein structure. Part 2: Selected applications. *Biophys. Rev.* **8**, 163-177.

Babu, MM (2016): The contribution of intrinsically disordered regions to protein function, cellular complexity, and human disease. *Biochem. Soc. Trans.* **44**, 1185-1200.

Bahram, F, von der Lehr, N, Cetinkaya, C, and Larsson, L-G (2000): c-Myc hot spot mutations in lymphomas result in inefficient ubiquitination and decreased proteasome-mediated turnover. *Blood* **95**, 2104-2110.

Balzani, V, Bergamini, G, Campagna, S, and Puntoriero, F (2007): Photochemistry and photophysics of coordination compounds: overview and general concepts: *Photochemistry and Photophysics of Coordination Compounds I*. Springer, pp. 1-36.

Baskakov, I, and Bolen, DW (1998): Forcing thermodynamically unfolded proteins to fold. *J. Biol. Chem.* **273**, 4831-4834.

Baskakov, I, Wang, A, and Bolen, DW (1998): Trimethylamine-N-oxide counteracts urea effects on rabbit muscle lactate dehydrogenase function: a test of the counteraction hypothesis. *Biophys. J.* **74**, 2666-2673.

Beechem, JM, and Brand, L (1985): Time-resolved fluorescence of proteins. *Annu. Rev. Biochem.* **54**, 43-71.

Belford, GG, Belford, RL, and Weber, G (1972): Dynamics of Fluorescence Polarization in Macromolecules. *Proc. Natl. Acad. Sci.* **69**, 1392-1393.

Belmont, LD, and Mitchison, TJ (1996): Identification of a protein that interacts with tubulin dimers and increases the catastrophe rate of microtubules. *Cell* **84**, 623-631.

Bent, DV, and Hayon, E (1975a): Excited state chemistry of aromatic amino acids and related peptides. II. Phenylalanine. *J. Am. Chem. Soc.* **97**, 2606-2612.

Bent, DV, and Hayon, E (1975b): Excited state chemistry of aromatic amino acids and related peptides. III. Tryptophan. *J. Am. Chem. Soc.* **97**, 2612-2619.

Berg, JM, Tymoczko, JL, and Stryer, L (2002): Biochemistry. *Freeman, New York*.

Bevington, PR, and Robinson, KD (1992): *Data reduction and error analysis for the physical sciences*. McGraw-Hill, Inc.

Bies, J, and Wolff, L (1997): Oncogenic activation of c-Myb by carboxyl-terminal truncation leads to decreased proteolysis by the ubiquitin-26S proteasome pathway. *Oncogene* **14**, 203-212.

Blackwell, TK, Kretzner, L, Blackwood, EM, Eisenman, RN, and Weintraub, H (1990): Sequence-specific DNA binding by the c-Myc protein. *Science* **250**, 1149-1151.

Blackwood, EM, and Eisenman, RN (1991): Max: a helix-loop-helix zipper protein that forms a sequence-specific DNA-binding complex with Myc. *Science* **251**, 1211-1217.

Bloomer, AC, Champness, JN, Bricogne, G, Staden, R, and Klug, A (1978): Protein disk of tobacco mosaic virus at 2.8 Å resolution showing the interactions within and between subunits. *Nature* **276**, 362-368.

Bode, W, Schwager, P, and Huber, R (1978): The transition of bovine trypsinogen to a trypsin-like state upon strong ligand binding: the refined crystal structures of the bovine trypsinogen-pancreatic trypsin inhibitor complex and of its ternary complex with Ile-Val at 1.9 Å resolution. *J. Mol. Biol.* **118**, 99-112.

Bolen, DW (2001): Protein stabilization by naturally occurring osmolytes: *Methods Mol. Biol.*, Vol. 168. Springer, pp. 17-36.

Bordone, L, and Campbell, C (2002): DNA ligase III is degraded by calpain during cell death induced by DNA damaging agents. *J. Biol. Chem.* **277**, 26673–26680.

Bousset, K, Henriksson, M, Lüscher-Firzlaff, JM, Litchfield, DW, and Luscher, B (1993): Identification of casein kinase II phosphorylation sites in Max: effects on DNA-binding kinetics of Max homo-and Myc/Max heterodimers. *Oncogene* **8**, 3211-3220.

Bracken, C (2001): NMR spin relaxation methods for characterization of disorder and folding in proteins. *J. Mol. Graphics Modell.* **19**, 3-12.

Brand, L, and Gohlke, JR (1972): Fluorescence probes for structure. *Annu. Rev. Biochem.* **41**, 843-868.

Brown, CJ, Takayama, S, Campen, AM, Vise, P, Marshall, TW, Oldfield, CJ, Williams, CJ, and Keith Dunker, A (2002): Evolutionary rate heterogeneity in proteins with long disordered regions. *J. Mol. Evol.* **55**, 104-110.

Burg, MB (1995): Molecular basis of osmotic regulation. *Am. J. Physiol. Renal. Physiol.* **268**, F983-F996.

Burgi, J, Xue, B, Uversky, VN, and van der Goot, FG (2016): Intrinsic disorder in transmembrane proteins: roles in signaling and topology prediction. *PloS one* **11**, e0158594.

Callebaut, I, Labesse, G, Durand, P, Poupon, A, Canard, L, Chomilier, J, Henrissat, B, and Mornon, JP (1997): Deciphering protein sequence information through hydrophobic cluster analysis (HCA): current status and perspectives. *Cell. Mol. Life Sci.* **53**, 621-645.

Campagna, S, Puntoriero, F, Nastasi, F, Bergamini, G, and Balzani, V (2007): Photochemistry and photophysics of coordination compounds: ruthenium: *Photochemistry and Photophysics of Coordination Compounds I*. Springer, pp. 117-214.

Campanero, MR, and Flemington, EK (1997): Regulation of E2F through ubiquitin–proteasome-dependent degradation: stabilization by the pRB tumor suppressor protein. *Proc. Natl. Acad. Sci.* **94**, 2221-2226.

Cheng, Y, LeGall, T, Oldfield, CJ, Dunker, AK, and Uversky, VN (2006): Abundance of intrinsic disorder in protein associated with cardiovascular disease. *Biochemistry* **45**, 10448-10460.

Chou, T-Y, Dang, CV, and Hart, GW (1995): Glycosylation of the c-Myc transactivation domain. *Proc. Natl. Acad. Sci.* **92**, 4417-4421.

Cooper, GM, and Ganem, D (1997): The cell: a molecular approach. *Nat. Med.* **3**, 1042-1042.

Cordero, OJ, Sarandeses, CS, Lopez, JL, and Nogueira, M (1992): On the anomalous behaviour on gel-filtration and SDS-electrophoresis of prothymosin-alpha. *Biochemistry* **28**, 1117-1124.

Cortese, MS, Uversky, VN, and Dunker, AK (2008): Intrinsic disorder in scaffold proteins: getting more from less. *Prog. Biophys. Mol. Biol.* **98**, 85-106.

Cotton, S (2006): Coordination chemistry of the actinides: *Lanthanide and Actinide Chemistry*. John Wiley & Sons, Ltd, pp. 173-199.

Cox, CJ, Dutta, K, Petri, ET, Hwang, WC, Lin, Y, Pascal, SM, and Basavappa, R (2002): The regions of securin and cyclin B proteins recognized by the ubiquitination machinery are natively unfolded. *FEBS Lett.* **527**, 303-308.

Creed, D (1984a): The photophysics and photochemistry of the near-UV absorbing amino acids–I. Tryptophan and its simple derivatives. *Photochem. Photobiol.* **39**, 537-562.

Creed, D (1984b): The photophysics and photochemistry of the near-UV absorbing amino acids–II. Tyrosine and its simple derivatives. *Photochem. Photobiol.* **39**, 563-575.

Crick, SL, Jayaraman, M, Frieden, C, Wetzel, R, and Pappu, RV (2006): Fluorescence correlation spectroscopy shows that monomeric polyglutamine molecules form collapsed structures in aqueous solutions. *Proc. Natl. Acad. Sci.* **103**, 16764-16769.

Crosby, GA (1975): Spectroscopic investigations of excited states of transition-metal complexes. *Acc. Chem. Res.* **8**, 231-238.

Csizmok, V, Szollosi, E, Friedrich, P, and Tompa, P (2006): A novel two-dimensional electrophoresis technique for the identification of intrinsically unstructured proteins. *Mol. Cell Proteomics* **5**, 265-273.

Dahlman-Wright, K, and McEwan, IJ (1996): Structural studies of mutant glucocorticoid receptor transactivation domains establish a link between transactivation activity in vivo and α-helix-forming potential in vitro. *Biochemistry* **35**, 1323-1327.

Dang, CV (1999): c-Myc target genes involved in cell growth, apoptosis, and metabolism. *Mol. Cell. Biol.* **19**, 1-11.

Daniel, RM, Dunn, RV, Finney, JL, and Smith, JC (2003): The role of dynamics in enzyme activity. *Annu. Rev. Biophys. Biomol. Struct.* **32**, 69-92.

Dawson, RMC, Elliott, DC, Elliott, WH, and Jones, KM (1969): *Data for biochemical research*. Clarendon Press Oxford.

Debye, P (1915): Zerstreuung von Röntgenstrahlen. *Ann. Phys.* **351**, 809-823.

di Prisco, G, Condo, SG, Tamburrini, M, and Giardina, B (1991): Oxygen transport in extreme environments. *Trends Biochem. Sci.* **16**, 471-474.

Dill, KA, and Shortle, D (1991): Denatured states of proteins. *Annu. Rev. Biochem.* **60**, 795-825.

Dougan, L, Li, J, Badilla, CL, Berne, BJ, and Fernandez, JM (2009): Single homopolypeptide chains collapse into mechanically rigid conformations. *Proc. Natl. Acad. Sci.* **106**, 12605-12610.

Dunker, AK, Brown, CJ, Lawson, JD, Iakoucheva, LM, and Obradovic, Z (2002a): Intrinsic disorder and protein function. *Biochemistry* **41**, 6573-6582.

Dunker, AK, Brown, CJ, and Obradovic, Z (2002b): Identification and functions of usefully disordered proteins. *Adv. Protein Chem.* **62**, 25-49.

Dunker, AK, Cortese, MS, Romero, P, Iakoucheva, LM, and Uversky, VN (2005): Flexible nets: the roles of intrinsic disorder in protein interaction networks. *FEBS J.* **272**, 5129-5148.

Dunker, AK, Garner, E, Guilliot, S, Romero, P, Albrecht, K, Hart, J, Obradovic, Z, Kissinger, C, and Villafranca, JE (1998): Protein disorder and the evolution of molecular recognition: theory, predictions and observations. *Pac. Symp. Biocomput.* **3**, 473-484.

Dunker, AK, Lawson, JD, Brown, CJ, Williams, RM, Romero, P, Oh, JS, Oldfield, CJ, Campen, AM, Ratliff, CM, and Hipps, KW (2001): Intrinsically disordered protein. *J. Mol. Graphics Modell.* **19**, 26-59.

Dunker, AK, and Obradovic, Z (2001): The protein trinity—linking function and disorder. *Nat. Biotechnol.* **19**, 805-806.

Dunker, AK, Romero, P, Obradovic, Z, Garner, EC, and Brown, CJ (2000): Intrinsic protein disorder in complete genomes. *Genome Inform.* **11**, 161-171.

Dunker, AK, Silman, I, Uversky, VN, and Sussman, JL (2008): Function and structure of inherently disordered proteins. *Curr. Opin. Struct. Biol.* **18**, 756-764.

Dyson, HJ, and Wright, PE (2002): Coupling of folding and binding for unstructured proteins. *Curr. Opin. Struct. Biol.* **12**, 54-60.

Dyson, HJ, and Wright, PE (2005): Intrinsically unstructured proteins and their functions. *Nat. Rev. Mol. Cell. Biol.* **6**, 197-208.

Eberhardy, SR, and Farnham, PJ (2002): Myc recruits P-TEFb to mediate the final step in the transcriptional activation of the cad promoter. *J. Biol. Chem.* **277**, 40156-40162.

Eilers, M, Schirm, S, and Bishop, JM (1991): The MYC protein activates transcription of the alpha-prothymosin gene. *EMBO J.* **10**, 133-141.

Ekman, D, Light, S, Björklund, ÅK, and Elofsson, A (2006): What properties characterize the hub proteins of the protein-protein interaction network of Saccharomyces cerevisiae? *Genome Biol.* **7**, R45.

Fasman, GD (1992): *Practical handbook of biochemistry and molecular biology*. CRC Press, New York.

Fink, AL (2005): Natively unfolded proteins. *Curr. Opin. Struct. Biol.* **15**, 35-41.

Fink, AL, Calciano, LJ, Goto, Y, Kurotsu, T, and Palleros, DR (1994): Classification of acid denaturation of proteins: intermediates and unfolded states. *Biochemistry* **33**, 12504-12511.

Fink, JC, Nass, CM, Chen, H, and Christenson, R (2005): N-terminal pro-B-type natriuretic peptide for predicting coronary disease and left ventricular hypertrophy in asymptomatic CKD not requiring dialysis. *Am. J. Kidney Dis.* **46**, 35-44.

Fontana, A, de Laureto, PP, De Filippis, V, Scaramella, E, and Zambonin, M (1997a): Probing the partly folded states of proteins by limited proteolysis. *Fold. Des.* **2**, R17-R26.

Fontana, A, Fassina, G, Vita, C, Dalzoppo, D, Zamai, M, and Zambonin, M (1986): Correlation between sites of limited proteolysis and segmental mobility in thermolysin. *Biochemistry* **25**, 1847-1851.

Fontana, A, Zambonin, M, de Laureto, PP, De Filippis, V, Clementi, A, and Scaramella, E (1997b): Probing the conformational state of apomyoglobin by limited proteolysis1. *J. Mol. Biol.* **21**, 223-230.

Forster, T (1948): Intermolecular energy transfer and fluorescence. *Ann. Phys. Leipzig.* **2**, 55-75.

Fox, SJ, and Kannan, S (2017): Probing the dynamics of disorder. *Prog. Biophys. Mol. Biol.* **128**, 57-62.

Galea, CA, Pagala, VR, Obenauer, JC, Park, C-G, Slaughter, CA, and Kriwacki, RW (2006): Proteomic studies of the intrinsically unstructured mammalian proteome. *J. Proteome Res.* **5**, 2839-2848.

Gatewood, JM, Schroth, GP, Schmid, CW, and Bradbury, EM (1990): Zinc-induced secondary structure transitions in human sperm protamines. *J. Biol. Chem.* **265**, 20667-20672.

Ghoda, L, van Daalen Wetters, T, Macrae, M, Ascherman, D, and Coffino, P (1989): Prevention of rapid intracellular degradation of ODC by a carboxyl-terminal truncation. *Science* **243**, 1493-1495.

Gianni, S, Dogan, J, and Jemth, P (2016): Coupled binding and folding of intrinsically disordered proteins: what can we learn from kinetics? *Curr. Opin. Struct. Biol.* **36**, 18-24.

Goldberg, ME, Semisotnov, GV, Friguet, B, Kuwajima, K, Ptitsyn, OB, and Sugai, S (1990): An early immunoreactive folding intermediate of the tryptophan synthase β2 subunit is a 'molten globule'. *FEBS Lett.* **263**, 51-56.

Goto, Y, Takahashi, N, and Fink, AL (1990): Mechanism of acid-induced folding of proteins. *Biochemistry* **29**, 3480-3488.

Grandori, C, Cowley, SM, James, LP, and Eisenman, RN (2000): The Myc/Max/Mad network and the transcriptional control of cell behavior. *Annu. Rev. Cell Dev. Biol.* **16**, 653-699.

Green, BR, and Parson, WW (2004): *Advances in Photosynthesis and Respiration, Light-Harvesting Antennas in Photosynthesis*, Vol. 13. Springer, Dordrecht, The Netherlands.

Greene, LH, Wijesinha-Bettoni, R, and Redfield, C (2006): Characterization of the molten globule of human serum retinol-binding protein using NMR spectroscopy. *Biochemistry* **45**, 9475-9484.

Gregory, MA, and Hann, SR (2000): c-Myc proteolysis by the ubiquitin-proteasome pathway: stabilization of c-Myc in Burkitt's lymphoma cells. *Mol. Cell. Biol.* **20**, 2423-2435.

Grinspan, H, Birnbaum, J, and Feitelson, J (1966): Environmental effects on the ultraviolet absorption spectrum of tyrosine. *Biochim. Biophys. Acta.* **126**, 13-18.

Gschneidner, KA (1994): *Lanthanides/actinides: chemistry*. Elsevier.

Habchi, J, Tompa, P, Longhi, S, and Uversky, VN (2014): Introducing protein intrinsic disorder. *Chem. Rev.* **114**, 6561-6588.

Hackel, M, Konno, T, and Hinz, H-J (2000): A new alternative method to quantify residual structure in 'unfolded'proteins. *Biochim. Biophys. Acta, Protein Struct. Mol. Enzymol.* **1479**, 155-165.

Ham, JS, and Platt, JR (1952): Far UV spectra of peptides. *J. Chem. Phys.* **20**, 335-336.

Harding, SE, and Jumel, K (1998): Light Scattering: *Curr. Protoc. Protein. Sci.* John Wiley & Sons, Inc., pp. 7.8.1-7.8.14.

Haynes, C, Oldfield, CJ, Ji, F, Klitgord, N, Cusick, ME, Radivojac, P, Uversky, VN, Vidal, M, and Iakoucheva, LM (2006): Intrinsic disorder is a common feature of hub proteins from four eukaryotic interactomes. *PLoS Comput. Biol.* **2**, e100.

Hemann, MT, Bric, A, Teruya-Feldstein, J, Herbst, A, Nilsson, JA, Cordon-Cardo, C, Cleveland, JL, Tansey, WP, and Lowe, SW (2005): Evasion of the p53 tumour surveillance network by tumour-derived MYC mutants. *Nature* **436**, 807-811.

Henriksson, M, and Luscher, B (1996): Proteins of the Myc network: essential regulators of cell growth and differentiation: *Advances in cancer research*, Vol. 68. Elsevier, pp. 109-182.

Herbst, A, Hemann, MT, Tworkowski, KA, Salghetti, SE, Lowe, SW, and Tansey, WP (2005): A conserved element in Myc that negatively regulates its proapoptotic activity. *EMBO Rep.* **6**, 177-183.

Hershey, PEC, McWhirter, SM, Gross, JD, Wagner, G, Alber, T, and Sachs, AB (1999): The Cap-binding protein eIF4E promotes folding of a functional domain of yeast translation initiation factor eIF4G1. *J. Biol. Chem.* **274**, 21297-21304.

Heyen, BJ, Alsheikh, MK, Smith, EA, Torvik, CF, Seals, DF, and Randall, SK (2002): The calcium-binding activity of a vacuole-associated, dehydrin-like protein is regulated by phosphorylation. *Plant Physiol.* **130**, 675-687.

Hill, JJ, and Royer, CA (1997): Fluorescence approaches to study of protein-nucleic acid complexation. *Methods Enzymol.* **278**, 390–416.

Hollstein, M, Sidransky, D, Vogelstein, B, and Harris, CC (1991): p53 mutations in human cancers. *Science* **253**, 49-53.

Holowka, D, Wensel, T, and Baird, B (1990): A nanosecond fluorescence depolarization study on the segmental flexibility of receptor-bound immunoglobulin E. *Biochemistry* **29**, 4607-4612.

Homchaudhuri, L, and Swaminathan, R (2001): Novel absorption and fluorescence characteristics of l-lysine. *Chem. Lett.* **30**, 844-845.

Homchaudhuri, L, and Swaminathan, R (2004): Near ultraviolet absorption arising from lysine residues in close proximity: A probe to monitor protein unfolding and aggregation in lysine-rich proteins. *Bull. Chem. Soc. Jpn.* **77**, 765-769.

Homocianu, M (2011): Solvent effects on the electronic absorption and fluorescence spectra. *J. Adv. Res. Phys.* **2**, 1-9.

Horiuchi, M, Kurihara, Y, Katahira, M, Maeda, T, Saito, T, and Uesugi, S (1997): Dimerization and DNA Binding Facilitate aaa-Helix Formation of Max in Solution. *J. Biochem.* **122**, 711-716.

Hua, QX, Jia, WH, Bullock, BP, Habener, JF, and Weiss, MA (1998): Transcriptional activator coactivator recognition: nascent folding of a kinase inducible transactivation domain predicts its structure on coactivator binding. *Biochemistry* **37**, 5858-5866.

Hubbard, SJ, Beynon, RJ, and Thornton, JM (1998): Assessment of conformational parameters as predictors of limited proteolytic sites in native protein structures. *Protein Eng.* **11**, 349-359.

Hubbard, SJ, Eisenmenger, F, and Thornton, JM (1994): Modeling studies of the change in conformation required for cleavage of limited proteolytic sites. *Protein Sci.* **3**, 757-768.

Huber, R, and Bennett Jr, WS (1983): Functional significance of flexibility in proteins. *Biopolymers* **22**, 261-279.

Hudson, EN, and Weber, G (1973): Synthesis and characterization of two fluorescent sulfhydryl reagents. *Biochemistry* **12**, 4154-4161.

Hulst, HC, and van de Hulst, HC (1957): *Light scattering by small particles*. John Wiley & Sons.

Hunt, HD, and Simpson, WT (1953): Spectra of Simple Amides in the Vacuum Ultraviolet1. *J. Am. Chem. Soc.* **75**, 4540-4543.

Iakoucheva, LM, Brown, CJ, Lawson, JD, Obradović, Z, and Dunker, AK (2002): Intrinsic disorder in cell-signaling and cancer-associated proteins. *J. Mol. Biol.* **323**, 573-584.

Iakoucheva, LM, Radivojac, P, Brown, CJ, O'Connor, TR, Sikes, JG, Obradovic, Z, and Dunker, AK (2004): The importance of intrinsic disorder for protein phosphorylation. *Nucleic Acids Res.* **32**, 1037-1049.

Imahori, K, and Tanaka, J (1959): Ultraviolet absorption spectra of poly-L-glutamic acid. *J. Mol. Biol.* **1**, 359-364.

Janes, R, and Moore, EA (2004): *Metal-ligand bonding*. Royal society of chemistry.

Jeganathan, S, von Bergen, M, Brutlach, H, Steinhoff, HJ, and Mandelkow, E (2006): Global hairpin folding of tau in solution. *Biochemistry* **45**, 2283-2293.

Johansson, J, Gudmundsson, GH, Rottenberg, MnE, Berndt, KD, and Agerberth, B (1998): Conformation-dependent antibacterial activity of the naturally occurring human peptide LL-37. *J. Biol. Chem.* **273**, 3718-3724.

Kalthoff, C (2003): A novel strategy for the purification of recombinantly expressed unstructured protein domains. *J. Chromatogr. B* **786**, 247-254.

Kalthoff, C, Alves, J, Urbanke, C, Knorr, R, and Ungewickell, EJ (2002): Unusual structural organization of the endocytic proteins AP180 and epsin 1. *J. Biol. Chem.* **277**, 8209–16.

Karnaukhova, E, Rutardottir, S, Rajabi, M, Wester Rosenlöf, L, Alayash, AI, and Åkerström, B (2014): Characterization of heme binding to recombinant α1-microglobulin. *Front. Physiol.* **5**, 465.

Kato, GJ, Barrett, J, Villa-Garcia, M, and Dang, CV (1990): An amino-terminal c-myc domain required for neoplastic transformation activates transcription. *Mol. Cell. Biol.* **10**, 5914-5920.

Kelly, SM, and Price, NC (1997): The application of circular dichroism to studies of protein folding and unfolding. *Biochim. Biophys. Acta. Protein Struct. Mol. Enzym.* **1338**, 161-185.

Kendrew, JC, Bodo, G, Dintzis, HM, Parrish, RG, Wyckoff, H, and Phillips, DC (1958): A three-dimensional model of the myoglobin molecule obtained by x-ray analysis. *Nature* **181**, 662-666.

Khoury, GA, Baliban, RC, and Floudas, CA (2011): Proteome-wide post-translational modification statistics: frequency analysis and curation of the swiss-prot database. *Sci. Rep.* **1**, 90.

Kim, TD, Ryu, HJ, Cho, HI, Yang, C-H, and Kim, J (2000): Thermal behavior of proteins: heat-resistant proteins and their heat-induced secondary structural changes. *Biochemistry* **39**, 14839-14846.

King, BA, Stanley, RJ, and Boxer, SG (1997): Excited state energy transfer pathways in photosynthetic reaction centers. 2. heterodimer special pair. *J. Phys. Chem. B* **101**, 3644-3648.

Konno, T, Tanaka, N, Kataoka, M, Takano, E, and Maki, M (1997): A circular dichroism study of preferential hydration and alcohol effects on a denatured protein, pig

calpastatin domain I. *Biochim. Biophys. Acta, Protein Struct. Mol. Enzym.* **1342**, 73-82.

Kovacs, D, Kalmar, E, Torok, Z, and Tompa, P (2008): Chaperone activity of ERD10 and ERD14, two disordered stress-related plant proteins. *Plant Physiol.* **147**, 381-390.

Kozlowski, LP, and Bujnicki, JM (2012): MetaDisorder: a meta-server for the prediction of intrinsic disorder in proteins. *BMC Bioinformatics* **13**, 111.

Kriwacki, RW, Hengst, L, Tennant, L, Reed, SI, and Wright, PE (1996): Structural studies of p21Waf1/Cip1/Sdi1 in the free and Cdk2-bound state: conformational disorder mediates binding diversity. *Proc. Natl. Acad. Sci.* **93**, 11504-11509.

Kumar, R, Lee, JC, Bolen, DW, and Thompson, EB (2001): The conformation of the glucocorticoid receptor af1/tau1 domain induced by osmolyte binds coregulatory proteins. *J. Biol. Chem.* **276**, 18146–18152.

Kumar, R, Serrette, JM, Khan, SH, Miller, AL, and Thompson, EB (2007): Effects of different osmolytes on the induced folding of the N-terminal activation domain (AF1) of the glucocorticoid receptor. *Arch. Biochem. Biophys.* **465**, 452-460.

Kumar, S, Ravi, VK, and Swaminathan, R (2008): How do surfactants and DTT affect the size, dynamics, activity and growth of soluble lysozyme aggregates? *Biochem. J.* **415**, 275-288.

Kurland, JF, and Tansey, WP (2008): Myc-mediated transcriptional repression by recruitment of histone deacetylase. *Cancer Res.* **68**, 3624-3629.

Lakowicz, JR (1983): Quenching of fluorescence: *Principles of fluorescence spectroscopy*. Springer, pp. 257-301.

Lakowicz, JR (2006): Protein fluorescence: *Principles of Fluorescence Spectroscopy*, Vol. 3rd edition. Springer US, New York, pp. 529-575.

Laporte, O, and Meggers, WF (1925): Some rules of spectral structure. *JOSA* **11**, 459-463.

Leermakers, PA, and Vesley, GF (1964): Organic photochemistry and the excited state. *J. Chem. Educ.* **41**, 535.

Lesk, AM (2001): Introduction to protein architecture: the structural biology of proteins. *Oxford University Press, Oxford*.

Lin, R, Beauparlant, P, Makris, C, Meloche, S, and Hiscott, J (1996): Phosphorylation of IkappaBalpha in the C-terminal PEST domain by casein kinase II affects intrinsic protein stability. *Mol. Cell. Biol.* **16**, 1401-1409.

Liu, J, Faeder, JR, and Camacho, CJ (2009): Toward a quantitative theory of intrinsically disordered proteins and their function. *Proc. Natl. Acad. Sci.* **106**, 19819-19823.

Liu, Z-P, Galindo, RL, and Wasserman, SA (1997): A role for CKII phosphorylation of the cactus PEST domain in dorsoventral patterning of the Drosophila embryo. *Genes Dev.* **11**, 3413-3422.

Liu, Z, and Huang, Y (2014): Advantages of proteins being disordered. *Protein Sci.* **23**, 539-550.

Lobley, A, Whitmore, L, and Wallace, BA (2002): DICHROWEB: an interactive website for the analysis of protein secondary structure from circular dichroism spectra. *Bioinformatics* **18**, 211-212.

Longworth, JW, Steiner, RF, and Weinryb, I (1971): Excited states of proteins and nucleic acids. *Plenum Press, New York*, 319-484.

Lowry, OH, Rosebrough, NJ, Farr, AL, and Randall, RJ (1951): Protein measurement with the Folin phenol reagent. *J. Biol. Chem.* **193**, 265-275.

Luscher, B, Kuenzel, EA, Krebs, EG, and Eisenman, RN (1989): Myc oncoproteins are phosphorylated by casein kinase II. *EMBO J.* **8**, 1111-1119.

Lynn, A, Chandra, S, Malhotra, P, and Chauhan, VS (1999): Heme binding and polymerization by Plasmodium falciparum histidine rich protein II: influence of pH on activity and conformation. *FEBS letters* **459**, 267-271.

Maki, CG, Huibregtse, JM, and Howley, PM (1996): In vivo ubiquitination and proteasome-mediated degradation of p53. *Cancer Res.* **56**, 2649-2654.

Mandal, I, Paul, S, and Venkatramani, R (2018): Optical backbone-sidechain charge transfer transitions in proteins sensitive to secondary structure and modifications. *Faraday Discuss.* **207**, 115-135.

Mao, AH, Crick, SL, Vitalis, A, Chicoine, CL, and Pappu, RV (2010): Net charge per residue modulates conformational ensembles of intrinsically disordered proteins. *Proc. Natl. Acad. Sci.* **107**, 8183-8188.

Marcu, KB, Bossone, SA, and Patel, AJ (1992): Myc function and regulation. *Annu. Rev. Biochem.* **61**, 809-858.

Mason, R (1959): Charge transfer processes in biological systems. *Discuss. Faraday Soc.* **27**, 129-133.

Mateos-Gil, P, Tsortos, A, Velez, M, and Gizeli, E (2016): Monitoring structural changes in intrinsically disordered proteins using QCM-D: application to the bacterial cell division protein ZipA. *Chem. Commun.* **52**, 6541-6544.

McConnell, H (1952): Effect of polar solvents on the absorption frequency of n→ π electronic transitions. *J. Chem. Phys.* **20**, 700-704.

McMillin, DR, and Morris, MC (1981): Further perspectives on the charge transfer transitions of blue copper proteins and the ligand moieties in stellacyanin. *Proc. Natl. Acad. Sci.* **78**, 6567-6570.

Mie, G (1908): Beiträge zur Optik trüber Medien, speziell kolloidaler Metallösungen. *Ann. Phys.* **330**, 377-445.

Milo, R, and Phillips, R (2015): *Cell biology by the numbers*. Garland Science.

Mittag, T, Kay, LE, and Forman-Kay, JD (2010a): Protein dynamics and conformational disorder in molecular recognition. *J. Mol. Recognit.* **23**, 105-116.

Mittag, T, Marsh, J, Grishaev, A, Orlicky, S, Lin, H, Sicheri, F, Tyers, M, and Forman-Kay, JD (2010b): Structure/function implications in a dynamic complex of the intrinsically disordered Sic1 with the Cdc4 subunit of an SCF ubiquitin ligase. *Structure* **18**, 494-506.

Moglich, A, Joder, K, and Kiefhaber, T (2006): End-to-end distance distributions and intrachain diffusion constants in unfolded polypeptide chains indicate intramolecular hydrogen bond formation. *Proc. Natl. Acad. Sci.* **103**, 12394-12399.

Mukhopadhyay, S, Krishnan, R, Lemke, EA, Lindquist, S, and Deniz, AA (2007): A natively unfolded yeast prion monomer adopts an ensemble of collapsed and rapidly fluctuating structures. *Proc. Natl. Acad. Sci.* **104**, 2649-2654.

Musci, G, Metz, GD, Tsunematsu, H, and Berliner, LJ (1985): 4, 4'-Bis [8-(phenylamino) naphthalene-1-sulfonate] binding to human thrombins: a sensitive exo site fluorescent affinity probe. *Biochemistry* **24**, 2034-2039.

Nash, P, Tang, X, Orlicky, S, Chen, Q, Gertler, FB, Mendenhall, MD, Sicheri, F, Pawson, T, and Tyers, M (2001): Multisite phosphorylation of a CDK inhibitor sets a threshold for the onset of DNA replication. *Nature* **414**, 514-521.

Nespoulous, C, Rofidal, V, Sommerer, N, Hem, S, and Rossignol, M (2012): Phosphoproteomic analysis reveals major default phosphorylation sites outside long intrinsically disordered regions of Arabidopsis plasma membrane proteins. *Proteome Sci.* **10**, 62.

Nilapwar, SM, Nardelli, M, Westerhoff, HV, and Verma, M (2011): Absorption spectroscopy: *Methods in enzymology*, Vol. 500. Elsevier, pp. 59-75.

Nimmo, GA, and Cohen, P (1978): The Regulation of Glycogen Metaabolism: Purification and Characterisation of Protein Phosphatase Inhibitor-1 from Rabbit Skeletal Muscle. *Eur. J. Biochem.* **87**, 341-351.

Olashaw, N, Bagui, TK, and Pledger, WJ (2004): Cell cycle control: a complex issue. *Cell Cycle* **3**, 261-262.

Oldfield, CJ, Cheng, Y, Cortese, MS, Brown, CJ, Uversky, VN, and Dunker, AK (2005): Comparing and combining predictors of mostly disordered proteins. *Biochemistry* **44**, 1989-2000.

Oliner, JD, Pietenpol, JA, Thiagalingam, S, Gyuris, J, Kinzler, KW, and Vogelstein, B (1993): Oncoprotein MDM2 conceals the activation domain of tumour suppressor p53. *Nature* **362**, 857-860.

Otey, MC, and Greenstein, JP (1954): Studies on polycysteine peptides and proteins. II. Apparent dissociation constants, and ultraviolet and infrared absorption spectra of isomeric cystinylcystine peptides. *Arch. Biochem. Biophys.* **53**, 501-513.

Patil, A, and Nakamura, H (2006): Disordered domains and high surface charge confer hubs with the ability to interact with multiple proteins in interaction networks. *FEBS Lett.* **580**, 2041-2045.

Pierloot, K, De Kerpel, JOA, Ryde, U, Olsson, MHM, and Roos, BO (1998): Relation between the structure and spectroscopic properties of blue copper proteins. *J. Am. Chem. Soc.* **120**, 13156-13166.

Plaxco, KW, and Gross, M (1997): The importance of being unfolded. *Nature* **386**, 657-659.

Prakash, S, Tian, L, Ratliff, KS, Lehotzky, RE, and Matouschek, A (2004): An unstructured initiation site is required for efficient proteasome-mediated degradation. *Nat. Struct. Biol.* **11**, 830-837.

Prasad, S, Mandal, I, Singh, S, Paul, A, Mandal, B, Venkatramani, R, and Swaminathan, R (2017): Near UV-Visible electronic absorption originating from charged amino acids in a monomeric protein. *Chem. Sci.* **8**, 5416-5433.

Prendergast, GC, and Ziff, EB (1991): Methylation-sensitive sequence-specific DNA binding by the c-Myc basic region. *Science* **251**, 186-189.

Ptitsyn, OB (1995a): Molten globule and protein folding: *Advances in protein chemistry*, Vol. 47. Elsevier, pp. 83-229.

Ptitsyn, OB (1995b): Structures of folding intermediates. *Curr. Opin. Struct. Biol.* **5**, 74-78.

Quickenden, TI, and Irvin, JA (1980): The ultraviolet absorption spectrum of liquid water. *J. Chem. Phys.* **72**, 4416-4428.

Radivojac, P, Iakoucheva, LM, Oldfield, CJ, Obradovic, Z, Uversky, VN, and Dunker, AK (2007): Intrinsic disorder and functional proteomics. *Biophys. J.* **92**, 1439-1456.

Rayleigh, L (1899): XXXIV. On the transmission of light through an atmosphere containing small particles in suspension, and on the origin of the blue of the sky. *Philos. Mag. Ser.* **47**, 375-384.

Rechsteiner, M, and Rogers, SW (1996): PEST sequences and regulation by proteolysis. *Trends Biochem. Sci.* **21**, 267-271.

Reddy, KH (2007): *Bioinorganic chemistry*. New Age International.

Reddy, SL, Endo, T, and Reddy, GS (2012): Electronic (absorption) spectra of 3d transition metal complexes: *Advanced Aspects of Spectroscopy*. InTech.

Riener, CK, Kada, G, and Gruber, HJ (2002): Quick measurement of protein sulfhydryls with Ellman's reagent and with 4, 4'-dithiodipyridine. *Anal. Bioanal. Chem.* **373**, 266-276.

Rogers, S, Wells, R, and Rechsteiner, M (1986): Amino acid sequences common to rapidly degraded proteins: the PEST hypothesis. *Science* **234**, 364-368.

Romero, P, Obradovic, Z, Li, X, Garner, EC, Brown, CJ, and Dunker, AK (2001): Sequence complexity of disordered protein. *Proteins* **42**, 38-48.

Rosenheck, K, and Doty, P (1961): The far ultraviolet absorption spectra of polypeptide and protein solutions and their dependence on conformation. *Proc. Natl. Acad. Sci.* **47**, 1775-1785.

Rusinova, E, Tretyachenko-Ladokhina, V, Vele, OE, Senear, DF, and Alexander Ross, JB (2002): Alexa and Oregon Green dyes as fluorescence anisotropy probes for measuring protein–protein and protein–nucleic acid interactions. *Anal. Biochem.* **308**, 18-25.

Salghetti, SE, Kim, SY, and Tansey, WP (1999): Destruction of Myc by ubiquitin-mediated proteolysis: cancer-associated and transforming mutations stabilize Myc. *EMBO J.* **18**, 717-726.

Sambrook, J, Fritsch, EF, and Maniatis, T (1989): *Molecular cloning: a laboratory manual*. Cold spring harbor laboratory press.

Schmid, FX (1989): Spectral probes of conformation: *Protein structure: a practical approach*. IRL Press, Oxford, UK, pp. 251-285.

Schuster, GB (2000): Long-range charge transfer in DNA: transient structural distortions control the distance dependence. *Acc. Chem. Res.* **33**, 253-260.

Showalter, SA (2014): Intrinsically Disordered Proteins: Methods for Structure and Dynamics Studies. *eMagRes* **3**, 181-190.

Siegel, R (2001): *Thermal radiation heat transfer*. CRC press.

Sigalov, AB (2010): Protein intrinsic disorder and oligomericity in cell signaling. *Mol. Biosyst.* **6**, 451-461.

Singh, GP, Ganapathi, M, Sandhu, KS, and Dash, D (2006): Intrinsic unstructuredness and abundance of PEST motifs in eukaryotic proteomes. *Proteins* **62**, 309-315.

Small, EW, and Isenberg, I (1977): Hydrodynamic properties of a rigid molecule: Rotational and linear diffusion and fluorescence anisotropy. *Biopolymers* **16**, 1907-1928.

Smyth, E, Syme, CD, Blanch, EW, Hecht, L, Vašák, M, and Barron, LD (2001): Solution structure of native proteins with irregular folds from Raman optical activity. *Biopolymers* **58**, 138-151.

Spencer, CA, and Groudine, M (1991): Control of c-myc regulation in normal and neoplastic cells: *Advances in cancer research*, Vol. 56. Elsevier, pp. 1-48.

Spolar, RS, and Record, MT (1994): Coupling of local folding to site-specific binding of proteins to DNA. *Science* **263**, 777-784.

Sreerama, N, and Woody, RW (2000): Estimation of Protein Secondary Structure from Circular Dichroism Spectra: Comparison of CONTIN, SELCON, and CDSSTR Methods with an Expanded Reference Set. *Anal. Biochem.* **287**, 252-260.

Sridharan, K (2016): *Spectral methods in transition metal complexes*. Elsevier.

Stancovski, I, Gonen, H, Orian, A, Schwartz, AL, and Ciechanover, A (1995): Degradation of the proto-oncogene product c-Fos by the ubiquitin proteolytic system in vivo and in vitro: identification and characterization of the conjugating enzymes. *Mol. Cell. Biol.* **15**, 7106-7116.

Steiner, RF (1991): Fluorescence Anisotropy: Theory and Applications: *Topics in Fluorescence Spectroscopy: Principles of fluorescence spectroscopy*, Vol. 2. Springer US, Boston, MA, pp. 1-55.

Stellwagen, E, Rysavy, R, and Babul, G (1972): The conformation of horse heart apocytochrome c. *J. Biol. Chem.* **247**, 8074-8077.

Stone, J, De Lange, T, Ramsay, G, Jakobovits, E, Bishop, JM, Varmus, H, and Lee, W (1987): Definition of regions in human c-myc that are involved in transformation and nuclear localization. *Mol. Cell. Biol.* **7**, 1697-1709.

Strutt, JW (1871a): LVIII. On the scattering of light by small particles. *Philos. Mag. Ser.* **41**, 447-454.

Strutt, JW (1871b): XXXVI. On the light from the sky, its polarization and colour. *Philos. Mag. Ser.* **41**, 274-279.

Stryer, L (1978): Fluorescence energy transfer as a spectroscopic ruler. *Annu. Rev. Biochem.* **47**, 819-846.

Sugase, K, Dyson, HJ, and Wright, PE (2007): Mechanism of coupled folding and binding of an intrinsically disordered protein. *Nature* **447**, 1021–1025.

Sun, X, Jones, WT, Harvey, D, Edwards, PJB, Pascal, SM, Kirk, C, Considine, T, Sheerin, DJ, Rakonjac, J, and Oldfield, CJ (2010): N-terminal domains of DELLA proteins are intrinsically unstructured in the absence of interaction with GID1/gibberellic acid receptors. *J. Biol. Chem.* **285**, 11557-11571.

Swaminathan, R, Periasamy, N, Udgaonkar, JB, and Krishnamoorthy, G (1994): Molten Globule-like Conformation of Barstar: A Study by Fluorescence Dynamics. *J. Phys. Chem.* **98**, 9270-9278.

Szilvay, GR, Blenner, MA, Shur, O, Cropek, DM, and Banta, S (2009): A FRET-based method for probing the conformational behavior of an intrinsically disordered repeat domain from Bordetella pertussis adenylate cyclase. *Biochemistry* **48**, 11273-11282.

Tansey, WP (2014): Mammalian MYC proteins and cancer. *New J. Sci.* **2014**, 1-27.

Tcherkasskaya, O, and Uversky, VN (2001): Denatured collapsed states in protein folding: example of apomyoglobin. *Proteins* **44**, 244-254.

Tennent, DL, and McMillin, DR (1979): A detailed analysis of the charge-transfer bands of a blue copper protein. Studies of the nickel (II), manganese (II), and cobalt (II) derivatives of azurin. *J. Am. Chem. Soc.* **101**, 2307-2311.

Thomas, LR, Wang, Q, Grieb, BC, Phan, J, Foshage, AM, Sun, Q, Olejniczak, ET, Clark, T, Dey, S, and Lorey, S (2015): Interaction with WDR5 promotes target gene recognition and tumorigenesis by MYC. *Mol. cell* **58**, 440-452.

Thomas, W-H, Weser, U, and Hempel, K (1977): Conformational changes induced by ionic strength and pH in two bovine myelin basic proteins. *Hoppe. Seylers. Z. Physiol. Chem.* **358**, 1345-1352.

Tompa, P (2002): Intrinsically unstructured proteins. *Trends Biochem. Sci.* **27**, 527-533.

Tompa, P (2003): The functional benefits of protein disorder. *J. Mol. Struct.* **666**, 361-371.

Tompa, P (2005): The interplay between structure and function in intrinsically unstructured proteins. *FEBS Lett.* **579**, 3346-3354.

Tompa, P (2010): *Structure and function of intrinsically disordered proteins*. CRC press.

Tompa, P, and Csermely, P (2004): The role of structural disorder in the function of RNA and protein chaperones. *FASEB J.* **18**, 1169-1175.

Treier, M, Staszewski, LM, and Bohmann, D (1994): Ubiquitin-dependent c-Jun degradation in vivo is mediated by the δ domain. *Cell* **78**, 787-798.

Tyndall, J (1868): On the Blue Colour of the Sky, the Polarization of Skylight, and on the Polarization of Light by Cloudy Matter Generally. *Proc. R. Soc. London* **17**, 223-233.

Uversky, VN (1993): Use of fast protein size-exclusion liquid chromatography to study the unfolding of proteins which denature through the molten globule. *Biochemistry* **32**, 13288-13298.

Uversky, VN (1994): Gel-permeation chromatography as a unique instrument for quantitative and qualitative analysis of protein denaturation and unfolding. *Int. J. Bio. Chromatogr.* **1**, 103-114.

Uversky, VN (2002): Natively unfolded proteins: a point where biology waits for physics. *Protein Sci.* **11**, 739-756.

Uversky, VN (2003): A protein-chameleon: conformational plasticity of α-synuclein, a disordered protein involved in neurodegenerative disorders. *J. Biomol. Struct. Dyn.* **21**, 211-234.

Uversky, VN (2009): Intrinsically disordered proteins and their environment: effects of strong denaturants, temperature, pH, counter ions, membranes, binding partners, osmolytes, and macromolecular crowding. *Protein J.* **28**, 305-325.

Uversky, VN (2011): Intrinsically disordered proteins from A to Z. *Int. J. Biochem. Cell Biol.* **43**, 1090-1103.

Uversky, VN (2013a): A decade and a half of protein intrinsic disorder: biology still waits for physics. *Protein Sci.* **22**, 693-724.

Uversky, VN (2013b): Unusual biophysics of intrinsically disordered proteins. *Biochim. Biophys. Acta, Proteins and Proteomics* **1834**, 932-951.

Uversky, VN, and Dunker, AK (2010): Understanding protein non-folding. *Biochim. Biophys. Acta, Proteins and Proteomics* **1804**, 1231-1264.

Uversky, VN, Gillespie, JR, and Fink, AL (2000a): Why are "natively unfolded" proteins unstructured under physiologic conditions? *Proteins* **41**, 415-427.

Uversky, VN, Gillespie, JR, Millett, IS, Khodyakova, AV, Vasilenko, RN, Vasiliev, AM, Rodionov, IL, Kozlovskaya, GD, Dolgikh, DA, and Fink, AL (2000b): Zn 2+-mediated structure formation and compaction of the "natively unfolded" human prothymosin α. *Biochem. Biophys. Res. Commun.* **267**, 663-668.

Uversky, VN, Gillespie, JR, Millett, IS, Khodyakova, AV, Vasiliev, AM, Chernovskaya, TV, Vasilenko, RN, Kozlovskaya, GD, Dolgikh, DA, and Fink, AL (1999): Natively unfolded human prothymosin α adopts partially folded collapsed conformation at acidic pH. *Biochemistry* **38**, 15009-15016.

Uversky, VN, Li, J, and Fink, AL (2001a): Evidence for a partially folded intermediate in α-synuclein fibril formation. *J. Biol. Chem.* **276**, 10737-10744.

Uversky, VN, Li, J, and Fink, AL (2001b): Metal-triggered structural transformations, aggregation, and fibrillation of human α-synuclein a possible molecular link between parkinson′ s disease and heavy metal exposure. *J. Biol. Chem.* **276**, 44284-44296.

Uversky, VN, Li, J, and Fink, AL (2001c): Trimethylamine-N-oxide-induced folding of α-synuclein. *FEBS Lett.* **509**, 31-35.

Uversky, VN, and Narizhneva, NV (1998): Effect of natural ligands on the structural properties and conformational stability of proteins. *Biochemistry* **63**, 420-433.

Uversky, VN, Oldfield, CJ, and Dunker, AK (2008): Intrinsically disordered proteins in human diseases: introducing the D2 concept. *Annu. Rev. Biophys.* **37**, 215-246.

Uversky, VN, Oldfield, CJ, Midic, U, Xie, H, Xue, B, Vucetic, S, Iakoucheva, LM, Obradovic, Z, and Dunker, AK (2009): Unfoldomics of human diseases: linking protein intrinsic disorder with diseases. *BMC genomics* **10**, S1-S7.

Vacic, V, Uversky, VN, Dunker, AK, and Lonardi, S (2007): Composition Profiler: a tool for discovery and visualization of amino acid composition differences. *BMC bioinformatics* **8**, 211.

Vitalis, A, Wang, X, and Pappu, RV (2007): Quantitative characterization of intrinsic disorder in polyglutamine: insights from analysis based on polymer theories. *Biophys. J.* **93**, 1923-1937.

Vucetic, S, Xie, H, Iakoucheva, LM, Oldfield, CJ, Dunker, AK, Obradovic, Z, and Uversky, VN (2007): Functional anthology of intrinsic disorder. II. Cellular components, domains, technical terms, developmental processes, and coding sequence diversities correlated with long disordered regions. *J. Proteome Res.* **6**, 1899-1916.

Waddell, WJ (1956): A simple ultraviolet spectrophotometric method for the determination of protein. *J. Lab. Clin. Med.* **48**, 311-314.

Walters, RH, and Murphy, RM (2009): Examining polyglutamine peptide length: a connection between collapsed conformations and increased aggregation. *J. Mol. Biol.* **393**, 978-992.

Wang, X, Vitalis, A, Wyczalkowski, MA, and Pappu, RV (2006): Characterizing the conformational ensemble of monomeric polyglutamine. *Proteins* **63**, 297-311.

Warrant, RW, and Kim, SH (1978): α-Helix–double helix interaction shown in the structure of a protamine-transfer RNA complex and a nucleoprotamine model. *Nature* **271**, 130-135.

Watts, JD, Cary, PD, Sautiere, P, and Crane-Robinson, C (1990): Thymosins: both nuclear and cytoplasmic proteins. *Eur. J. Biochem.* **192**, 643-651.

Weber, G (1952): Polarization of the fluorescence of macromolecules. 1. Theory and experimental method. *Biochem. J.* **51**, 145-155.

Weinreb, PH, Zhen, W, Poon, AW, Conway, KA, and Lansbury, PT (1996): NACP, a protein implicated in Alzheimer's disease and learning, is natively unfolded. *Biochemistry* **35**, 13709-13715.

Wetlaufer, DB (1963): Ultraviolet spectra of proteins and amino acids: *Advances in protein chemistry,* Vol. 17. Elsevier, pp. 303-390.

Whitmore, L, and Wallace, BA (2004): DICHROWEB, an online server for protein secondary structure analyses from circular dichroism spectroscopic data. *Nucleic Acids Res.* **32**, W668-W673.

Whitmore, L, and Wallace, BA (2008): Protein secondary structure analyses from circular dichroism spectroscopy: Methods and reference databases. *Biopolymers* **89**, 392-400.

Wiederschain, GY (2011): *The Molecular Probes handbook. A guide to fluorescent probes and labeling technologies*. Springer.

Wildegger, G, Liemann, S, and Glockshuber, R (1999): Extremely rapid folding of the C-terminal domain of the prion protein without kinetic intermediates. *Nat. Struct. Biol.* **6**, 550-553.

Williams, RM, Obradovic, Z, Mathura, V, Braun, W, Garner, EC, Young, J, Takayama, S, Brown, CJ, and Dunker, AK (2001): The protein non-folding problem: amino acid determinants of intrinsic order and disorder. *Pac. Symp. Biocomput.*, 89-100.

Worbs, M, Huber, R, and Wahl, MC (2000): Crystal structure of ribosomal protein L4 shows RNA-binding sites for ribosome incorporation and feedback control of the S10 operon. *EMBO J.* **19**, 807-818.

Wright, PE, and Dyson, HJ (1999): Intrinsically unstructured proteins: re-assessing the protein structure-function paradigm. *J. Mol. Biol.* **293**, 321-331.

Wright, PE, and Dyson, HJ (2015): Intrinsically disordered proteins in cellular signalling and regulation. *Nat. Rev. Mol. Cell. Biol.* **16**, 18-29.

Wu, PG, and Brand, L (1994): Resonance energy transfer: methods and applications. *Anal. Biochem.* **218**, 1-13.

Xie, H, Vucetic, S, Iakoucheva, LM, Oldfield, CJ, Dunker, AK, Obradovic, Z, and Uversky, VN (2007): Functional anthology of intrinsic disorder. 3. Ligands, post-translational modifications, and diseases associated with intrinsically disordered proteins. *J. Proteome Res.* **6**, 1917-1932.

Xue, B, W Williams, R, J Oldfield, C, Kian-Meng Goh, G, Keith Dunker, A, and N Uversky, V (2010): Viral disorder or disordered viruses: do viral proteins possess unique features? *Protein Pept. Lett.* **17**, 932-951.

Yaglom, J, Linskens, MH, Sadis, S, Rubin, DM, Futcher, B, and Finley, D (1995): p34Cdc28-mediated control of Cln3 cyclin degradation. *Mol. Cell. Biol.* **15**, 731-741.

Yancey, PH, Clark, ME, Hand, SC, Bowlus, RD, and Somero, GN (1982): Living with water stress: evolution of osmolyte systems. *Science* **217**, 1214-1222.

Yguerabide, J, Epstein, HF, and Stryer, L (1970): Segmental flexibility in an antibody molecule. *J. Mol. Biol.* **51**, 573-590.

Zaccai, NR, Serdyuk, IN, and Zaccai, J (2017): *Methods in molecular biophysics*. Cambridge University Press.

Zhang, X-y, DeSalle, LM, and McMahon, SB (2006): Identification of novel targets of MYC whose transcription requires the essential MbII domain. *Cell Cycle* **5**, 238-241.